平成 24 年度

修 士 論 文

Seismic Structural Monitoring of World Heritage Masonry Monuments in Earthquake-prone Countries

指導教員　　花里利一　教授

三重大学大学院工学研究科
建築学専攻

小柳津菜都美

Seismic Structural Monitoring of World Heritage Masonry Monuments in Earthquake-prone Countries

Contents

Chapter1 Introduction

1.1 ABSTRACT

In order to study actual behaviors and to grasp the fundamental dynamic characteristics, earthquake monitoring has been undertaken at the Parthenon Athens, Greece and the Prambanan Temples, Indonesia, both registered as World Cultural Heritage. Furthermore, monitoring of crack displacement with temperature and humidity has been carried out to assess the present structural stability at the Prambanan Temples.

In the present study, the natural frequencies of these heritage structures were evaluated from the earthquake records. At the Parthenon Athens, two small earthquakes were recorded in 2010 and the end of 2011. Four earthquakes were recorded at the Prambanan Temple as well. Three of these records were enough large to compare the characteristics of the seismic performance of the structure.

The present state of structural stability of Chandi Shiva, the highest monument of the Prambanan Temples, was successfully assessed on the basis of the crack displacement performance before/after the seismic events. The long-term structural stability affected by temperature was also discussed. In addition, variation of temperature and humidity at the different monitoring points of the monuments were found at the Prambanan Temples.

Seismic response analyses of both the Parthenon Athens and the Prambanan Temples were conducted by using these earthquake records. The analysis employing finite element method was also carried out for simulation of the seismic response of Chandi Shiva of which inside structural condition has been unknown. The finite element model was verified by the earthquake monitoring data of 2010.

1.2 BACKGROUND

Today, a number of historical masonry heritage monuments exist in the earthquake-prone countries. These monuments were affected by earthquakes and by the other natural or human disasters. Furthermore, they were investigated, restored and improved during their long histories. However, there is no general index to assess structural stability or anti-seismic capacity of masonry heritage monuments. In the present study, monitoring surveys have been employed to provide effective suggestion from the view of structural safety. Throughout the earthquake monitoring, their actual behaviors under seismic motions were clarified. Those two objects of the World heritage masonry monuments also have been affected by the past earthquakes, and restoration projects were carried out. Structural monitoring survey has been carried out for the historical buildings, mentioned in the following sections. Hence, “monitoring” was introduced as one article of principles for the analysis, conservation and structural restoration of architectural

heritage in 2003 by ISCARSAH (the International Scientific Committee on the Analysis and Restoration of Structures of Architectural Heritage) [1].

A project, NIKER (New Integrated Knowledge based approaches to the protection of cultural heritage from Earthquake-induced Risk) [2], works to present guidelines of assessment procedures and final validation on real case studies. This project aims at developing new integrated methodologies with a systemic approach which includes also design methods, advanced monitoring and early warning techniques for cultural heritage assets. Structural monitoring of masonry monuments is included in this international project. NIKER was established in 2010 by 18 participations of research centers, enterprises, industry, public authority and end-users from EU countries, countries around the Mediterranean Sea, AC, ICPC and MPC. They have conducted studies to develop and validate innovative materials and technologies for systemic improvement of seismic behaviors of cultural heritage assets. They have 10 work packages. In work package 9, the knowledge-based assessment procedures to real case studies develop. Monitoring is a useful tool not only for knowledge based assessment but also for early warning. How to conduct monitoring effectively is discussed in order to keep cultural heritage asset having its targeted performance.

1.3 PURPOSE

This research focuses on the structural monitoring to assess the present state of the seismic structural stability of heritage masonry monuments. It is also aimed that recording data are used for both studying actual seismic behaviors and structural analyses for both of the Parthenon Athens and the Prambanan Temples. When analyzing structures, numerical models were verified by the earthquake monitoring records. Furthermore, the seismic ground motions at the site could be used for input motions for the earthquake response analysis. As the structural monitoring, monitoring of earthquakes, as well as, that of crack displacement, temperature and humidity have been conducted for the case of the Prambanan Temples.

1.4 PAST STUDIES

G. Creazza reported the investigation program of the San Marco Basilica, Venice, which was built in Romanesque-Byzantine architecture dates from the 5th century [3]. It was underwent considerable restration between the 11th and 12th centuries. The Basilica showed clear signs of the structural deformations and damages caused during its long life. This investigation program started in 1991. His study was based on combination approach of analysis and experiments. It consisted of the following eight major steps; topographic and photogrammetric surveys, historical analysis based on the study of existing documents and drawings, detailed crack pattern survey of the supporting masonry structures, geotechnical investigations by in situ and laboratory tests,

analysis of the structural characteristics of the masonry by means of coring, video camera survey, sonic tomography and radar inspection, flat-jack testing of the actual state of stress, analysis of physical and chemical characteristics of the mortars, structural analysis of the Basilica by means of a three-dimensional finite element model, and monitoring of the opening of the major cracks, the relative movements of the pillars and the relative settlements of the foundations. The instruments of the monitoring system were connected to an automatic data acquisition and to processing unit which was able to check in real-time the deformation behavior of the structure. The results were interpreted in an interdisciplinary way.

Hanazato et al. conducted the survey of resistance to earthquakes at the same time they performed structural monitoring of the Hagia Sophia in Istanbul, Turkey [4 to 8]. Their study was conducted as an international collaborative scientific research. They reviewed the history of the major earthquakes and the damages of its dome celling. They also evaluated its structural health by monitoring of structure and environment. As results, they found its fundamental dynamic characteristics, and evaluated the input earthquake motions that could be utilized for structural reinforcement plan. They installed monitoring equipment inside and outside the Hagia Sophia; 31 measuring points for temperature, 13 points for humidity and 24 points for crack displacement during September, 1995 and February, 2000. Long-term crack monitoring was conducted, because record of crack displacement was considered to be useful as safety monitoring of structure.

T. Ueshima et al. conducted long-term continuous observation of microtremor/seismic motion at the crest of an aged arch dam, the Ohkura Dam in Miyagi Prefecture, Japan, which was constructed approximately fifty years ago [9]. They installed accelerographs of three components at two points of the surface. They compared the natural frequencies of the dam with microtremor data during approximately five months from summer to winter. The 2011 East Japan Earthquake was recorded at the dam. From the results of identification of the dynamic characteristics every five minutes during the period from August to December, it was noticed that natural frequency was getting lower from summer toward winter. They considered that the mechanism of decrease of the natural frequency following the dam surface temperature was as follows. As the dam body temperature decrease, the dam shrinks, arch effect is lost, the compressive stress of the dam body concrete decreases and as the result, Young’s modulus decreases. Otherwise the natural frequency decrease was considered to be caused by the joint rigidity decrease following the compressive stress decrease.

Chapter 2 Case Study at the Parthenon Athens

2.1 INTRODUCTION

The Parthenon Athens shown in Fig. 2-1 was constructed approximately 25 centuries ago. The monument has not been damaged severely despite it has experienced earthquakes throughout its history. A total of 125 historical earthquakes were utilized to calculate the peak accelerations at the Acropolis hill, where the Parthenon Athens stands, in the past study by the authors. As results, the peak acceleration values considered to exceed 94 gal (cm/s^2) only 10 times [10]. However it was damaged slightly by the recent earthquake in 1981. The restoration works for this monument had been conducted many times before 1981. The present restoration work has been carried out by the ministry of Greece government since 1999. Since 2008, international collaborative research had been established with the National Technical University of Athens (NTUA). The main purpose is to understand the actual seismic performance of this monument that has survived against earthquakes. The present study was conducted for proposing the structural restoration plan.

Fig. 2-1 View of the Parthenon Athens from the Southeast corner

2.2 EARTHQUAKE MONITORING

Since September of 2008, the earthquake monitoring system has been initiated on the Northwest corner. The seismographs were replaced with new ones in April 2010. One small earthquake was recorded on September 2nd, 2010. However, the earthquake was only recorded at the base as the trigger system had trouble at that time. After having revised the system, we could record a minor earthquake both at the base and the roof on December 8th, 2011. In the following section, the earthquake record on December 8th, 2011 is described.

2.2.1 MONITORING SYSTEM

The earthquake monitoring system has two seismographs both on the base (Master) on the top of the cornice (Slave). Fig. 2-2 shows the schematic representation of the system. Fig. 2-3 shows

brief image of the arrangement of the devices in stainless boxes. The specification of accelerograph is shown in Table. 2-1. Fig. 2-4 shows the sensor used in the present monitoring. The location of the equipment and the view of each ones are shown in Figs. 2-5 and 2-6, respectively.

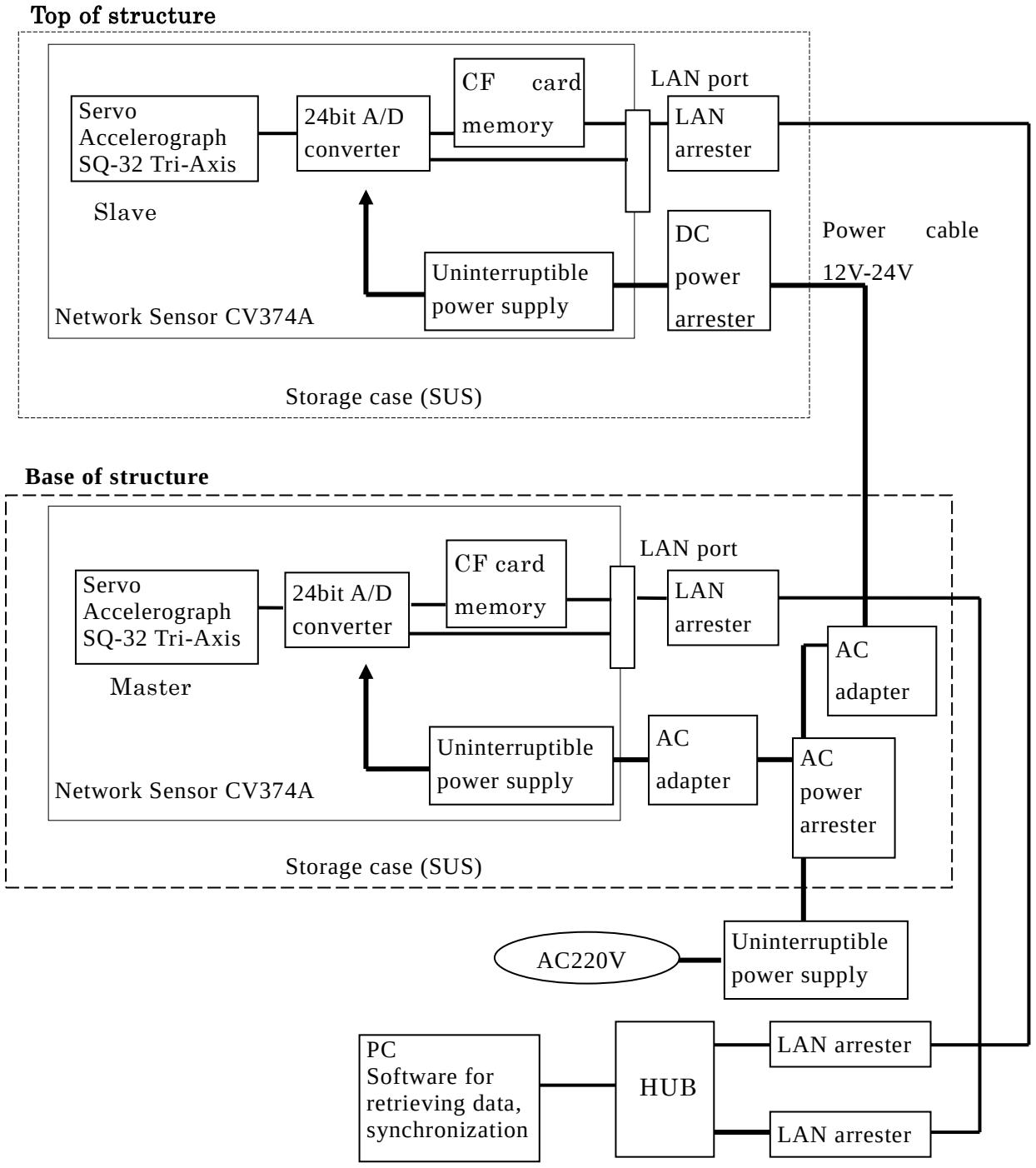

Fig. 2-2 Earthquake monitoring system (Data acquisition system using CV374)

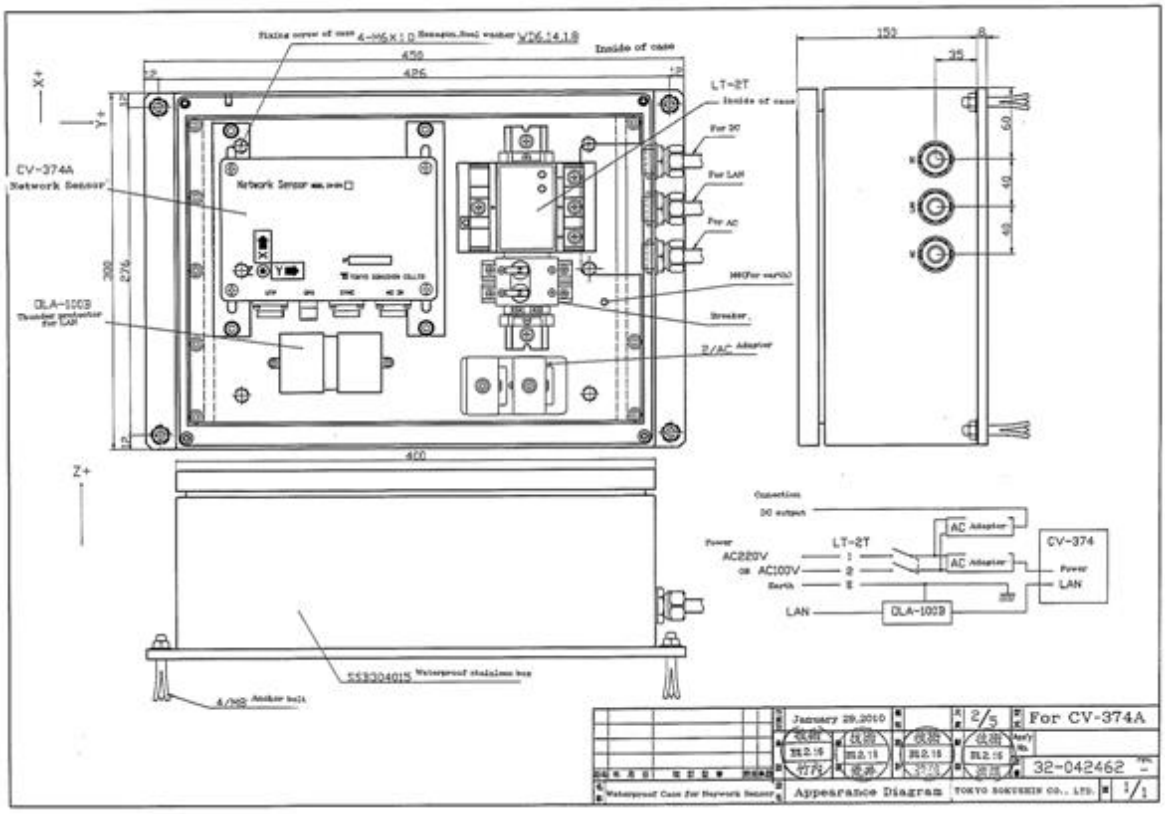

(a) Arrangement of devices in a stainless steel box for CV374A (Master)

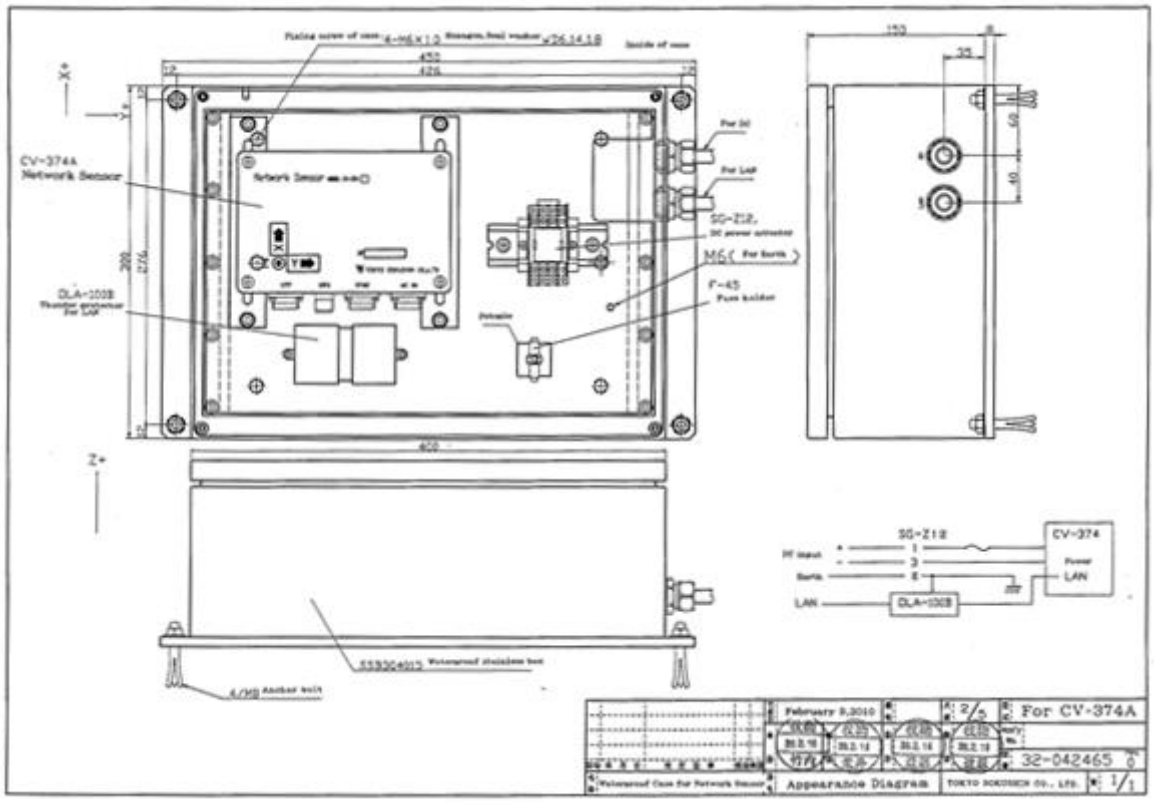

Fig. 2-3 (b) Arrangement of devices in a stainless steel box for CV374A (Slave)

Table. 2-1 Specifications of the servo-type accelerograph (after Tokyo Sokushin)

Data	Number of Channels	3
	Full Scale	±2000 cm/s^2
	Sampling	100 Hz,200 Hz
	Bandwidth	DC to 100 Hz
	AD converter	24bit
	Resolution	0.001cm/s^2
Sensor	Accelerometer	Servo accelerometer
	Components	Tri-axial
Event recorder	Trigger level	0.5 – 100 cm/s^2
	Pre trigger time	1 – 30 s
	Post trigger time	10 – 200 s
	Memory	CF card
	Duration (Total)	160 h
Clock	Accuracy	0.62 ppm
	Time synchronization	NTP or GPS
Internal UPS (Battery)	Duration	90 min
Dimension	W×D×H	180×120×100 mm^3

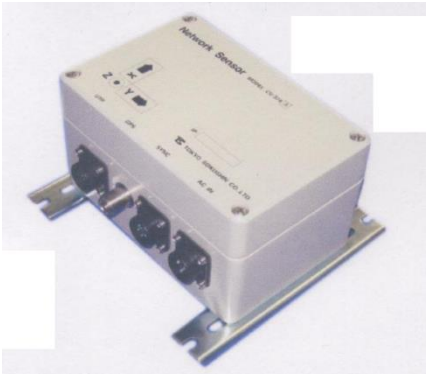

Fig. 2-4 CV374A Network sensor

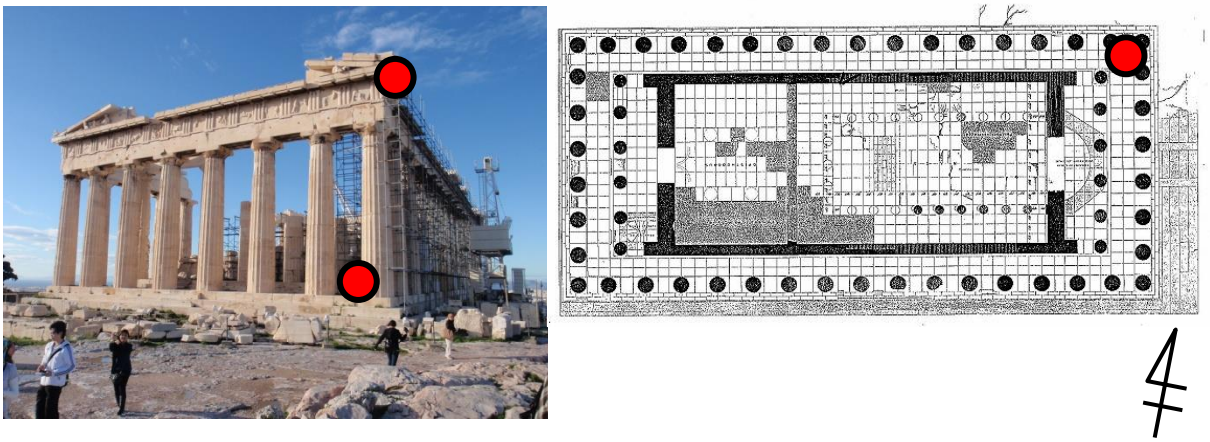

Fig. 2-5 Location of seismographs

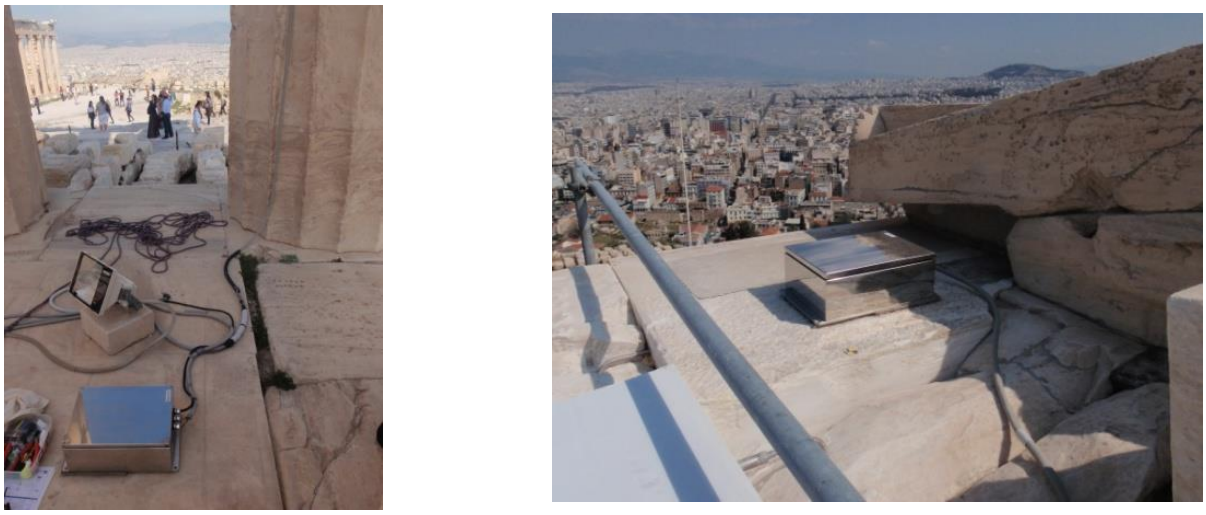

(A) Master sensor **(B) Slave sencor**

Fig. 2-6 View of seismographs

2.2.2 EARTHQUAKE RECORD

As these seismographs can record seismic motions as acceleration data, both velocity and displacement were calculated by integration from the acceleration records through Frequency filtering with the software TDAP III (ARK Information systems).

$$H(f) = 1 / (1 - (f0 / f)^2 - 2h (f0 / f) I) / (1+ (f1 / f)^2)^{1/2}$$

where f0=0.16666667 (Hz), f1=0.1 (Hz) and h=0.552.

I) Earthquake record on September 2nd, 2010

On September 2nd, 2010, a time history of small earthquake was recorded. Table. 2-2 shows the earthquake data. Fig. 2-7 shows the location of the epicenter and the Parthenon. Only the seismograph at the base could record the earthquake. Fig. 2-8, 2-9 and 2-10 show the time

histories of acceleration, velocity and displacement, respectively. Table. 2-3 shows the peak values of those time histories.

Table. 2-2 Earthquake data of the event on September 2nd, 2010

Local Time	Lat.	Lon.	Depth	M_L	Epicentral Dist.
5:53	38.2 N	23.2 E	26 km	4.3	56 km

Table. 2-3 Peak amplitude of the records on the September 2nd, 2010 event

		Acceleration (gal)		Velocity (cm/s)		Displacement (cm)	
		Max	Min	Max	Min	Max	Min
Master	EW	0.4	-0.4	0.032	-0.043	0.0029	-0.0034
	NS	0.7	-0.5	0.029	-0.024	0.0024	-0.0026
	UD	0.2	-0.2	0.012	-0.014	0.0023	-0.0017

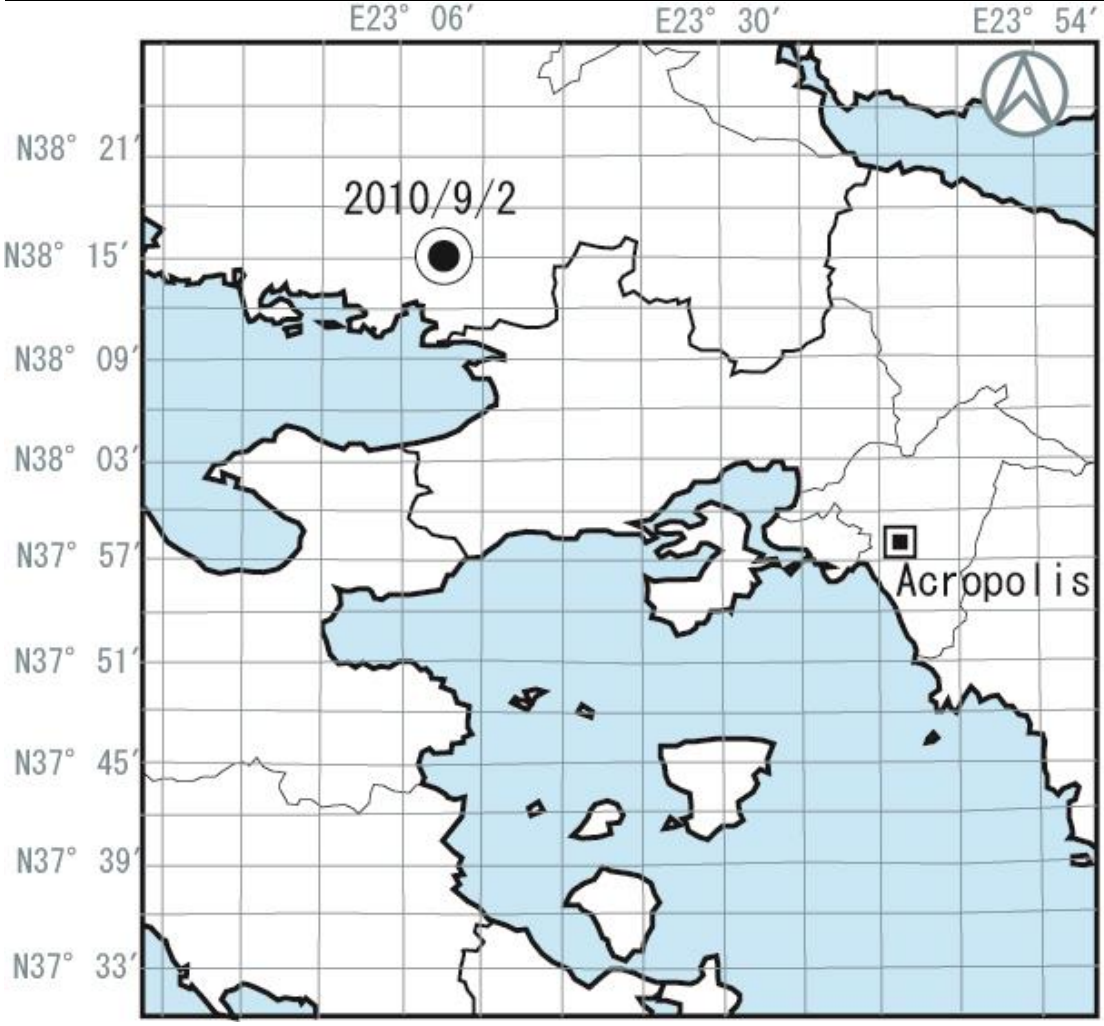

Fig. 2-7 Epicenter of the event on September 2nd, 2010

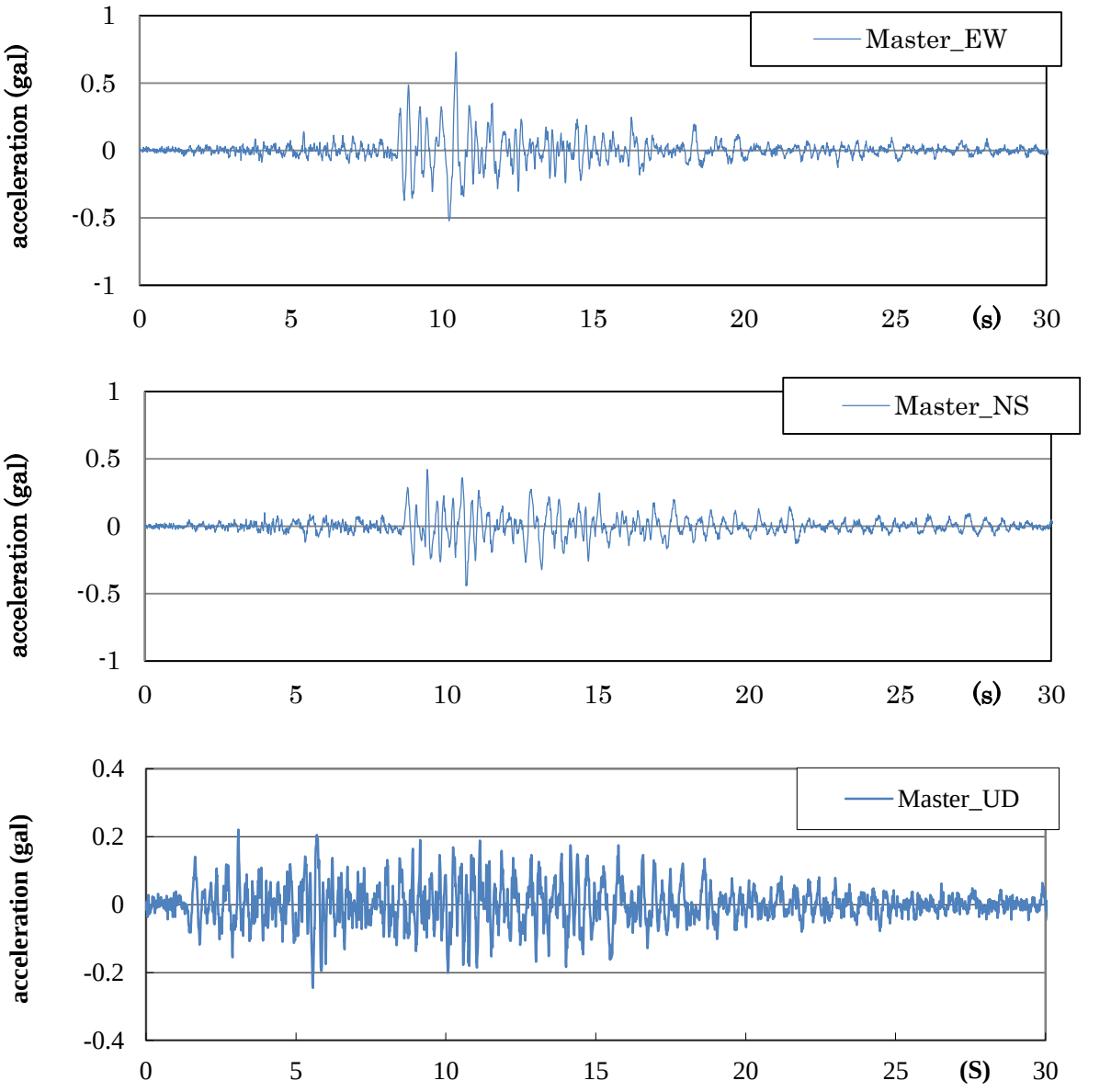

* 980gal = 1G

Fig. 2-8 Acceleration time history recorded at the base

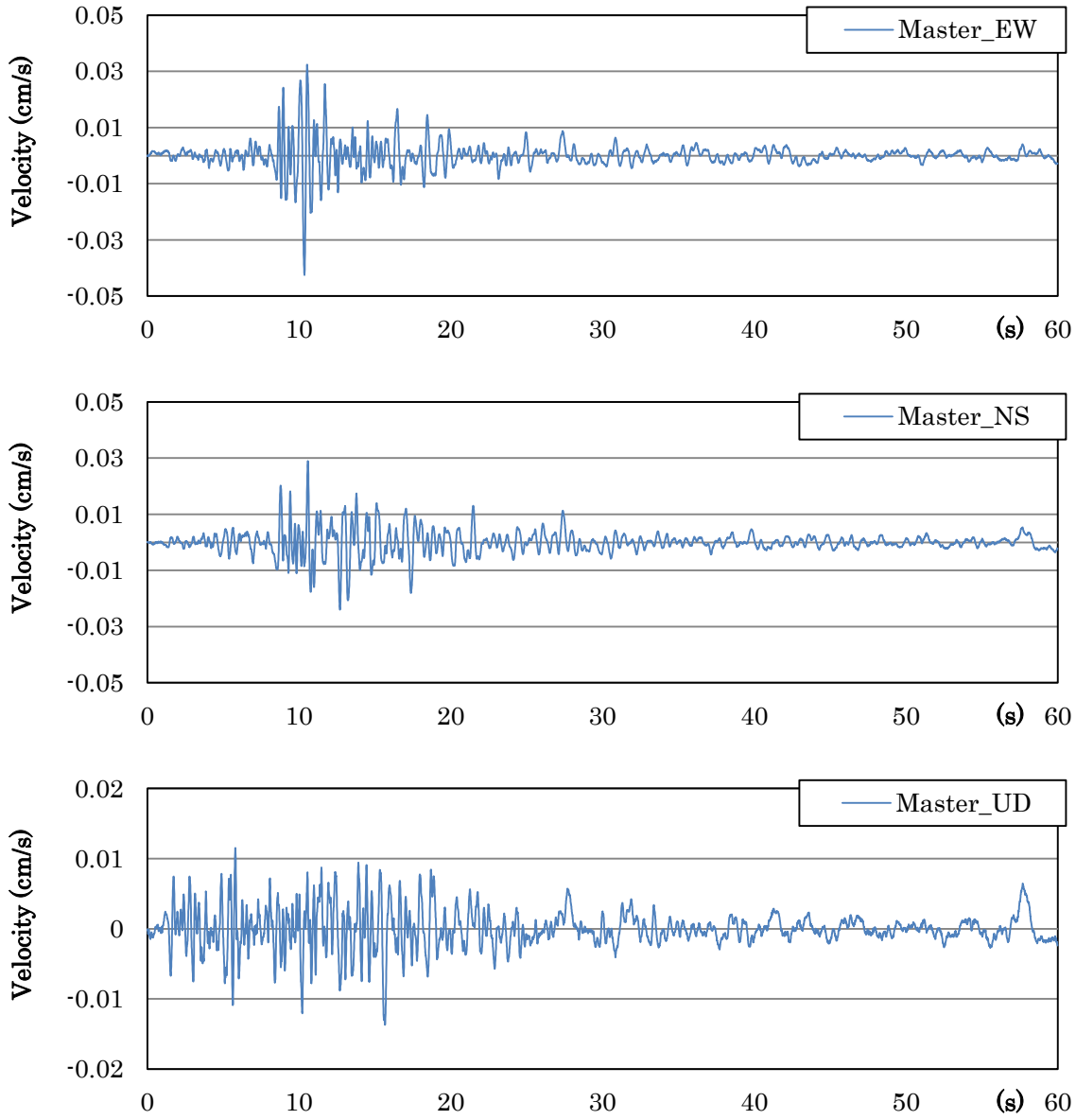

Fig. 2-9 Velocity time history recorded at the base

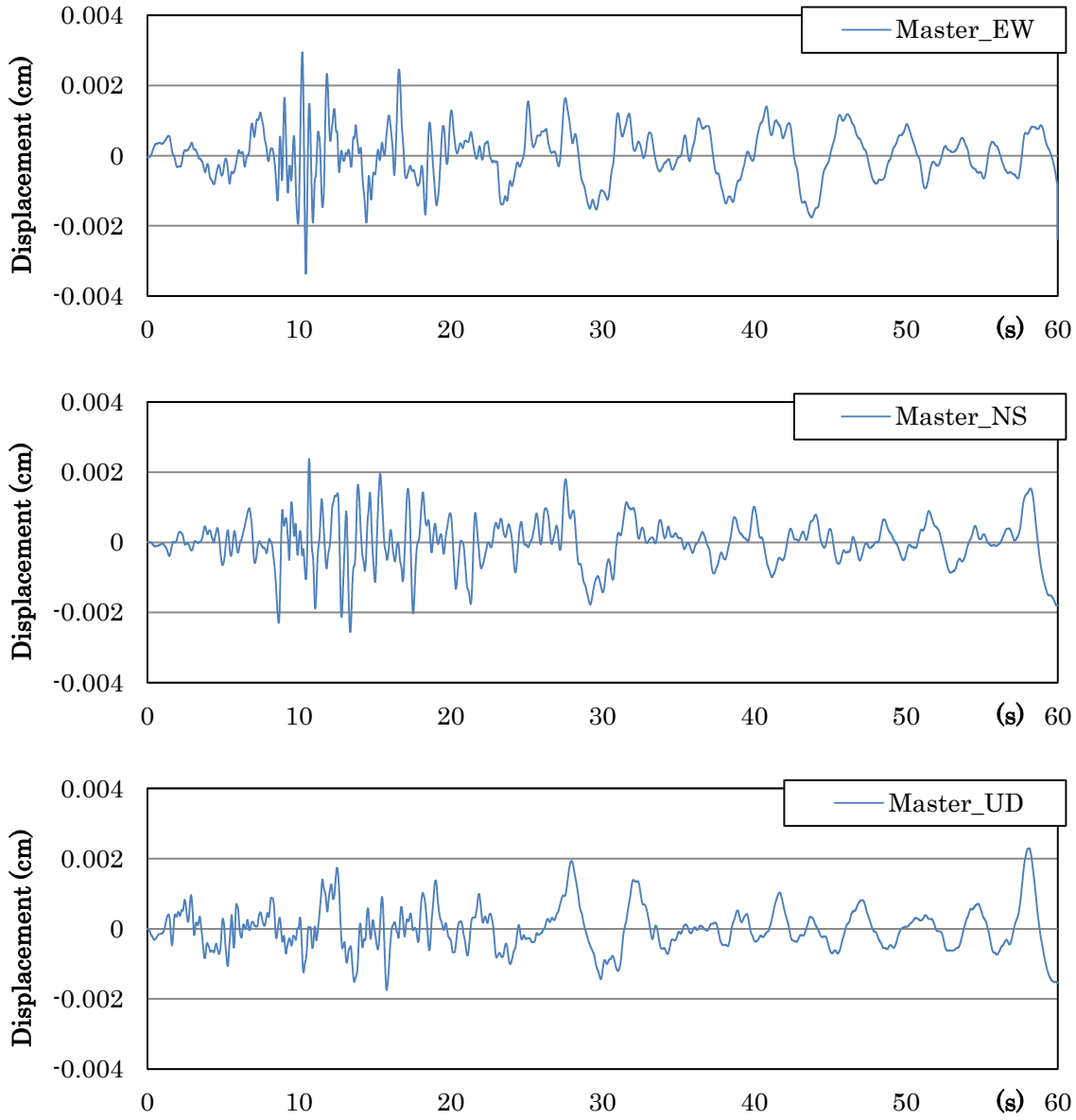

Fig. 2-10 Displacement time history recorded at the base

Fourier spectra of the acceleration data were calculated from the acceleration time histories by using the software Pwave32 with Hanning spectral window of 20 times, shown in Figs. 2-11. Fig. 2-12 shows the acceleration response spectra.

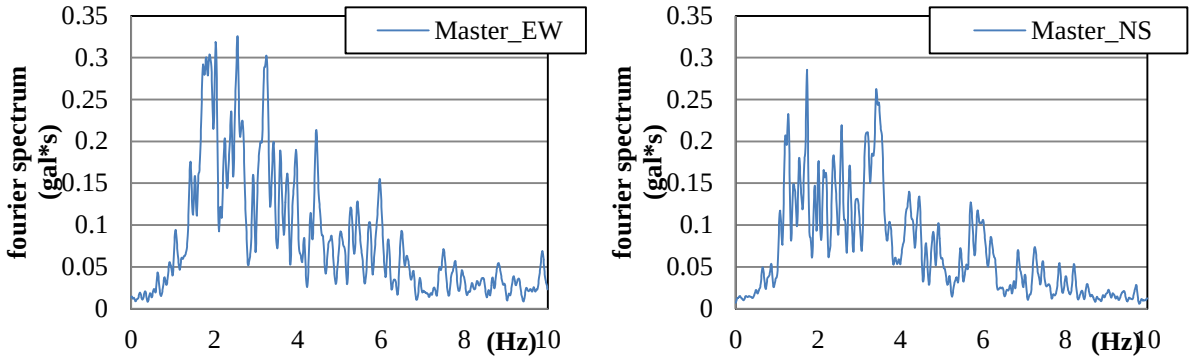

Fig. 2-11 Acc. Fourier Spectra

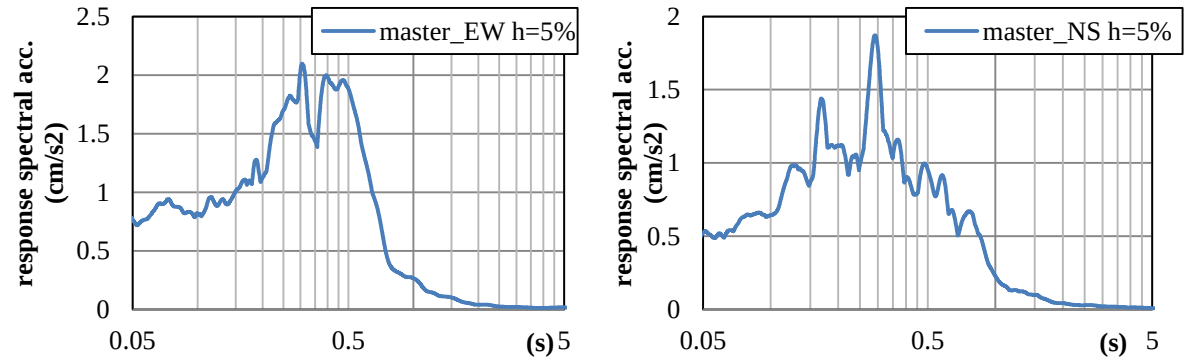

Fig. 2-12 Acc. Response Spectra

II) Earthquake record on December 8th, 2011

On December 8th, 2011, a time history of minor earthquake was recorded. Table. 2-4 shows the earthquake data. Fig.2-13 also shows the location of the epicenter and the Parthenon. Figs. 2-14 to 2-16 show acceleration time histories. Figs. 2-17 to 2-19 show velocity time histories and Figs. 2-20 to 2-22 show displacement time histories. The peak values of those time histories are summarized in Table. 2-5.

Table. 2-4 Earthquake data of the event on December 8th, 2011

Local Time	Lat.	Lon.	Depth	M_L	Epicentral Dist.
23:04	19.9 N	38.1 E	12 km	1.1	28 km

Table. 2-5 Peak amplitude of the records on the December 8th, 2011 event

		Acceleration (gal)		Velocity (cm/s)		Displacement (cm)	
		Max	Min	Max	Min	Max	Min
EW	Slave	3.9	-2.5	0.105	-0.099	0.0052	-0.0040
	Master	0.9	-0.6	0.035	-0.024	0.0022	-0.0023
NS	Slave	1.5	-1.9	0.052	-0.042	0.0026	-0.0033
	Master	0.4	-0.5	0.020	-0.016	0.0018	-0.0017
UD	Slave	1.3	-1.2	0.008	-0.015	0.0020	-0.0017
	Master	0.4	-0.3	0.009	-0.008	0.0018	-0.0021

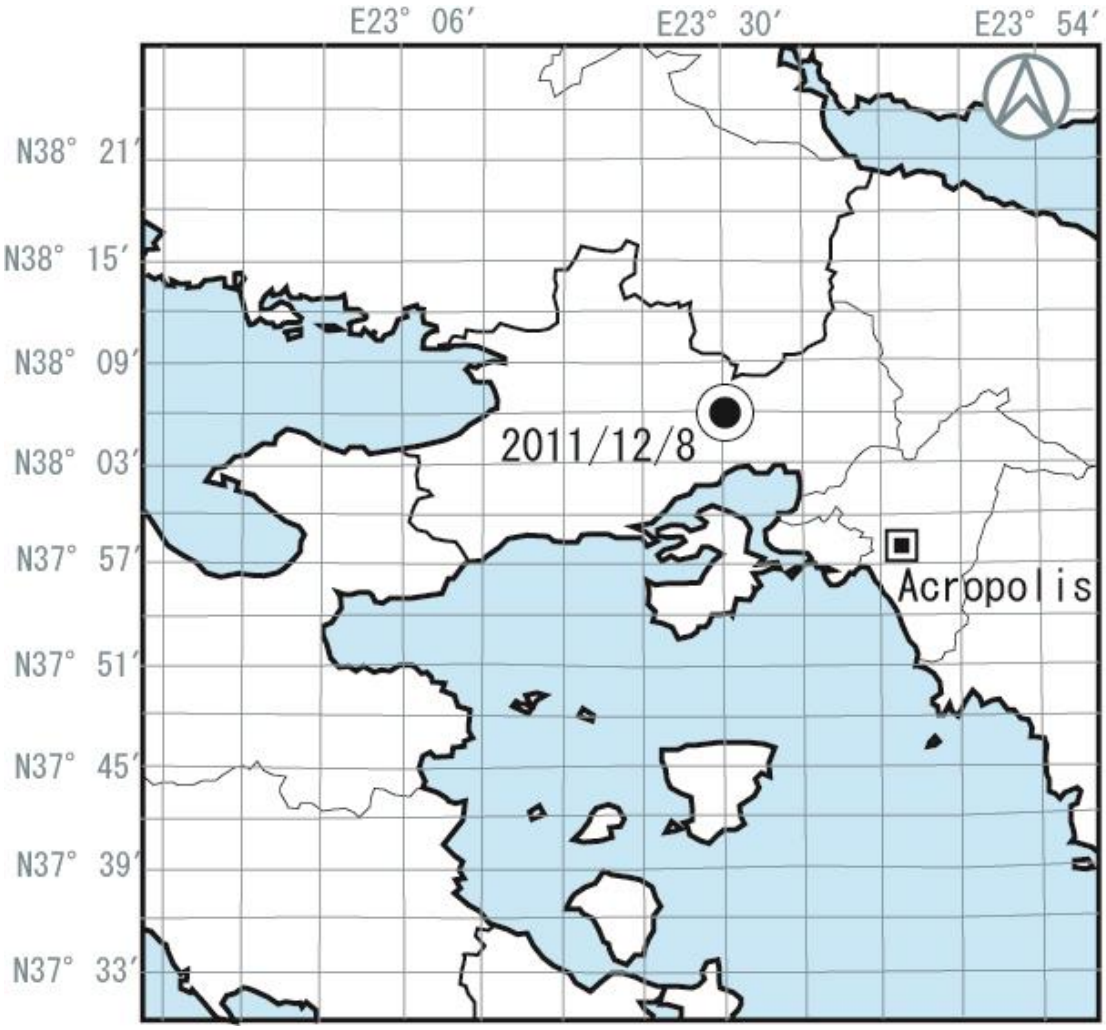

Fig. 2-13 Epicenter of the event on December 8th, 2011

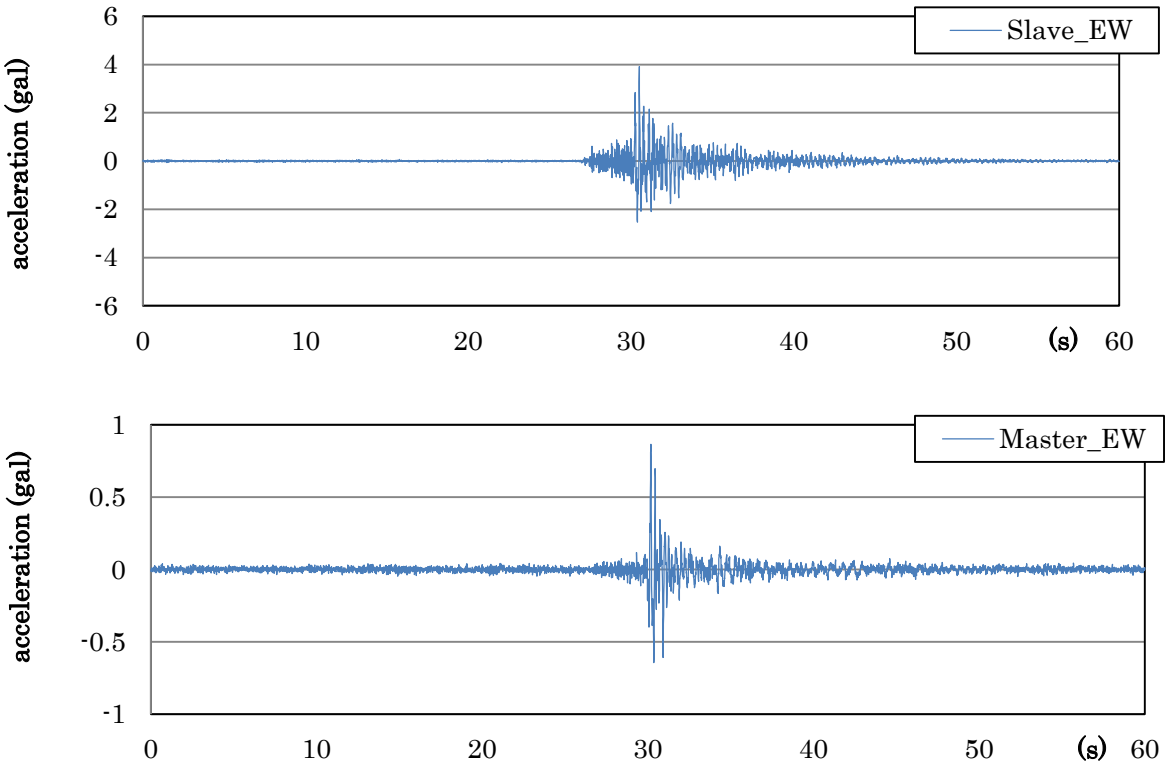

* 980 gal = 1 G

Fig. 2-14　Acceleration time history recorded in the EW direction

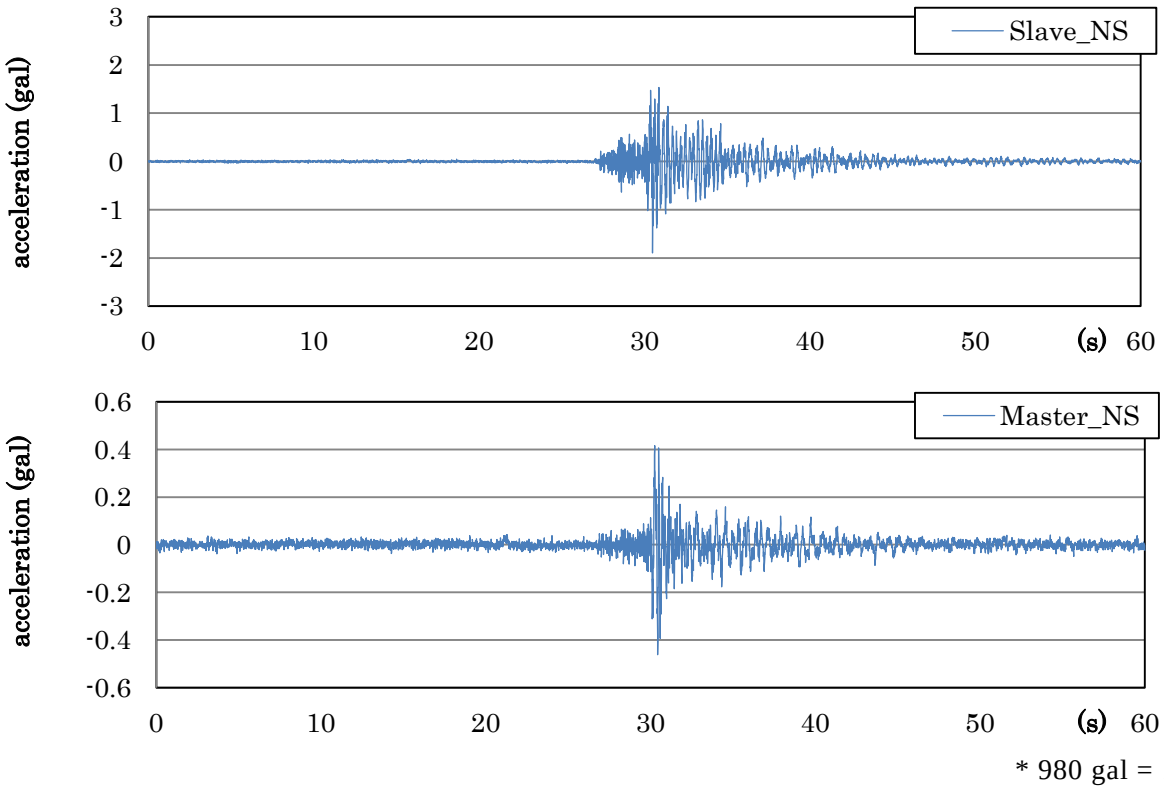

* 980 gal = 1 G

Fig. 2-15　Acceleration time history recorded in the NS direction

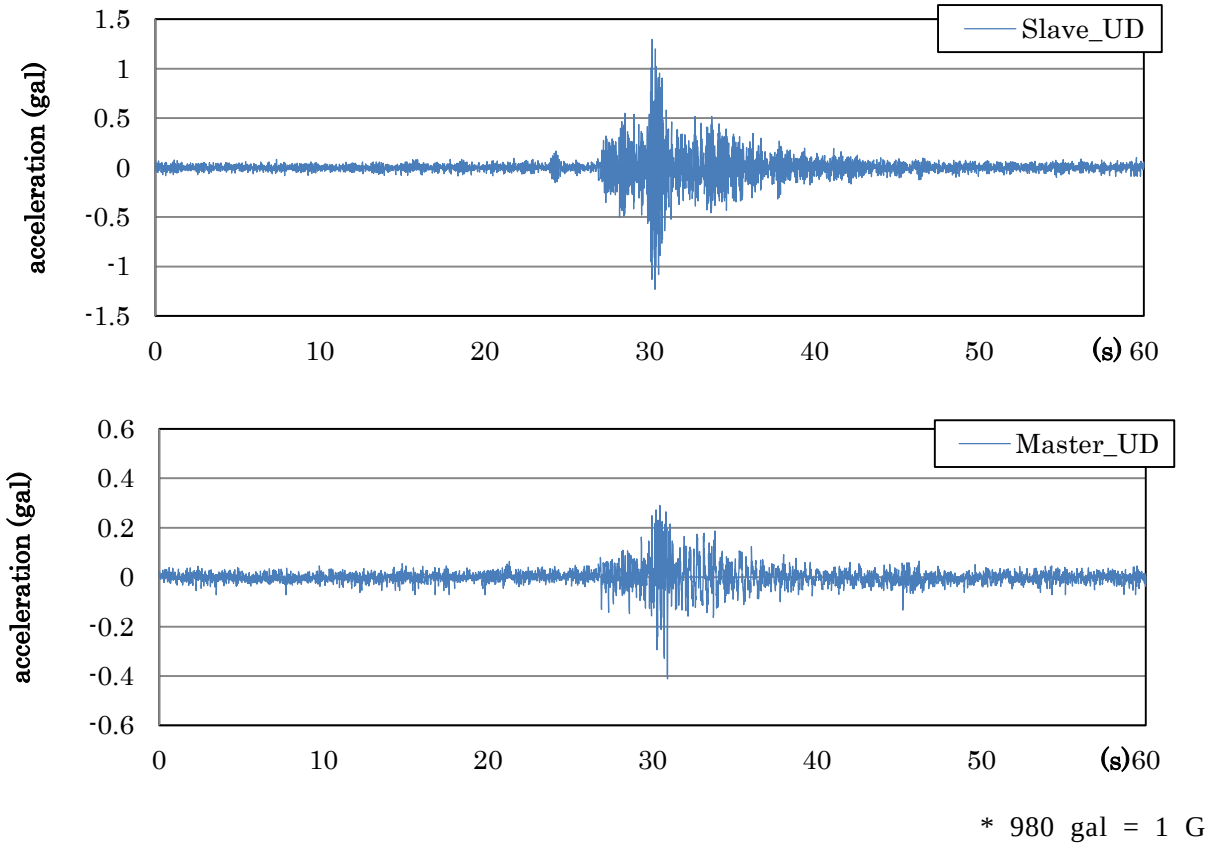

* 980 gal = 1 G

Fig. 2-16　Acceleration time history recorded in the UD direction

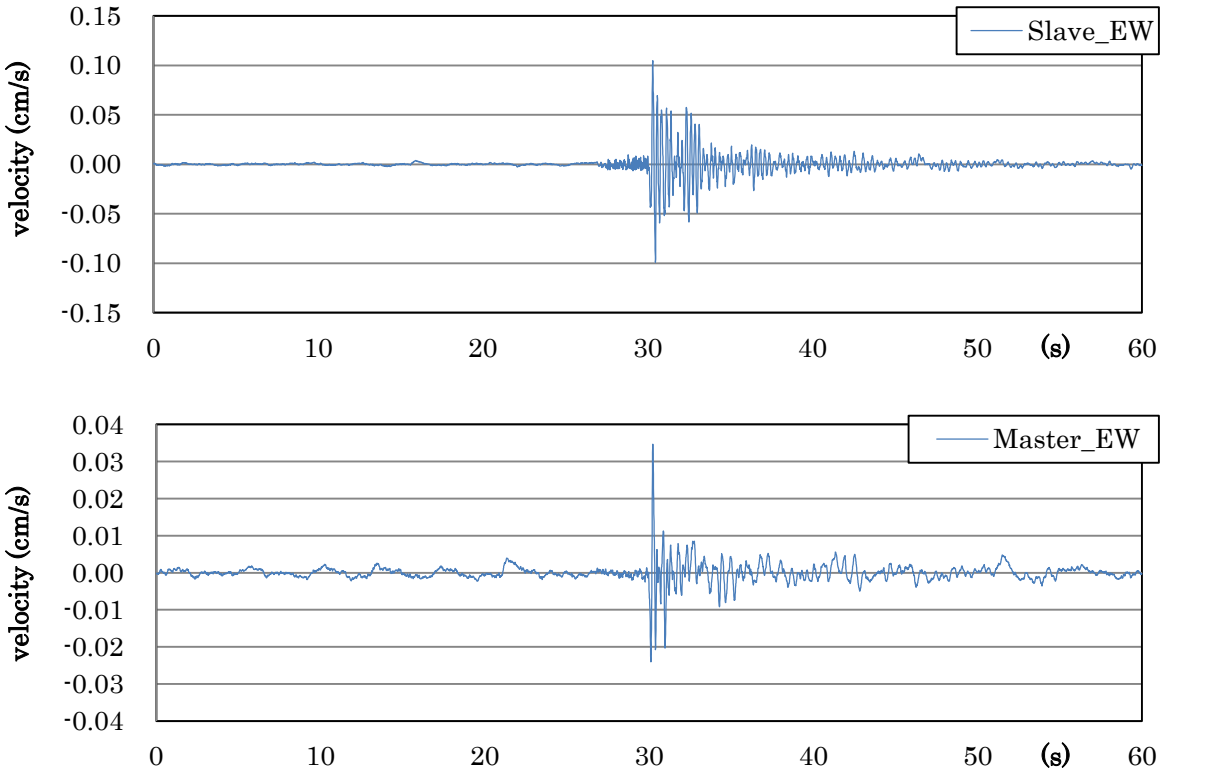

Fig. 2-17　Velocity time history recorded in the EW direction

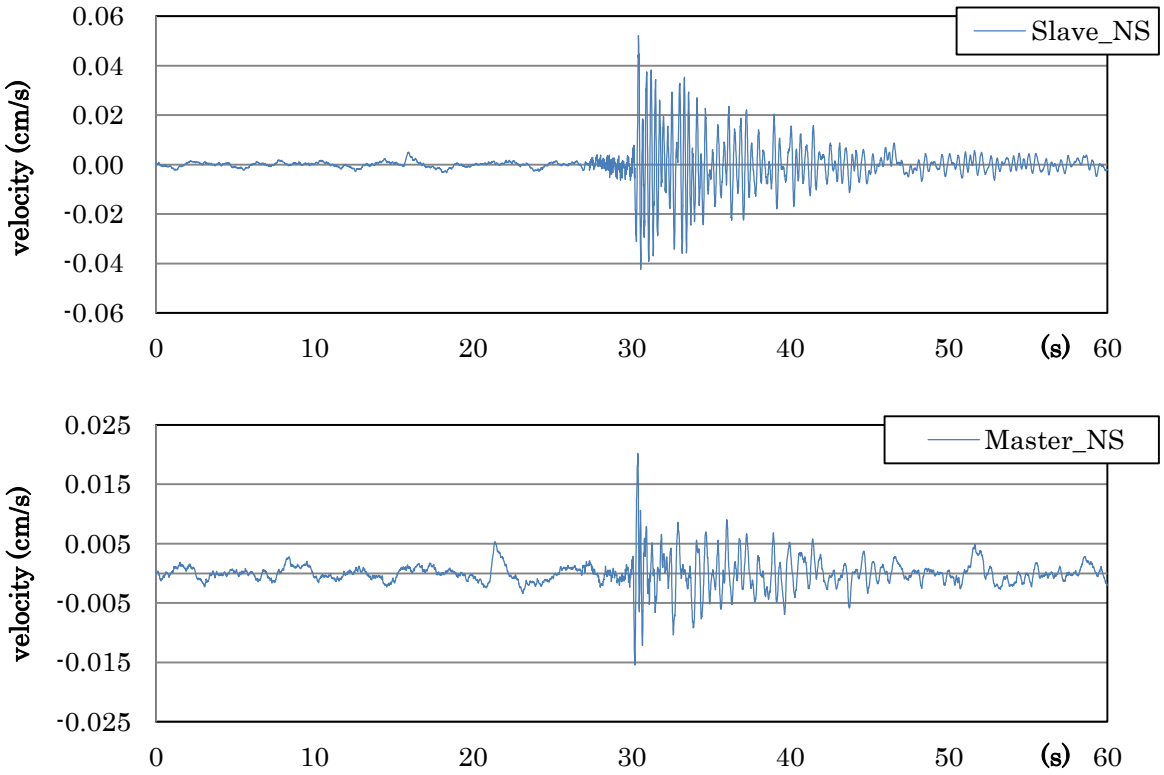

Fig. 2-18　Velocity time history recorded in the NS direction

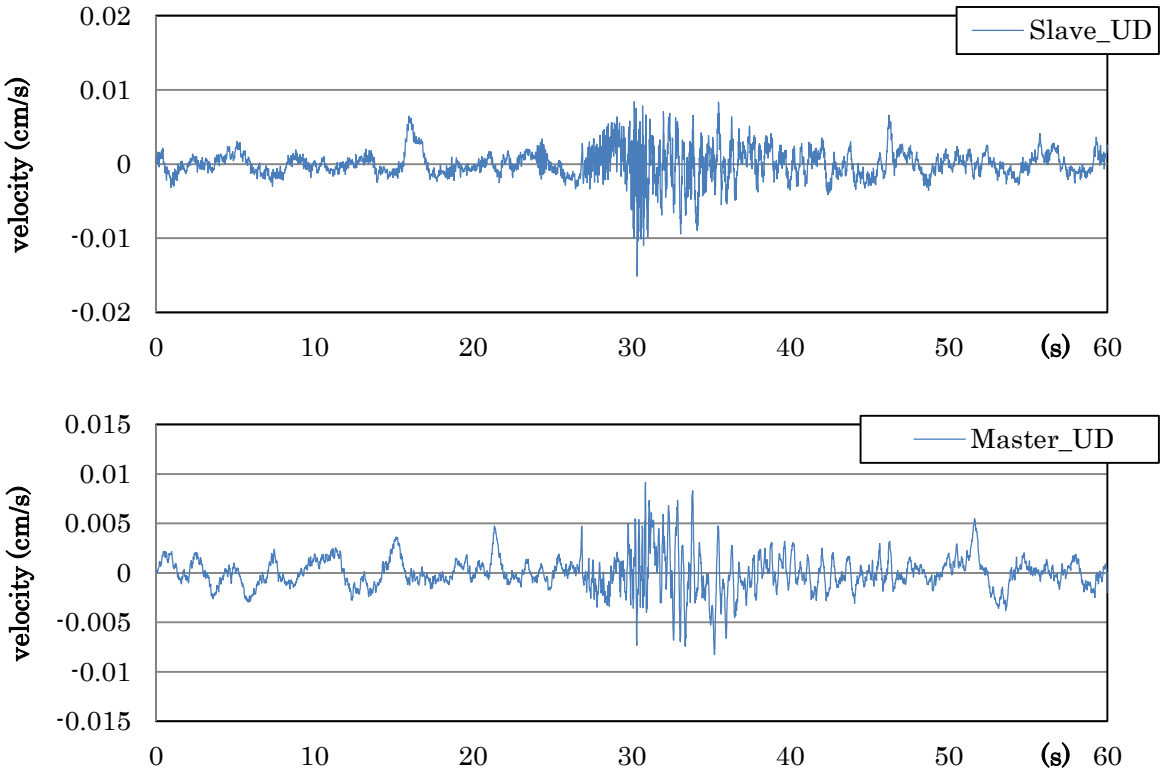

Fig. 2-19　Velocity time history recorded in the UD direction

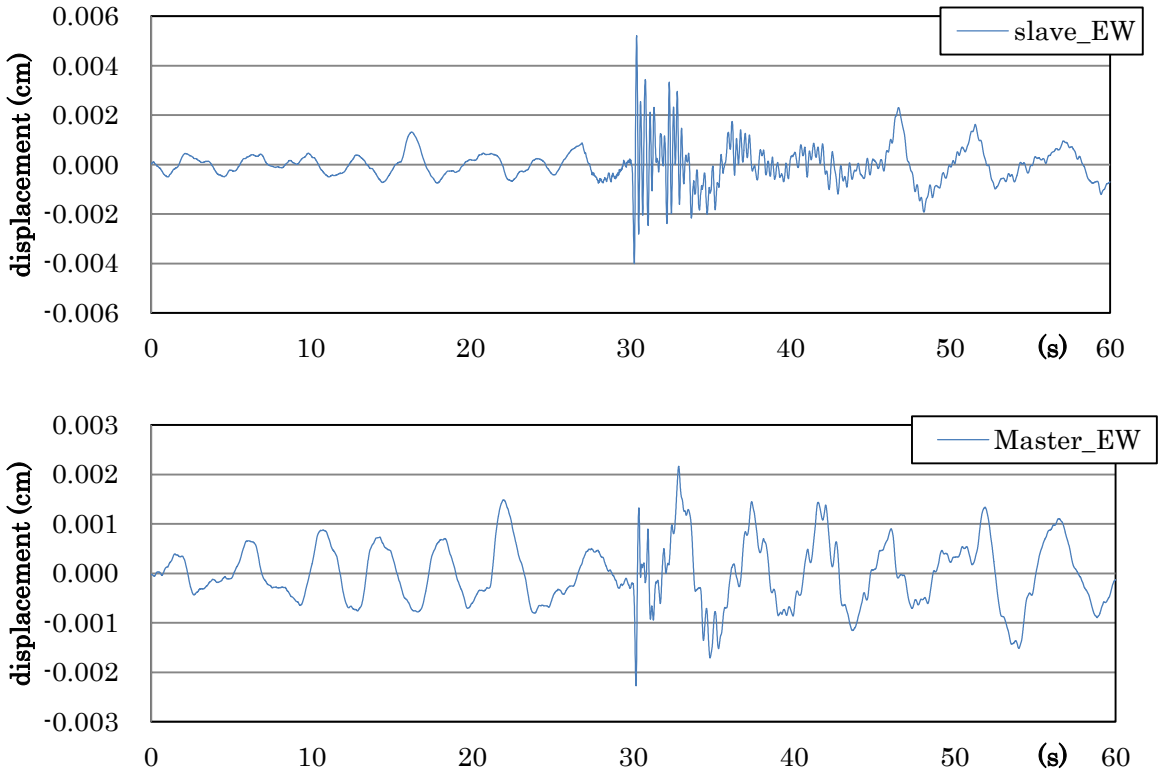

Fig. 2-20　Displacement time history recorded in the EW direction

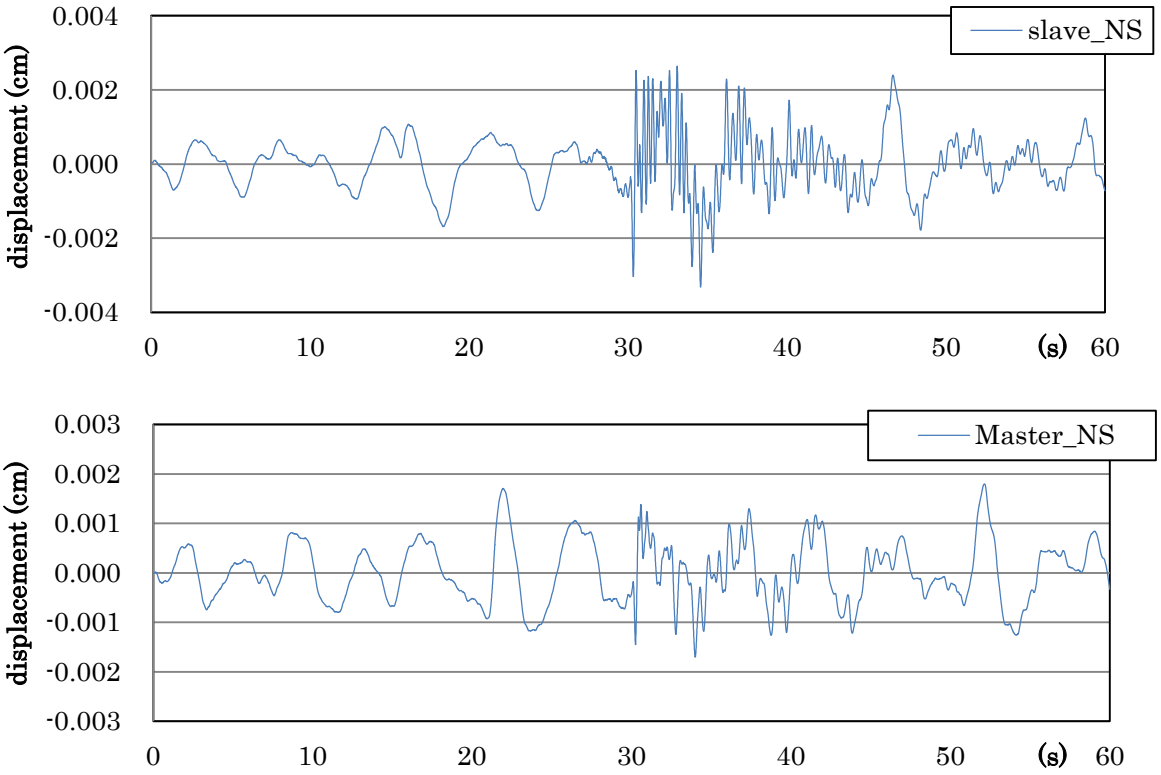

Fig. 2-21　Displacement time history recorded in the NS direction

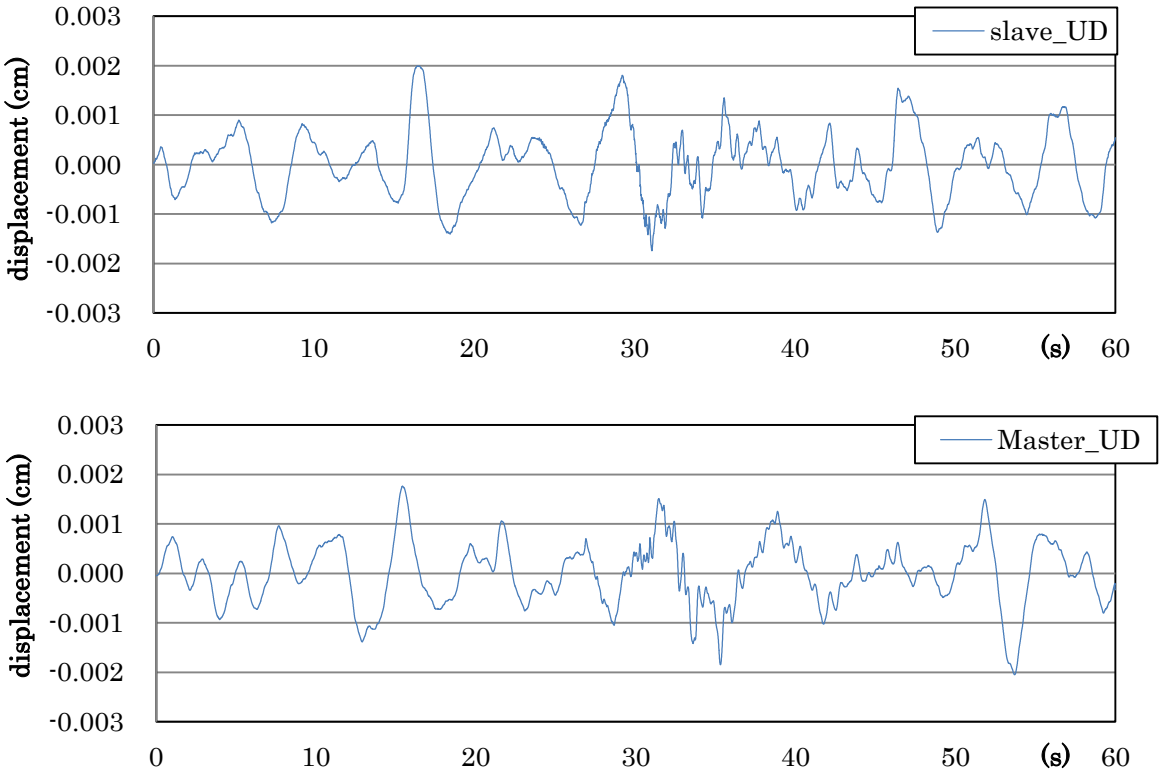

Fig. 2-22　Displacement time history recorded in the UD direction

Fig. 2-23 shows the orbit of both the Master and the Slave.

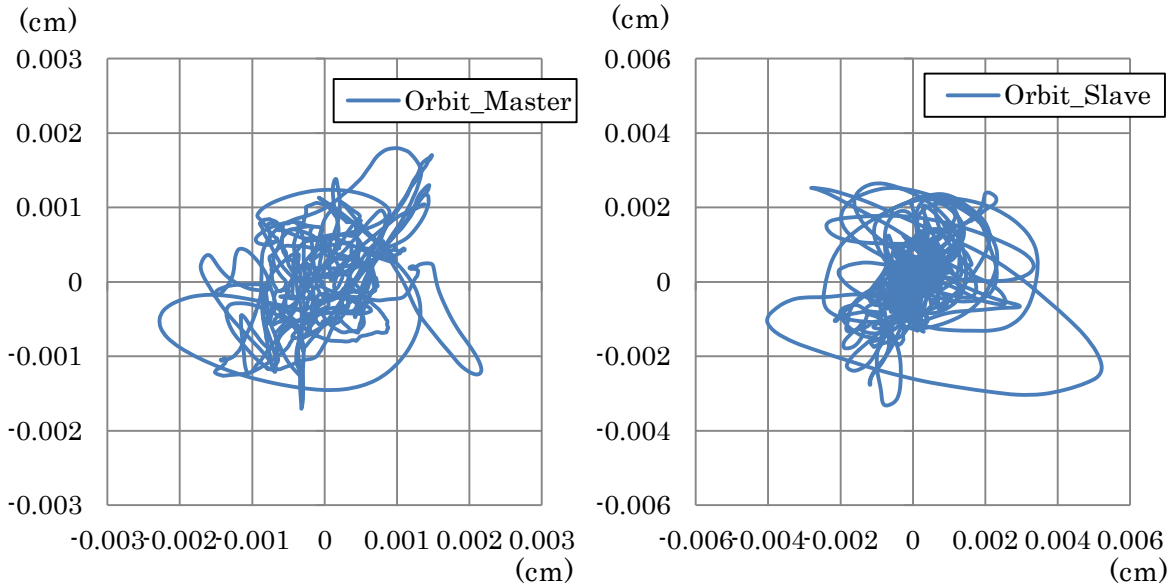

Fig. 2-23　Orbit of displacement

Fourier spectra of the acceleration data were calculated from the acceleration time histories by using the software Pwave32 with Hanning spectral window of 20 times, shown in Figs. 2-24 and 2-25.

Acceleration response spectra shown in Fig. 2-26 were calculated with TDAP III.

Transfer functions described in Fig. 2-27 show the ratio of the Fourier spectra of Slave to those of Master.

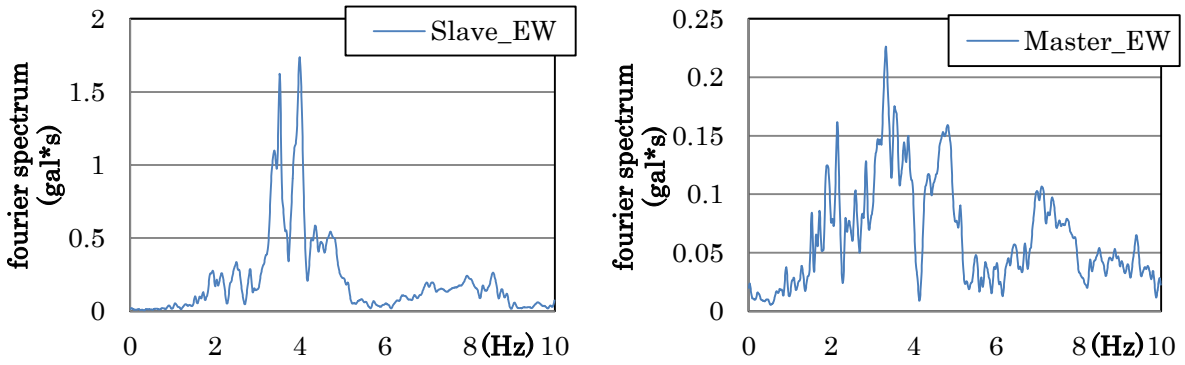

Fig. 2-24 Acc. Fourier Spectra; EW direction

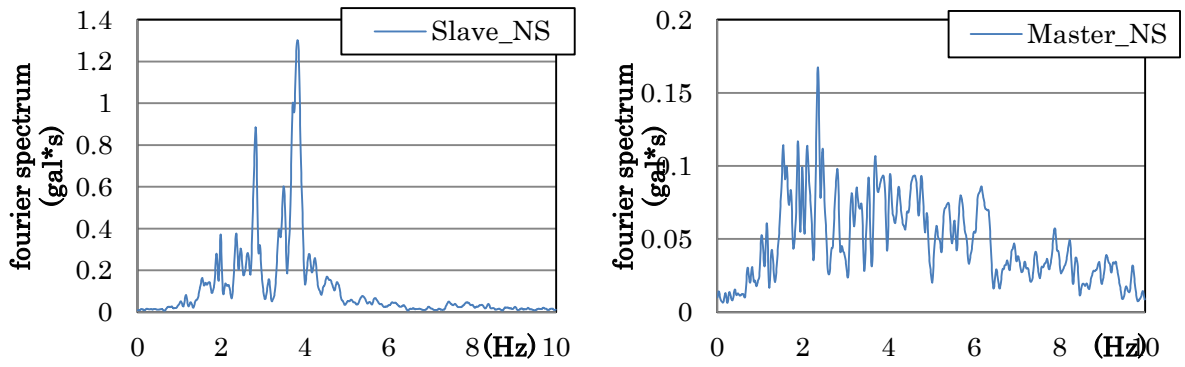

Fig. 2-25 Acc. Fourier Spectra; NS direction

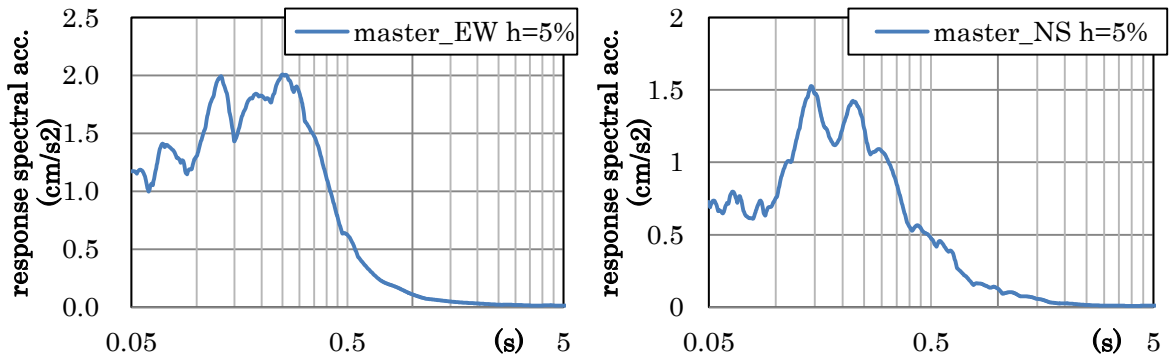

Fig. 2-26 Acc. Response Spectra

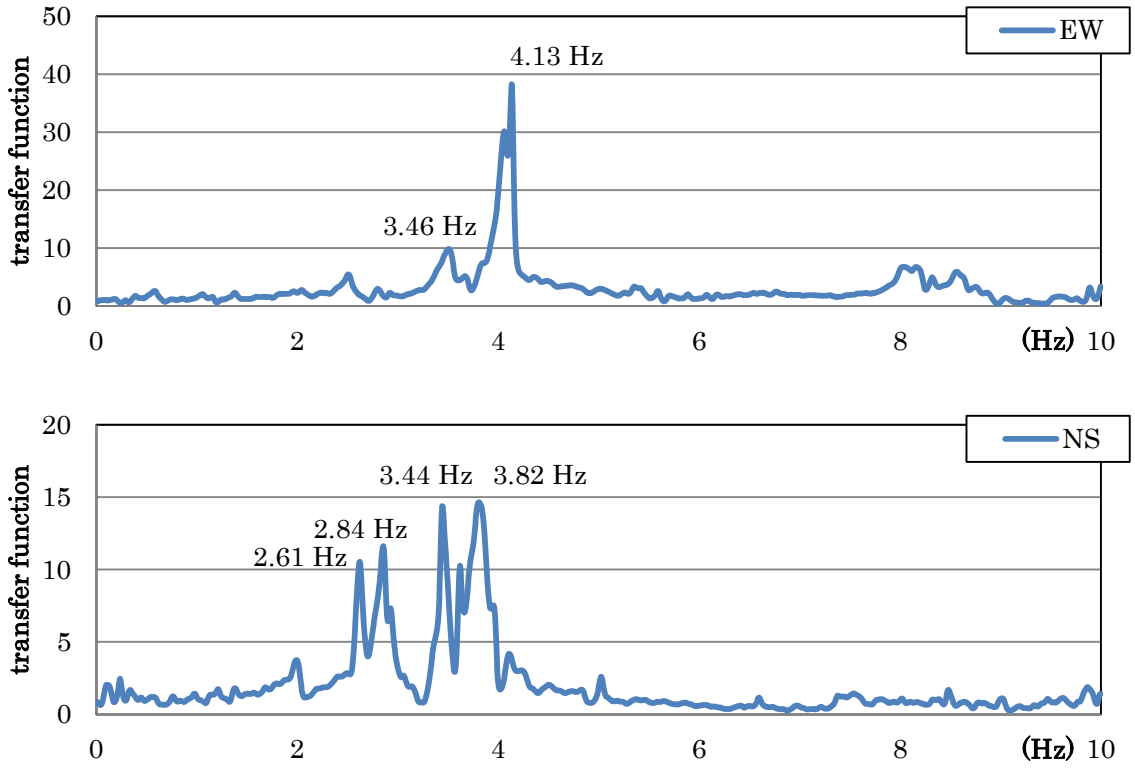

Fig. 2-27 Transfer Function

2.2.3 EARTHQUAKE MONITORING RESULTS

Fig. 2-28 and 2-29 show the comparison of acceleration fourier spectra and acceleration response spectra, respectively. The peak acceleration level at the base of the Parthenon Athens did not exceed 1 gal during the recorded earthquakes both in 2010 and in 2011. The response spectra did not show the topographic effect of the Acropolis hill clearly. The predominant period of the acceleration response spectra of the earthquake record in 2011 was shorter than that of the record in 2010, because the epicentral distance of the earthquake in 2011 was shorter than that in 2010. Moreover, the magnitude of 2011 event was smaller than that of 2010 event.

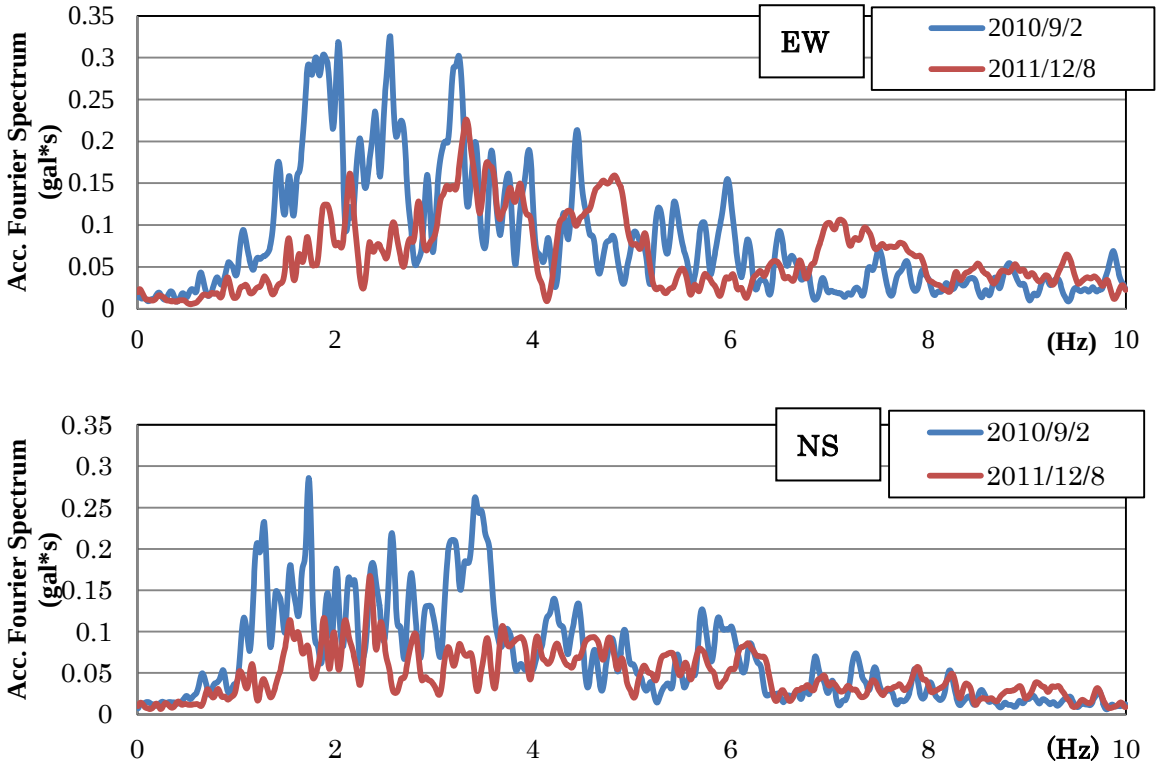

Fig. 2-28　Comparison of Acceleration fourier spectra at the base

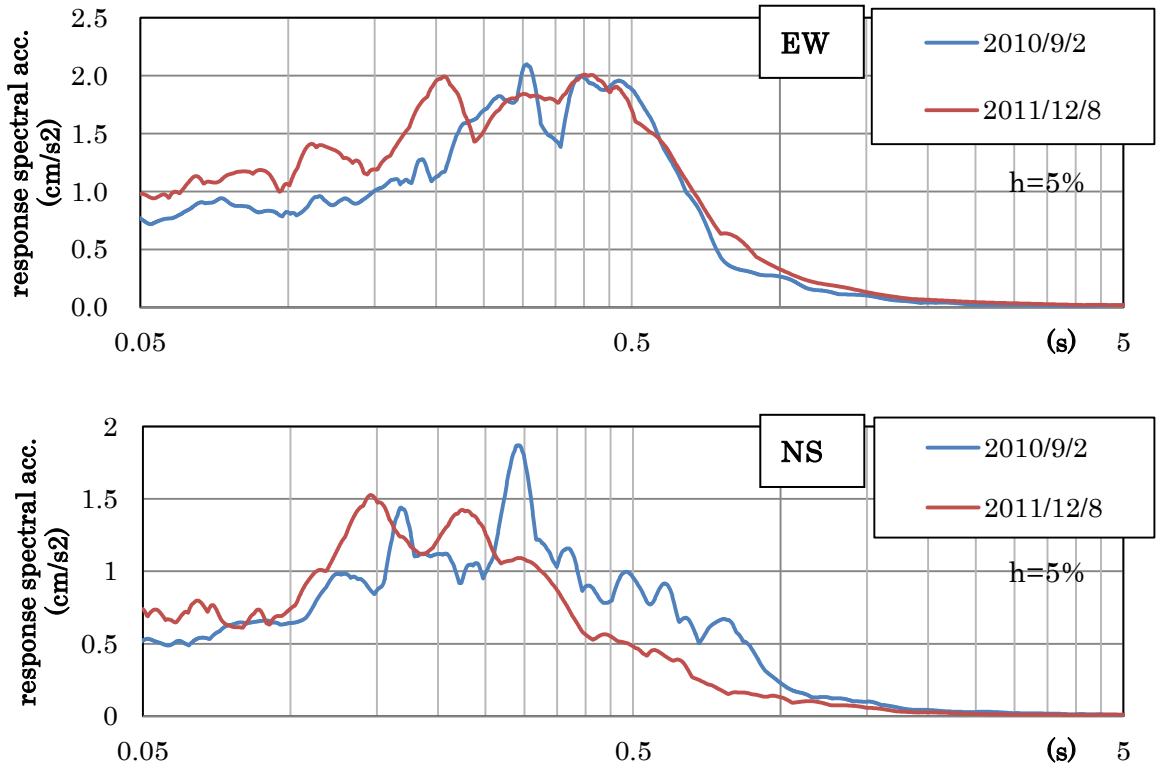

Fig. 2-29　Comparison of Acceleration response spectra of ground motions

The attenuation relationship formula in Greece was proposed by Theodulidis & Papazachos (1992) as follow.

$$\ln A = 3.88 + 1.12\,Ms - 1.65 \ln(R + 15) + 0.41\,S$$

where A is peak ground acceleration (gal (cm/s^2)), R is epicentral distance (km) and S=1 for stiff soil. The peak acceleration at the base of two recorded earthquakes and the calculated peak acceleration at the Acroopolis hill are presented in Figs. 2-30 and 2-31. The earthquake of September 2nd, 2010 occurred at the epicenter beyond the mountainous area. It might be caused by the soil response that peak acceleration value of the monitoring in 2010 was lowere than that of calculation. It should be needed to know the soil conditions around Athens.

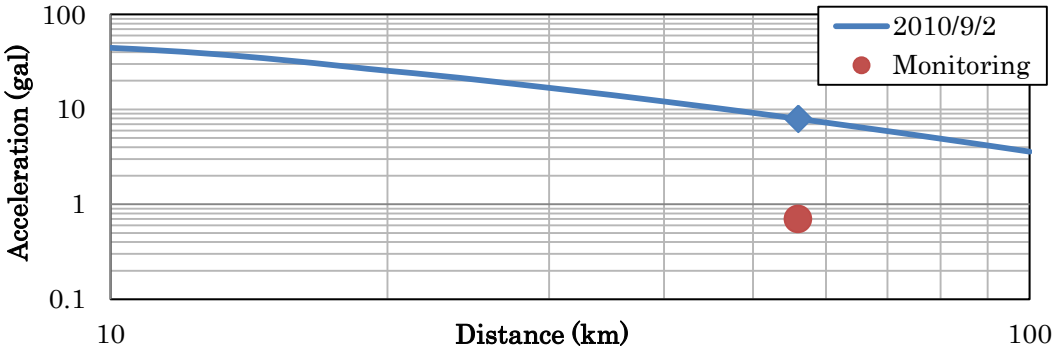

Fig. 2-30 Attenuation relationship for peak ground acceleration on September 2nd, 2010

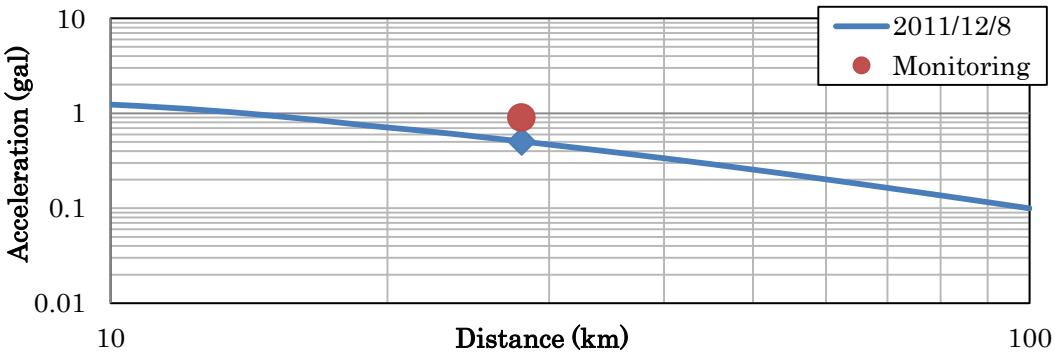

Fig. 2-31 Attenuation relationship for peak ground acceleration on December 8th, 2011

2.2.4 COMPARISON OF NATURAL FREQUENCIES

The peak frequency of the transfer function agreed well at the most measuring points of the microtremor measurements in 2008, shown in Fig. 2-32 in the past study [11]. In order to compare the transfer functions of the microtremor measurements with those of the earthquake monitoring results, transfer function was evaluated from CH 1 to CH 6 in the case of the north colonnade

numbered (1). In the case of the east colonnade numbered (2), transfer function was calculated as the same way as the case (1) from CH 1 to CH 2. The former is called 2008(1), while the latter is called 2008(2) in the following sections. In both cases, a sensor of CH 1 was arranged at the base of the middle of the colonnade. Fig. 2-33 shows the transfer functions of 2008(1) and 2008(2). It can be noticed that the peak frequency well agree in the NS direction at approximately 3.7 Hz. On the other hand, the peak frequency did not agree in EW direction. The natural frequency observed in every point in the north colonnade was 3.7 Hz in in-plane direction (EW direction). However, in out-of-plane direction (NS direction), the natural frequency was not observed clearly. The natural frequencies of whole structure of the east colonnade were 3.7 Hz and 2.7 Hz in-plane direction (NS direction) and in out-of-plane direction (EW direction), respectively. Transfer functions of 2008(1) and 2008(2) in EW direction did not show the same peaks shown in Fig. 2-33. The difference caused by the different situation of CH 1.

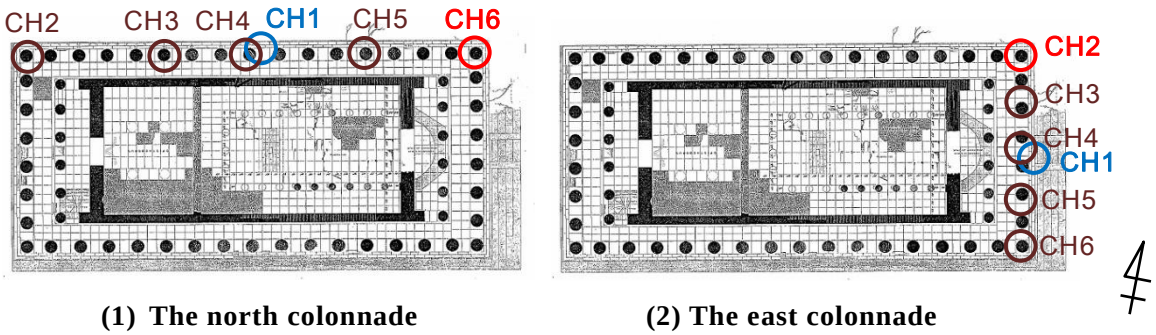

(1) The north colonnade **(2) The east colonnade**

Fig. 2-32 Arrangement of the microtremor sensors

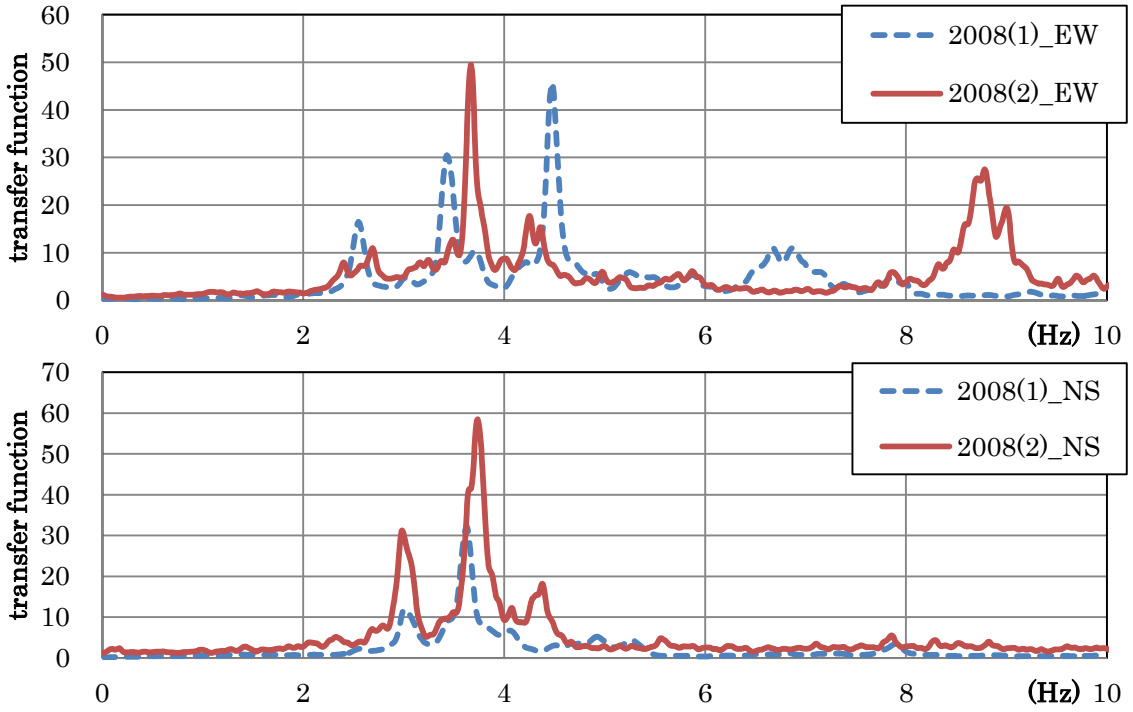

Fig. 2-33 Comparison of transfer functions of microtremor measurements

The transfer function of the earthquake on December 8th, 2011 was described in the former section. The black square in Fig. 2-34 shows the acceleration time history of the earthquake. It is called 2011/12/8EQ in the following sections. Furthermore, red square in Fig. 2-34 indicated a microtremor called 2011/12/8. Transfer functions calculated from 2011/12/8 and 2011/12/8EQ are shown in Fig. 2-35. These two figures show overlapping. Therefore, peak amplitude of the transfer functions of 2011/11/8 and 2011/11/8EQ shown in Table. 2-6. These figures indicated that the structure did not show the non-linear behavior during the minor earthquake of 2011. The reason why the non-linear effect was not observed was that the earthquake motion was so small.

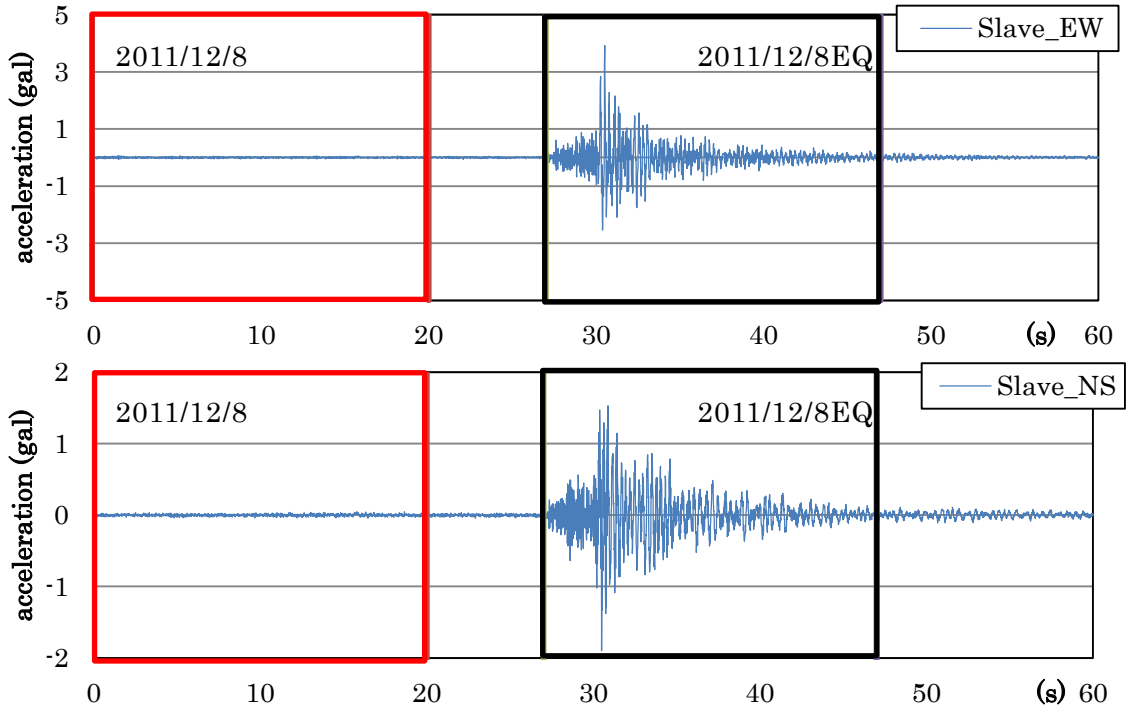

Fig. 2-34　Time section for analysis of the earthquake record for 60 second

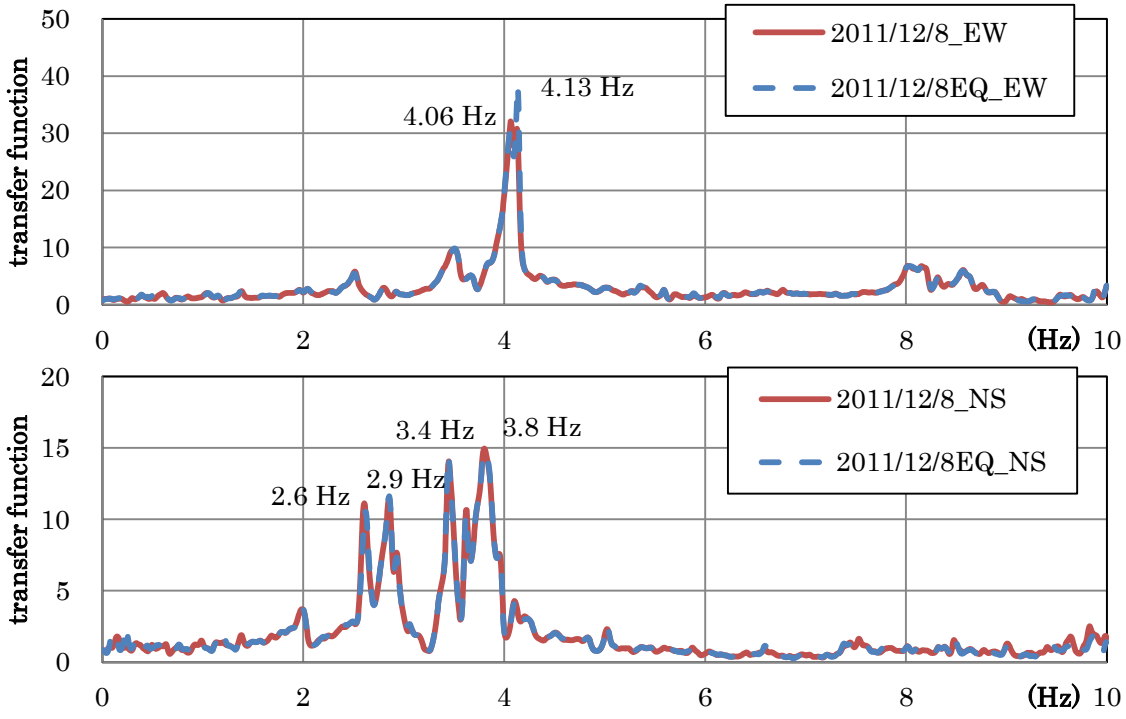

Fig. 2-35　Comparison of transfer functions of the Earthquake record and the microtremor

Table. 2-6 Transfer function

	Peak frequency	Transfer function (amplitude)	
	(Hz)	Micro tremor	Earthquake
EW	4.1	32.1	36.0
NS	2.6	11.1	10.5
	2.9	11.5	11.6
	3.5	10.7	14.4
	3.8	15	14.7

Table. 2-7 shows the natural frequencies evaluated from the transfer functions described above. The natural frequency in NS direction was in roughly agreement with each other. On the other hand, the natural frequencies of the microtremor measurements did not correspond to those of the record of 2011 in EW direction. The difference of the natural frequencies in the EW direction considered to be caused by the restoration work. During the recent restoration work, the cracks of the marbles were repaired by grouting, furthermore, new marble materials were inserted. As the restoration work proceeded, the north colonnade showed variation in dynamic behaviors in in-plane direction, EW direction.

Table. 2-7 Natural frequencies

	Natural Frequency (Hz)	
	EW	NS
2008(1)	4.48	3.63
2008(2)	3.67	3.74
2011/12/8	4.06	3.80
2011/12/8EQ	4.13	3.82

2.2.5 LONG TERM VERIATION OF NATURAL FREQUENCY

The trigger level of the seismographs was set at level as small as 0.5 cm/s^2. Therefore, a lot of records which exceeded the trigger level of the vibrations caused by heavy machinery during restoration work, were recorded. These records included a lot of noise. In this section, transfer functions of such records were calculated in every 6 month since June of 2011. Table. 2-8 listed the peak frequency shown in Figs. 2-36 and 2-37. These figures show the transfer functions of both in EW and NS direction. The transfer functions of the microtremor measurements recorded both before and during the earthquake of 2011 were also indicated.

Shown in Table. 2-8, Figs. 2-36 and 2-37, the natural frequency in EW direction ranged from 3.5 to 4.0 Hz. In the NS direction, the natural frequency was observed to be approximately 3.8 Hz for most of the cases.

Table. 2-8 Predominant frequency evaluated from transfer functions

Date	Time (GMT)	Predominant frequency (Hz)											
		EW							NS				
2008(1)		2.55		3.43			**4.48**		3.00	**3.63**			
2008(2)					**3.67**				2.98		**3.74**		
2011/6/10	18:44				3.70	**3.96**	4.27	2.85	2.93			**3.96**	
2011/6/12	13:08			**3.55**				2.98		**3.58**	3.80	4.01	
2011/12/8	23:04	2.51		3.53		**4.06**		2.86		3.45	**3.80**		
2011/12/8EQ	23:04			3.46			**4.13**	2.84		3.44	**3.82**		
2012/6/1(1)	11:37		3.22	3.50	**3.70**					3.37	**3.85**		
2012/6/1(2)	11:56			**3.50**	3.74				3.03	**3.39**			
2012/11/22	14:51	2.59			**3.69**	**4.03**			2.95	3.32	**3.74**		

*__Thick letter__: the largest peak

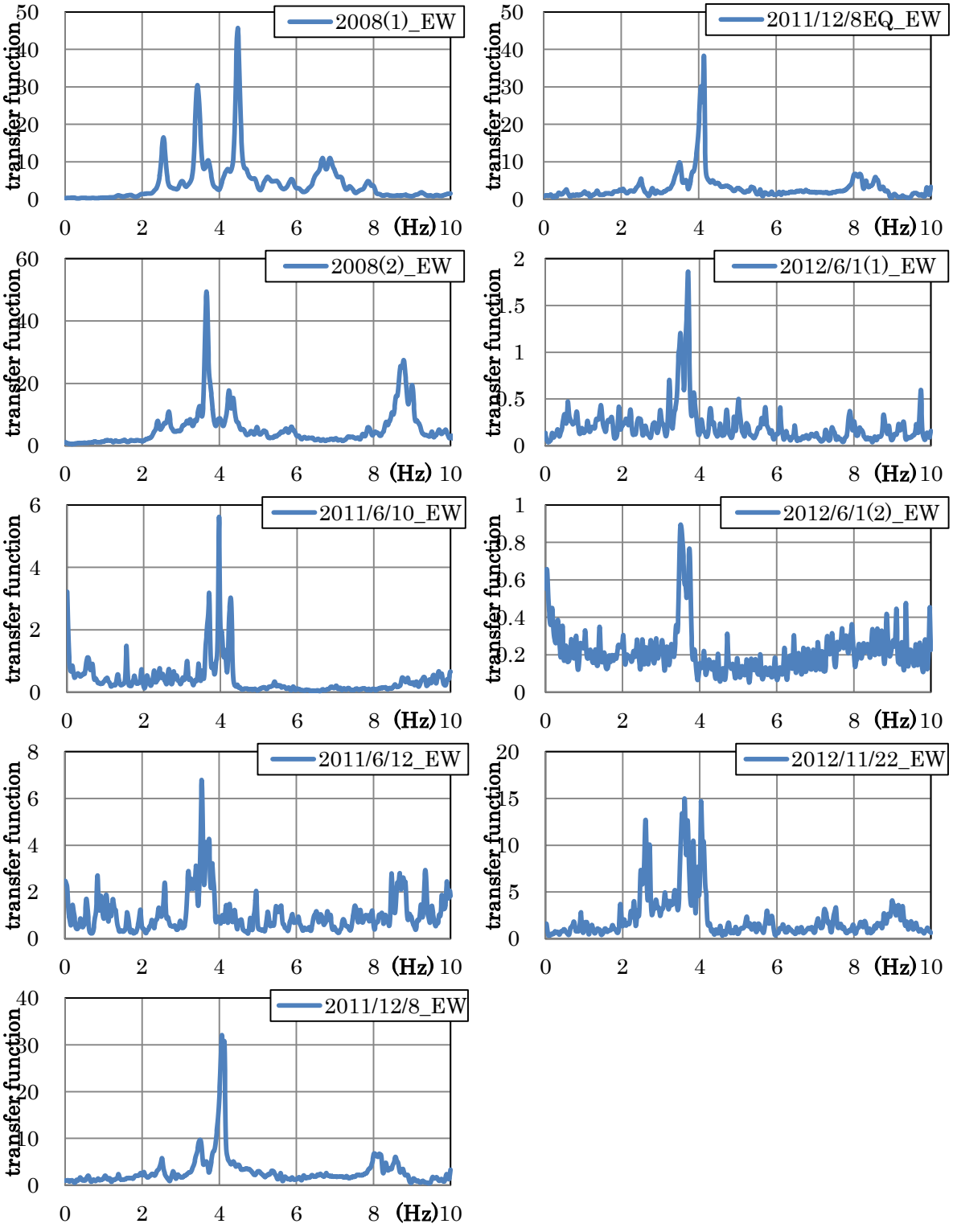

Fig. 2-36　Transfer function in the EW direction

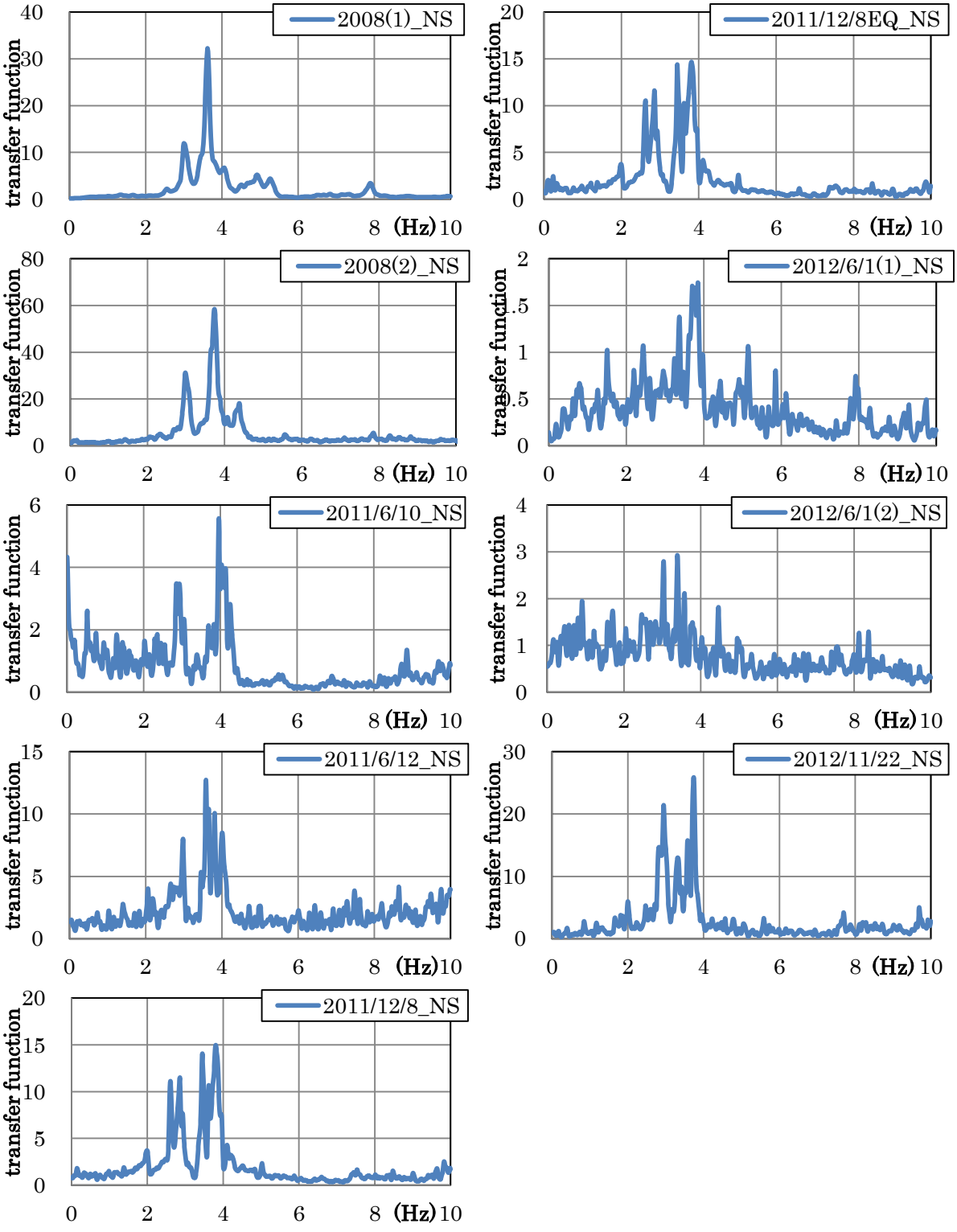

Fig. 2-37　Transfer function in NS direction

2.3 ANALYSIS

2.3.1 ANALYSIS MODEL

Linear analysis models were introduced by Ohmura in the past study [12]. The analysis was conducted with the software TDAP III (ARK Information Systems). These models, shown in Fig. 2-38, were verified with the result of microtremor measurements. In this section, the same model called the model 1, in the past study was used. Furthermore, the model 2 which was assumed to explain the difference between the stiffness of the beam elements of the model 1 was also used. The model 2 was almost the same as the model 1, but the model 2 has the weak rotational spring acting in horizontal plane at joint of horizontal beams as Table. 2-11. Tables. 2-9 and 2-10 show the parameters used for the analysis models.

Input motion was the earthquake record of the Master in December 8th, 2011. The column at the Northeast corner where the earthquake monitoring conducted corresponds to the Column 735 indicated by red square in Fig. 2-38 and shown in Fig. 2-39. In this seismic response analysis, Rayleigh damping model was assumed to be 1 % both for the primary and secondary modes, since the earthquake record was quite small. Table. 2-12 shows the natural frequencies of the colonnades of the models. The analysis model was successfully identified by the microtremor measurement.

Table. 2-9 Parameters used for columns of the analysis model

Mass	Weight [tf]	Height [m]	Vertical element	Young's modulus [tf / m^2]	Shear modulus of rigidity [tf / m^2]
M 14	363.48	12.779	k 14	77000000	-
M 13	232.06	11.204	L 13	1351198	3010000
M 12	64.97	10.080	L 12	363740	1646670
M 11	42.73	9.135	L 11	1113884	3102251
M 10	44.88	8.265	L 10	1123115	3100930
M 9	47.04	7.395	L 9	1131999	3106048
M 8	49.20	6.525	L 8	1137962	3098563
M 7	51.55	5.655	L 7	1144850	3097182
M 6	53.61	4.785	L 6	1155627	3111361
M 5	56.15	3.915	L 5	1159457	3093117
M 4	58.51	3.045	L 4	1173899	3090823
M 3	60.96	2.175	L 3	1174212	3089491
M 2	63.41	1.305	L 2	1187057	3092325
M 1	66.15	0.435	L 1	1192193	3080128

Table 2-10 Parameters used for horizontal beams of the analysis model 1

	Young's modulus [tf / m^2]	Shear modulus of rigidity [tf / m^2]	Reduction factor*
West colonnade	616000	269600	2 / 25
East colonnade	462000	202200	3 / 50
North colonnade	4235000	1853500	11 /20
South colonnade	4235000	1853500	11 /20

* Reduction factor denotes the ration of the stiffness of the model to that of the marble material

Table. 2-11 Parameters of the horizontal elements for model 2

	Young's modulus [tf / m^2]	Shear modulus of rigidity [tf / m^2]	Spring constant [tf * m]
L_H	7700000	3370000	-
k_R	-	-	1000

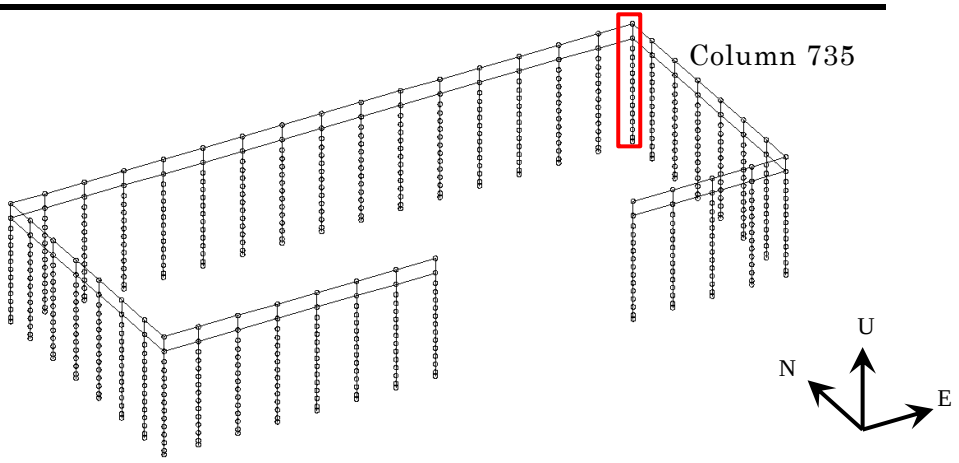

Fig. 2-38 Analysis model

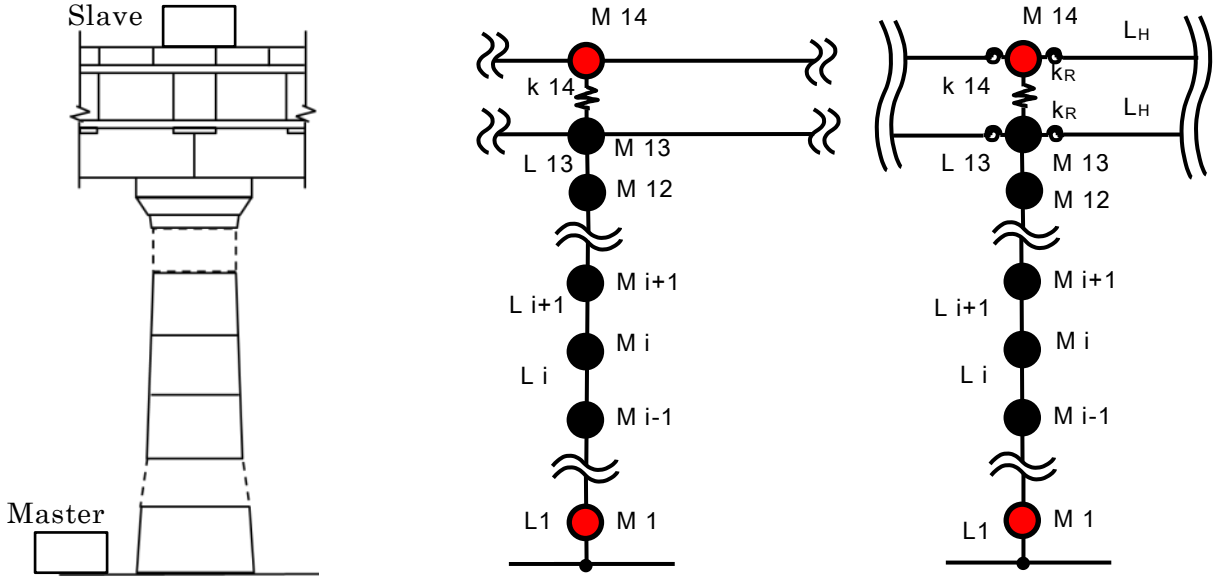

(A) Schematic drawing of marble drums and seismographs **(B) Analysis model 1 of one column** **(C) Analysis model 2 of one column**

Fig. 2-39 Marble drum with seismographs and analysis model

Table. 2-12 Comparison of natural frequency evaluated from analysis model 1, model 2 and microtremor measurement

	Natural frequency (Hz)					
	In-plane			out-of-plane		
	Model 1	Model 2	Measurement	Model 1	Model 2	Measurement
West colonnade	3.94	3.52	3.3	2.49	2.45	2.4
East colonnade	3.29	3.83	3.7	2.74	2.93	2.7
North colonnade	3.64	3.90	3.7	2.67	2.27	2.7
South colonnade	3.64	3.88	-	2.67	2.30	-

2.3.2 ANALYSIS RESULTS

Figs. 2-40 and 2-41 show the acceleration wave forms of the analysis using model 1 and model 2 (Mass No.14) and the monitoring (Slave) during the period of 5 seconds. Fig. 2-42 compares the orbits of the analysis result with that of the monitoring. Furthermore, in Fig. 2-43, the transfer functions evaluated by the same way described in the former section, 2.2.2, were compared between the analysis and the monitoring. Natural frequencies evaluated from transfer functions of the analysis, the earthquake monitoring record and the microtremor measurement of the North colonnade are shown in Table. 2-13.

Judging from Fig. 2-42, the orbit of the analysis using model 2 show smoother line than those of the monitoring and the analysis using model 1. The comparison between the time histories of the monitoring and those of the analysis also shows the same situation. Therefore, the behavior of this monument during the earthquake was simulated better with using model 1. There was a significant difference in natural frequencies of the microtremor measurement and those of the analysis with the earthquake monitoring in NS direction shown in Fig. 2-43, in particular between the natural frequencies evaluated from the monitoring and from the analysis using model 1. In EW direction, the natural frequencies evaluated from the monitoring and the analysis using model 1 show good agreements. On the other hand, the natural frequencies at the monitoring and the analysis using model 2 were in good agreement in NS direction. These results indicate that the East colonnade behaved dynamically as stiffer structure than the North colonnade. It was supposed that the weight of the pediment on the east colonnade affected the rigidity of the horizontal beam as the normal stress at the joints was larger.

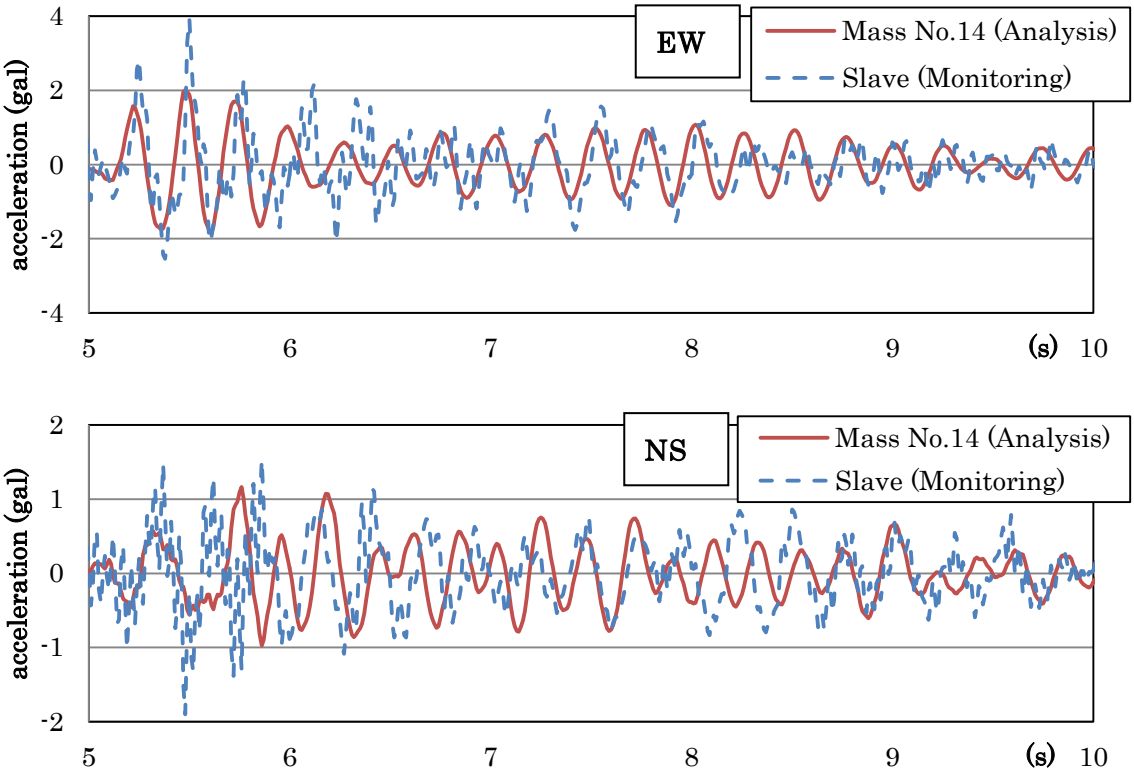

Fig. 2-40　Comparison of accleration time histories of model 1 and monitoring

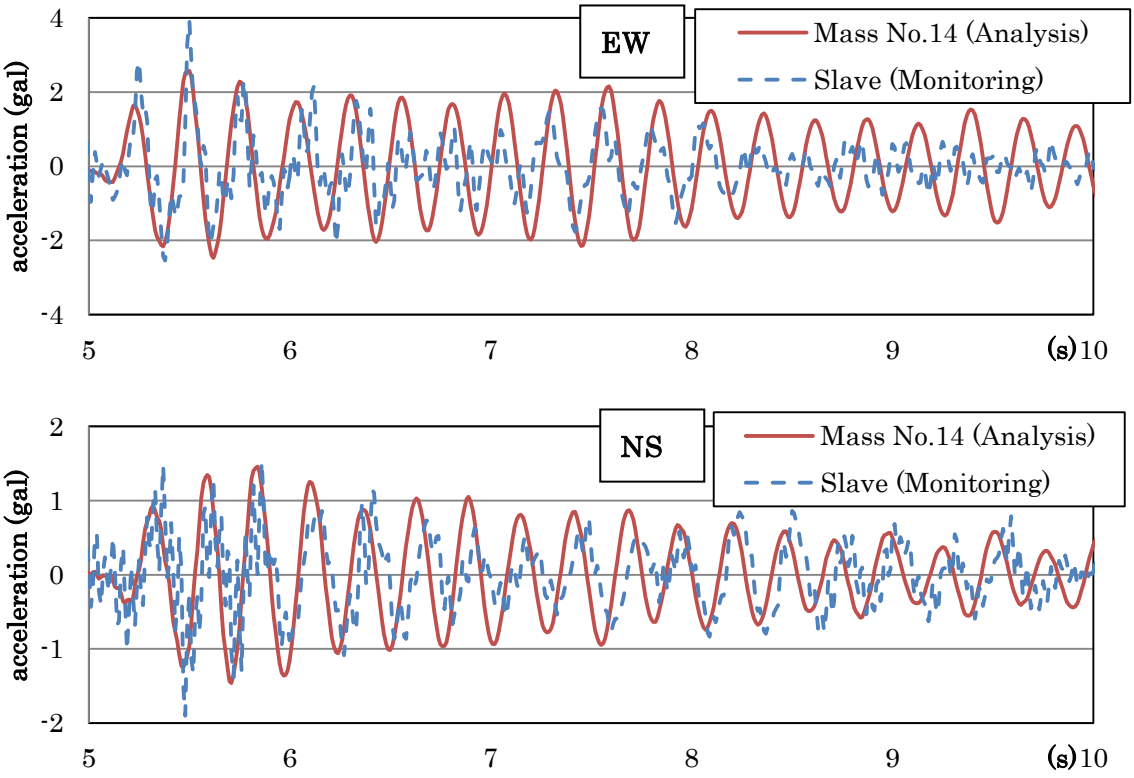

Fig. 2-41　Comparison of accleration time histories of model 2 and monitoring

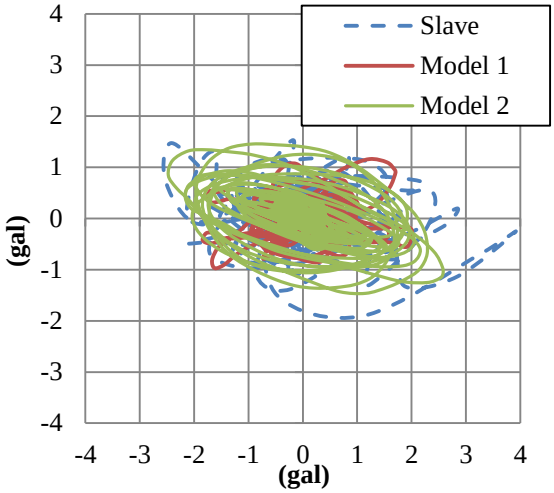

Fig. 2-42　Comparison of the orbit between the analysis and the monitoring

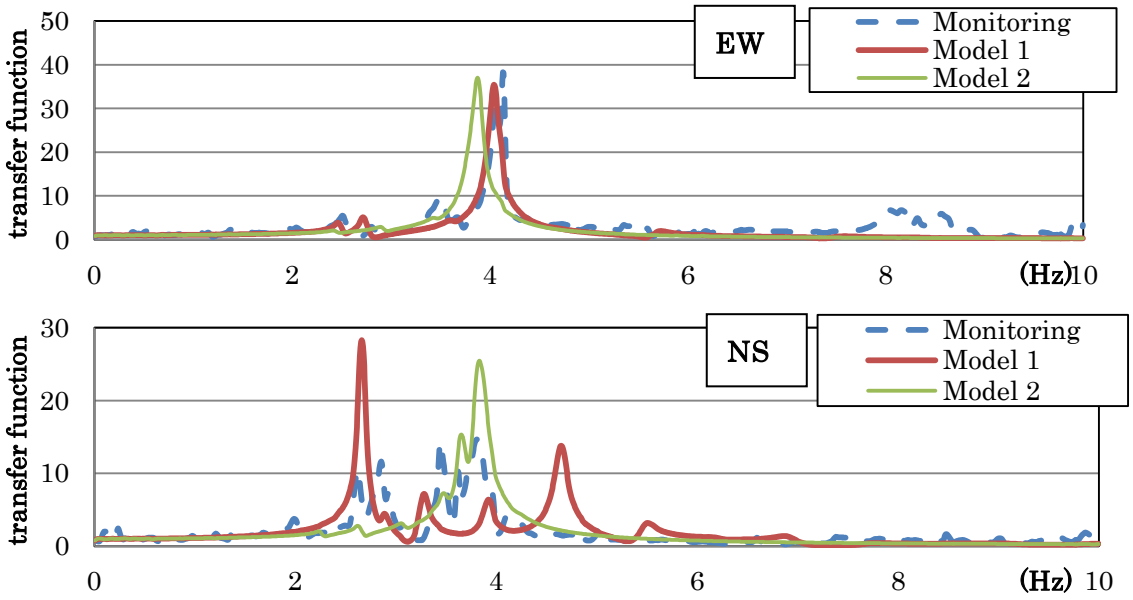

Fig. 2-43　Comparison of the transfer functions between the analysis and the monitoring

Table. 2-13　Natural frequency from transfer functions of the Analysis and Measurements

	Natural frequency (Hz)	
	EW	NS
Microtremor (North colonnade)	3.7	2.7
Monitoring at the NE corner	4.13	3.82
Analysis model 1 (Column 735)	4.04	2.66
Analysis model 2 (Column 735)	3.88	3.83

2.4 CONCLUDING REMARKS

One earthquake monitoring record of December 8th, 2011 revealed the actual behavior during a small level earthquake such as the peak ground acceleration was as small as 0.9 cm/s^2. The observed natural frequencies were 4.1 Hz in EW direction and 3.8 Hz in NS direction during the event of 2011. These natural frequencies were in good agreement with the ones of microtremor recorded just before the small earthquake. The acceleration responses at the base during the earthquake on September 2nd, 2010 were compared with those of December 8th, 2011. However, the predominant frequency due to topographic effect of the Acropolis hill was not recognized.

The observed natural frequencies by the microtremor measurements in the past studies were compared with those of the earthquake event. The natural frequencies in NS direction were in roughly agreement with each other. On the other hand, the natural frequencies in EW direction did not show good agreement. It would be needed to add monitoring points at the Parthenon Athens, and at the same time, at the Acropolis hill in order to reveal the topographical effect.

Vibration due to construction works were recorded at a number of times during the seismic the monitoring, as the peak exceeded trigger level was small as 0.5 cm/s^2. Those data also gave us the microtremor records. The natural frequency in NS direction was verified to be approximately 3.8 Hz since July of 2011 until now. However, the natural frequency in EW direction had variation.

The seismic response analysis utilizing the earthquake record of 2011 was conducted. The damping ratio during the small earthquake was revealed to be 1 %. As results of the analysis utilized two types of analysis models, it was understood that connection of horizontal beams affected mainly the earthquake response of the Parthenon Athens. As the recorded earthquakes were so small, it is necessary to continue monitoring.

Chapter 3 Case Study at the Prambanan Temples

3.1 INTRODUCTION

The Prambanan Temple Compounds, the World Heritages of stone structures were built in the 9th century in the suburbs at Yogyakarta, Indonesia (See Fig. 3-1). A total of 8 monuments compose the Prambanan Temple. Although they had ruined during their long histories, the structures were reconstructed in 20th century. Chandi Shiva, which is the largest monument in the Prambanan Temples, was reconstructed in around 1980; the others were reconstructed in around 1990. Historical earthquake records since only 19th century are reported by European residents as shown in Table. 3-1 and Fig. 3-2 [12]. Although all the parameters of the historical earthquake records were not clear, we calculated peak ground acceleration values at the site of the Prambanan Temples using magnitude and location of epicenters. Since an attenuation relationship formula has not been proposed in Indonesia, we used the attenuation equation given by Fukushima et al. (1999). The effectiveness of this equation in Indonesia was confirmed by Putra et al., 2012 [13].

$$\text{Log } A = 0.41\ Mw - \log\left(R + 0.032 * 10^{(0.41\ Mw)} \right) - 0.0034\ R + 1.3$$

In this equation, A denotes peak ground acceleration, Mw denotes moment magnitude and R denotes the shortest distance to epicenter. Various magnitude scales were converted into moment magnitude. Calculated peak ground acceleration are shown in Table. 3-1. Though the magnitude of the earthquake of 1867 was not reported, it was estimated as almost same as that of 2006 from the review of the locations of epicenters and the damages in the report; 375 government and private buildings collapsed or heavily damaged including the water castle at the Sultan's Palace in Yogyakarta in 1867 (See Fig. 3-3). As a result, it was found that the Prambanan Temples experienced severe earthquakes three times in the last two hundred years. Three major events affected were the 1867, 1943 and 2006 earthquakes.

The earthquake of May 27th, 2006 was called the Central Java earthquake, of which magnitude was 6.3. It affected a number of architectural heritages in and around the one of the historic cities in Indonesia, Yogyakarta. The Prambanan Temple Compounds also suffered severe damages; many "ratna" and "stupa" that decorated the nave roof fell. The upper part of the roof of Chandi Garuda appeared seriously unstable, significant relative displacement and horizontal openings between the stone elements were found at the freestanding gate on the platform in front of the entrance. Furthermore, Chandi Shiva suffered serious cracks at its base and wall of the nave [14].

As the Indonesian government requested in emergency the cooperation of Japanese Government to assess the earthquake damage to the Prambanan Temples by the Central Java earthquake for starting the restoration project, an interdisciplinary team of Japanese experts was organized in collaboration of Indonesian experts. Mie University took charge of survey of the

architectural structure of these stone temples for the restoration. At the same time the present stability of these structures has been studied. The present project had been conducted during 2006 and 2007 by the expert team organized in Japan Consortium for International Cooperation in Cultural Heritage being set up at National Research Institute for Cultural Properties, Tokyo. Since 2008, our activities have been financially supported by Grant-Aid for Scientific Research, provided by Japanese Government.

Fig. 3-1 Prambanan Temple Compounds

Table. 3-1 Historical earthquakes around Yogyakarta

Date	Lat.(S)	Lon.(E)	Depth (km)	Mw	Epicentral Dist. (km)	Calculated Acc. (cm/s^2)
1840/1/4	7.4	110	-	-	67	-
1859/10/20	-	-	-	-	-	-
1867/6/10	7.8	110.5	-	-	5	-
1875/3/28	-	-	-	-	-	-
1924/11/12	7.3	109.5	-	-	121	-
1924/12/2	7.3	109.9	-	-	83	-
1937/9/27	8.9	110.7	-	7.1	127	-
1943/7/23	8.6	109.9	90	8.2	115	66.6
1957/10/12	8.3	110.3	-	6.4	64	-
1979/11/2	7.7	108.3	25	6	248	3.2
1981/3/14	7.2	109.3	33	5.9	145	10.4
1992/6/9	8.5	111.1	106	6.6	103	18.6
2001/5/25	8.6	110.1	56	6.2	105	20.1
2004/8/19	9.2	109.6	55	6.3	194	7.4
2005/7/19	8.6	111.1	33	5.4	101	12.7
2006/5/27	8.0	110.5	12	6.3	24	158.4

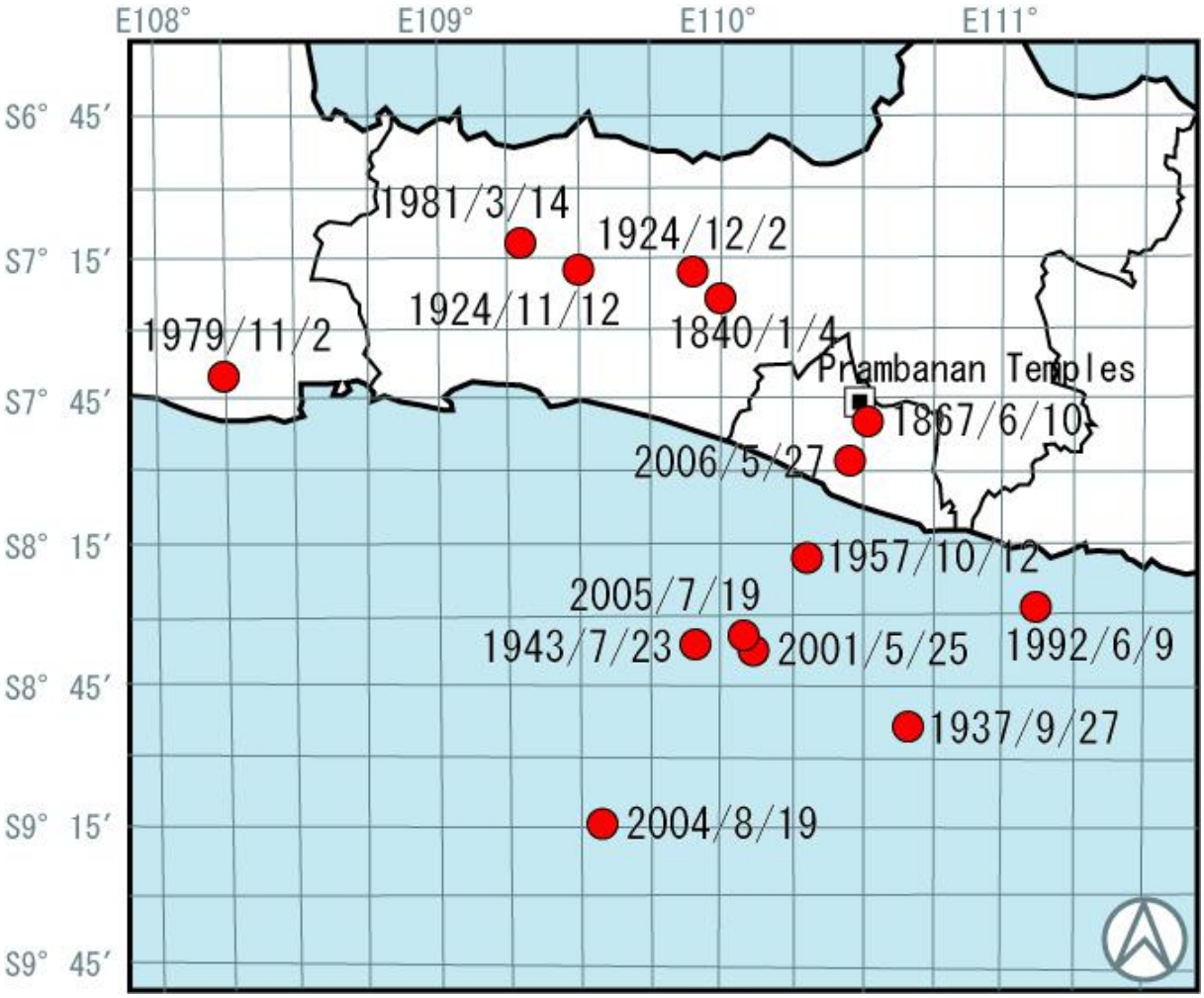

Fig. 3-2 Epicenters of historical earthquakes around Yogyakarta

Fig. 3-3 Damaged water castle at the Sultan's Palace

3.2 EARTHQUAKE MONITORING

Earthquake monitoring was initiated in the end of November 2007 to verify the analysis model, and at the same time, to observe the actual dynamic behaviors during strong motions. A total of 4 seismograms were installed at Chandi Hangsa as large as Chandi Garuda, the most severely damaged building of the six temples and an object of structural analysis. Chandi Hangsa is 22 m high as approximately half of Chandi Shiva. The earthquake monitoring equipment was replaced with new equipment at Chandi Shiva, the largest building which has a height of 47 m, because of the improvements of Chandi Hansa in July 2010. In this chapter, method of monitoring system and the record at Chandi Shiva are shown.

3.2.1 MONITORING SYSTEM

A total 4 seismographs connect up a power cable and a LAN cable these length are less than 60 cm, as shown in Fig. 3-4. NTP server and UPS were installed in the interior room. Electric power has been already supplied for monitoring of crack there. Components of these seismographs are Tri-axial.

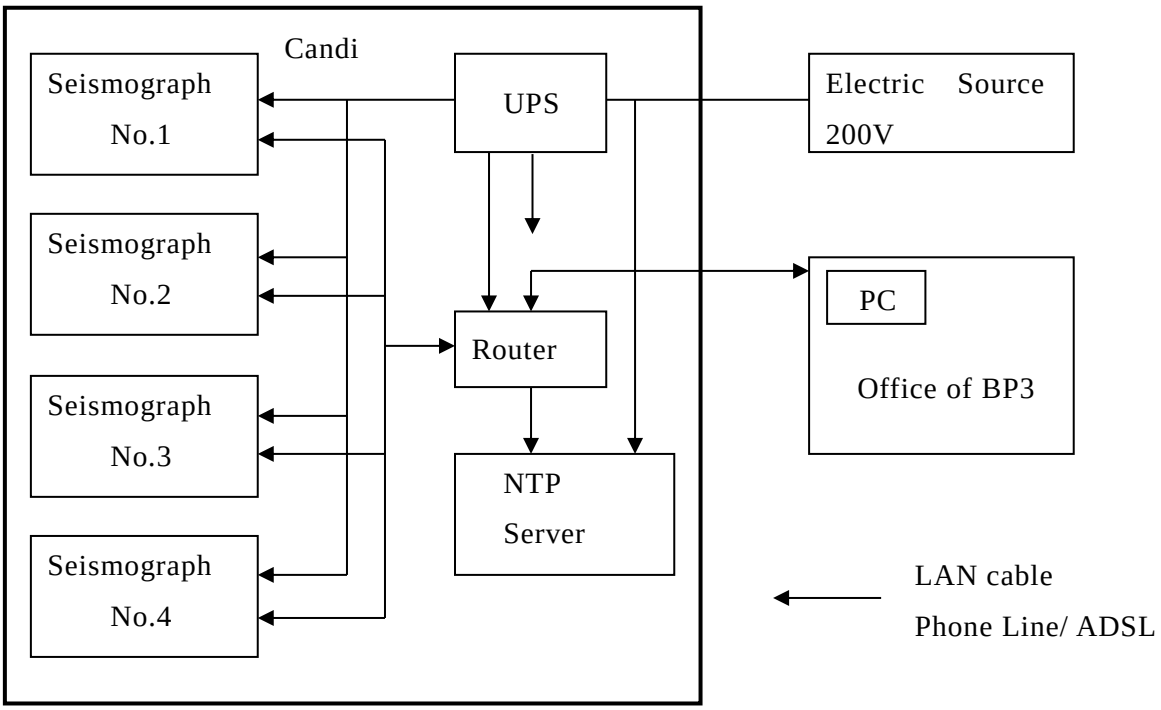

Fig. 3-4 Earthquake monitoring system

Table. 3-2 shows the specification of the seismographs installed. Figs. 3-5 and 3-6 show photographs of the seismograph and cover box preventing from sunshine and water.

Table. 3-2 Specification of the accelerograph

Sensor	Made in Japan	1 V = 1 G, 5 V = 24 bits, output: X = WE, Y = NS, Z = DU acceleration, temperature, DC = 6 V AC 220 V Electricity consumption 4 W, 0.8 A, cal = 0.000292 cm/s/s/D
Router (Hub)	Made in Japan	5 channel, 220 V, Electricity consumption 3 W, 10 m LANcable – NTP Server
NTP Server	Made in Japan	Drawing up time code, Record, Observation Toshba Dynabook Mxi/33LBL Windows 7, HD 320 G, Duration(battery) 9 hours, Electricity consumption 80 W
UPS	Made in Indonesia	APC - 800 VA, 400 W 10 minute
Cable	Made in Indonesia	LAN cable: Top 60 m, Middle 45 m, Base 3 m, Ground 30 + 5 m Power cable: Top 50 m, Middle 45 m, Ground 50 m φ = 1.5 mm

Fig. 3-5 Seismograph

Fig. 3-6 Shield weatherproof box

Figs. 3-7 and 3-8 show the location of seismographs. Figs. 3-9 to 3-12 show the view of seismographs on each point. Equipments except seismographs were set inside the central room of Chandi Shiva where electric powers were supplied. These recording equipment were connected with cable from seismographs, as shown in Figs. 3-11 and 3-14. Cable wiring diagram is shown in Fig. 3-17.

Seismographs are boxed in shield weatherproof boxes. These boxes were fasten on the pavement stone with Epoxy mortar and insulated from heat and prevented water from splashing in, after that, installed with mortar which gives less chemical change on stones of Chandi Shiva, as shown in Fig. 3-15. The height of 25 cm pavement stone for the seismograph on the Ground was buried a depth of 15 cm, furthermore all of them were covered with wooden box, as shown in Fig. 3-16.

Fig. 3-7 Location of seismographs

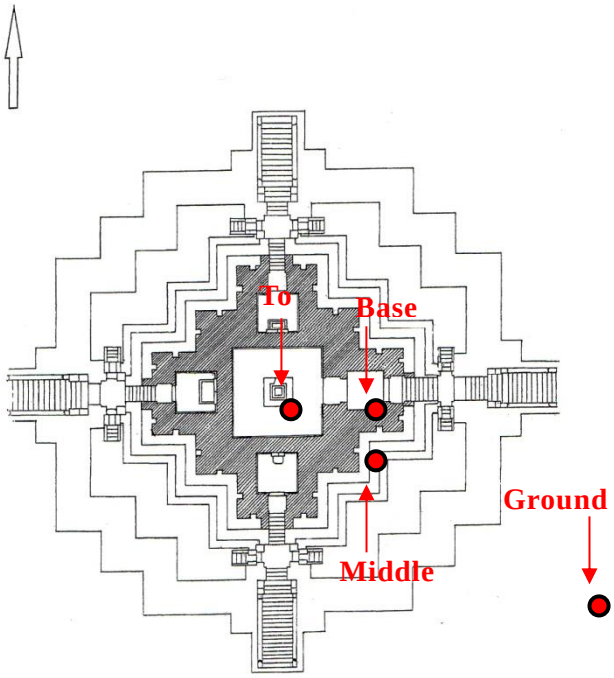

Fig. 3-8 Location of seismographs

Fig. 3-9 View of seismographs (Top)

Fig. 3-10 View of seismographs (Middle)

Fig. 3-11 View of seismographs (Base)

Fig. 3-12 View of seismographs (Ground)

Fig. 3-13 View of NTP Server

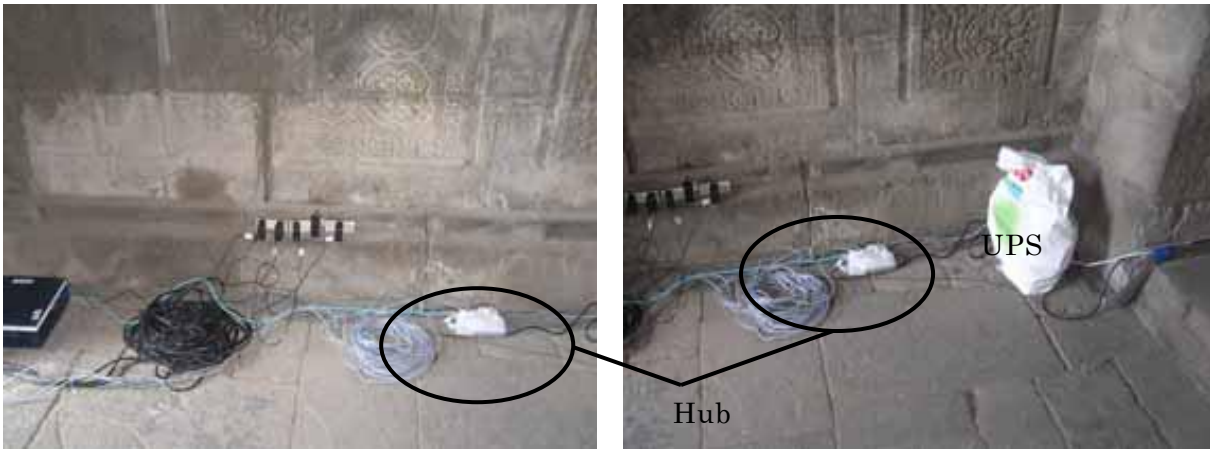

Fig. 3-14 (a)(b) View of electrical equipment at the entrance of the central room of Chandi Shiva

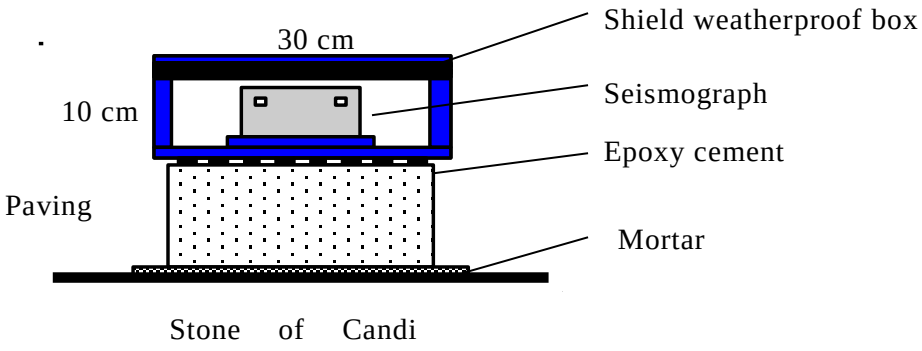

Fig. 3-15 Installation of seismograph on the Top, Middle and Base

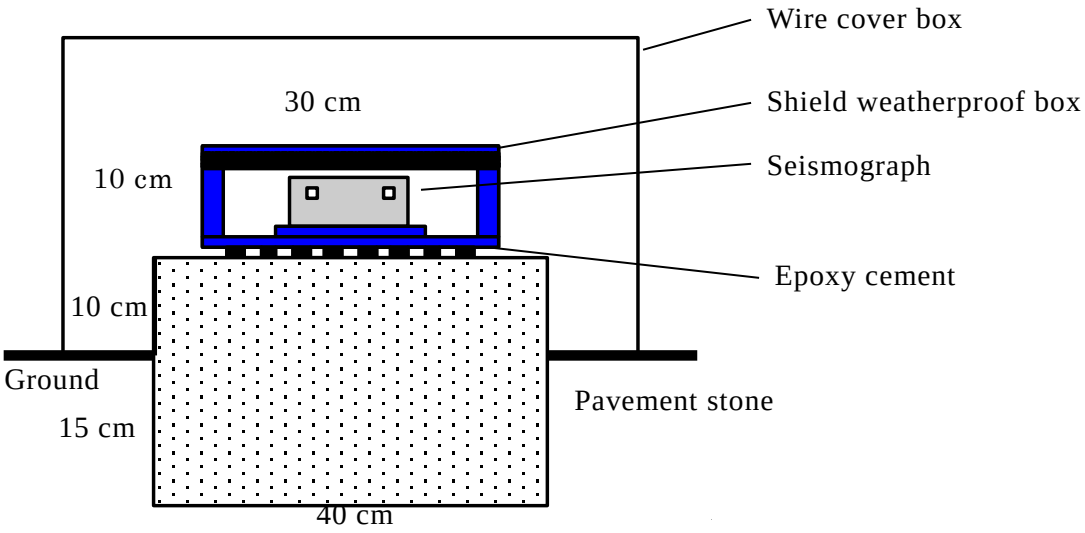

Fig. 3-16 Installation of seismograph on the Ground

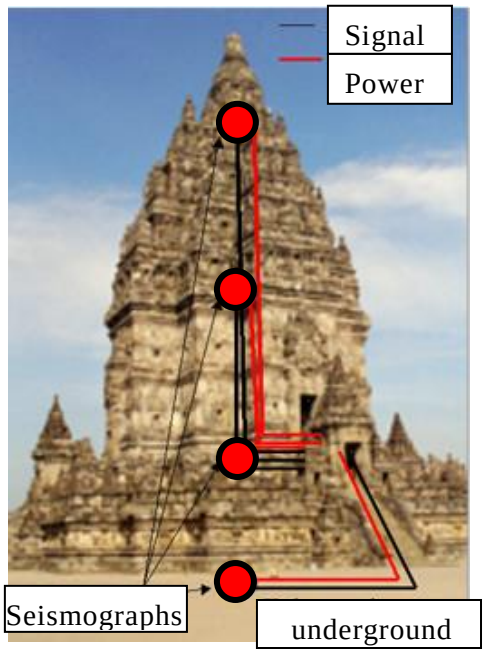

Fig. 3-17 Cable wiring

On January 10th and 11th, 2013, cables for signal, shield for connection and shield weatherproof boxes were replaced. Because, indoor LAN cables were used for the cables for signal from the Top, the Middle and the Ground, we replaced by outdoor use ones. Wooden shield weatherproof boxes of three seismographs have been deteriorated as shown in Figs. 3-18 and 3-20. Therefore shield weatherproof boxes were replaced with new ones as shown in Figs. 3-19 and 3-21.

Fig. 3-18 Before maintenance (Ground)

Fig. 3-19 After maintenance (Ground)

Fig. 3-20 Before maintenance (Top)

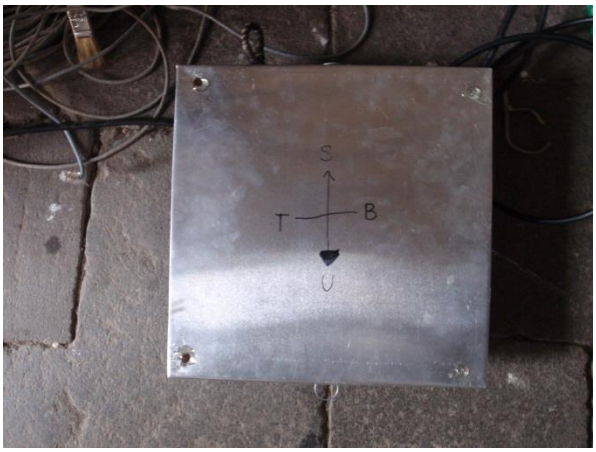

Fig. 3-21 After maintenance (Top)

3.2.2 EARTHQUAKE RECORDS

Four earthquake motions were recorded at Chandi Shiva, on September 12th, 2010, November 24th, 2011, March 19th and May 22th, 2012.

These seismographs recorded acceleration. Therefore, velocity and displacement were calculated from the acceleration records by Frequency filtering method with TDAP III. The following equation was applied for frequency filtering, where f0=0.16666667 Hz, f1=0.1 Hz and h=0.552. After filtering process, those data were integrated.

$$H(f) = 1 / (1 - (f0 / f)^2 - 2h (f0 / f) I) / (1+ (f1 / f)^2)^{1/2}$$

I) Earthquake record on September 12th, 2010

On September 12th, 2010, a time history of earthquake was recorded. Table. 3-3 lists the detail of this earthquake. Fig. 3-22 also shows the location of the epicenter and the Prambanan temples. Figs. 3-23 to 3-25 present the recorded acceleration time histories. Figs. 3-26 to 3-28 and 3-29 to 3-31 describe velocity time histories and displacement time histories, respectively.

The time histories as disordered line at the Base on the UD direction were considered to be miss-recording. Therefore, comparison and examination were carried out with using data except the data at the Base UD direction.

The peak amplitudes of the time histories at each point are presented in Table. 3-4.

Table. 3-3 Earthquake data of the event on September 12th, 2010

Local Time	Lat.	Lon.	Depth	M_L	Epicentral Dist.
23:37	7.85 S	110.5 E	48 km	5.0	11 km

Table. 3-4 Peak amplitudes of the records on September 12th, 2010 event

		Acceleration (gal)		Velocity (kine)		Displacement (cm)	
		Max	Min	Max	Min	Max	Min
EW	Top	26.1	-23.7	1.94	-2.09	0.182	-0.219
	Middle	15.7	-15.0	1.33	-1.15	0.133	-0.162
	Base	10.0	-10.4	0.86	-0.44	0.086	-0.114
	Ground	8.6	-7.2	0.36	-1.82	0.055	-0.056
NS	Top	21.1	-23.6	1.60	-1.47	0.142	-0.185
	Middle	15.9	-16.0	1.37	-0.89	0.143	-0.130
	Base	8.3	-12.1	0.74	-0.89	0.077	-0.041
	Ground	8.0	-9.3	0.39	-0.33	0.044	-0.032
UD	Top	4.3	-4.0	0.24	-0.21	0.024	-0.036
	Middle	4.3	-4.7	0.35	-0.32	0.029	-0.010
	Base	0.1	-0.1	0.02	-0.02	0.100	-0.010
	Ground	7.7	-6.6	0.24	-0.20	0.021	-0.021

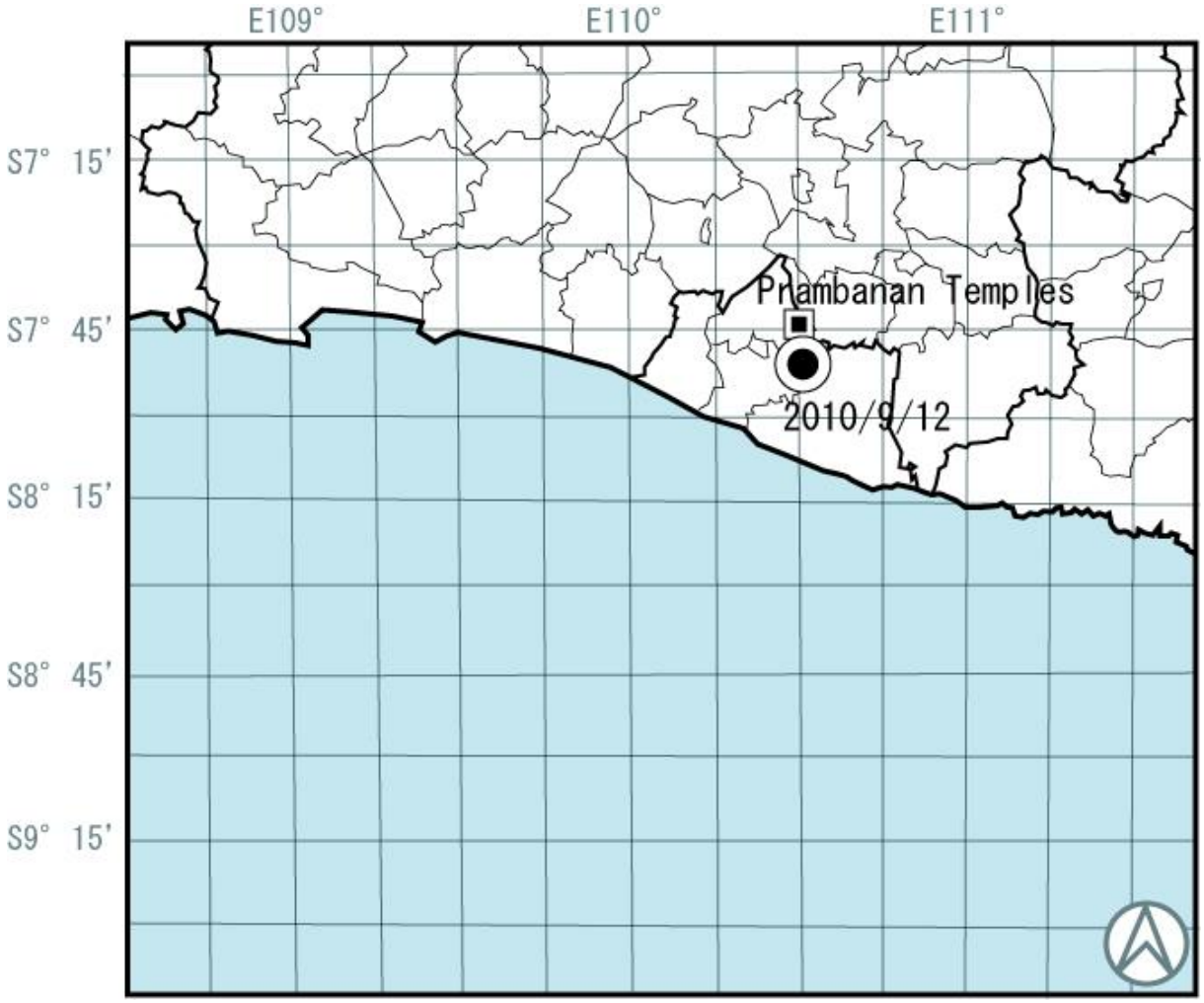

Fig. 3-22 Epicenter of the event on September 12th, 2010

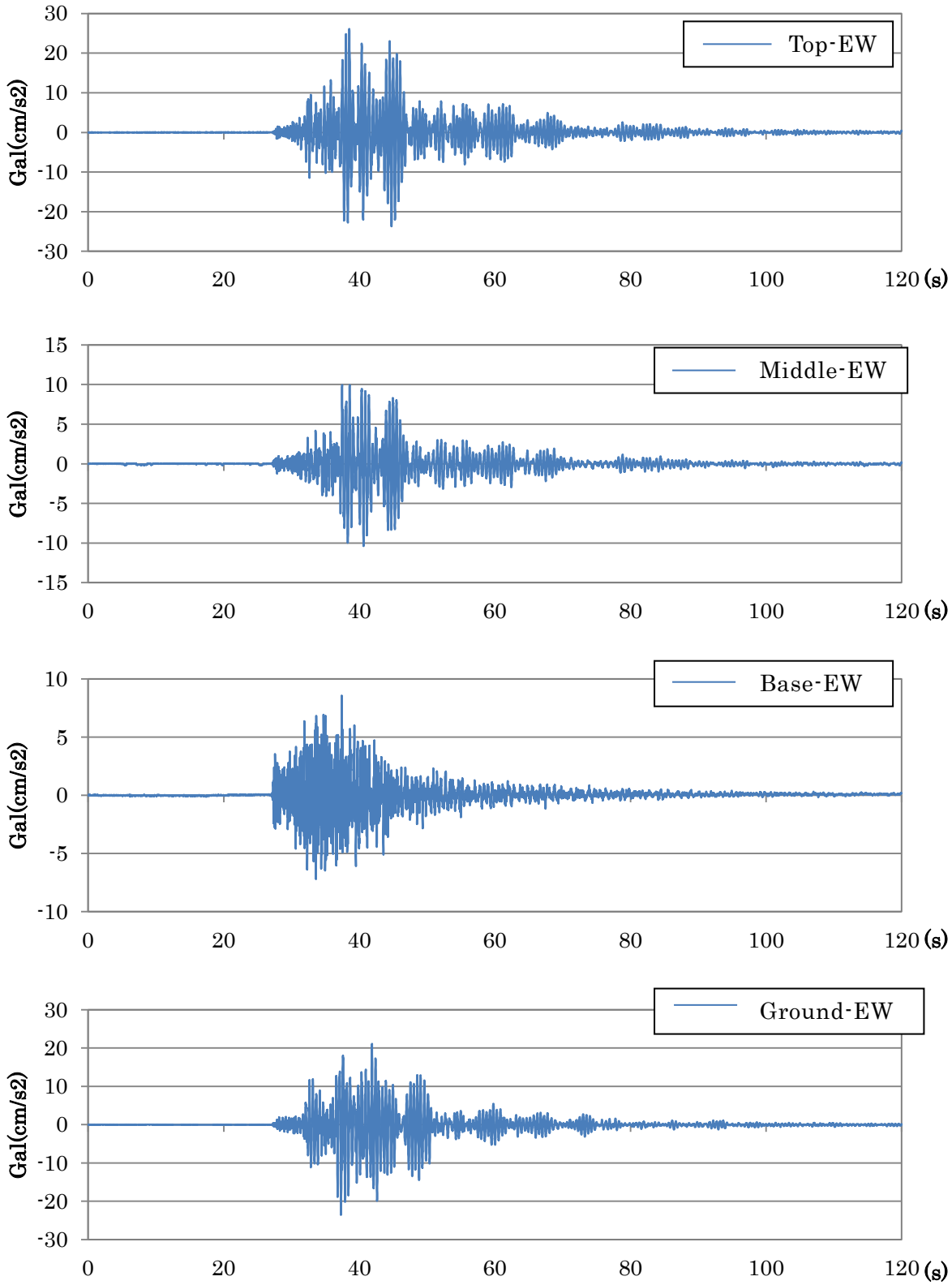

* 980 gal = 1 G

Fig. 3-24　Acceleration time history of the record in EW direction

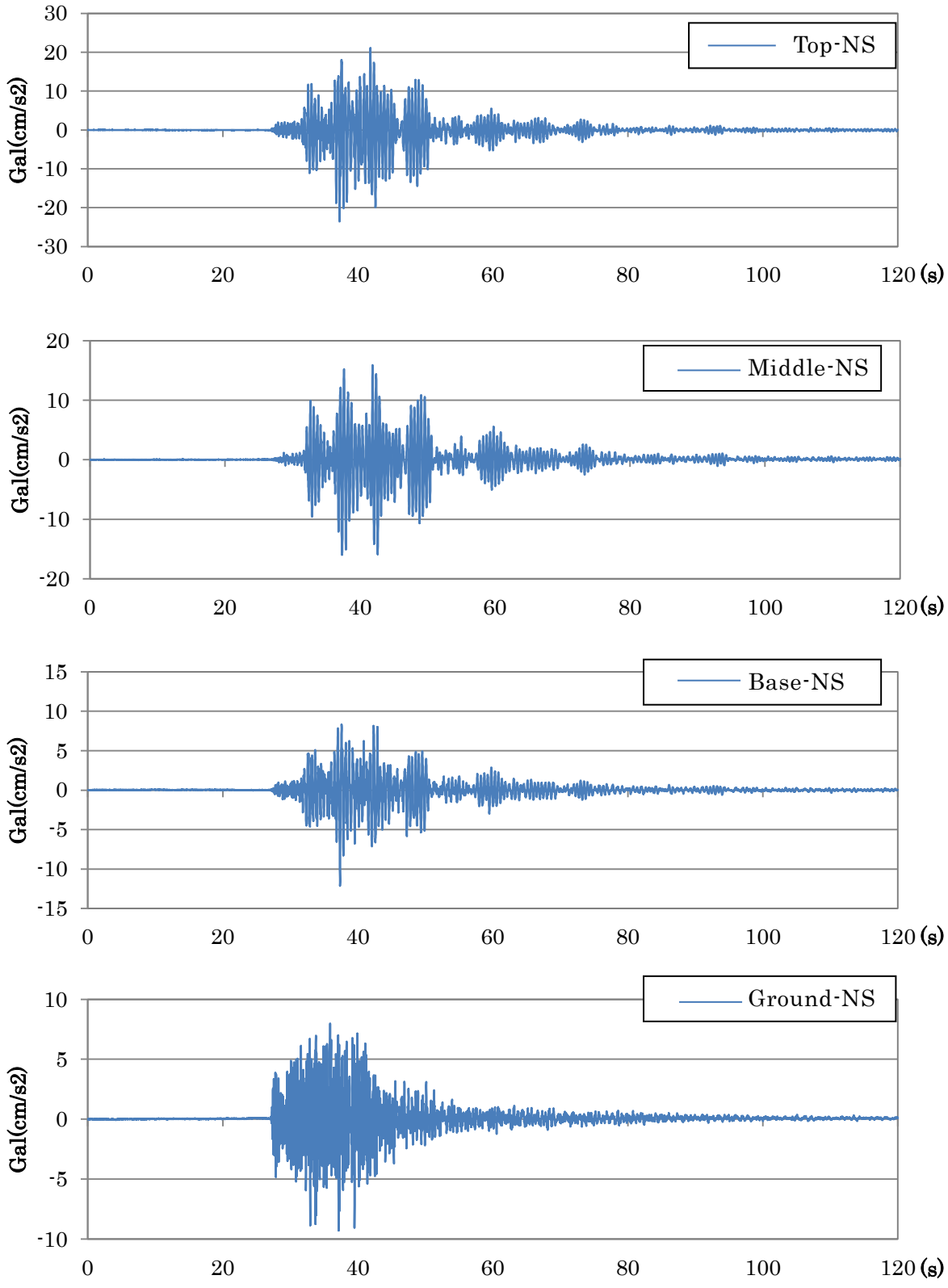

* 980 gal = 1 G

Fig. 3-25　Acceleration time history of the record in NS direction

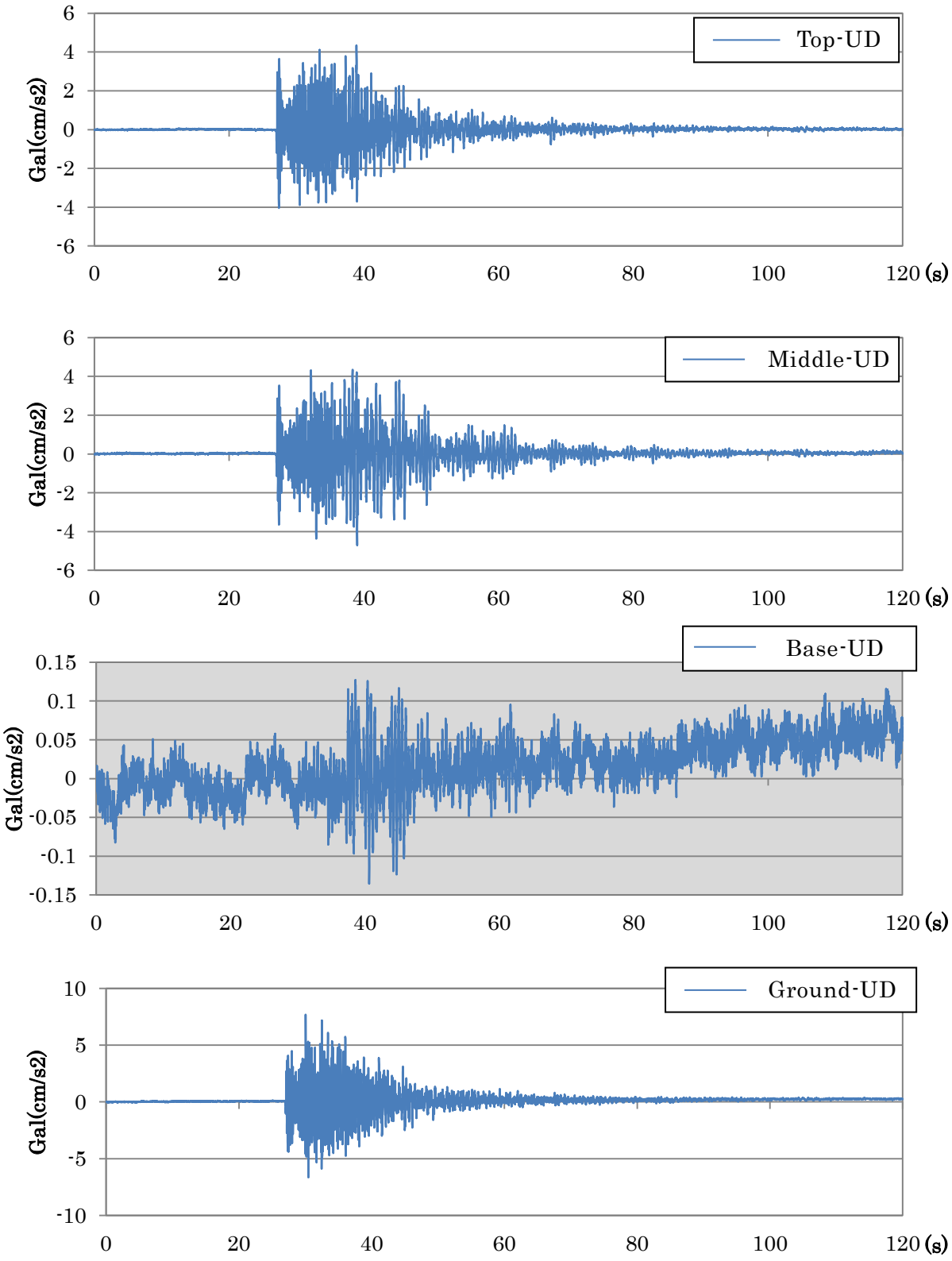

* 980 gal = 1 G

Fig. 3-26　Acceleration time history of the record in UD direction

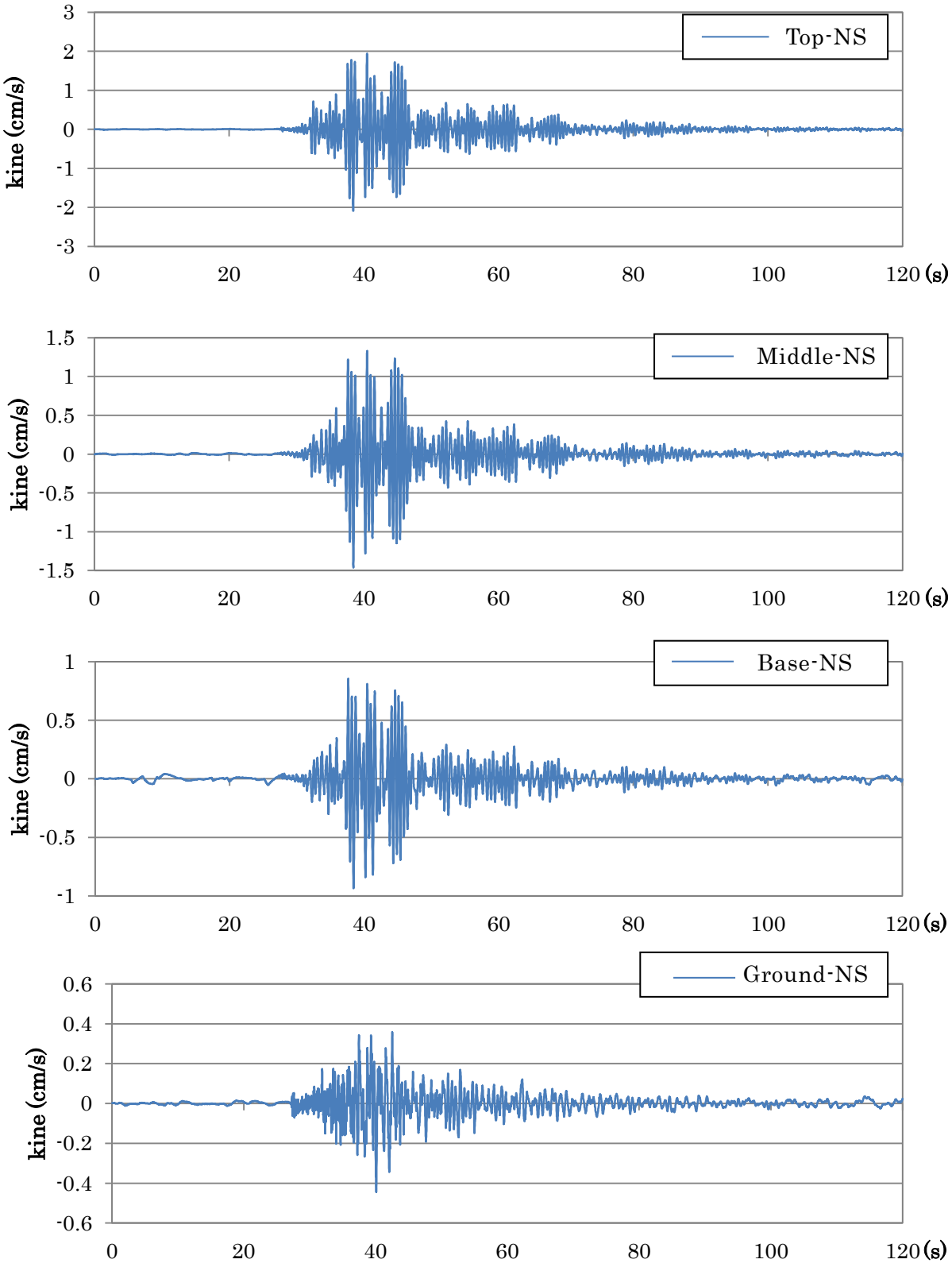

Fig. 3-27　Velocity time history of the record in EW direction

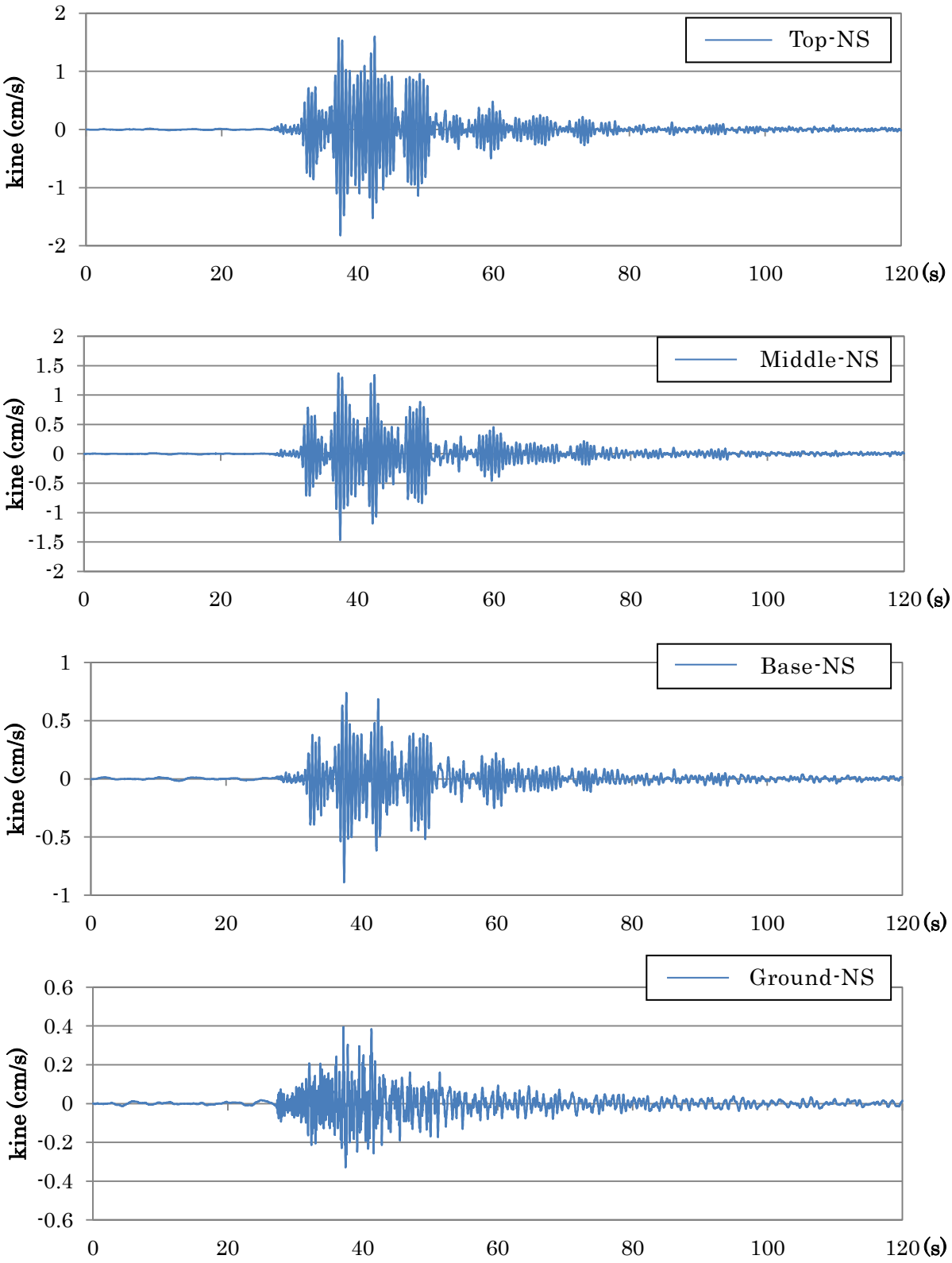

Fig. 3-28　Velocity time history of the record in NS direction

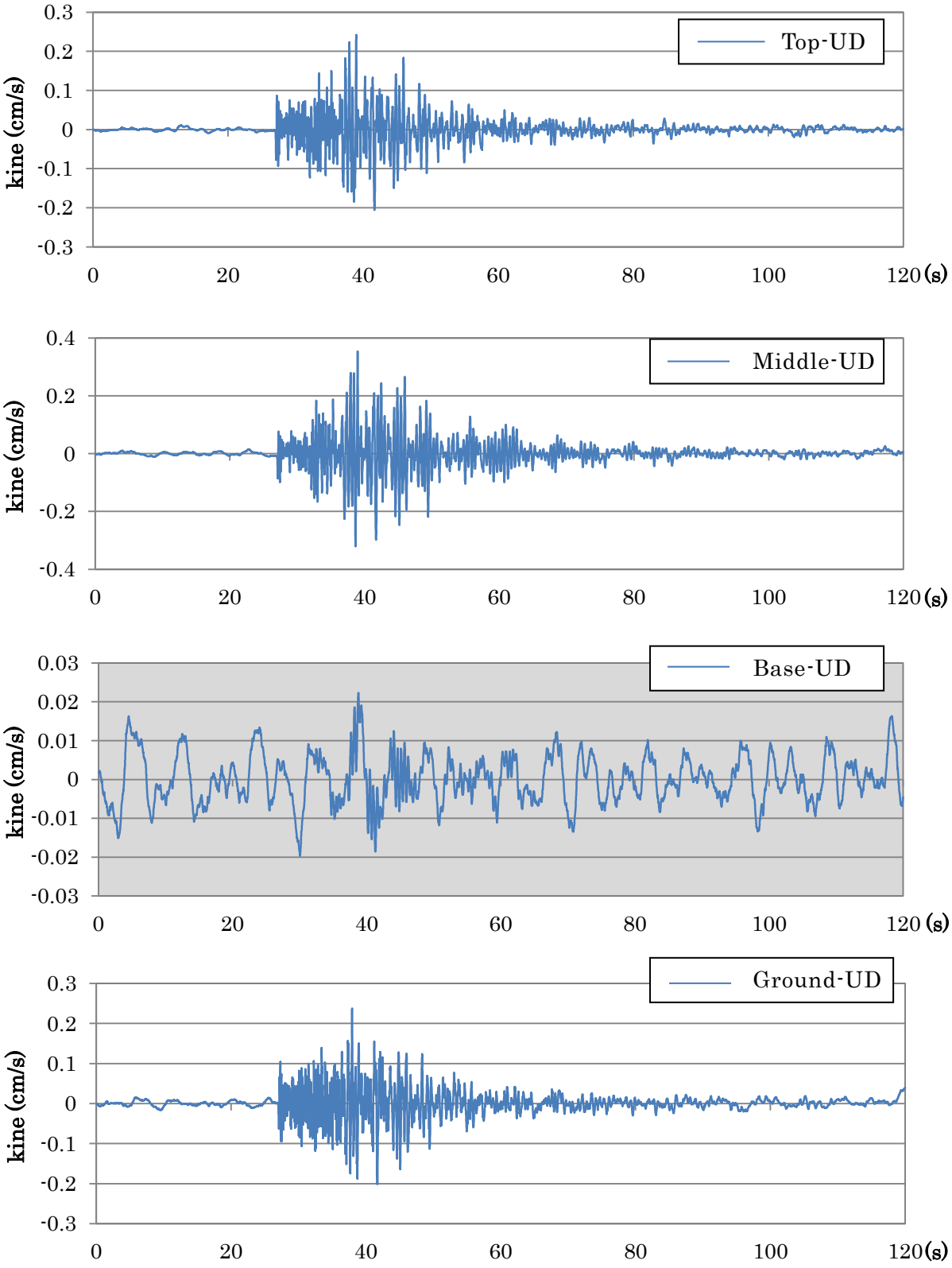

Fig. 3-29　Velocity time history of the record in UD direction

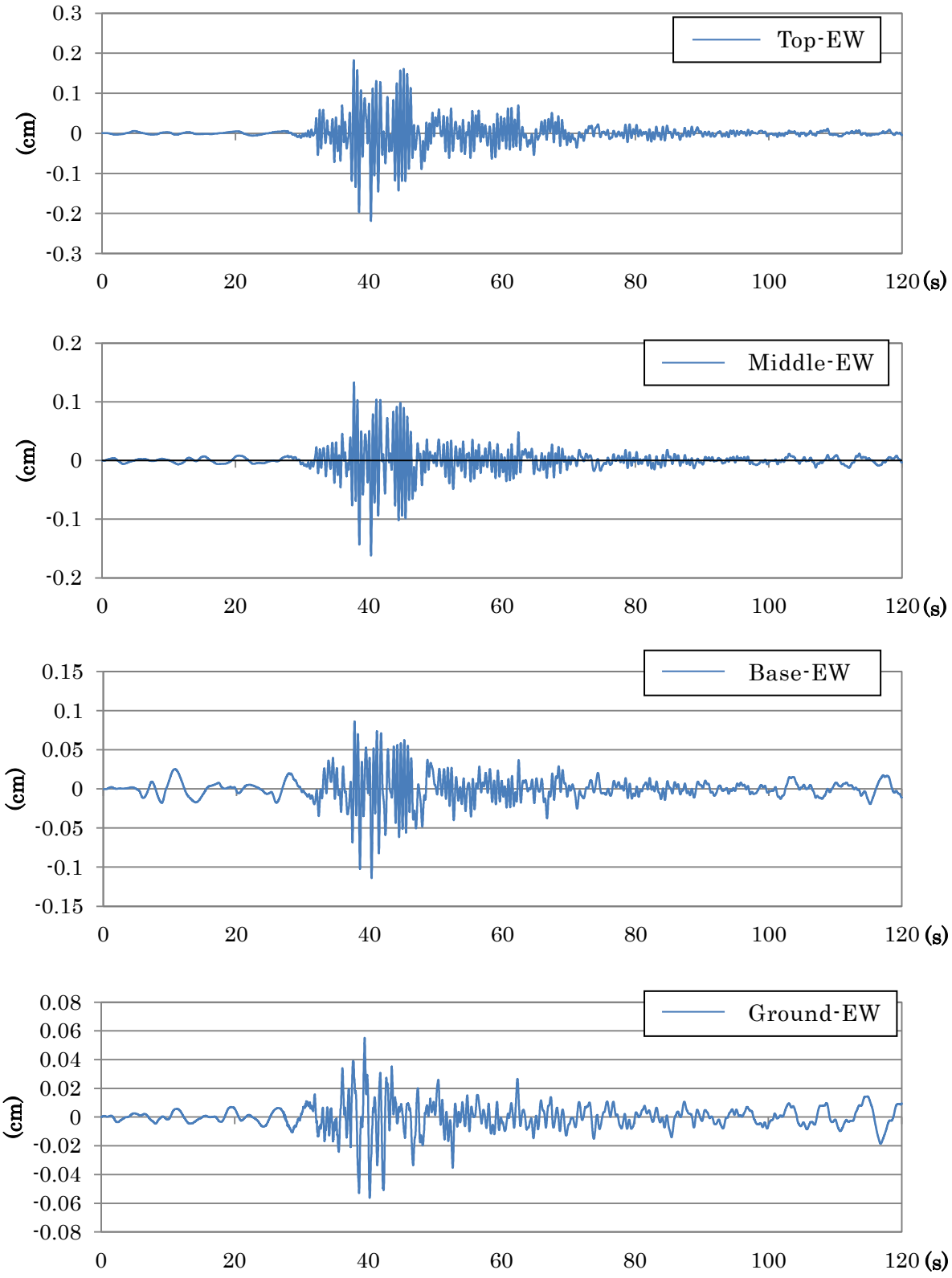

Fig. 3-30　Displacement time history of the record in EW direction

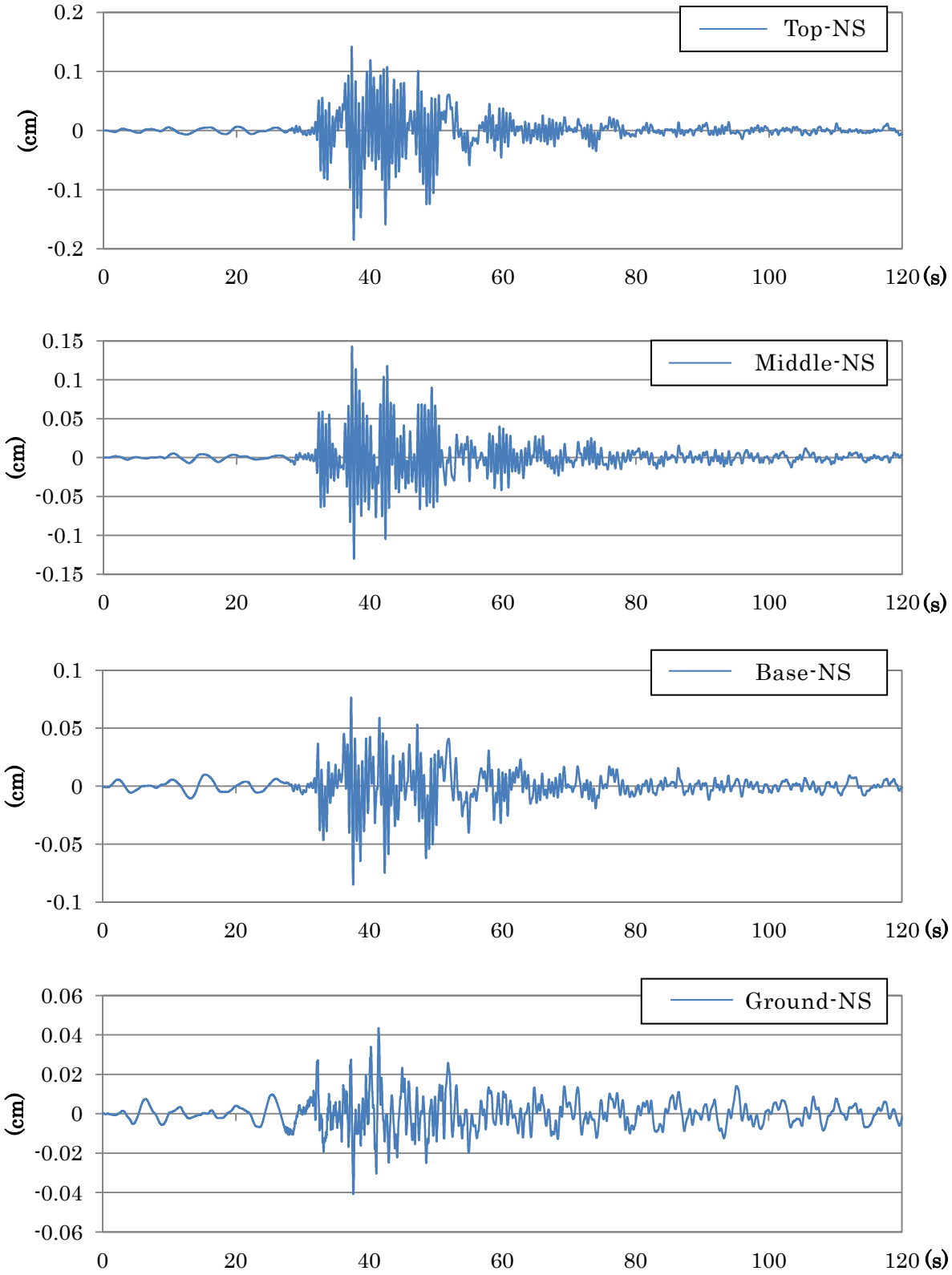

Fig. 3-31　Displacement time history of the record in NS direction

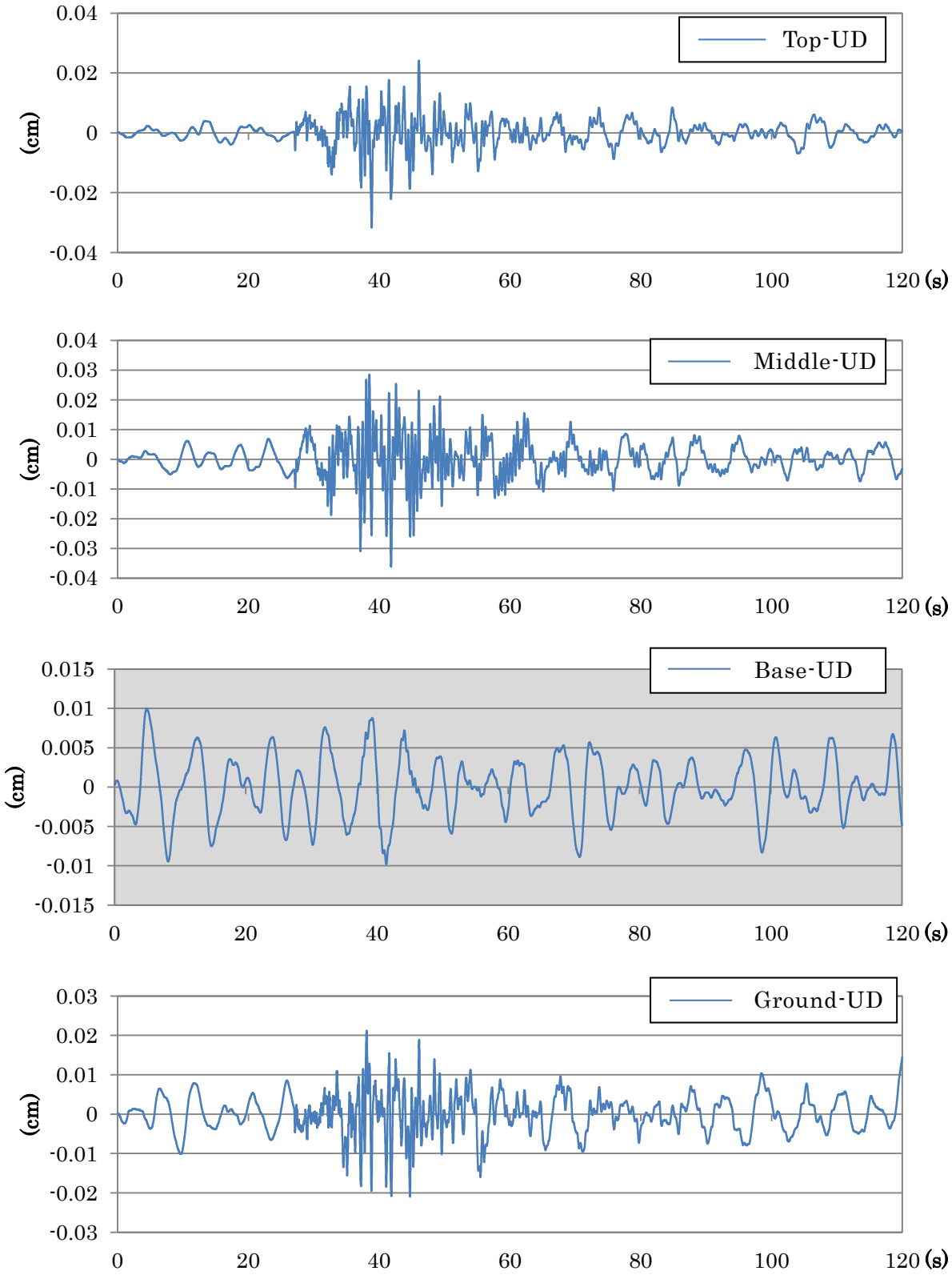

Fig. 3-32　Displacement time history of the record in UD direction

Fig. 3-33 shows the orbit at the Top, Middle, Base and Ground respectively.

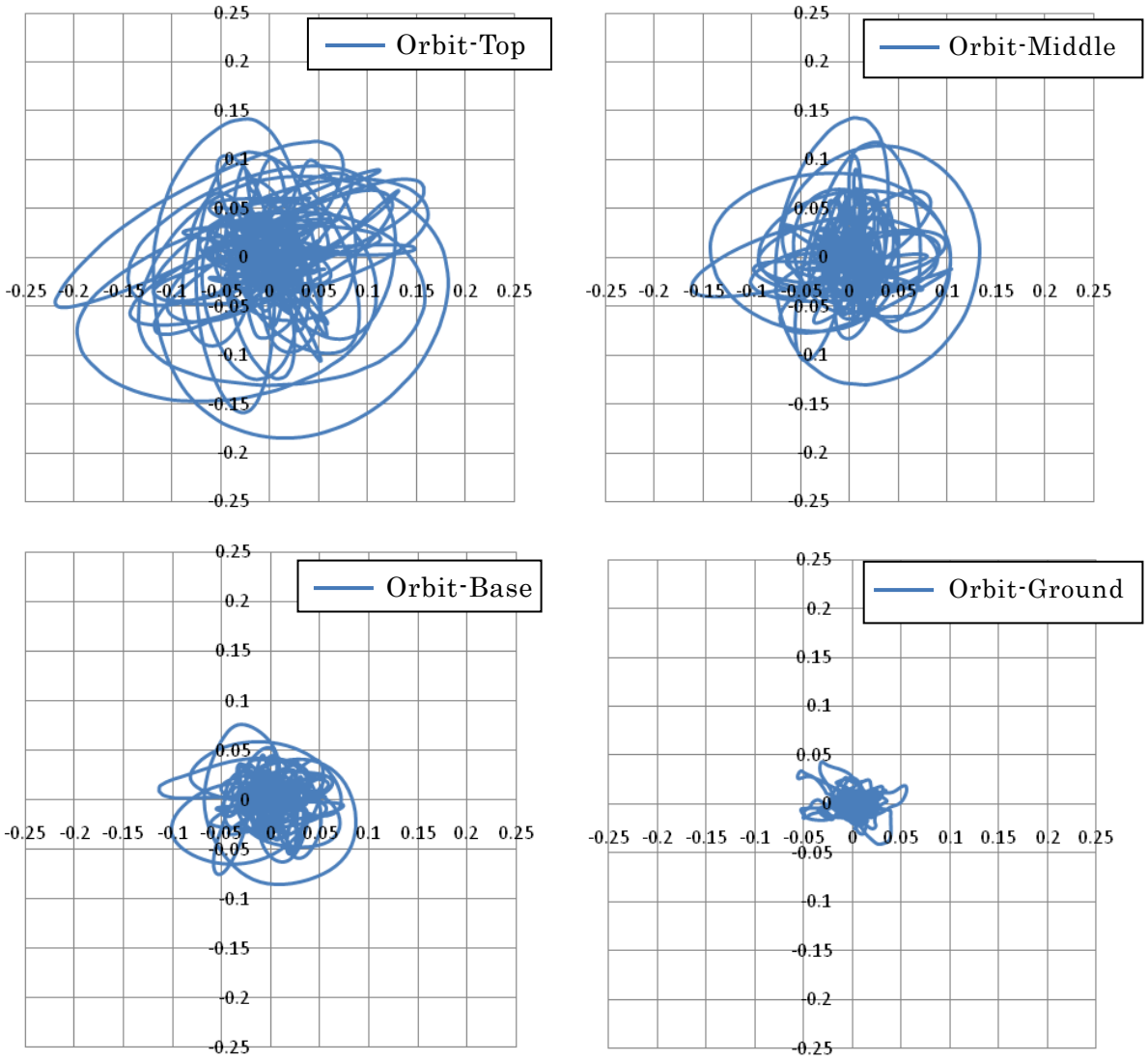

Fig. 3-33　Particle orbit at the point of the seismograms

Figs. 3-34 and 3-35 show Acceleration Fourier spectra for the EW and NS directions of the earthquake record at the Top, Middle, Base and Ground, respectively. These were drawn through smoothing with the Parzen spectral window of 0.5 Hz.

Figs. 3-36 and 3-37, Figs. 3-38 to 3-41 show the acceleration response spectra and the transfer function, respectively.

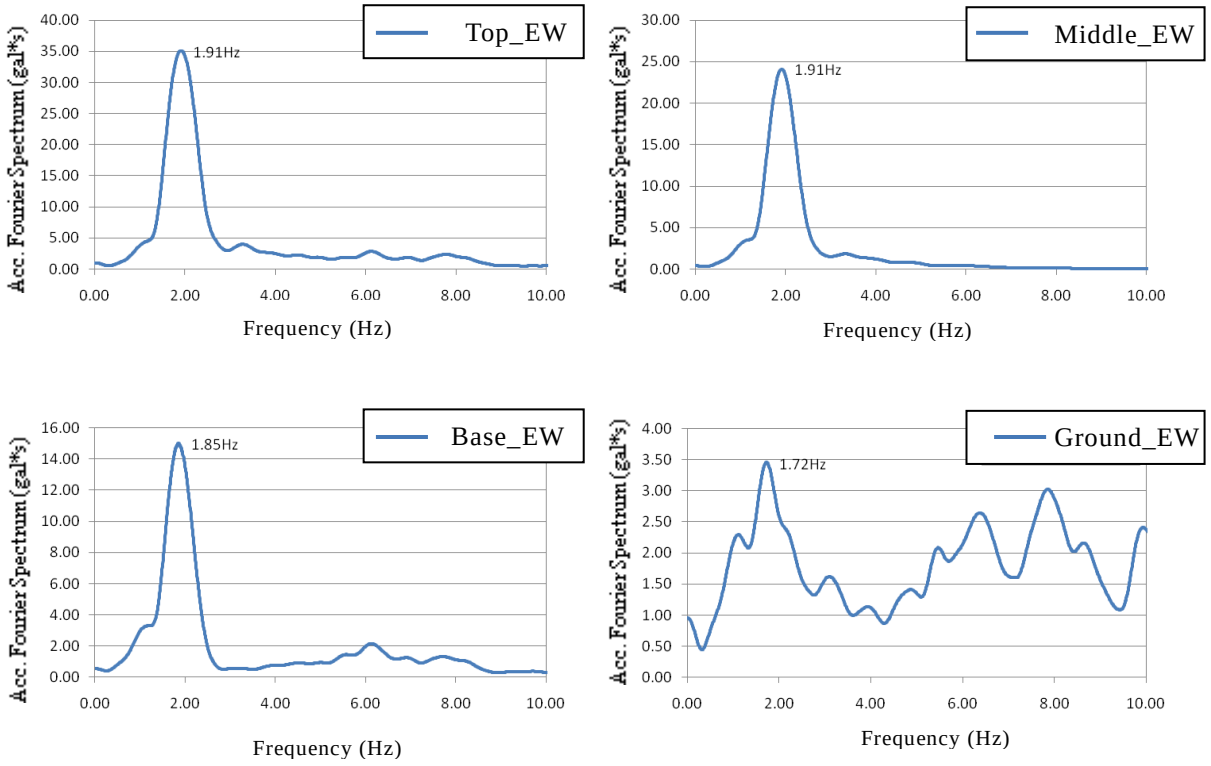

Fig. 3-34　Acc. Fourier Spectra; EW direction

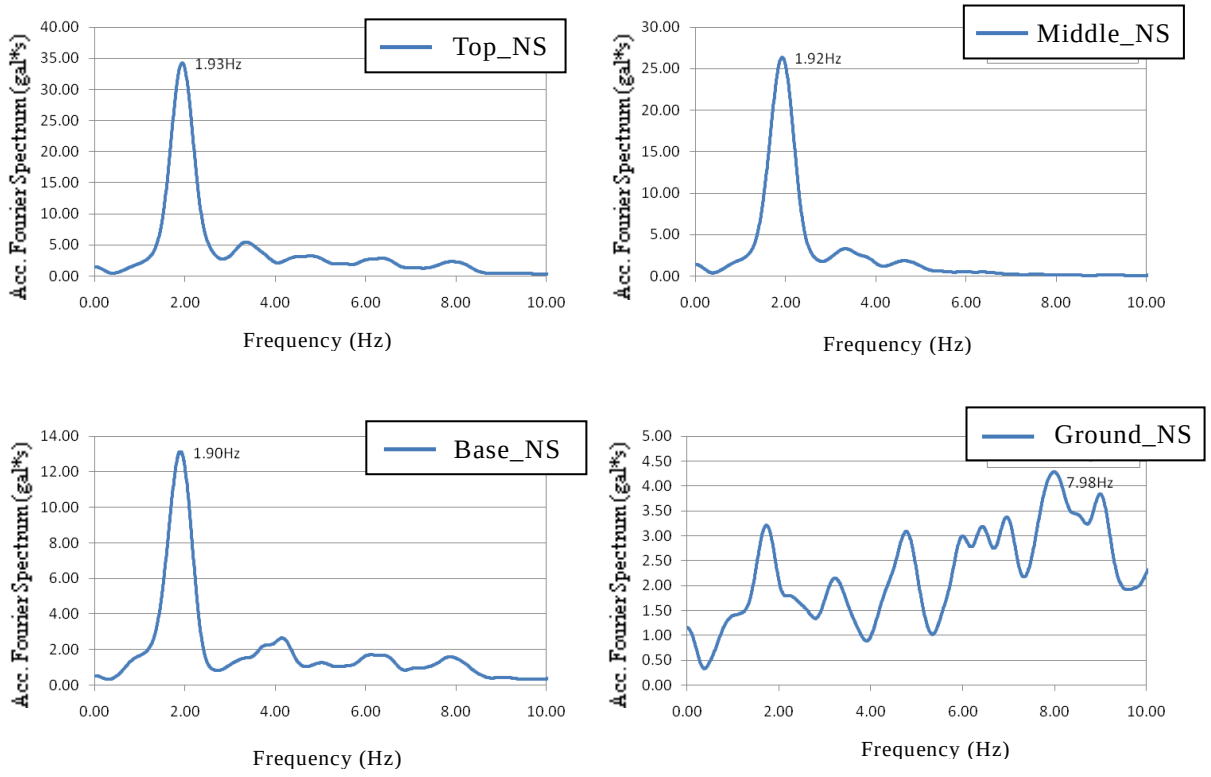

Fig. 3-35　Acc. Fourier Spectra; NS direction

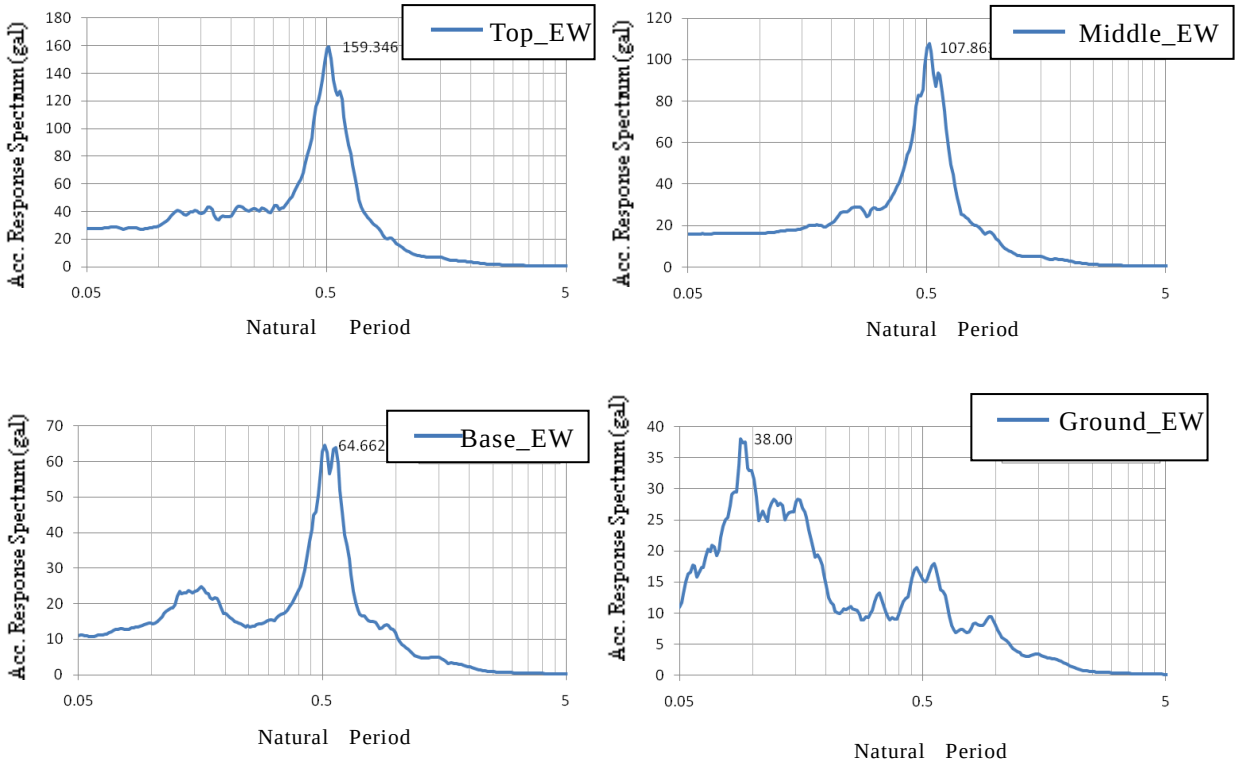

Fig. 3-36 Acc. Response Spectra; EW direction

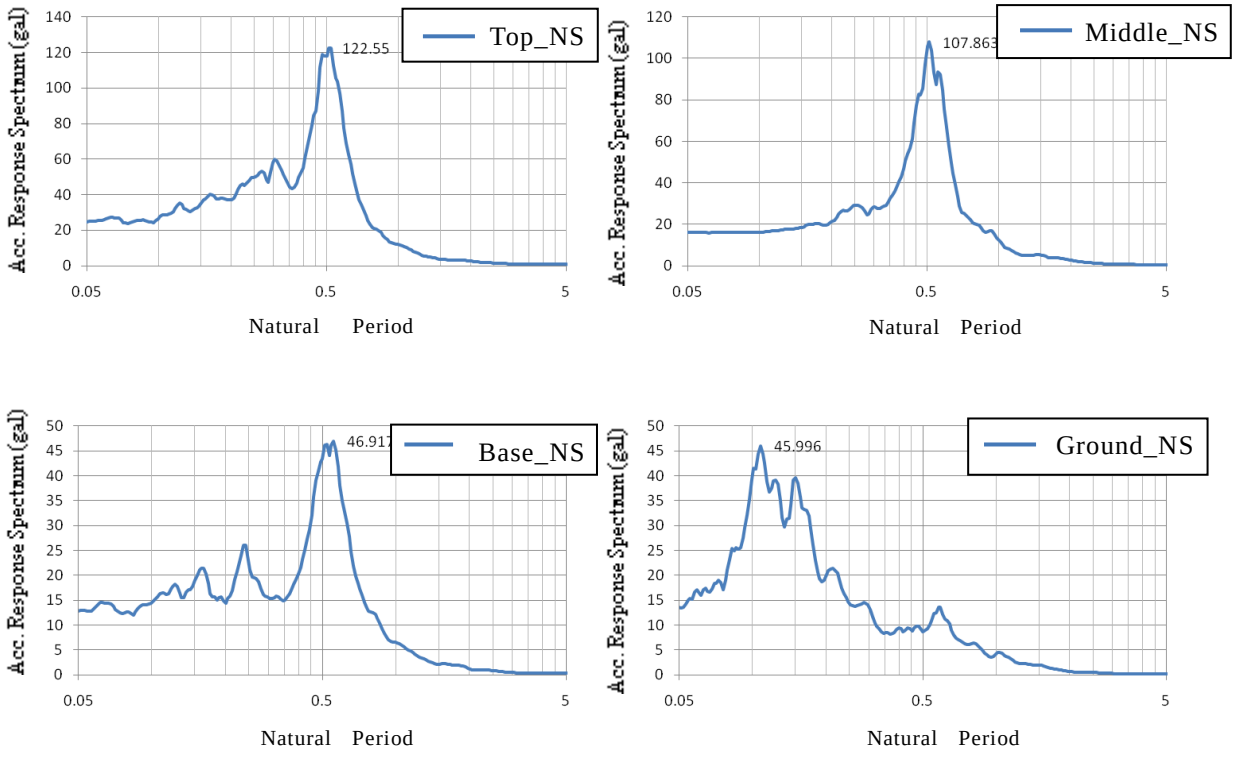

Fig. 3-37 Acc. Response Spectra; NS direction

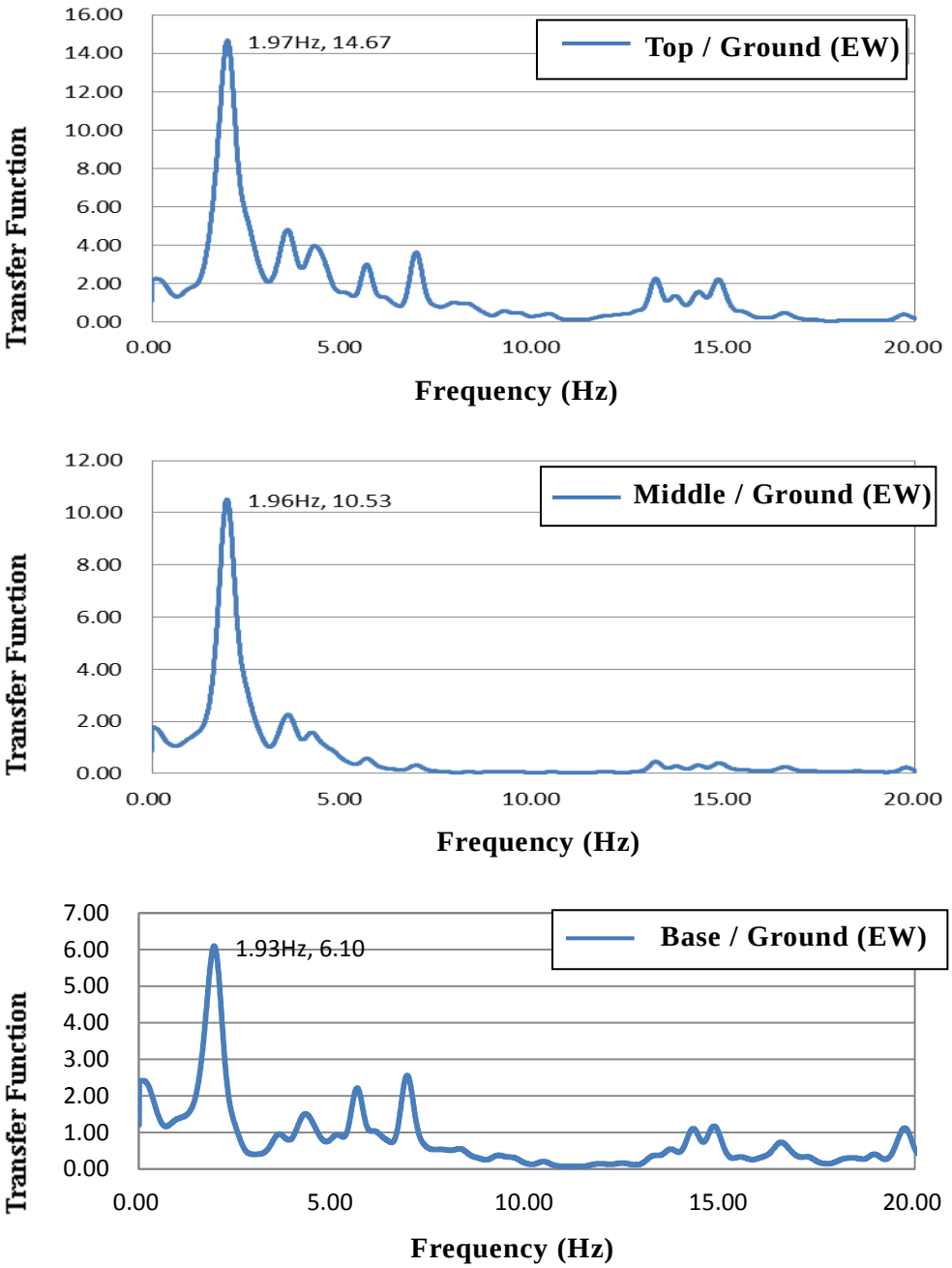

Fig. 3-38　Transfer Function of the record at the Ground; EW direction

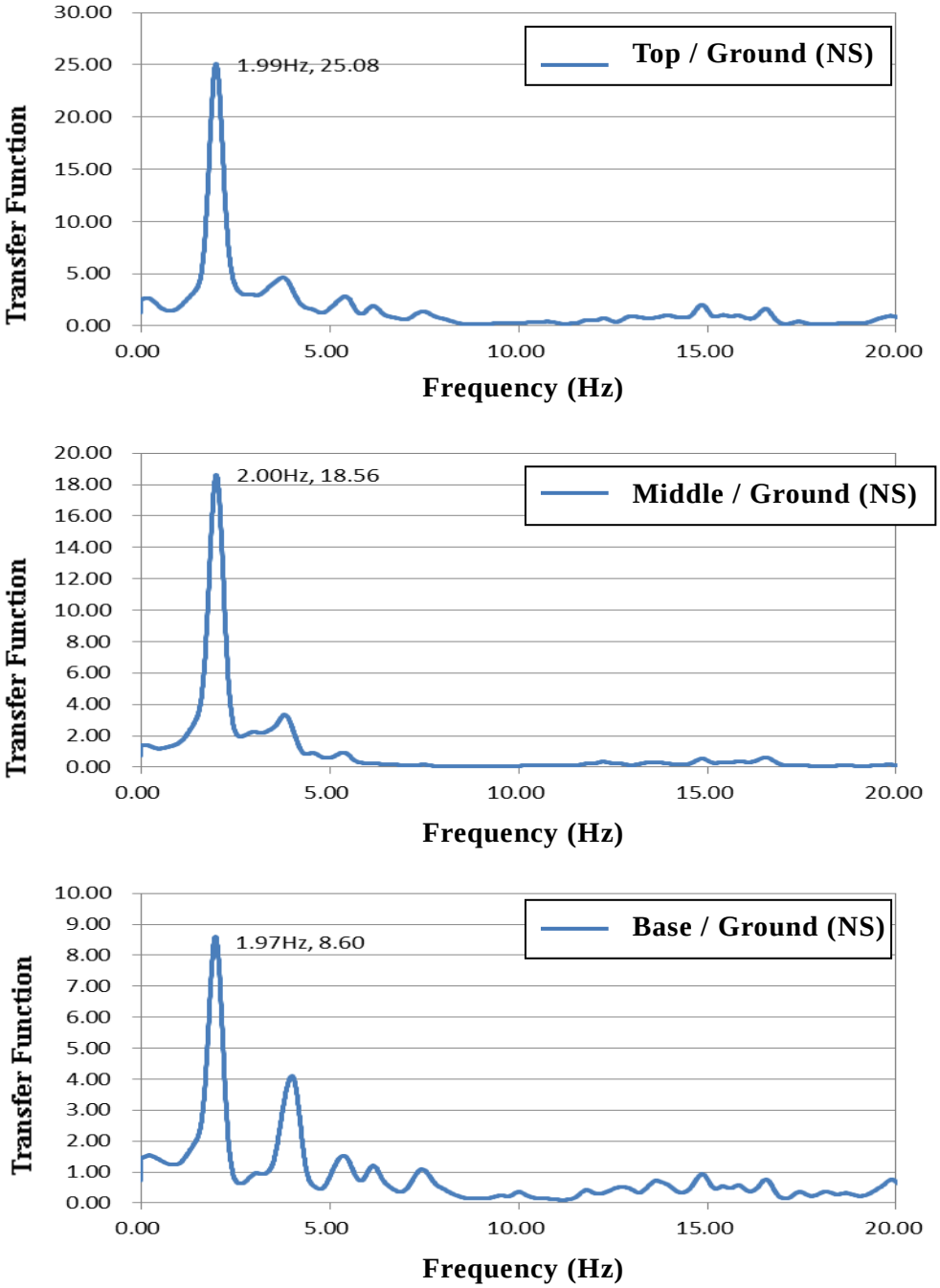

Fig. 3-39　Transfer Function of the record at the Ground; NS direction

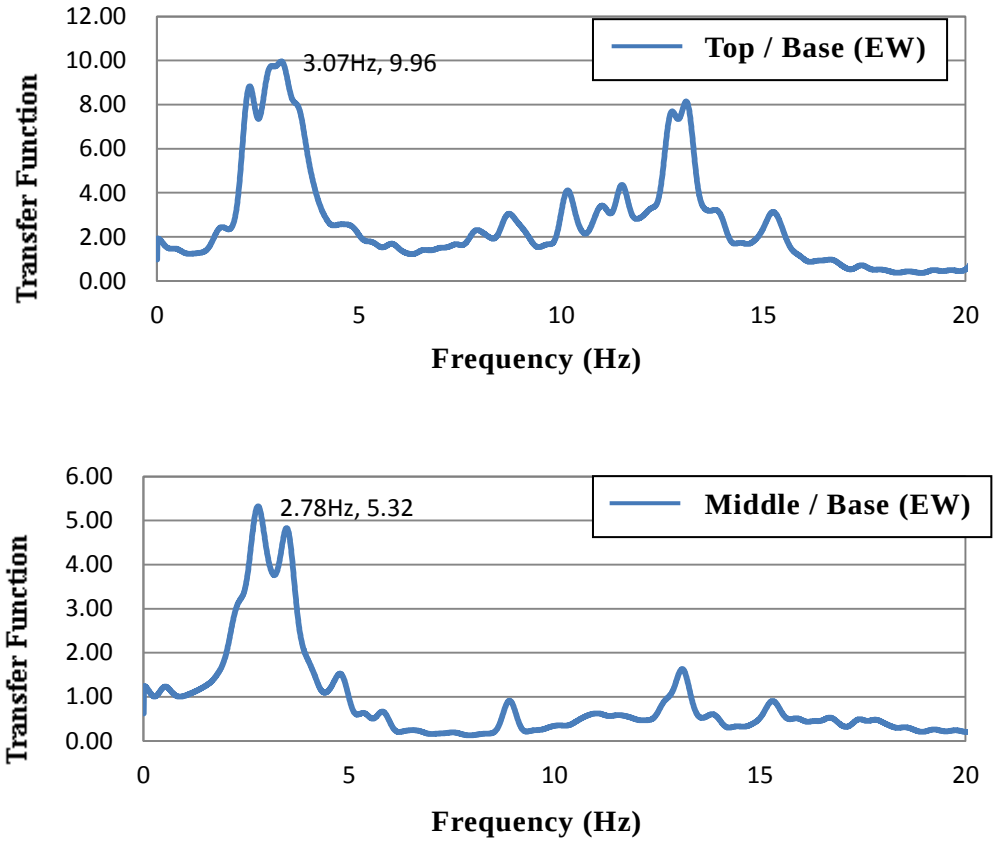

Fig. 3-40　Transfer Function of the record at the Base; EW direction

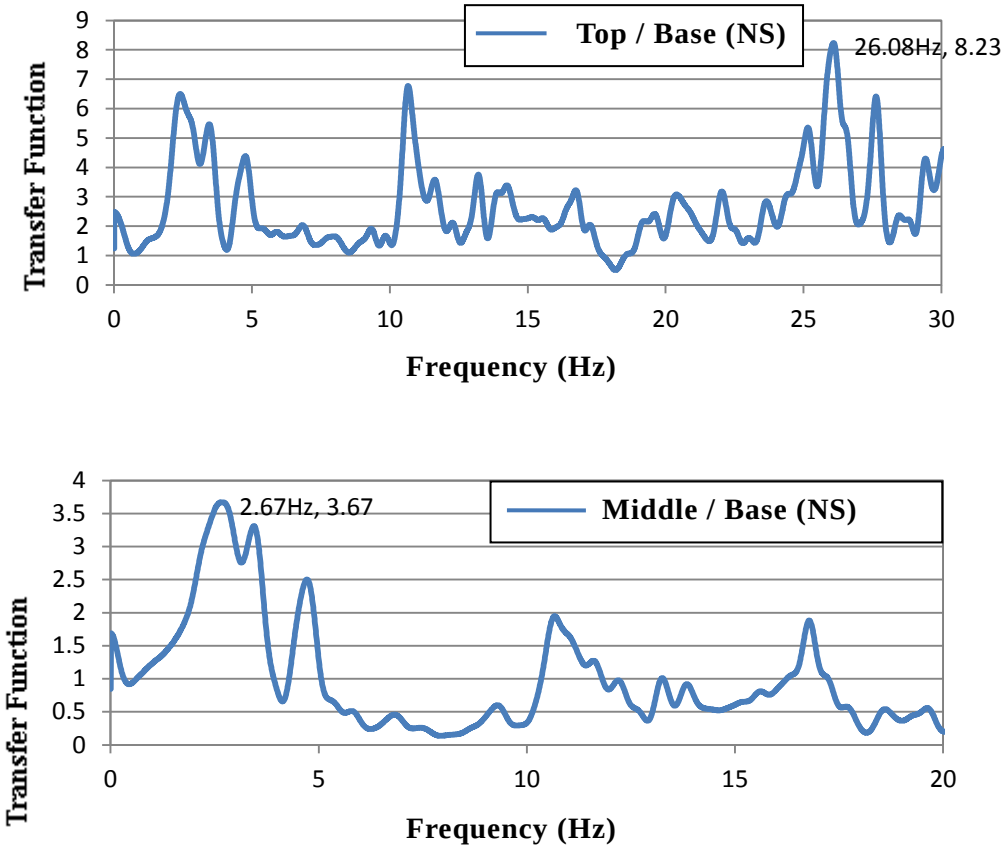

Fig. 3-41　Transfer Function of the record at the Base; NS direction

The natural frequency was evaluated to be 1.95 Hz in EW direction and 1.99 Hz in NS direction from the transfer functions shown in Figs. 3-38 and 3-39.

II) Earthquake record on November 24th, 2011

At 10:55 a.m. (local time) on November 24th, 2011 an earthquake was recorded at Chandi Shiva. The earthquake details are shown in Table. 3-5. The epicentral distance at the Prambanan Temples was estimated to be approximately 165 km. Fig. 3-42 shows the locational relation between the Prambanan Temples and the epicenter.

Table. 3-6 shows the peak values of the time histories. Figs. 3-43 to 3-45 show acceleration time histories at the Top, Middle, Base and Ground for EW, NS and UD directions, respectively. In the same way, Figs. 3-46 to 3-48 and Figs. 3-49 to 3-51 show velocity time histories and displacement time histories, respectively.

Table. 3-5 Earthquake data of the event on November 24th, 2011

Local Time	Lat.	Lon.	Depth	M_L	Epicentral Dist.
10:55	9.04 S	109.8 E	10 km	5.1	165 km

Table. 3-6 Peak amplitude of the records on the November 24th, 2011 event

		Acceleration (gal)		Velocity (kine)		Displacement (cm)	
		Max	Min	Max	Min	Max	Min
EW	Top	3.8	-4.0	0.25	-0.26	0.022	-0.025
	Middle	2.0	-2.2	0.15	-0.17	0.019	-0.017
	Base	1.7	-1.6	0.22	-0.21	0.075	-0.085
	Ground	1.8	-2.6	0.20	-0.15	0.090	-0.069
NS	Top	2.0	-2.0	0.15	-0.17	0.017	-0.017
	Middle	1.4	-1.4	0.10	-0.12	0.016	-0.014
	Base	1.8	-1.5	0.08	-0.12	0.021	-0.032
	Ground	2.5	-2.3	0.06	-0.06	0.023	-0.035
UD	Top	1.1	-1.0	0.03	-0.03	0.011	-0.009
	Middle	1.0	-1.1	0.04	-0.04	0.012	-0.009
	Base	1.1	-1.0	0.05	-0.05	0.011	-0.012
	Ground	1.5	-1.6	0.04	-0.05	0.012	-0.015

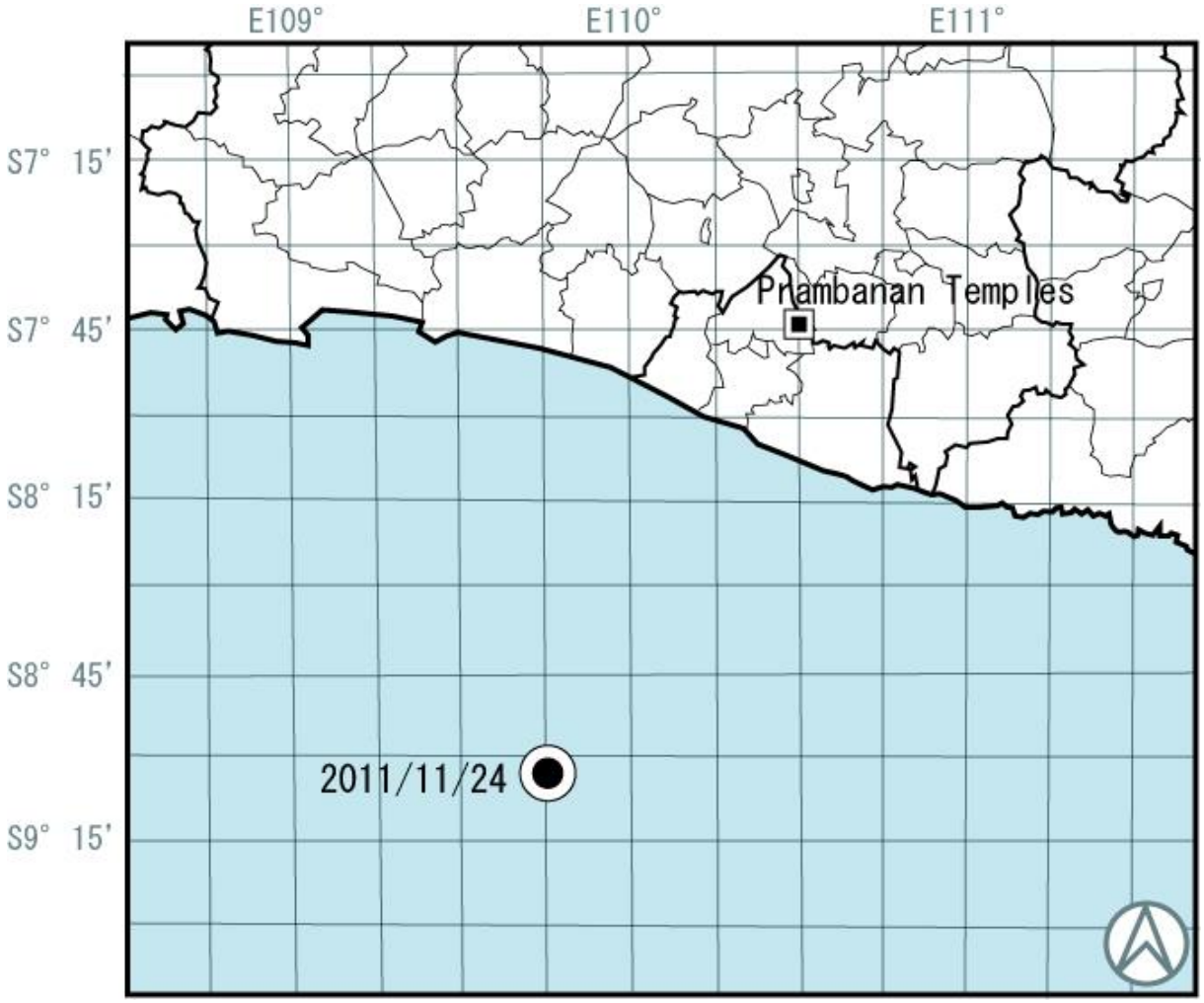

Fig. 3-42 Epicenter of the event on November 24th, 2011

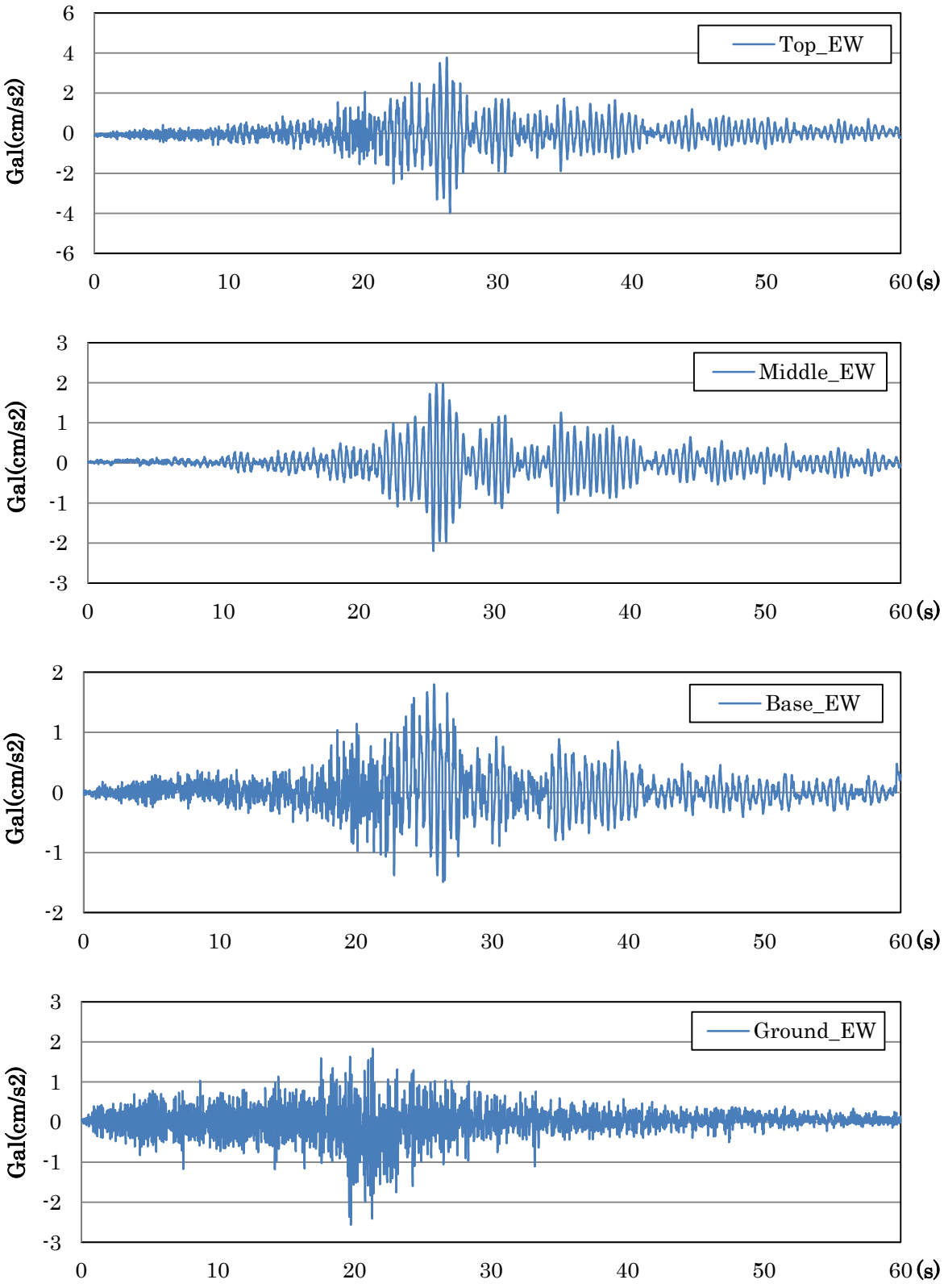

* 980 gal = 1 G

Fig. 3-43 Acceleration time history of the record in EW direction

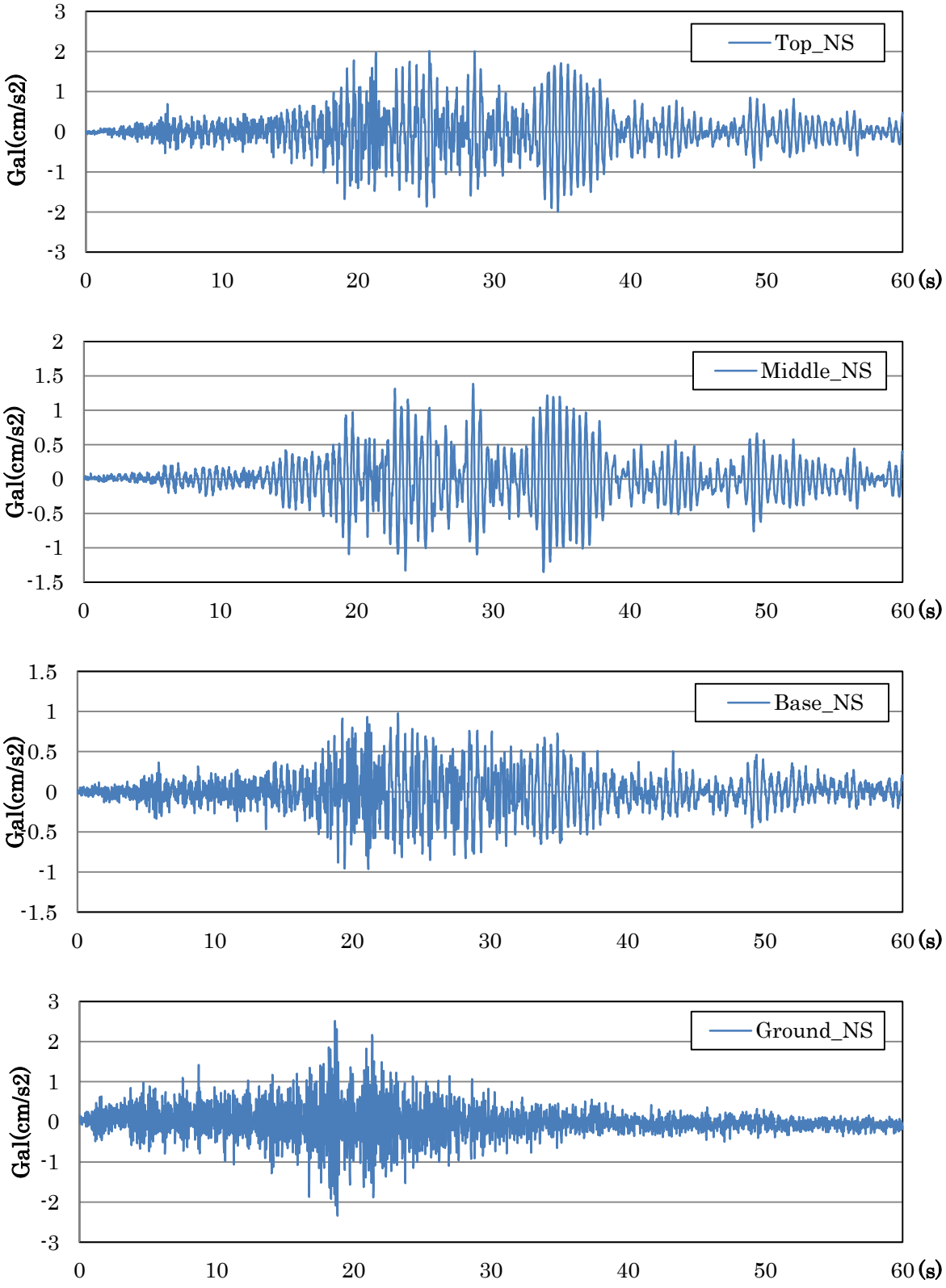

* 980 gal = 1 G

Fig. 3-44　Acceleration time history of the record in NS direction

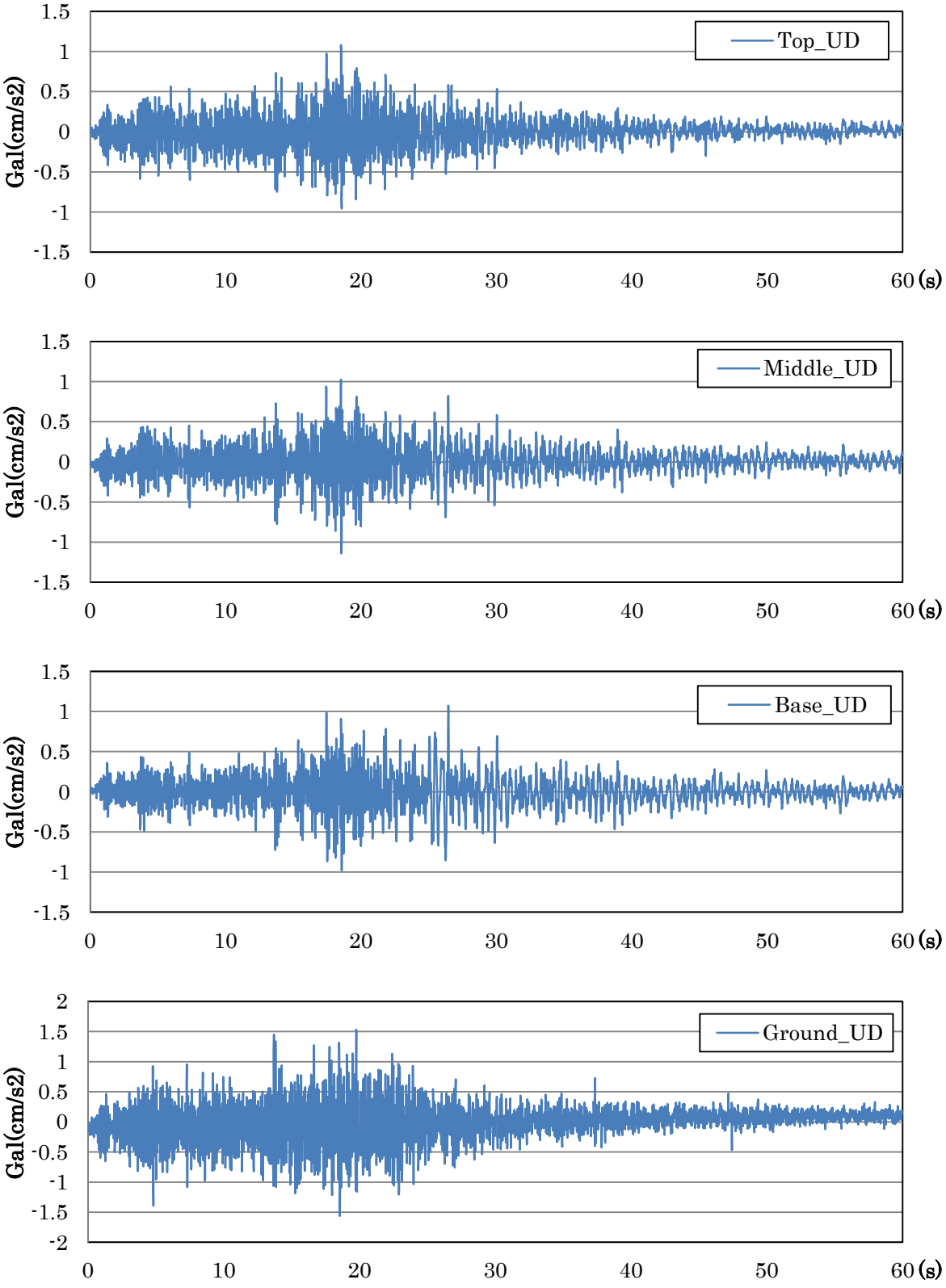

* 980 gal = 1 G

Fig. 3-45　Acceleration time history of the record in UD direction

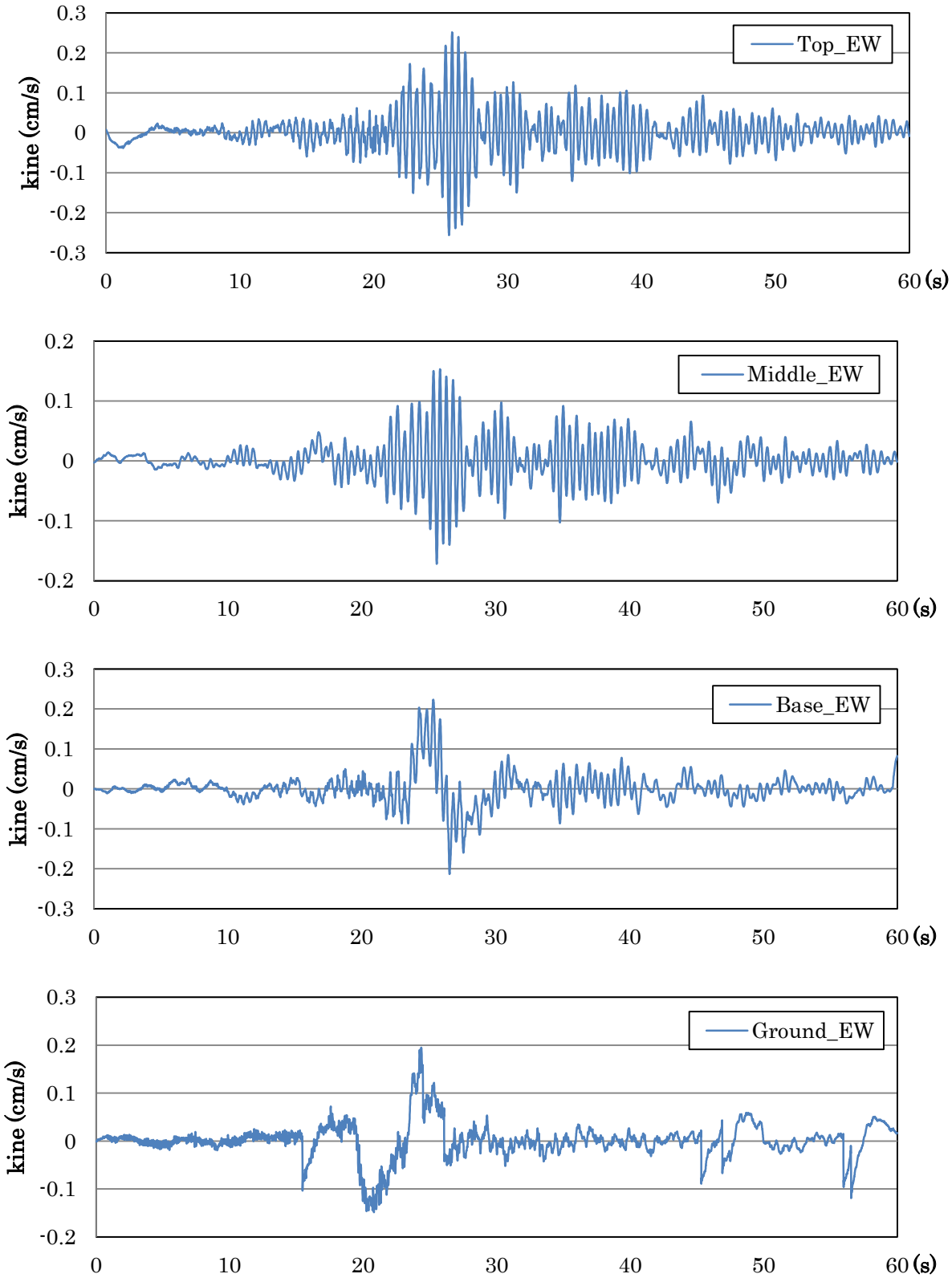

Fig. 3-46　Velocity time history of the record in EW direction

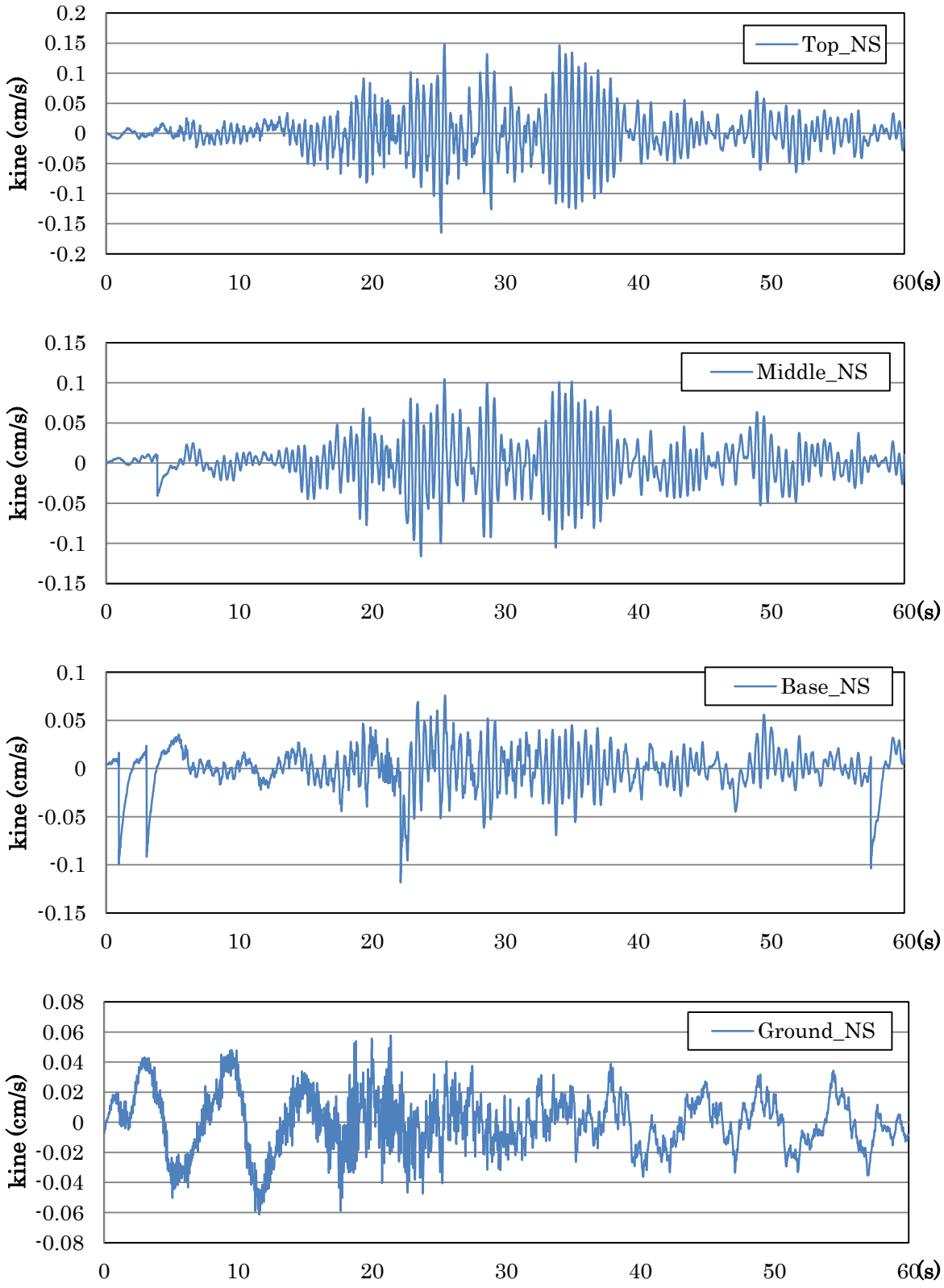

Fig. 3-47　Velocity time history of the record in NS direction

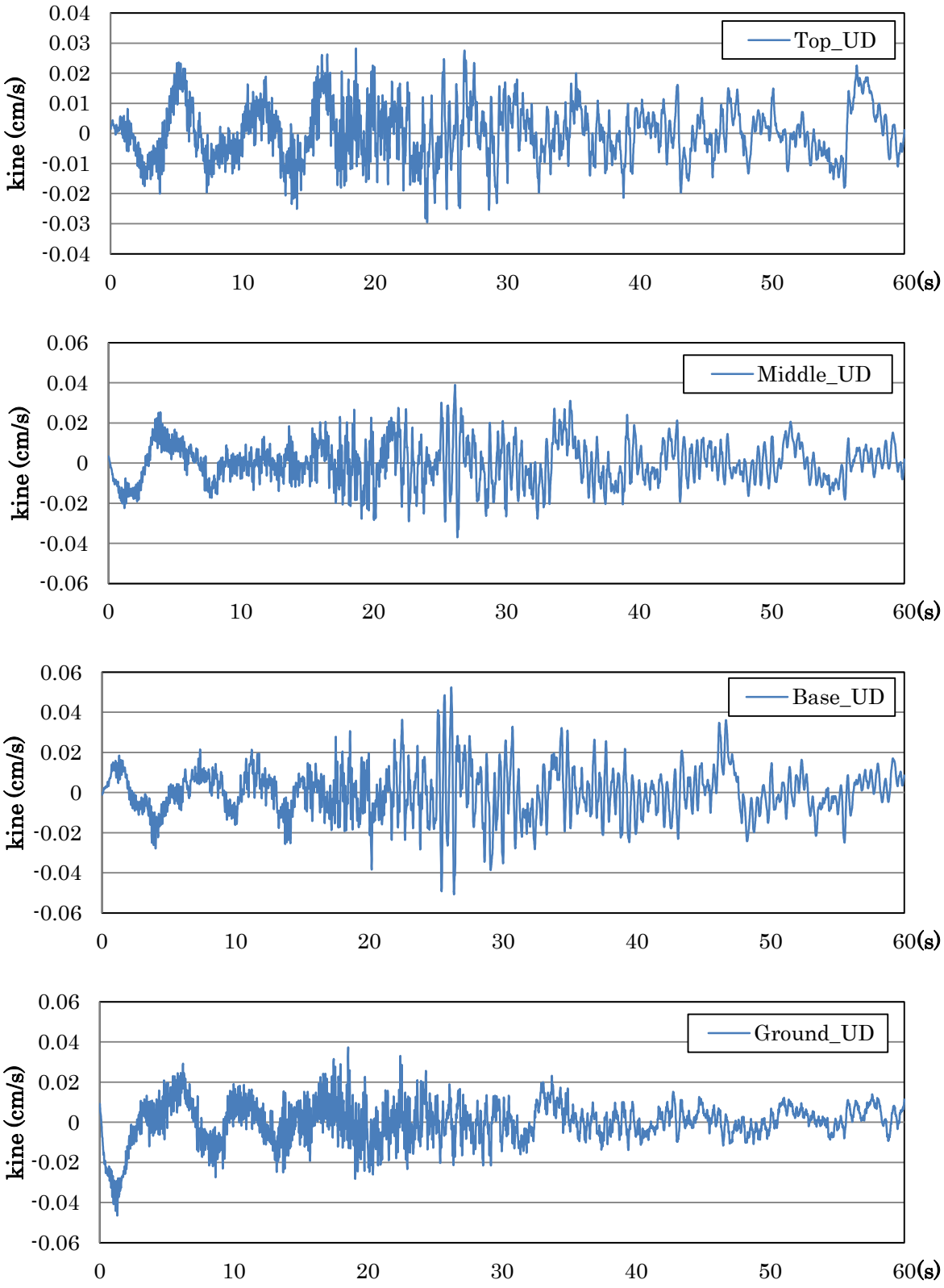

Fig. 3-48　Velocity time history of the record in UD direction

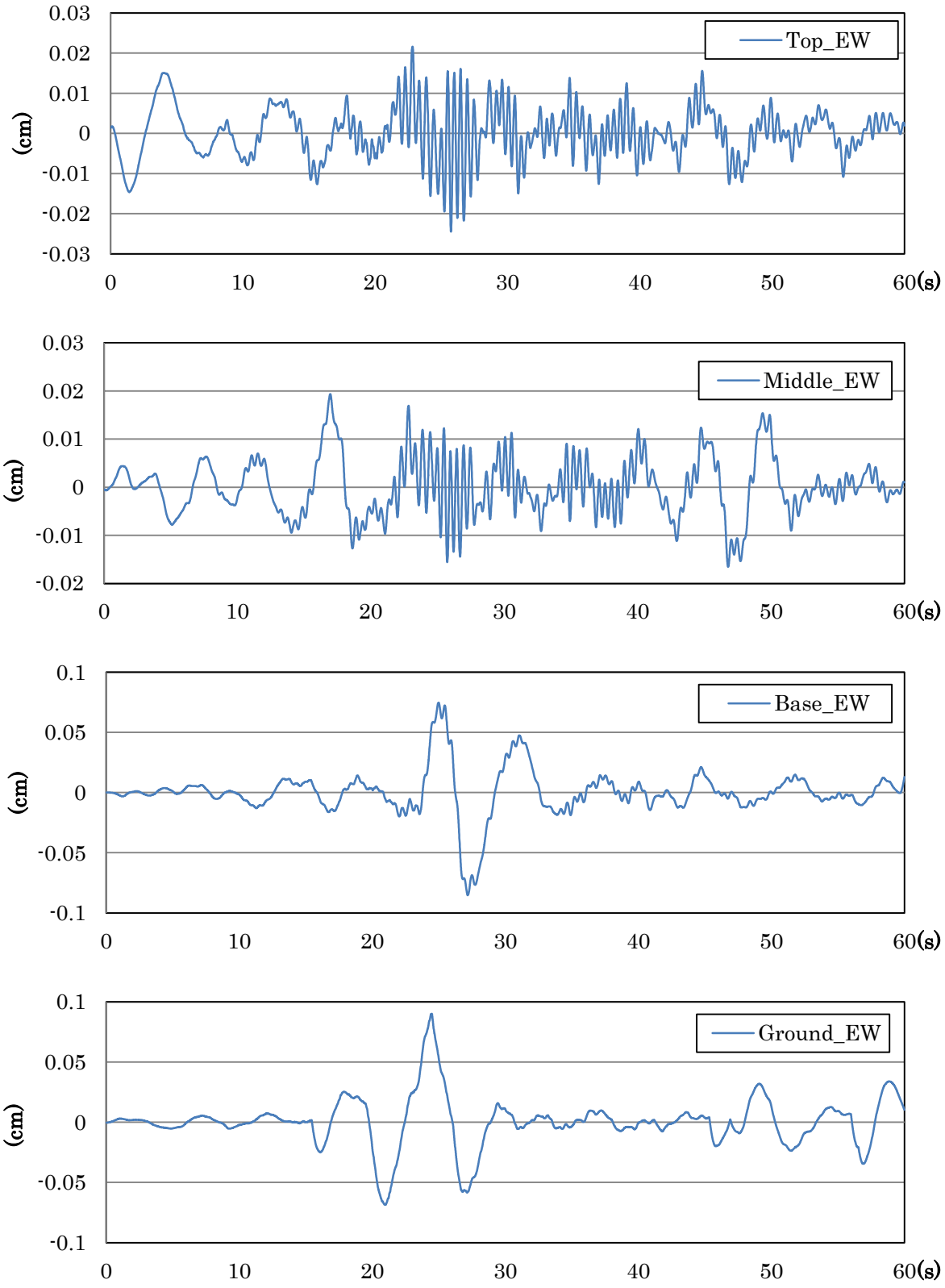

Fig. 3-49　Displacement time history of the record in EW direction

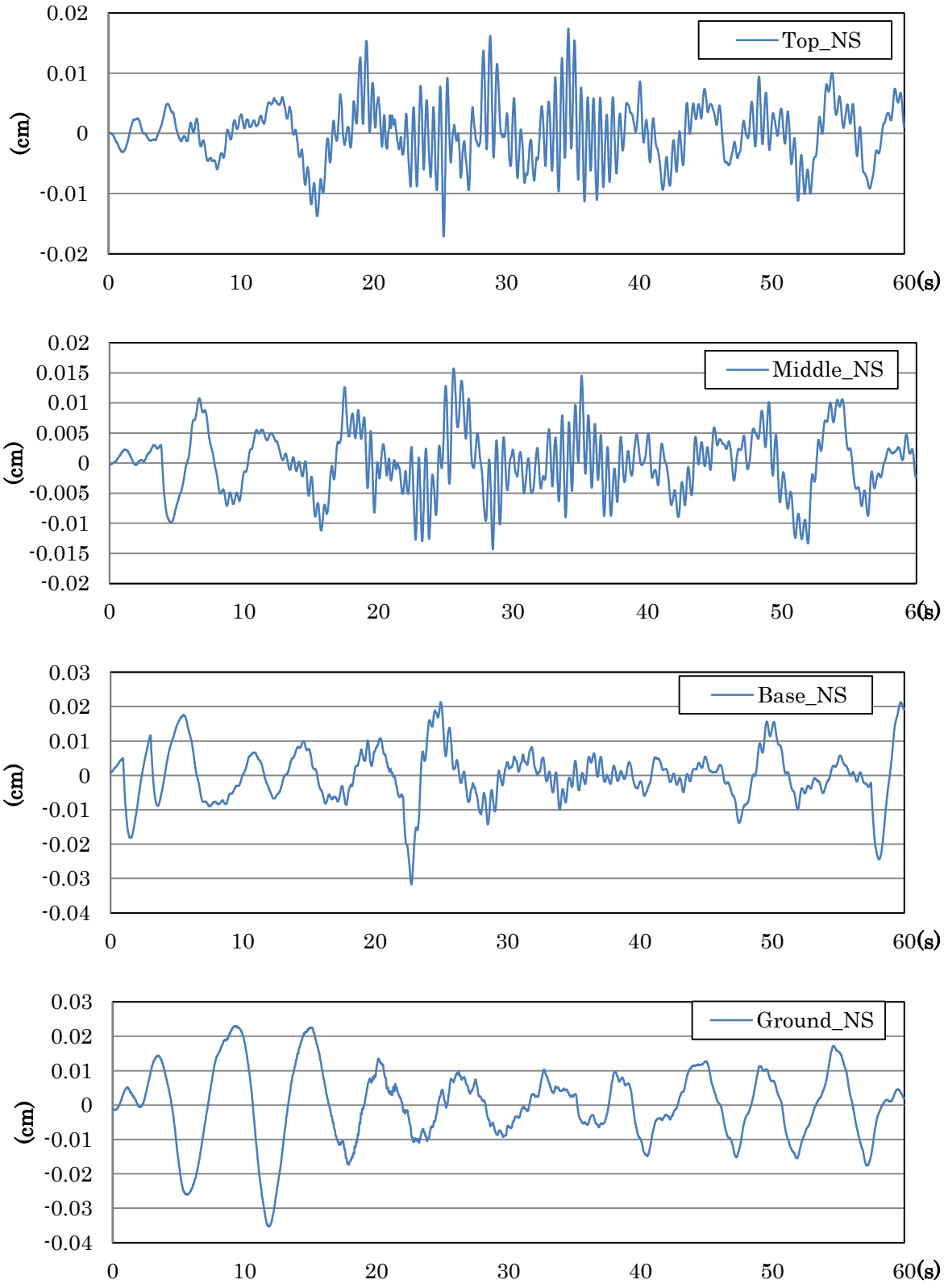

Fig. 3-50　Displacement time history of the record in NS direction

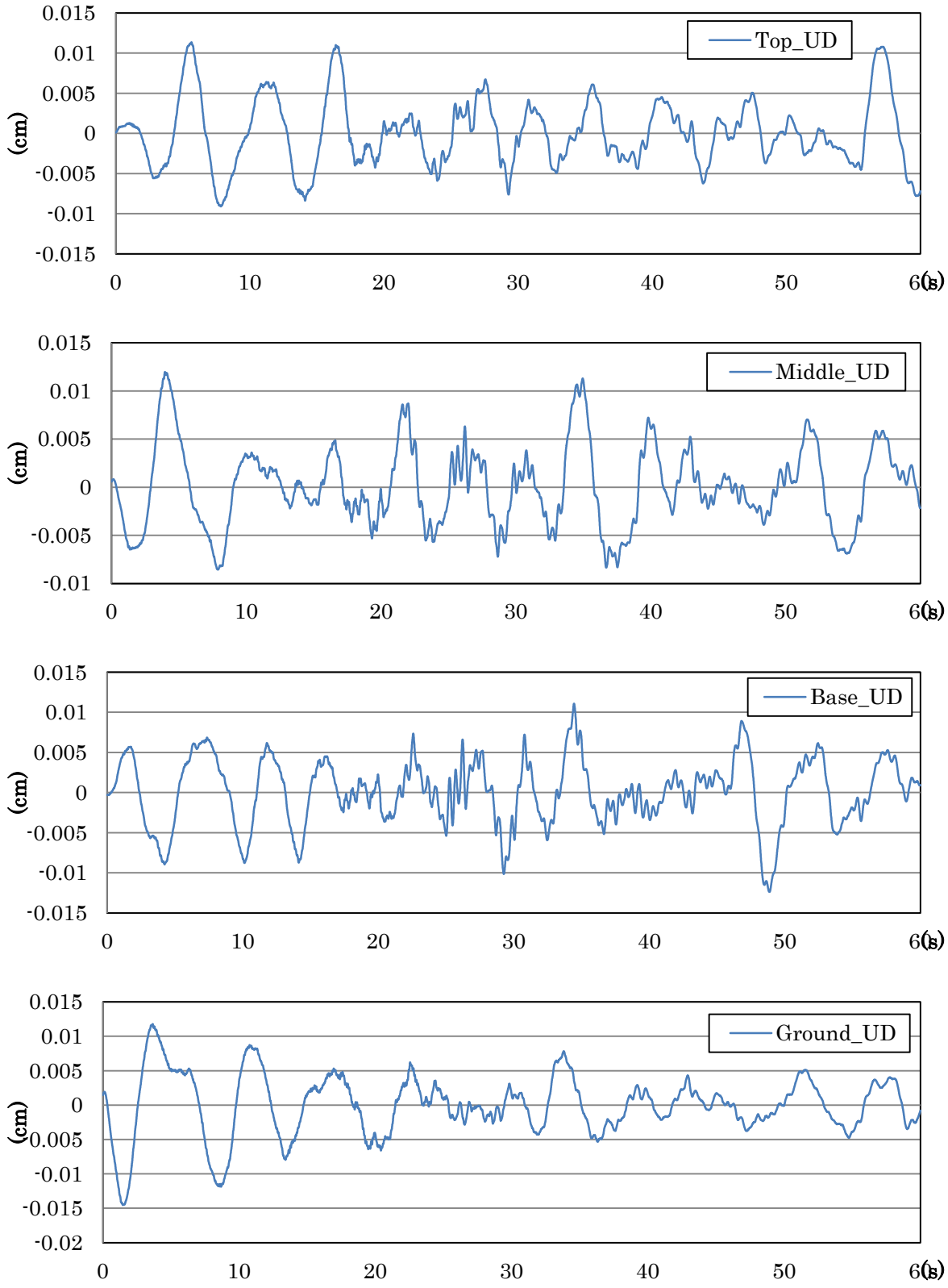

Fig. 3-51　Displacement time history of the record in UD direction

Fig. 3-52 shows the orbit at the Top, Middle, Base and Ground, respectively.

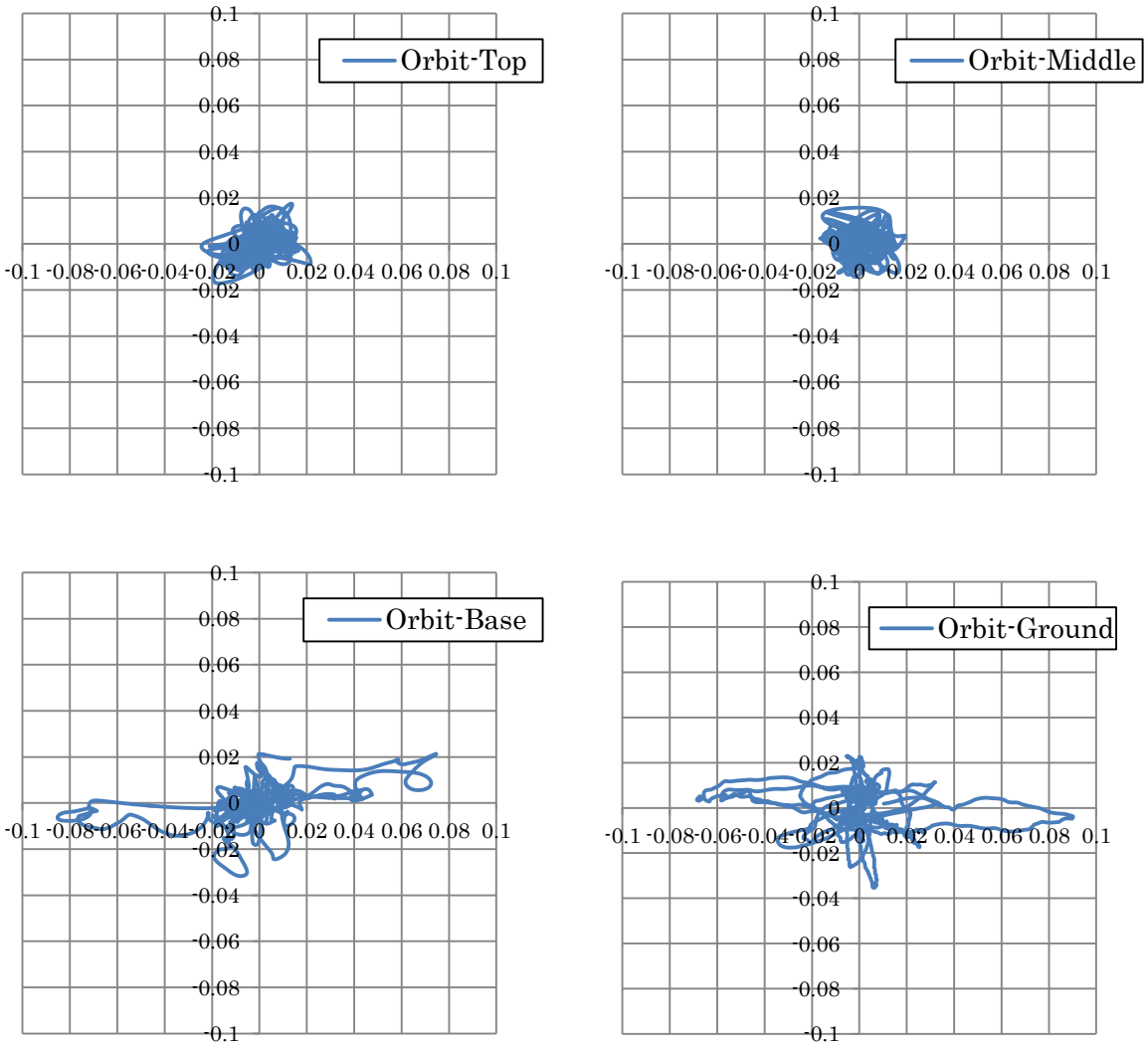

Fig. 3-52 Orbit at the point of the seismographs

Figs. 3-53 and 3-54 show Acceleration Fourier spectra in the EW and NS directions at the four points. Those spectra were smoothed with the Parzen Spectrum Window of 0.5 Hz.

Figs. 3-55 and 3-56 show Acceleration response spectra.

Figs. 3-57 to 3-60 show transfer functions calculated that were smoothed with the Parzen Spectrum Window of 0.5 Hz.

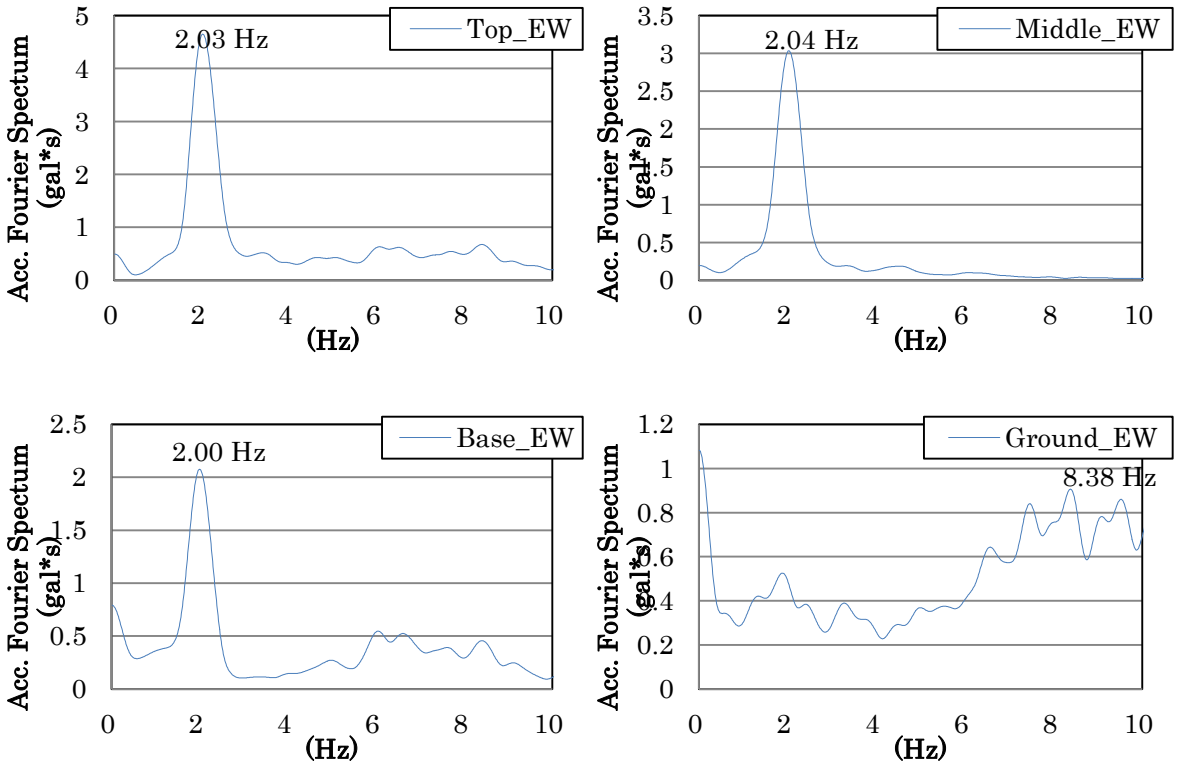

Fig. 3-53　Acc. Fourier Spectra; EW direction

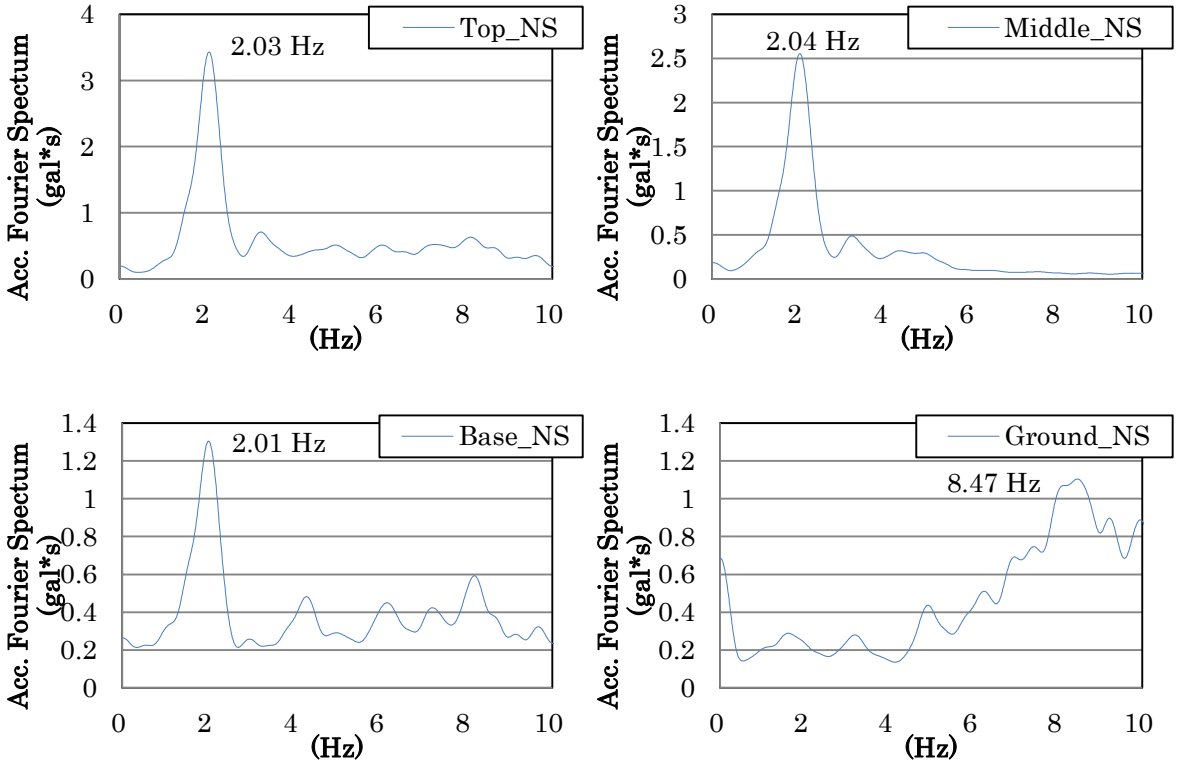

Fig. 3-54　Acc. Fourier Spectra; NS direction

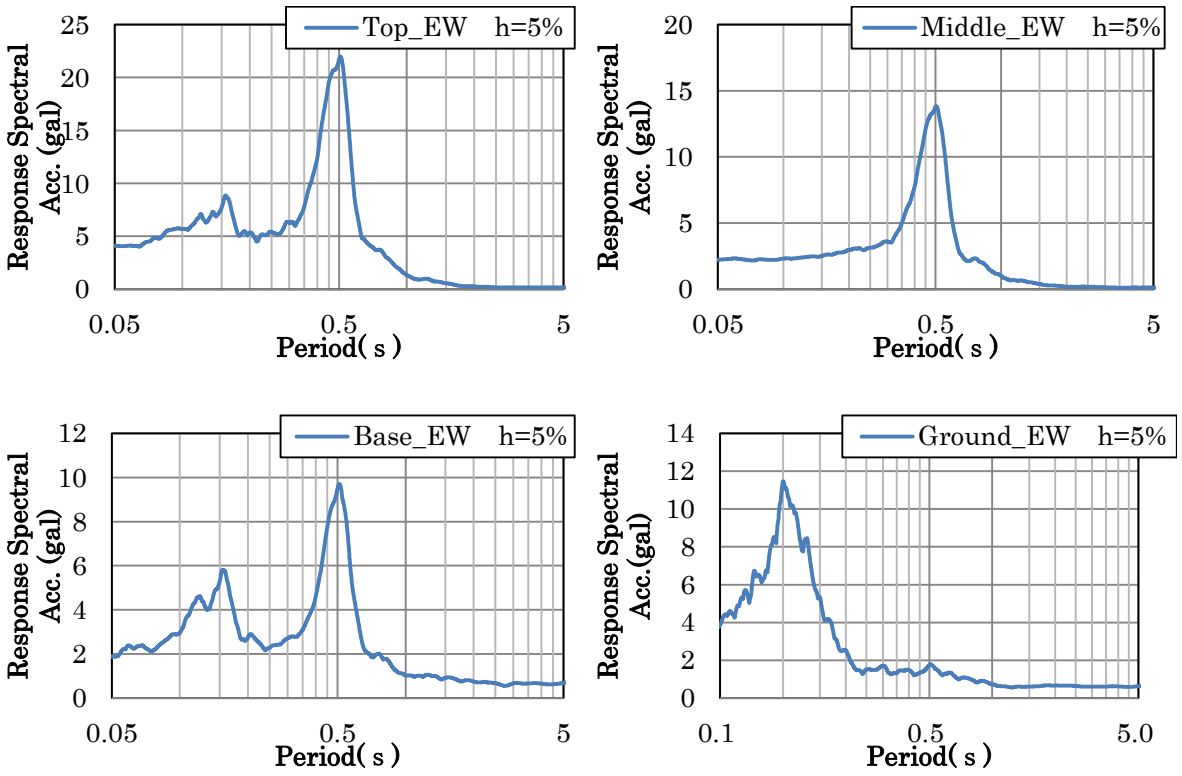

Fig. 3-55 Acc. Response Spectra; EW direction

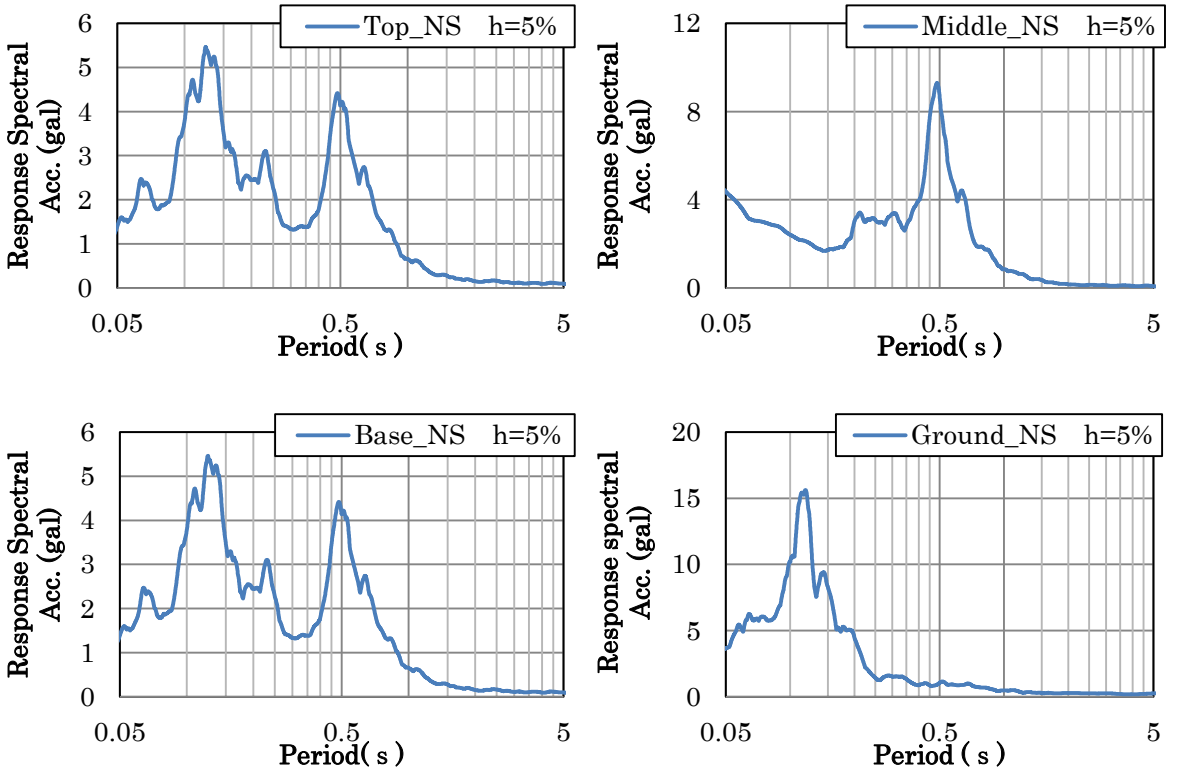

Fig. 3-56 Acc. Response Spectra; NS direction

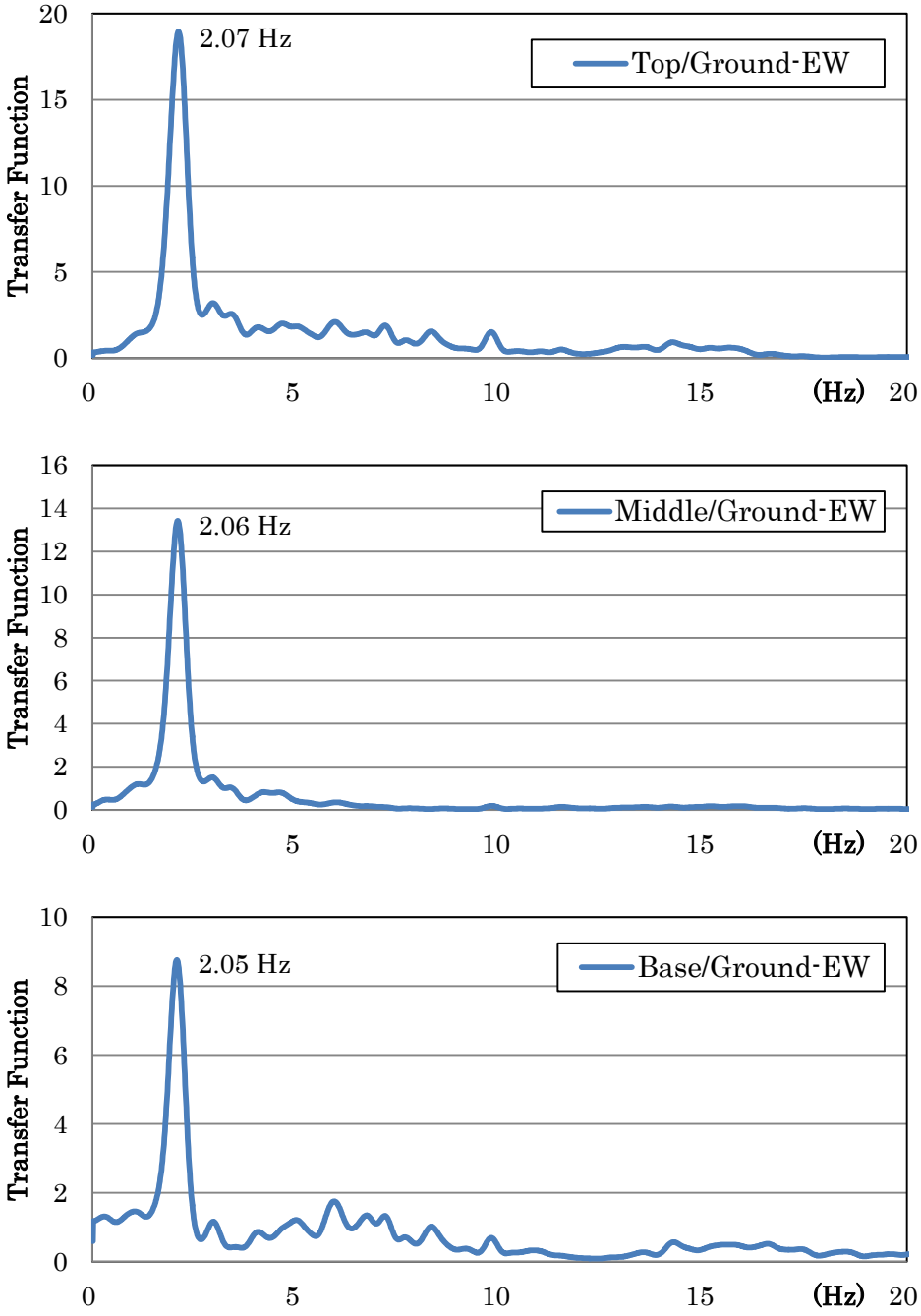

Fig. 3-57　Transfer Function of the record at the Ground; EW direction

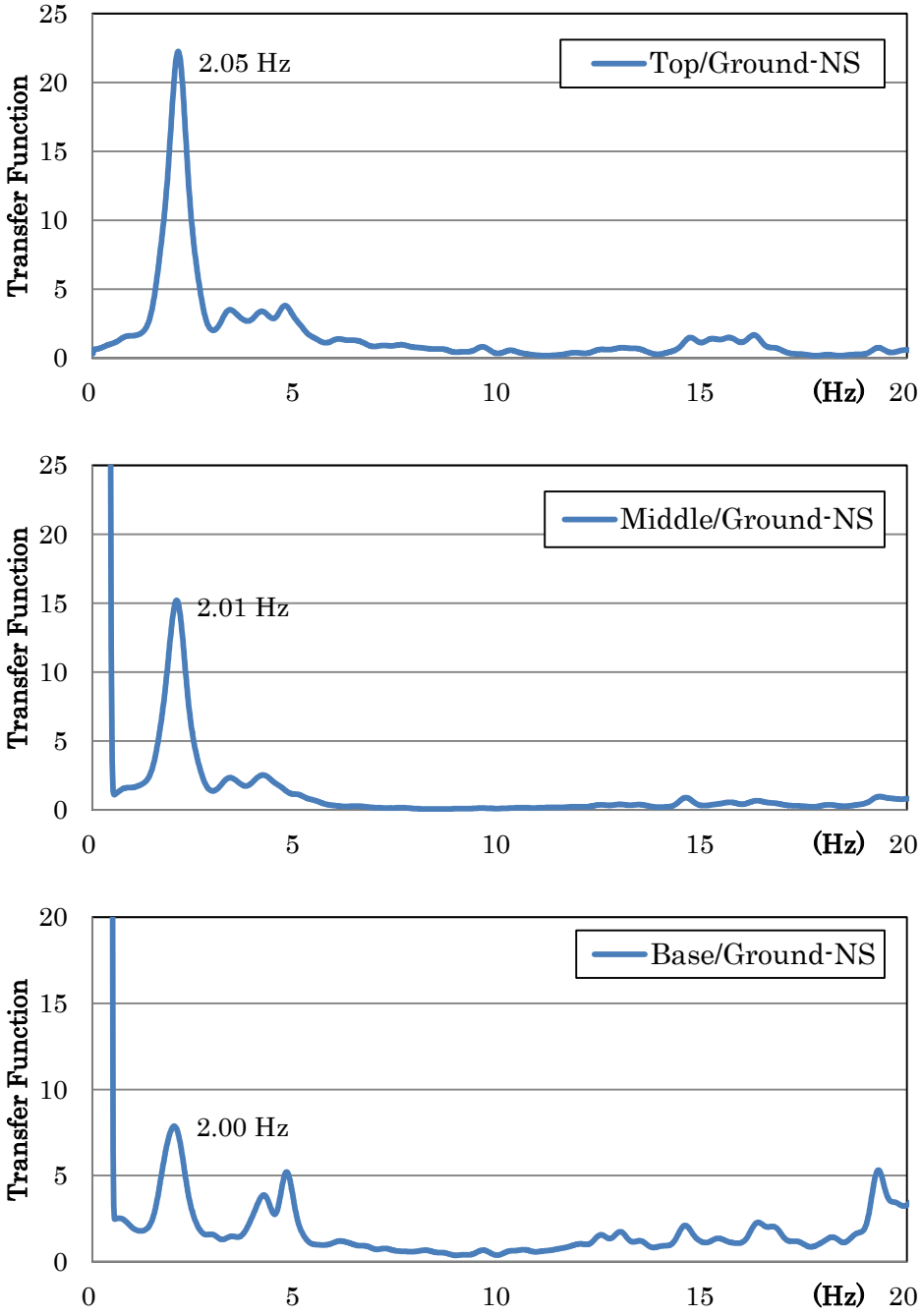

Fig. 3-58　Transfer Function of the record at the Ground; NS direction

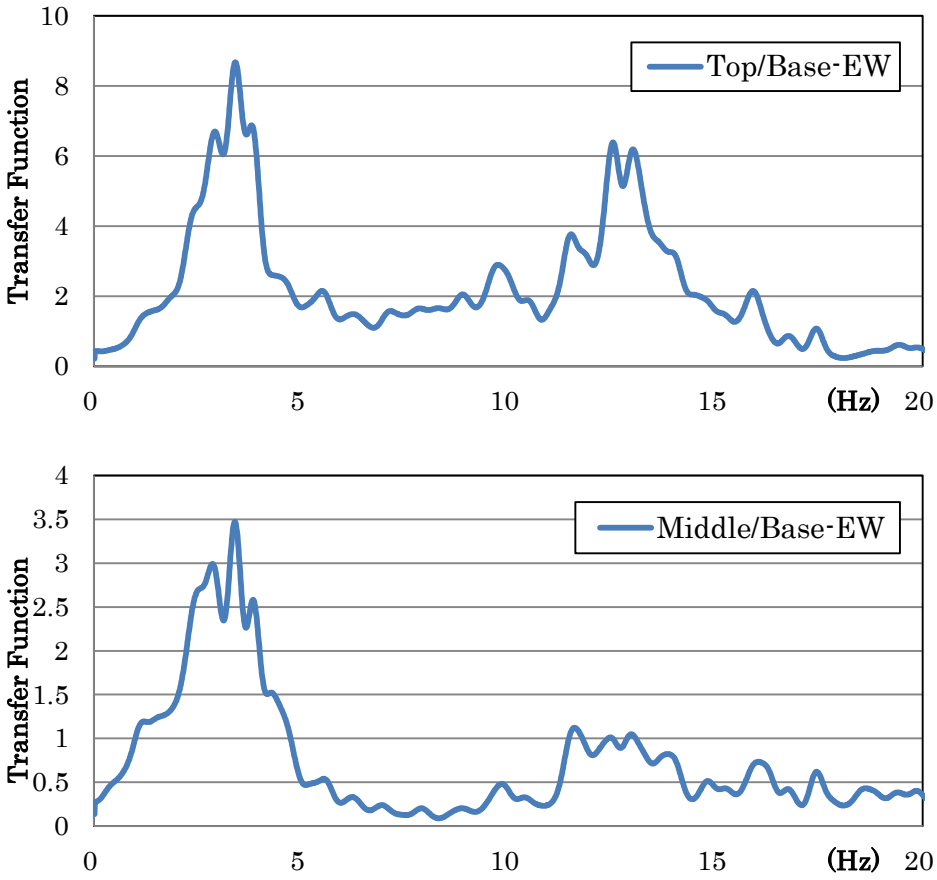

Fig. 3-59　Transfer Function of the record at the Base; EW direction

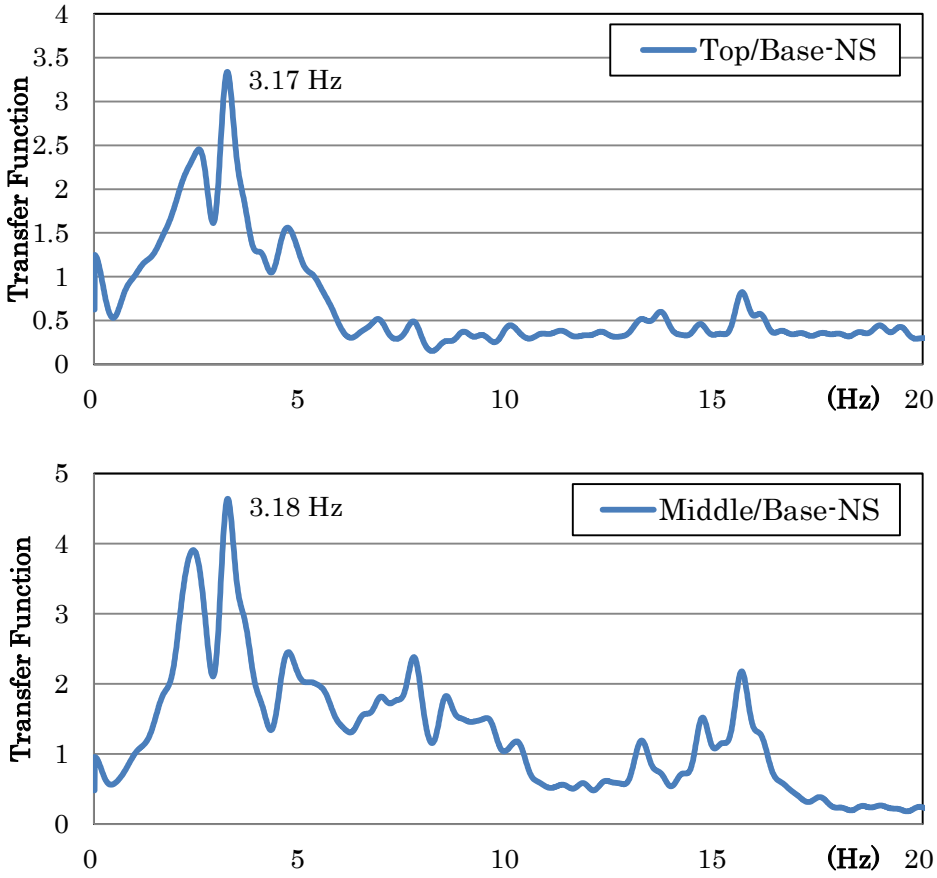

Fig. 3-60　Transfer Function of the record at the Base; NS direction

Transfer functions showed their natural frequency was 2.06 Hz in EW direction and 2.00 Hz in NS direction at the event on November 24th, 2011.

III) Earthquake record on March 19th, 2010

An earthquake occurred at 9:19 in the morning (local time) on March 19th, 2012. Table. 3-7 shows the detail of this earthquake. Its epicenter was located at 8.09 S, 110.3 E at a distance of 20km Southeast from Bantul with the focal depth of 10 km. The local magnitude was reported to be 4.2. The location of the epicenter is estimated to be shown in Fig. 3-61. The epicentral distance to the Prambanan Temple was estimated to be approximately 40 km. Table. 3-8 shows the peak amplitudes of these time histories, as shown in Figs. 3-62 to 3-64. Figs. 3-65 to 3-67 and Figs. 3-68 to 3-70 show the velocity time histories and the displacement time histories, respectively.

Table. 3-7 Earthquake data of the event on March 19th, 2012

Local Time	Lat.	Lon.	Depth	M_L	Epicentral Dist.
9:19	8.09 S	110.3 E	10 km	4.2	40 km

Table. 3-8 Peak amplitudes of the records on the March 19th, 2012 event

		Acceleration (gal)		Velocity (kine)		Displacement (cm)	
		Max	Min	Max	Min	Max	Min
EW	Top	12.3	-12.7	0.77	-0.54	0.061	-0.038
	Middle	4.9	-4.9	0.39	-0.30	0.027	-0.026
	Base	6.3	-6.9	0.27	-0.33	0.079	-0.070
	Ground	9.1	-9.8	0.19	-0.21	0.076	-0.092
NS	Top	17.2	-8.7	0.556	-0.62	0.018	-0.018
	Middle	8.1	-5.9	0.45	-0.37	0.024	-0.024
	Base	5.5	-5.9	0.28	-0.26	0.033	-0.029
	Ground	9.7	-11.0	0.25	-0.24	0.029	-0.051
UD	Top	3.5	-3.8	0.09	-0.11	0.013	-0.013
	Middle	4.3	-3.8	0.13	-0.15	0.010	-0.012
	Base	4.5	-3.7	0.17	-0.15	0.018	-0.017
	Ground	6.2	-5.7	0.15	-0.14	0.011	-0.016

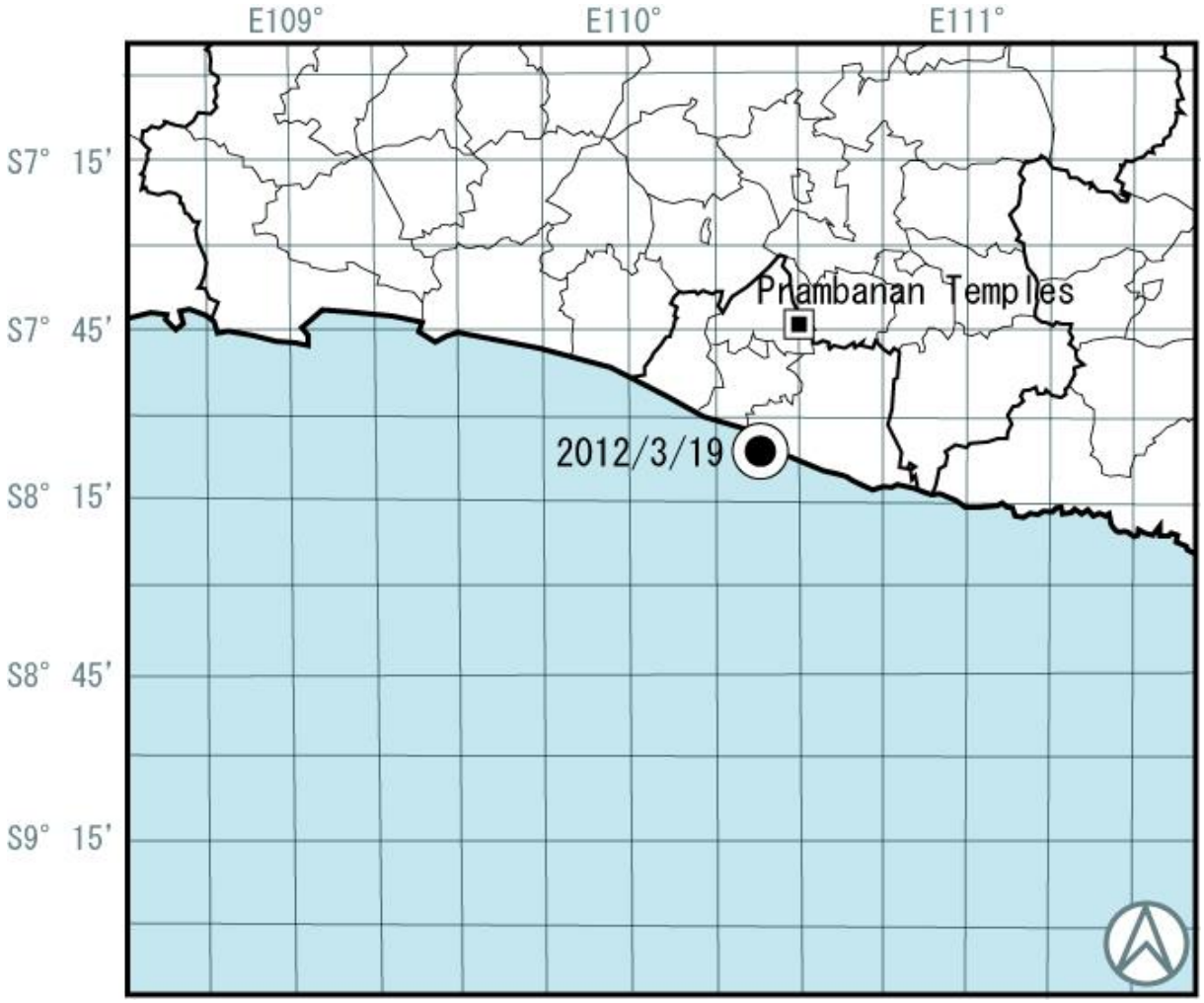

Fig. 3-61　Epicenter of the event on March 19th, 2012

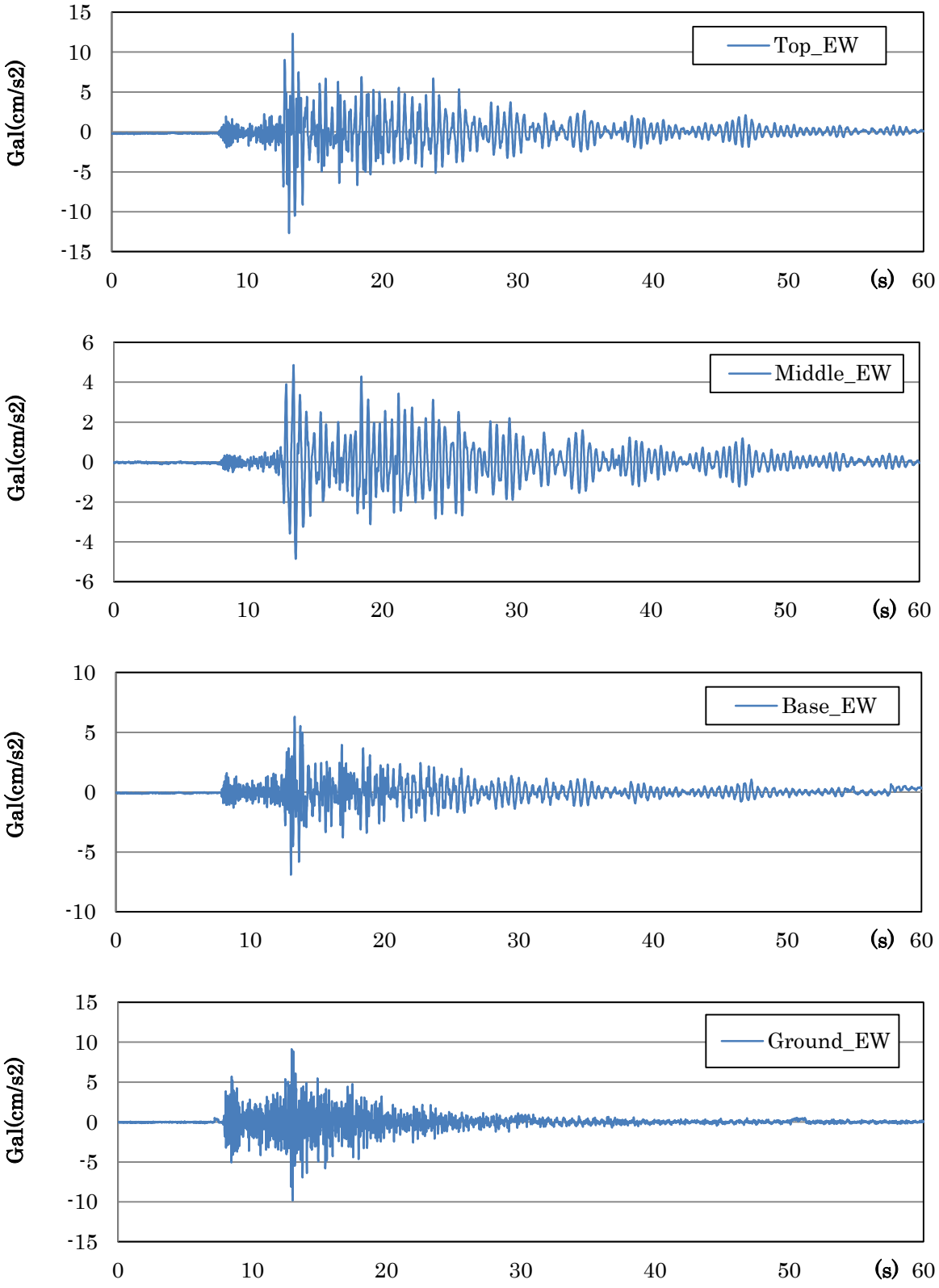

* 980 gal = 1 G

Fig. 3-62　Acceleration time history of the record in EW direction

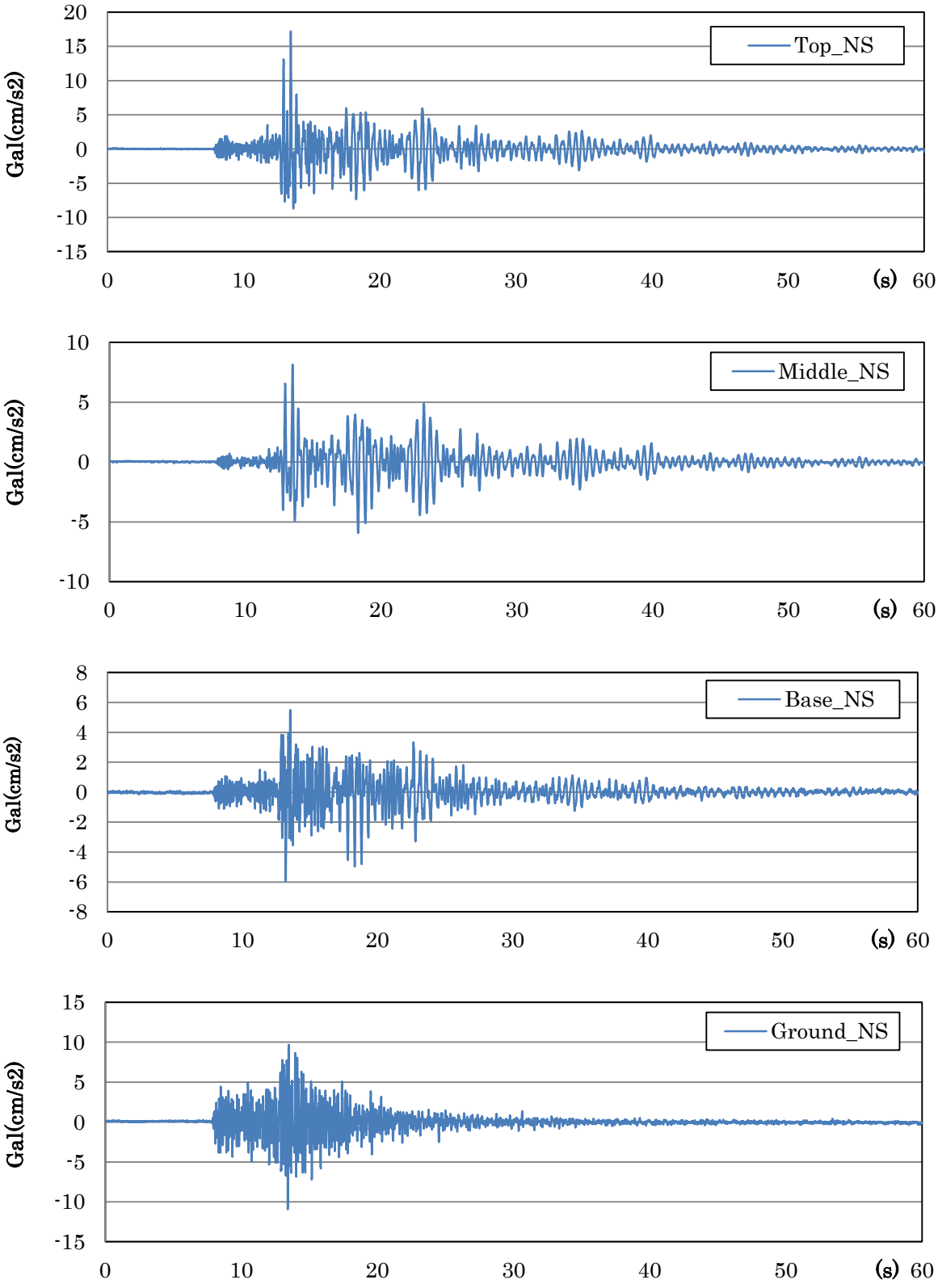

* 980 gal = 1 G

Fig. 3-63　Acceleration time history of the record in NS direction

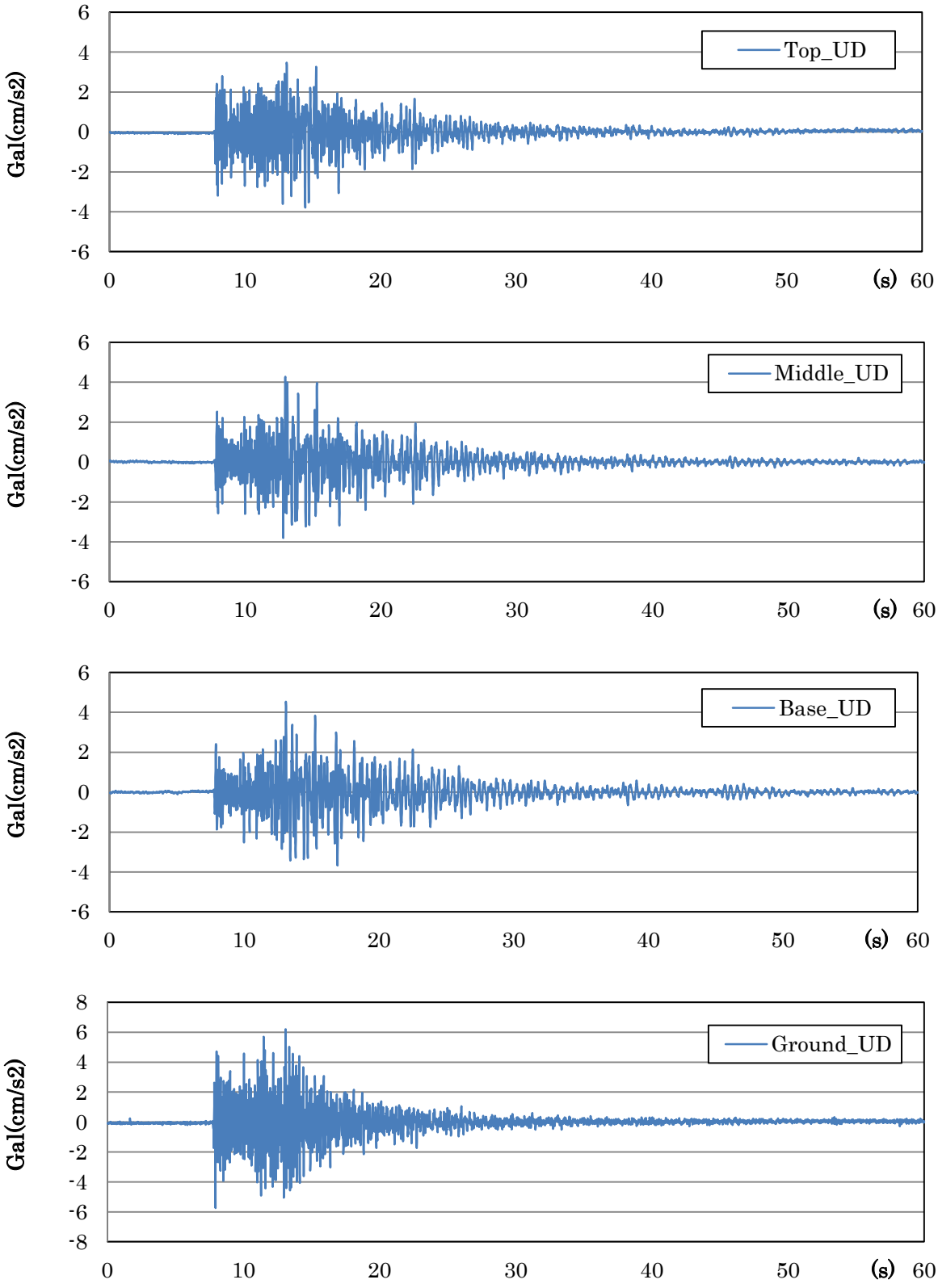

* 980 gal = 1 G

Fig. 3-64　Acceleration time history of the record in UD direction

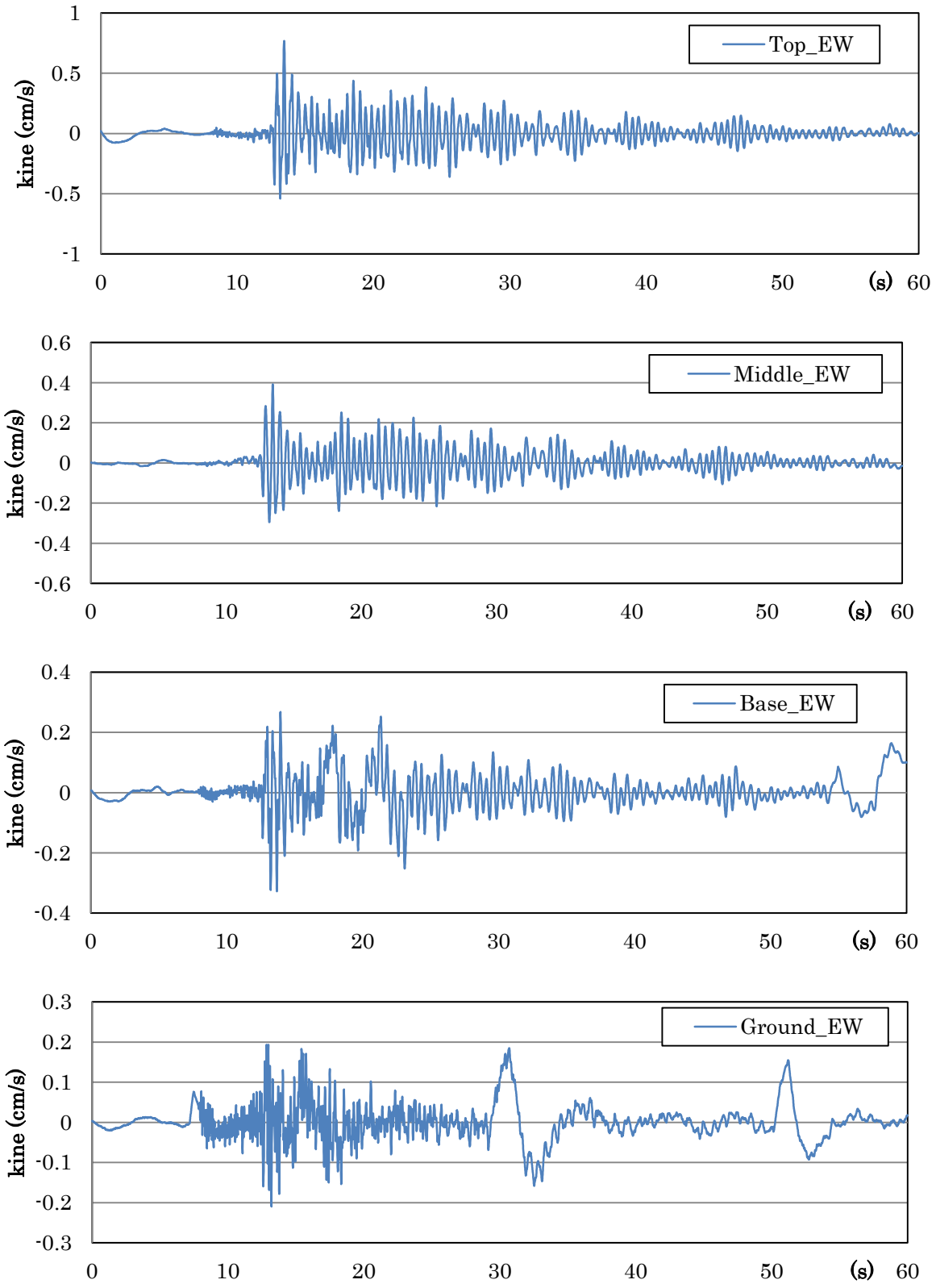

Fig. 3-65　Velocity time history of the record in EW direction

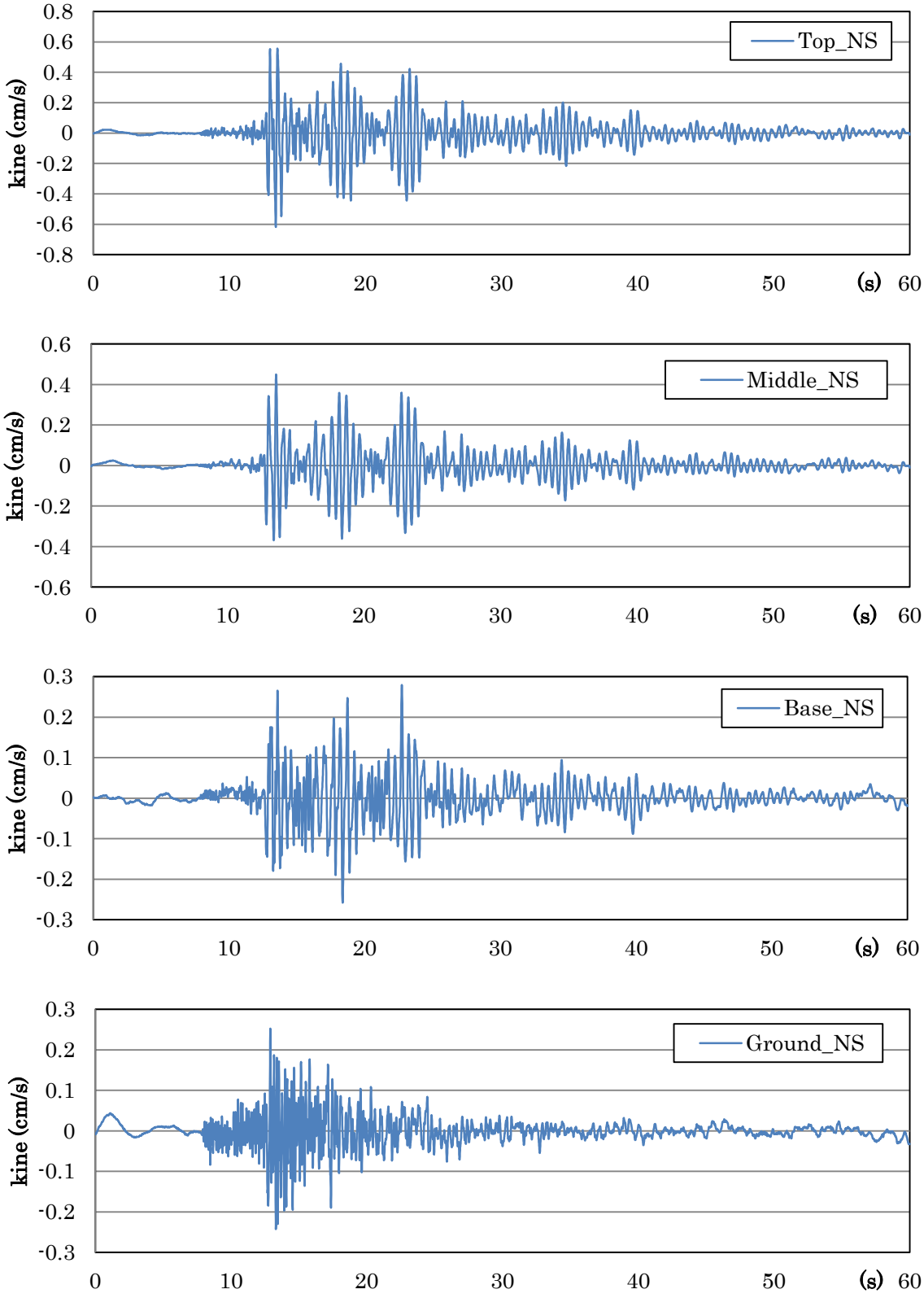

Fig. 3-66　Velocity time history of the record in NS direction

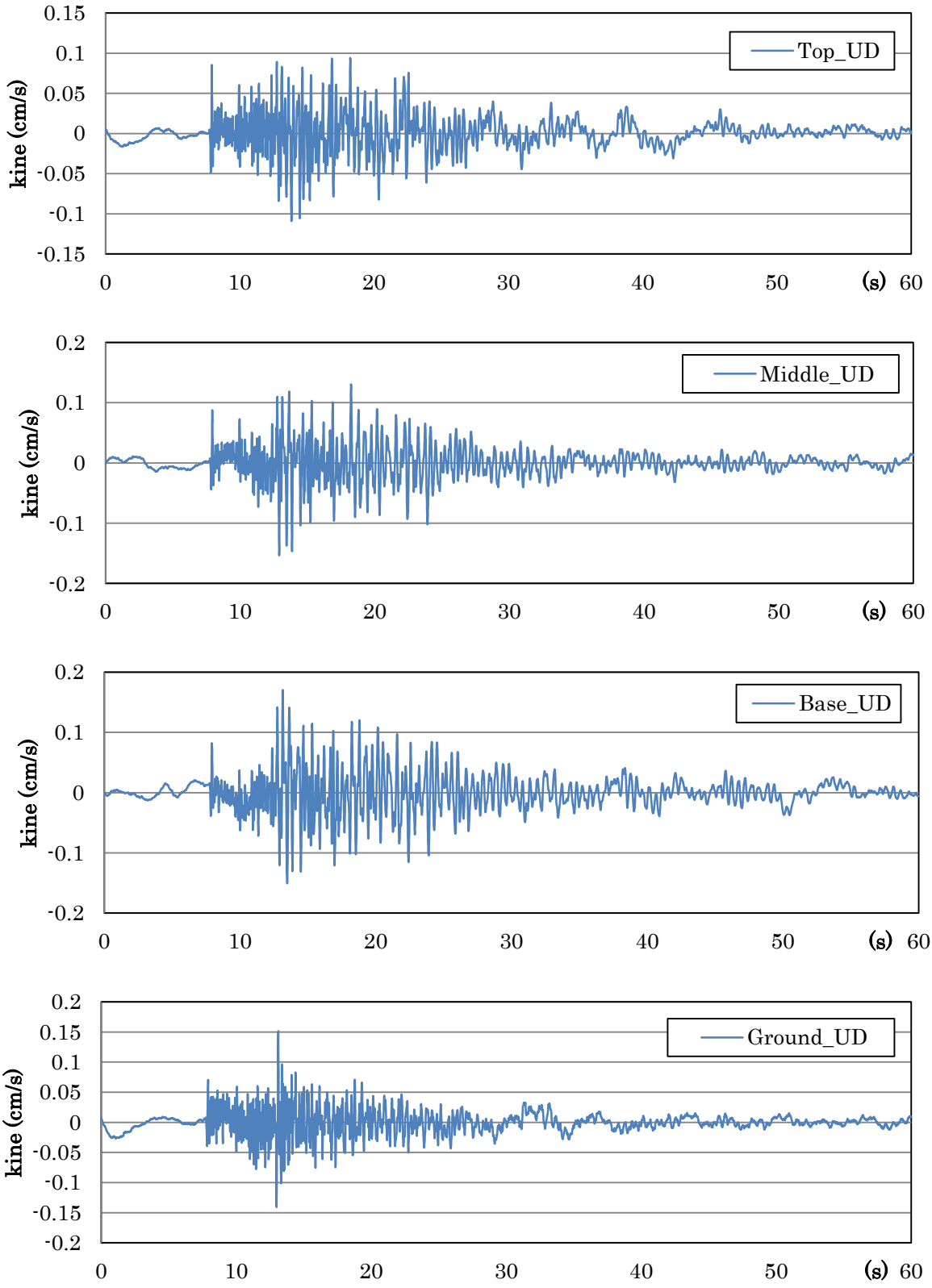

Fig. 3-67　Velocity time history of the record in UD direction

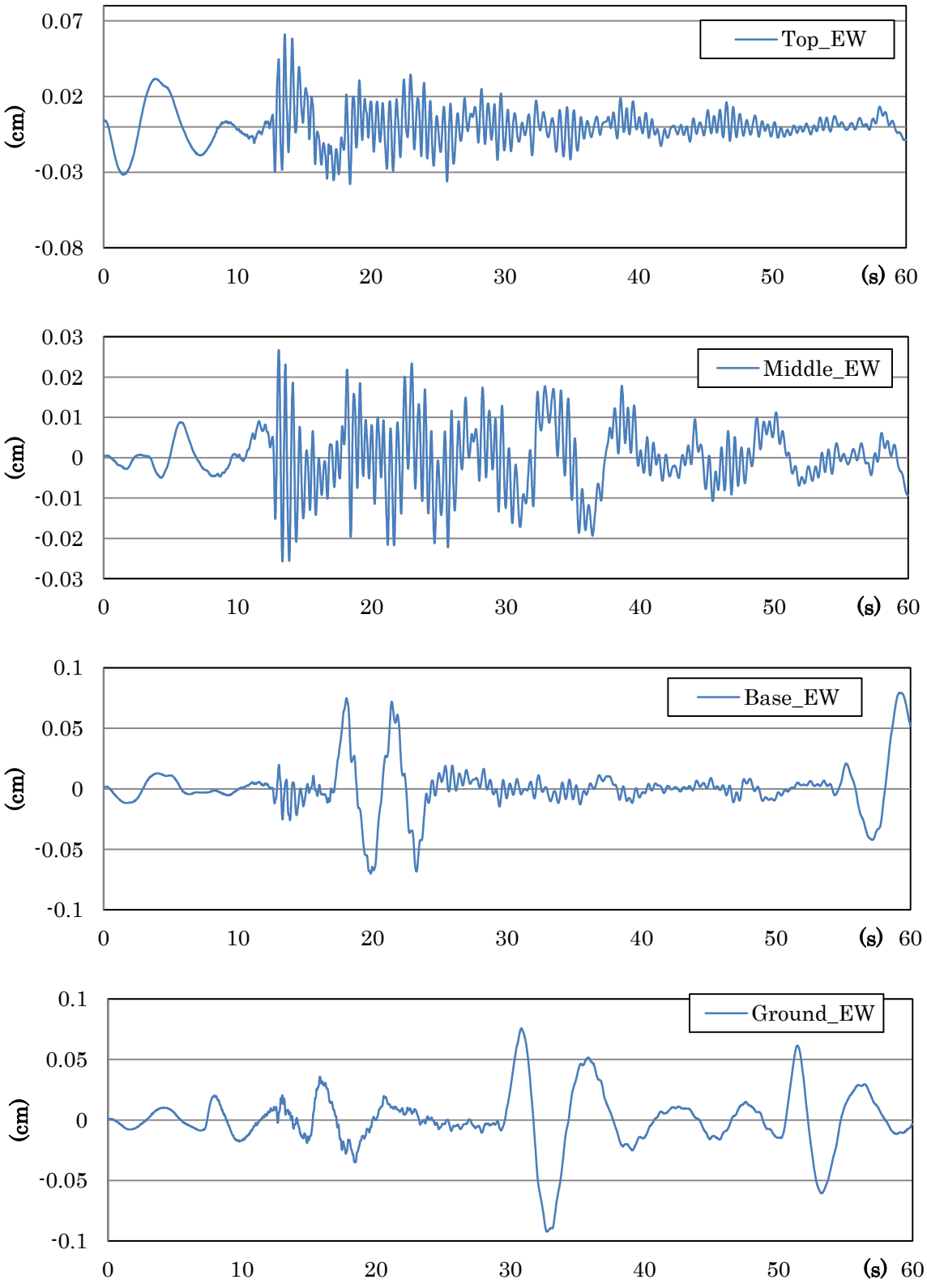

Fig. 3-68　Displacement time history of the record in EW direction

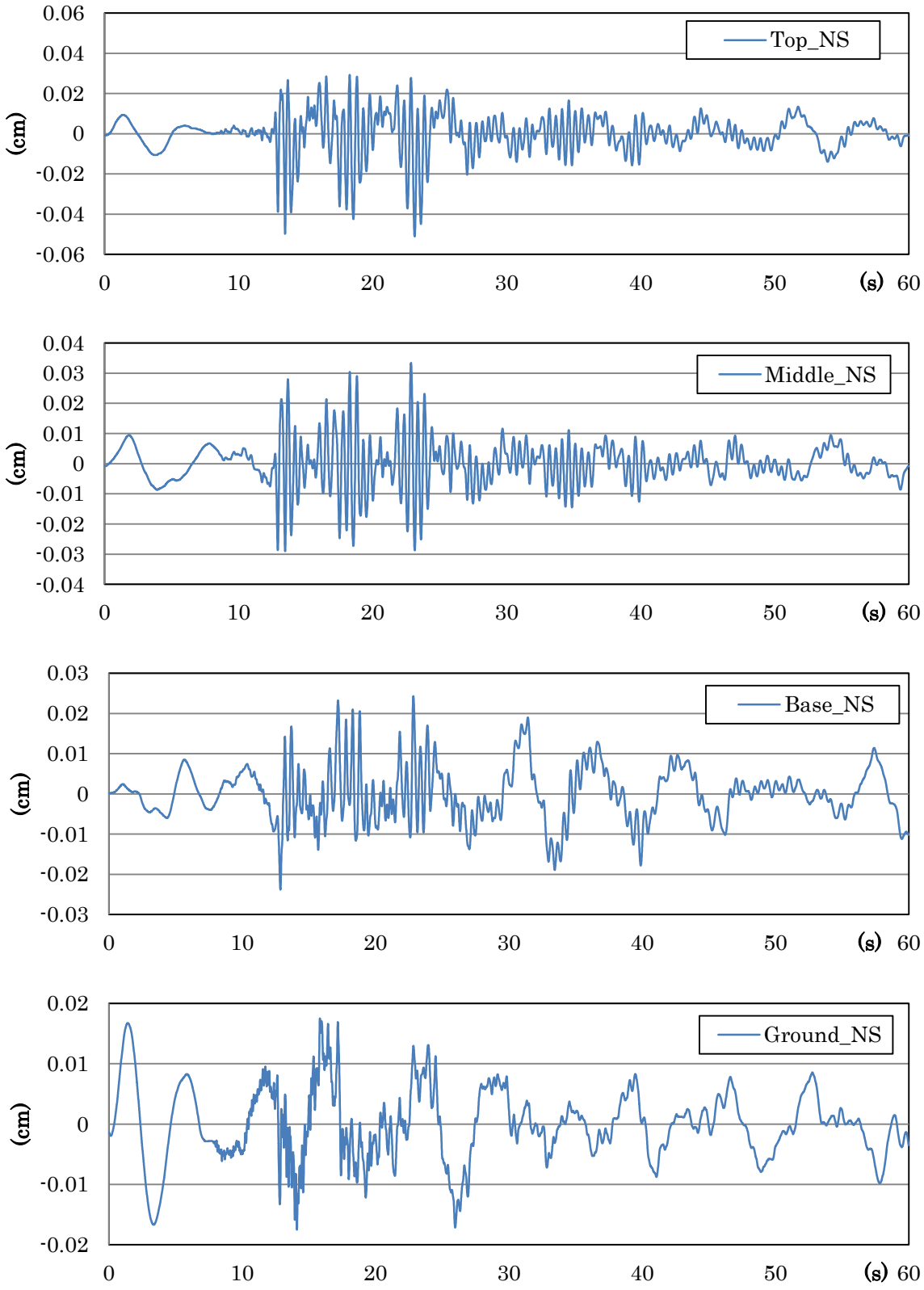

Fig. 3-69　Displacement time history of the record in NS direction

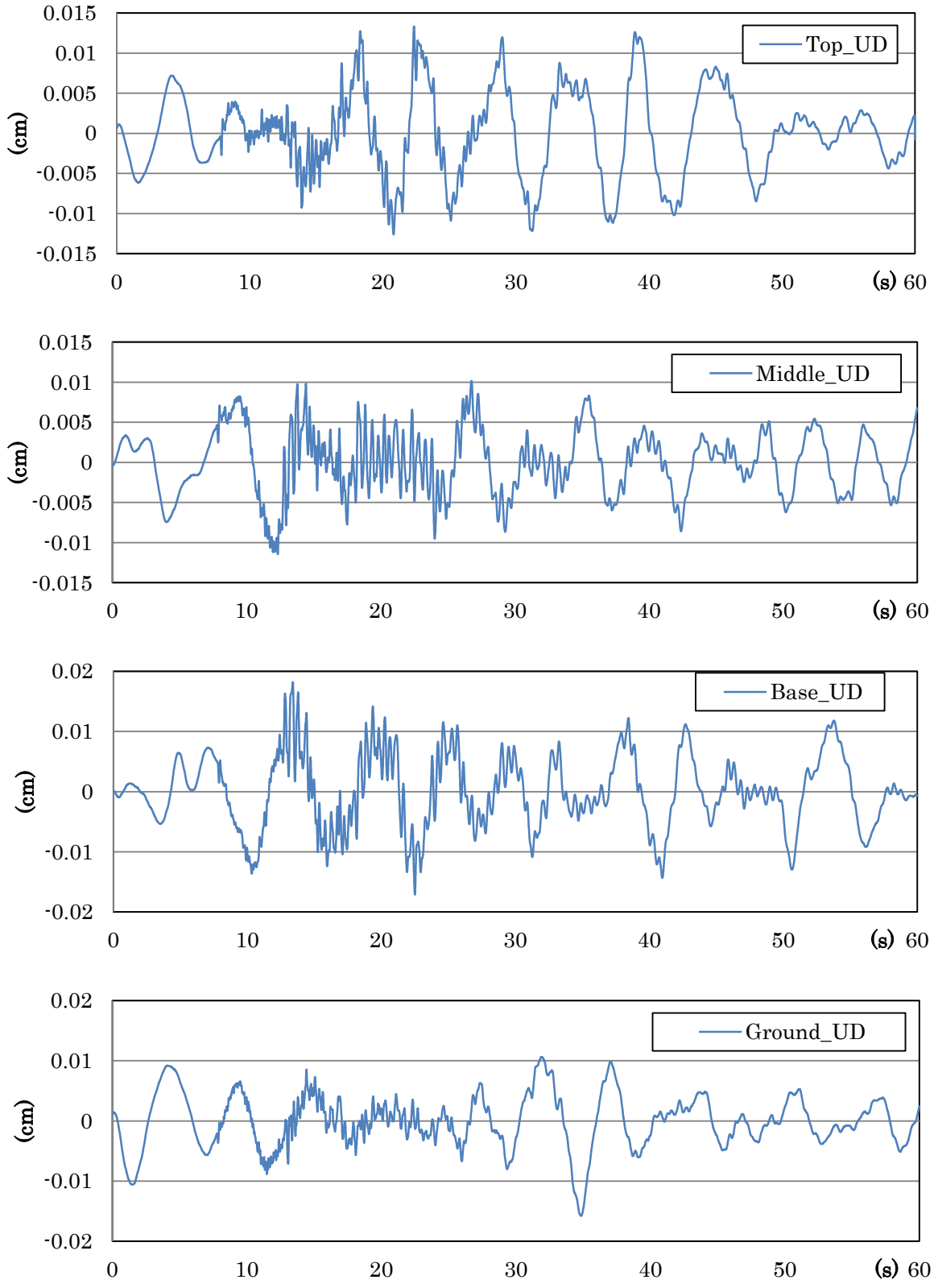

Fig. 3-70　Displacement time history of the record in UD direction

Figs. 3-71 shows the orbit at the Top, Middle, Base and Ground, respectively.

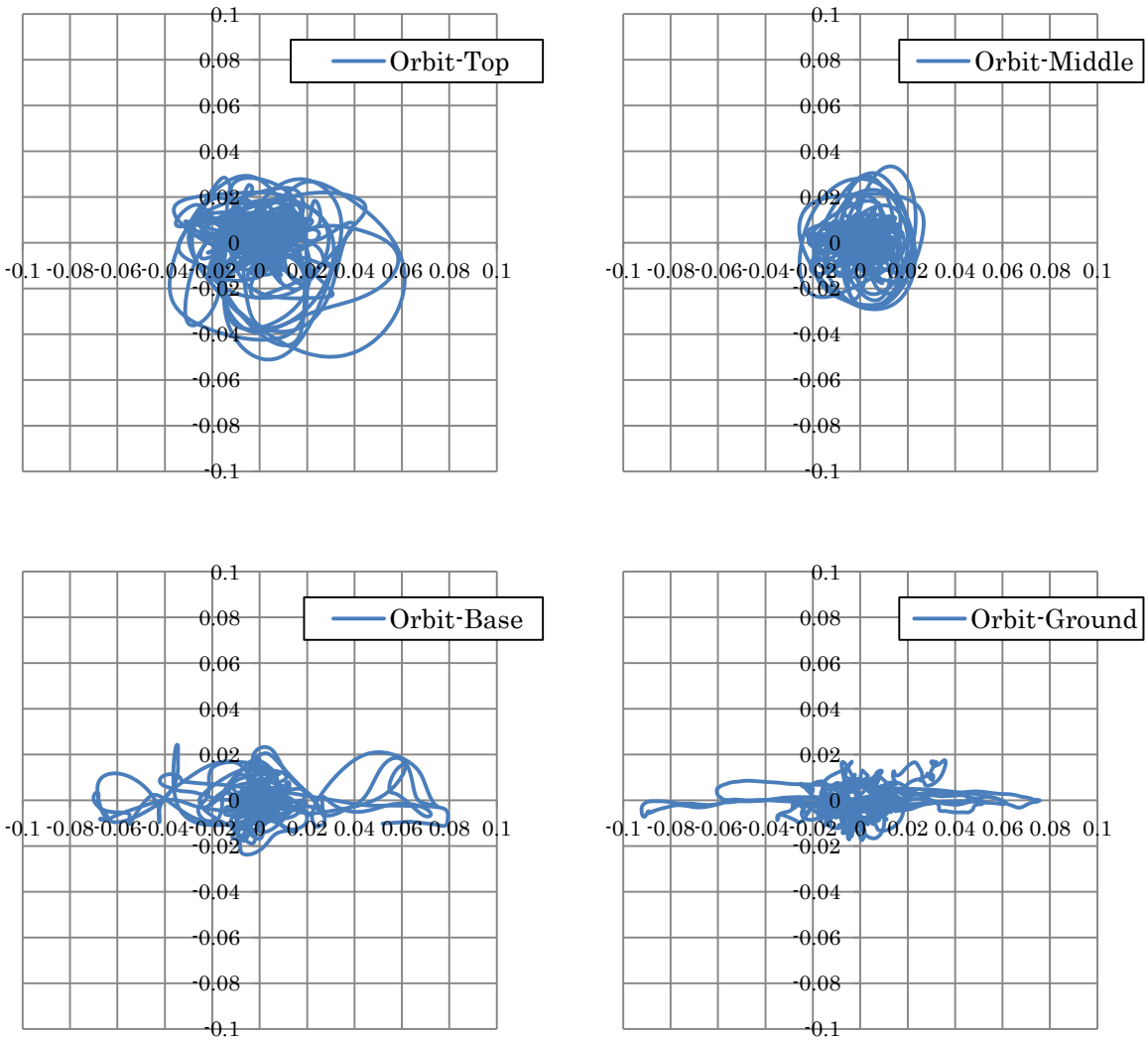

Fig. 3-71　Particle orbit at the point of the seismograms

Acceleration Fourier spectra, Acceleration response spectra and transfer functions are shown in Figs. 3-72 to 3-79. Acceleration Fourier spectra and transfer functions were smoothed with the Parzen Spectrum Window of 0.5 Hz.

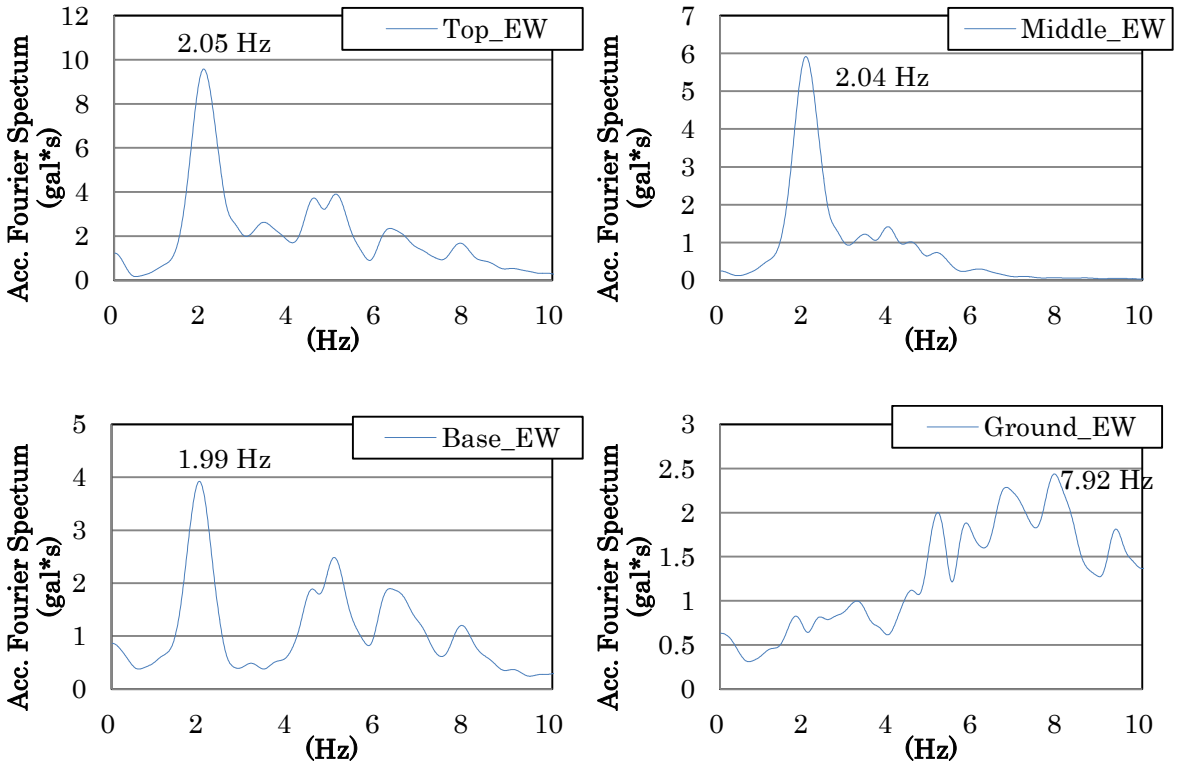

Fig. 3-72　Acc. Fourier Spectra; EW direction

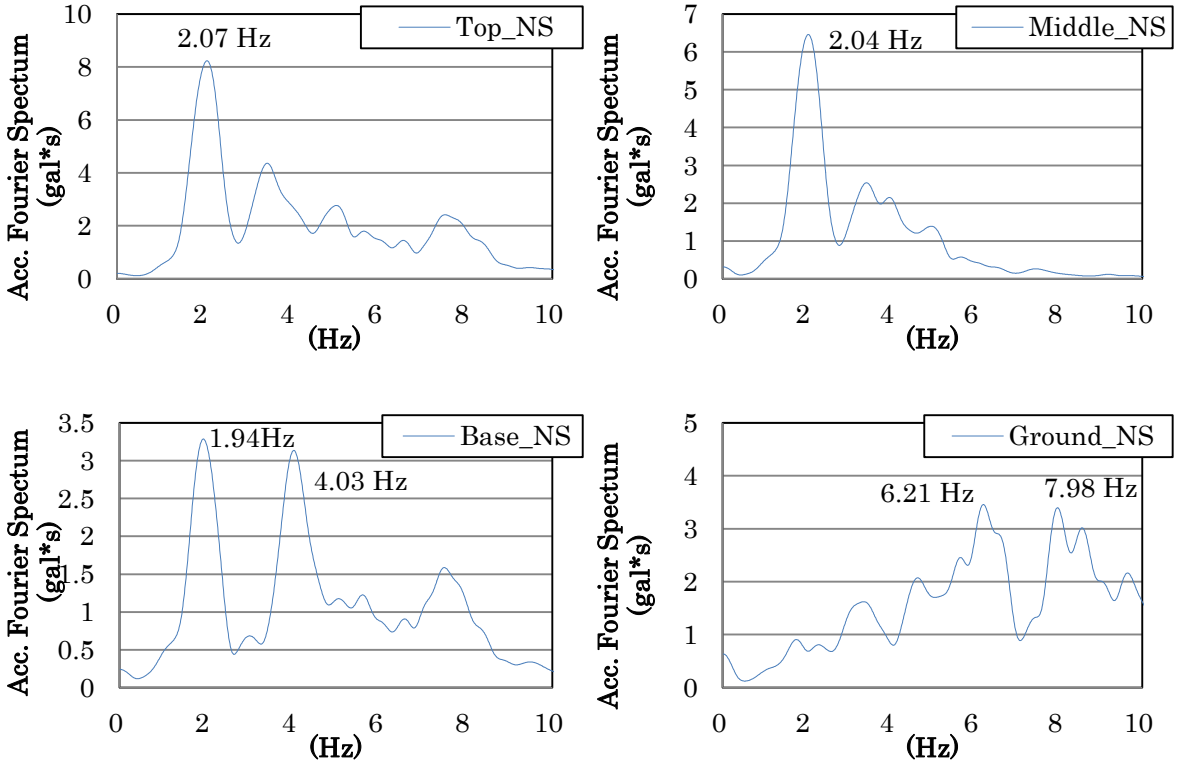

Fig. 3-73　Acc. Fourier Spectra; NS direction

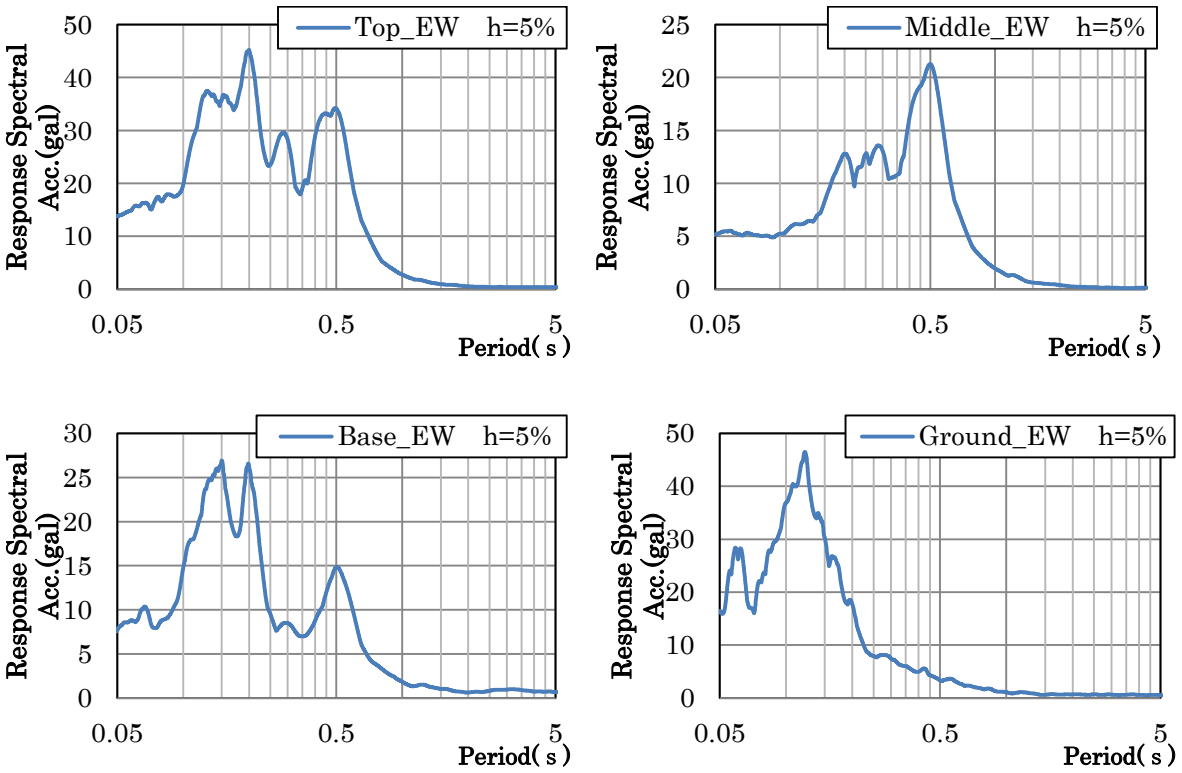

Fig. 3-74 Acc. Response Spectra; EW direction

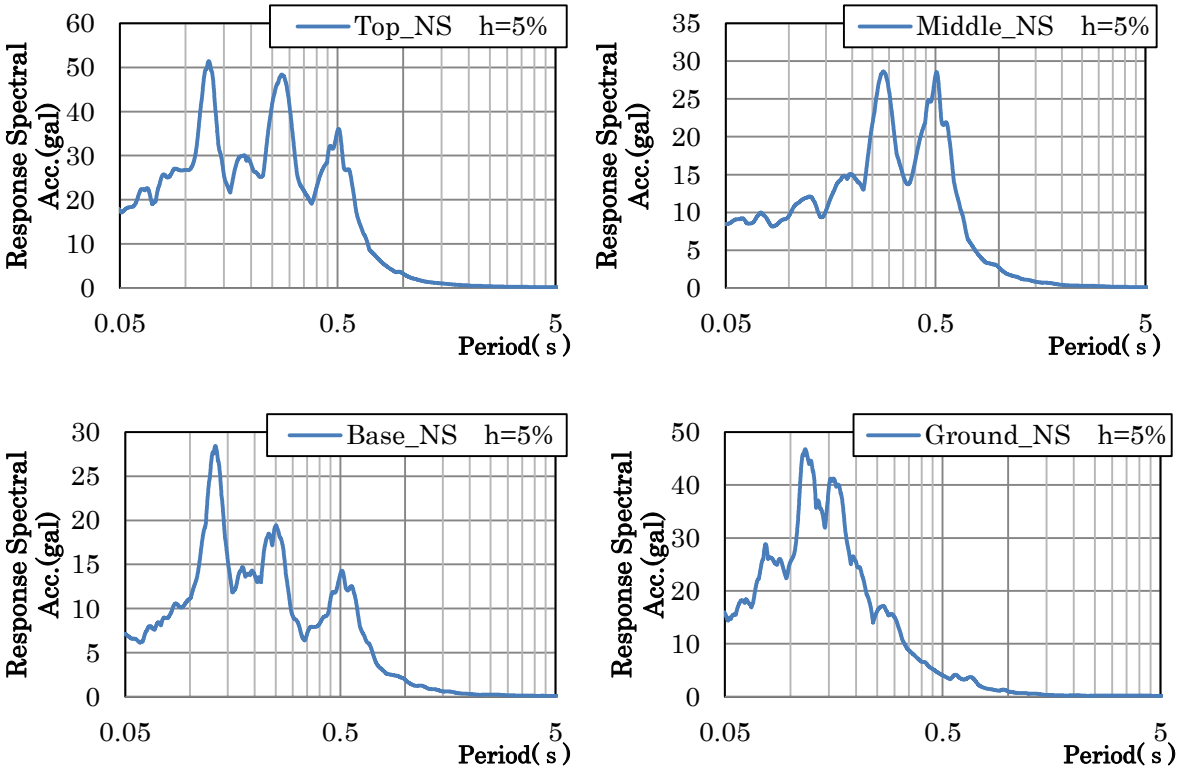

Fig. 3-75 Acc. Response Spectra; NS direction

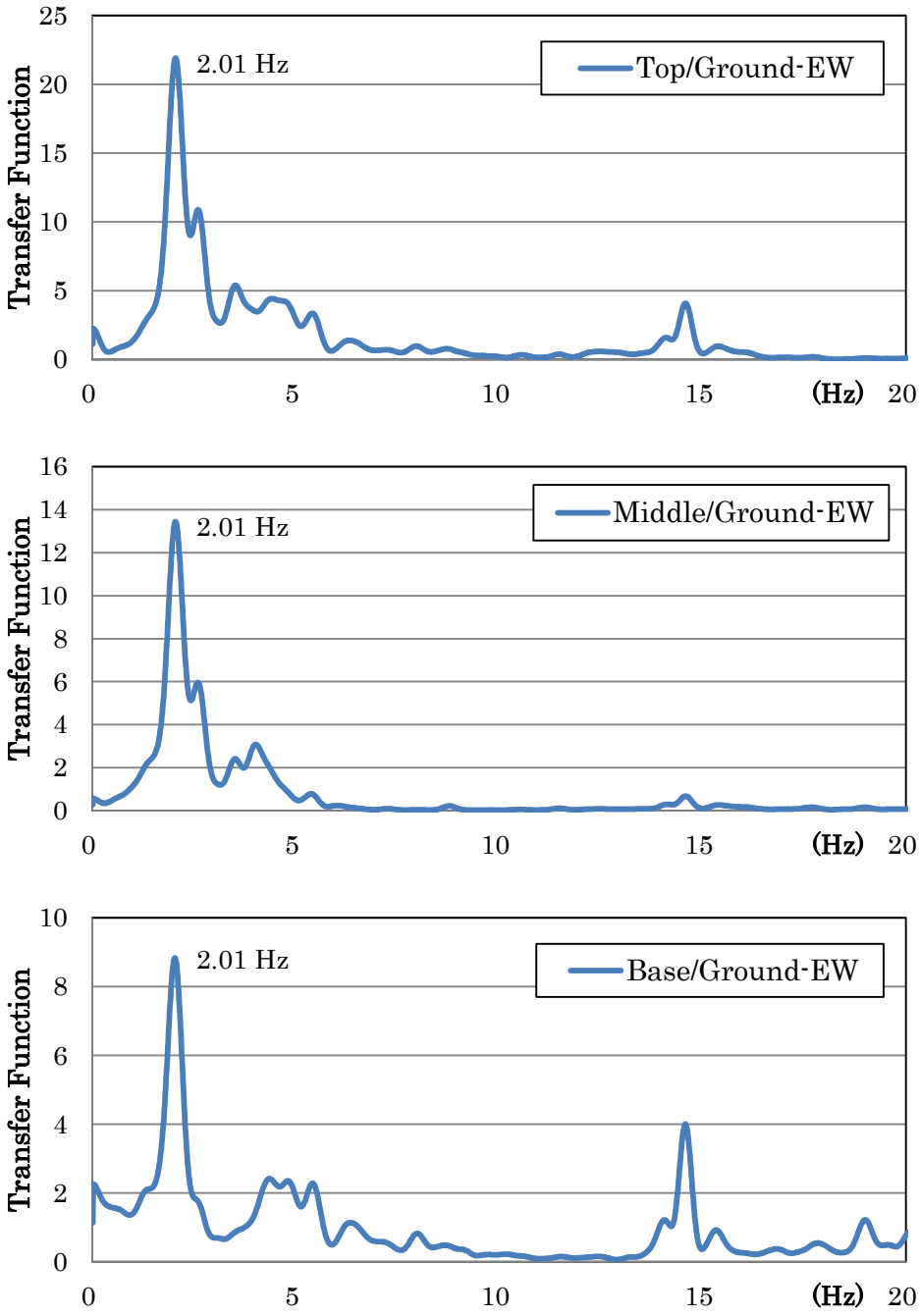

Fig. 3-76　Transfer Function of the record at the Ground; EW direction

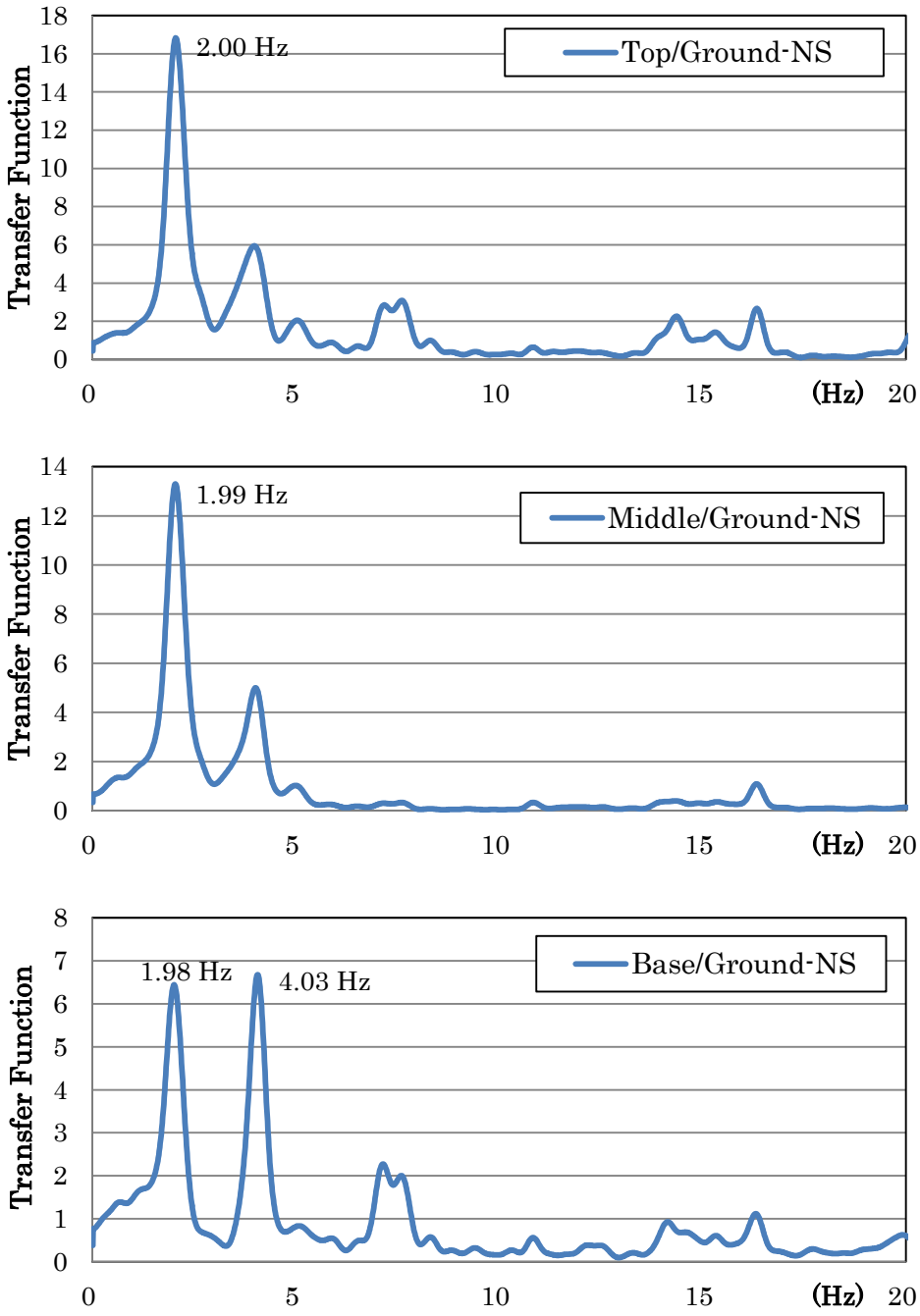

Fig. 3-77　Transfer Function of the record at the Ground; NS direction

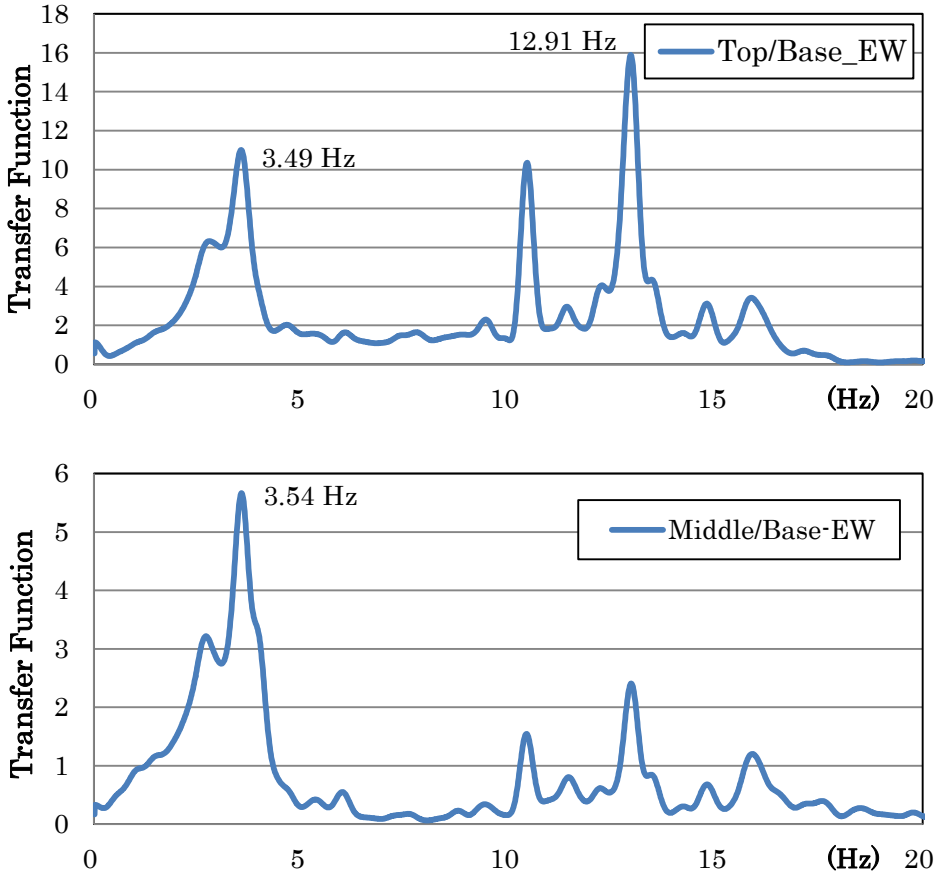

Fig. 3-78　Transfer Function of the record at the Base; EW direction

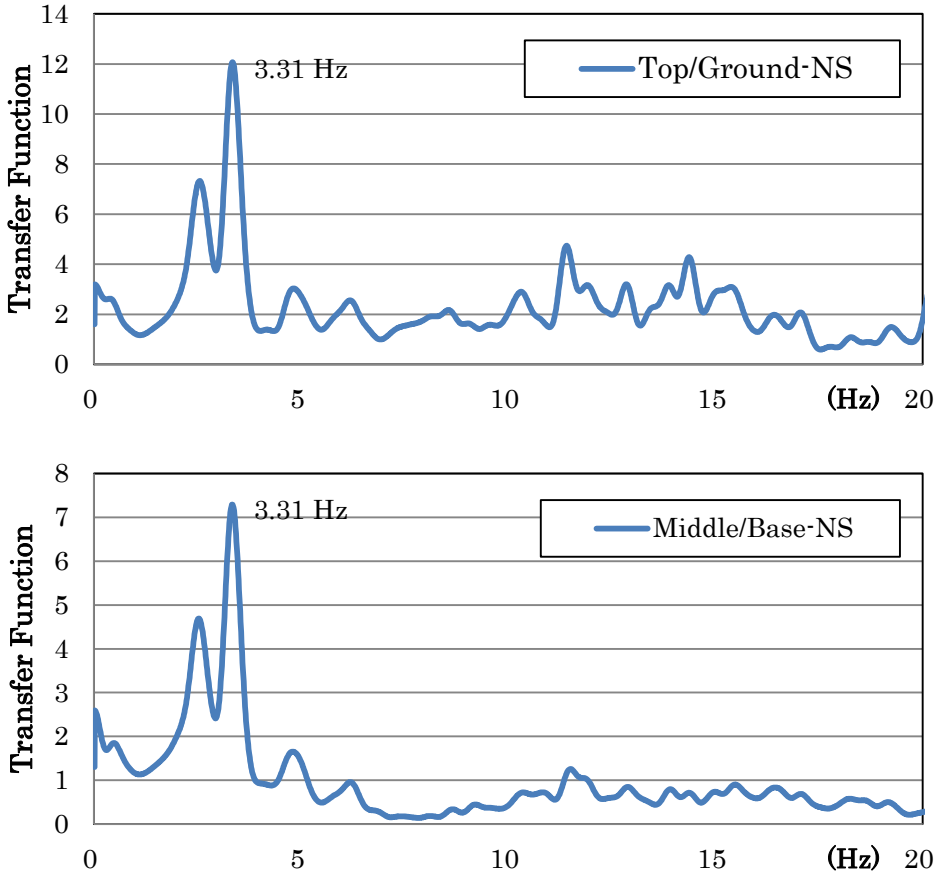

Fig. 3-79　Transfer Function of the record at the Base; NS direction

Transfer functions show the natural frequency of the Siva temple of 2.01 Hz in EW direction and 1.99 Hz in NS direction at this earthquake on March 19th, 2012.

IV) Earthquake record on May 22th, 2012

On May 22th, 2013, a small earthquake was recorded. Table. 3-9 shows the detail of this earthquake and Fig. 3-80 shows the location of the epicenter and the Prambanan temples. Figs. 3-81 to 3-83 show acceleration time histories. Figs. 3-84 to 3-86 and 3-87 to 3-89 show velocity time histories and displacement time histories, respectively.

The distorted time histories at the Top in the UD direction were considered to be miss-recording.

The peak amplitudes of the time histories at each point are shown in Table. 3-10.

Table. 3-9 Earthquake data of the event on May 22th, 2012

Local Time	Lat.	Lon.	Depth	M_L	Epicentral Dist.
22:36	8.81 S	110.16 E	63 km	4.7	123 km

Table. 3-10 Peak amplitudes of the records on the May 22th, 2012 event

		Acceleration (gal)		Velocity (kine)		Displacement (cm)	
		Max	Min	Max	Min	Max	Min
EW	Top	0.5	-0.4	0.04	-0.04	0.011	-0.010
	Middle	0.3	-0.2	0.02	-0.02	0.009	-0.009
	Base	0.3	-0.3	0.02	-0.04	0.012	-0.013
	Ground	0.2	-0.3	0.03	-0.02	0.011	-0.012
NS	Top	0.3	-0.4	0.06	-0.05	0.026	-0.027
	Middle	0.2	-0.3	0.03	-0.04	0.021	-0.021
	Base	0.2	-0.2	0.02	-0.03	0.009	-0.009
	Ground	0.3	-0.2	0.02	-0.02	0.009	-0.009
UD	Top	0.2	-0.2	0.03	-0.03	0.017	-0.015
	Middle	0.1	-0.1	0.01	-0.01	0.008	-0.008
	Base	0.1	-0.1	0.02	-0.02	0.009	-0.009
	Ground	0.2	-0.2	0.02	-0.02	0.010	-0.008

Fig. 3-80　Epicenter of the event on May 22th, 2012

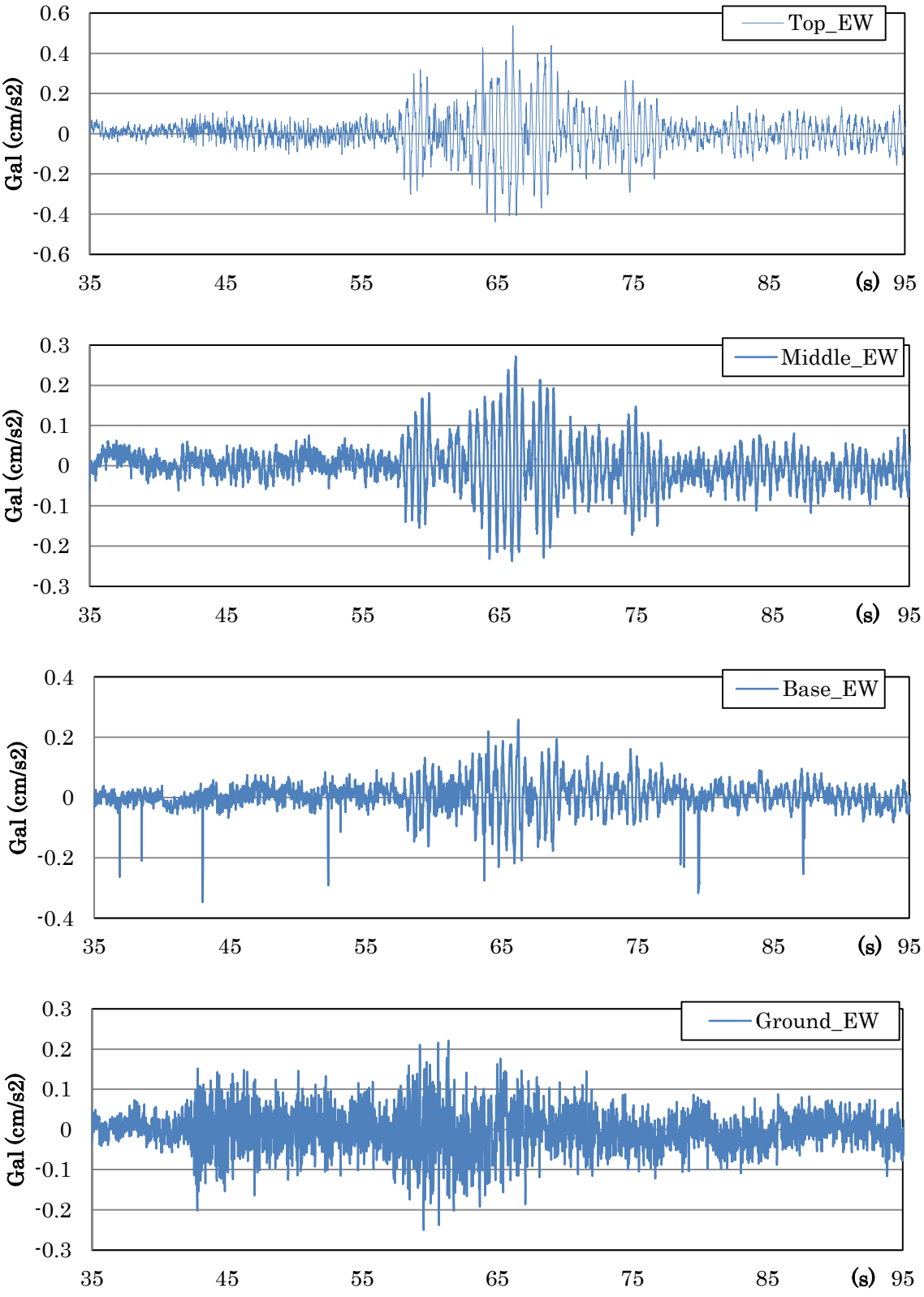

Fig. 3-81　Acceleration time history of the record in EW direction

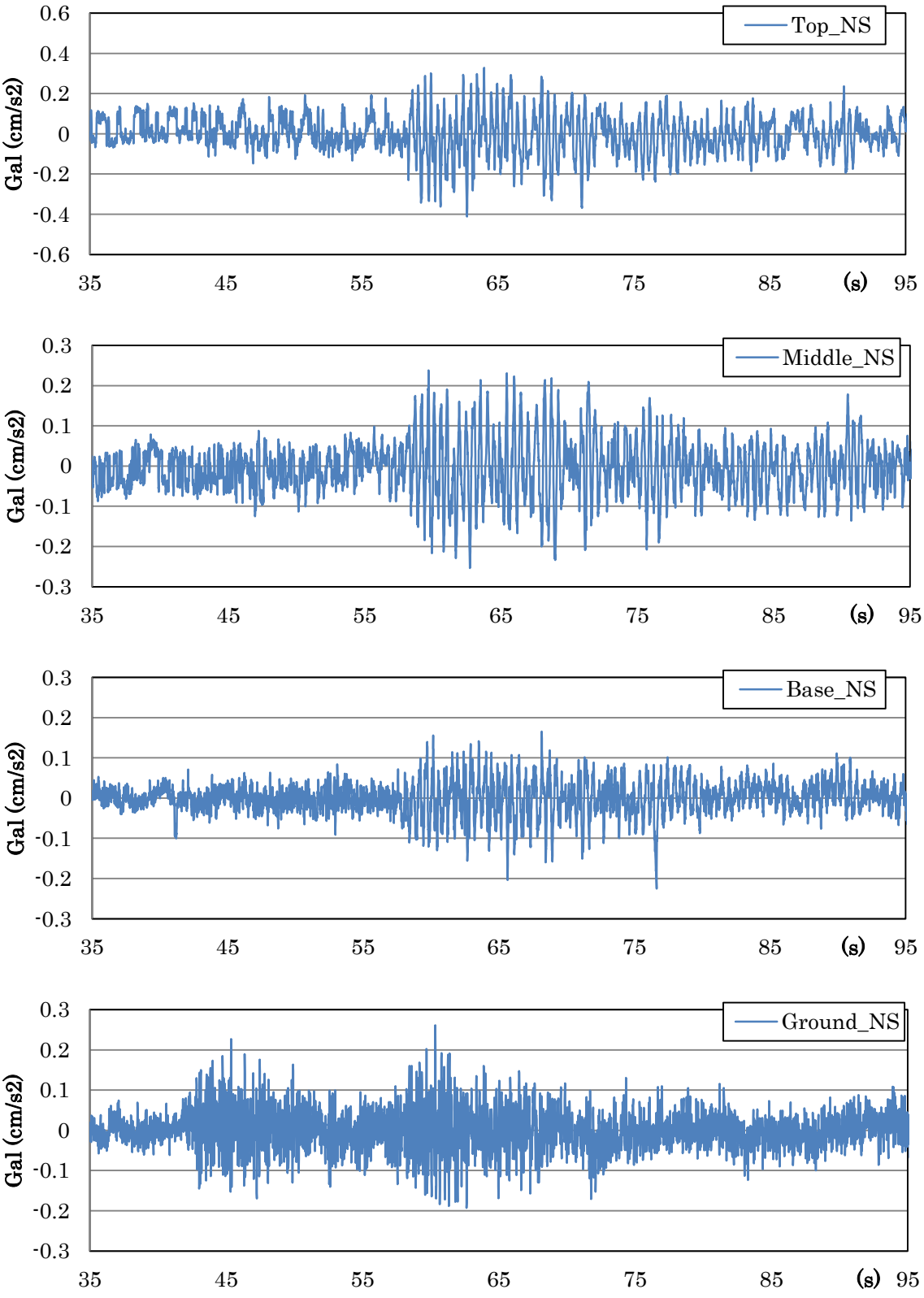

Fig. 3-82　Acceleration time history of the record in EW direction

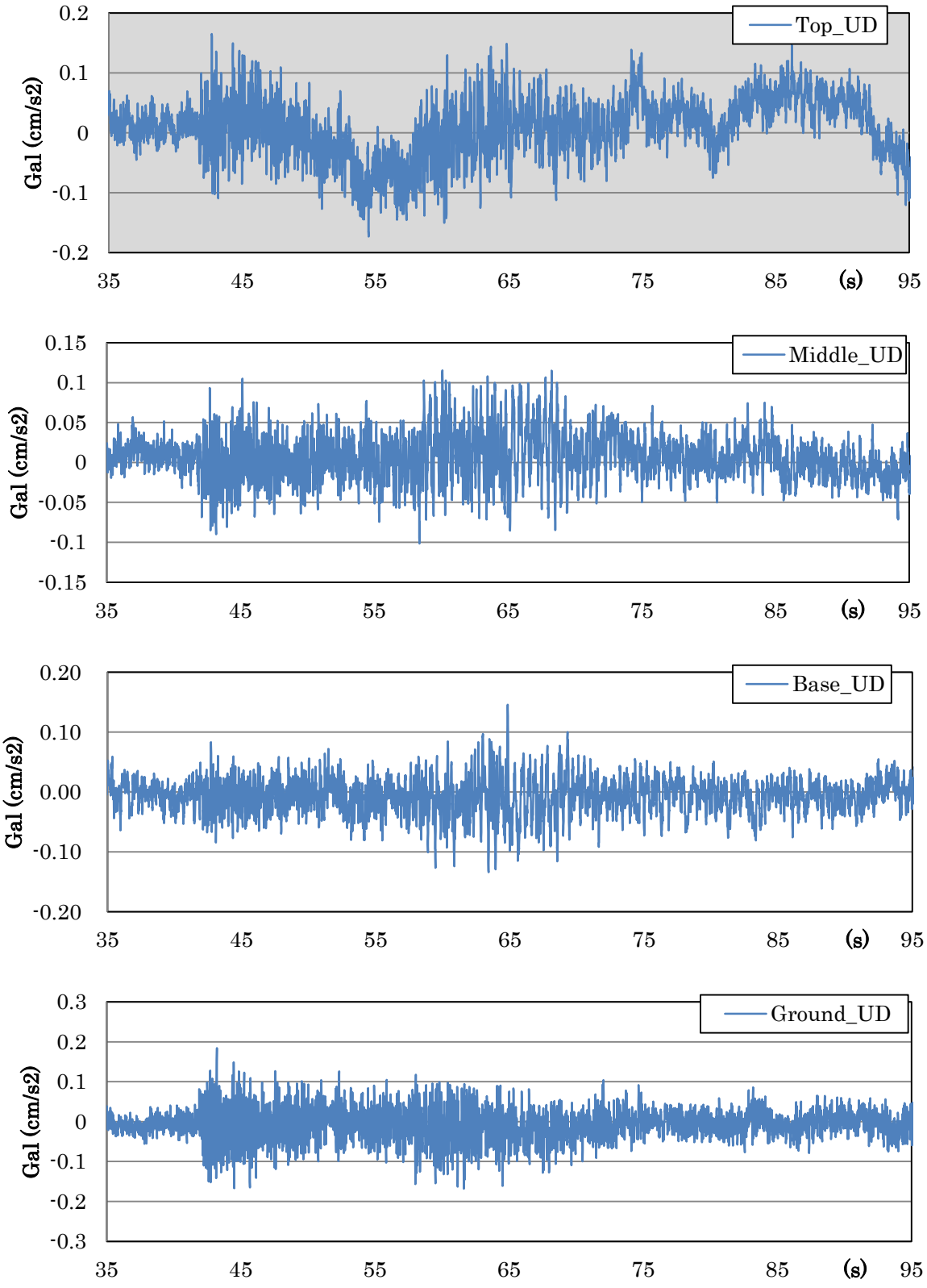

Fig. 3-83　Acceleration time history of the record in EW direction

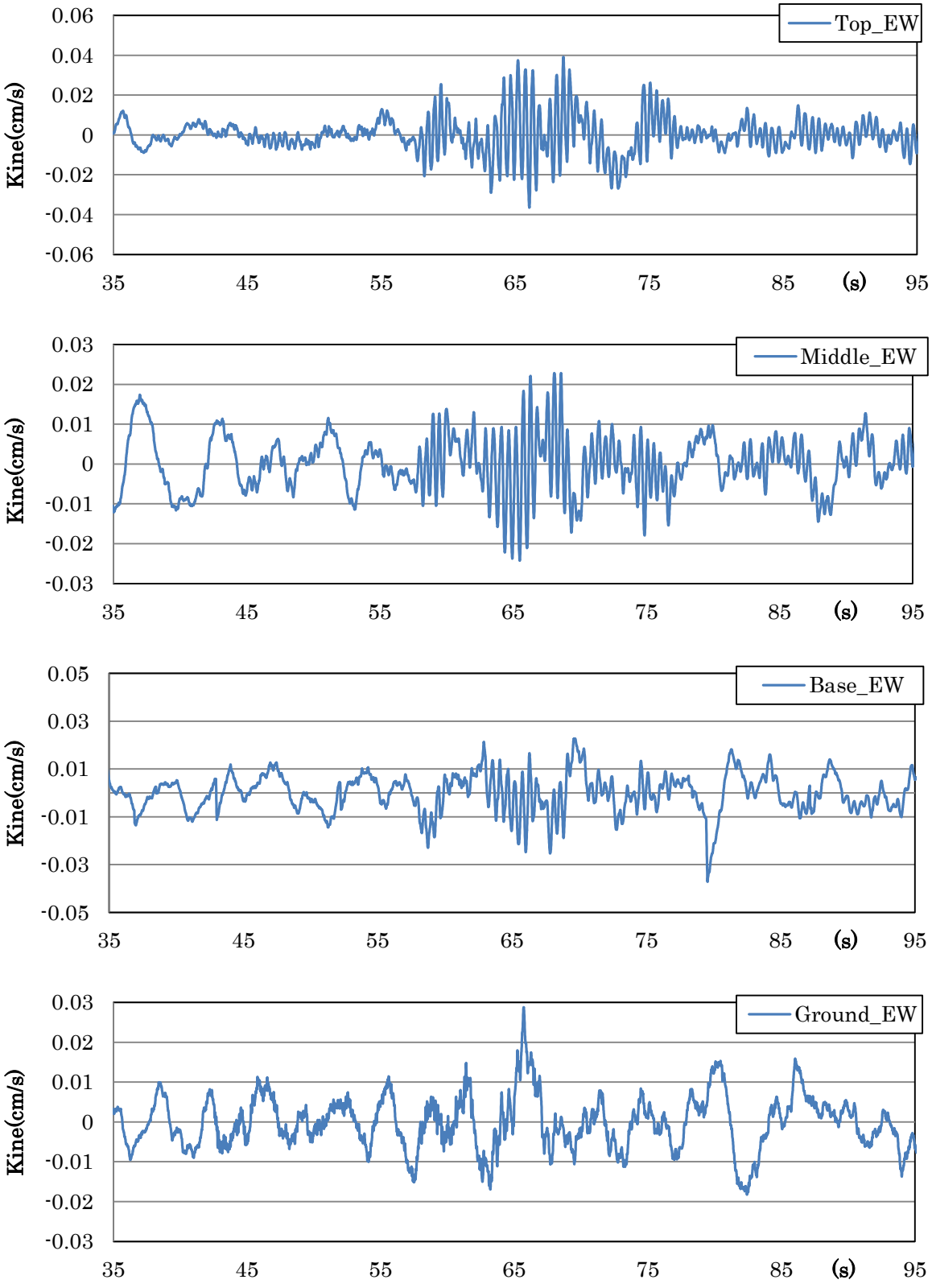

Fig. 3-84　Velocity time history of the record in EW direction

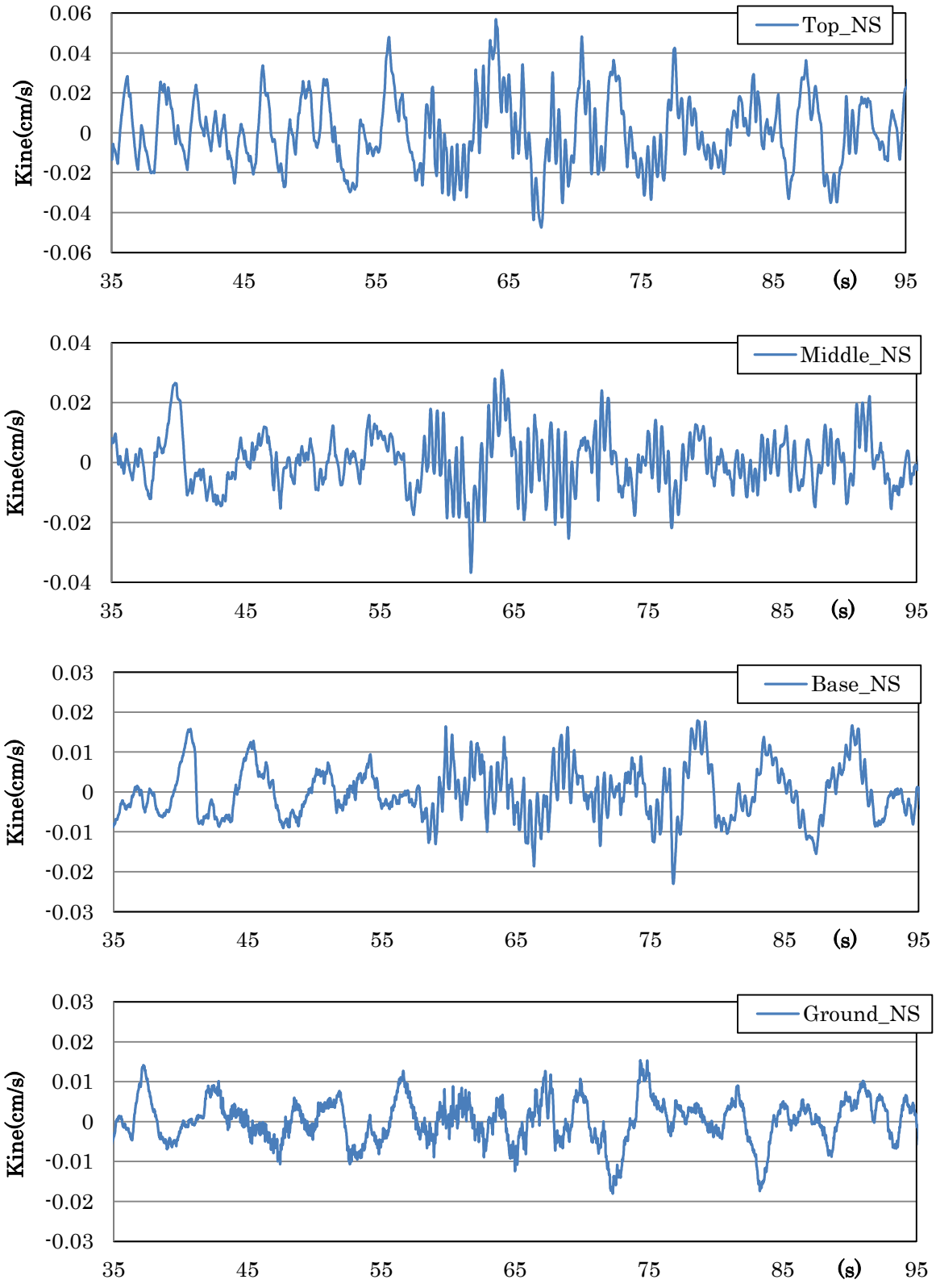

Fig. 3-85　Velocity time history of the record in EW direction

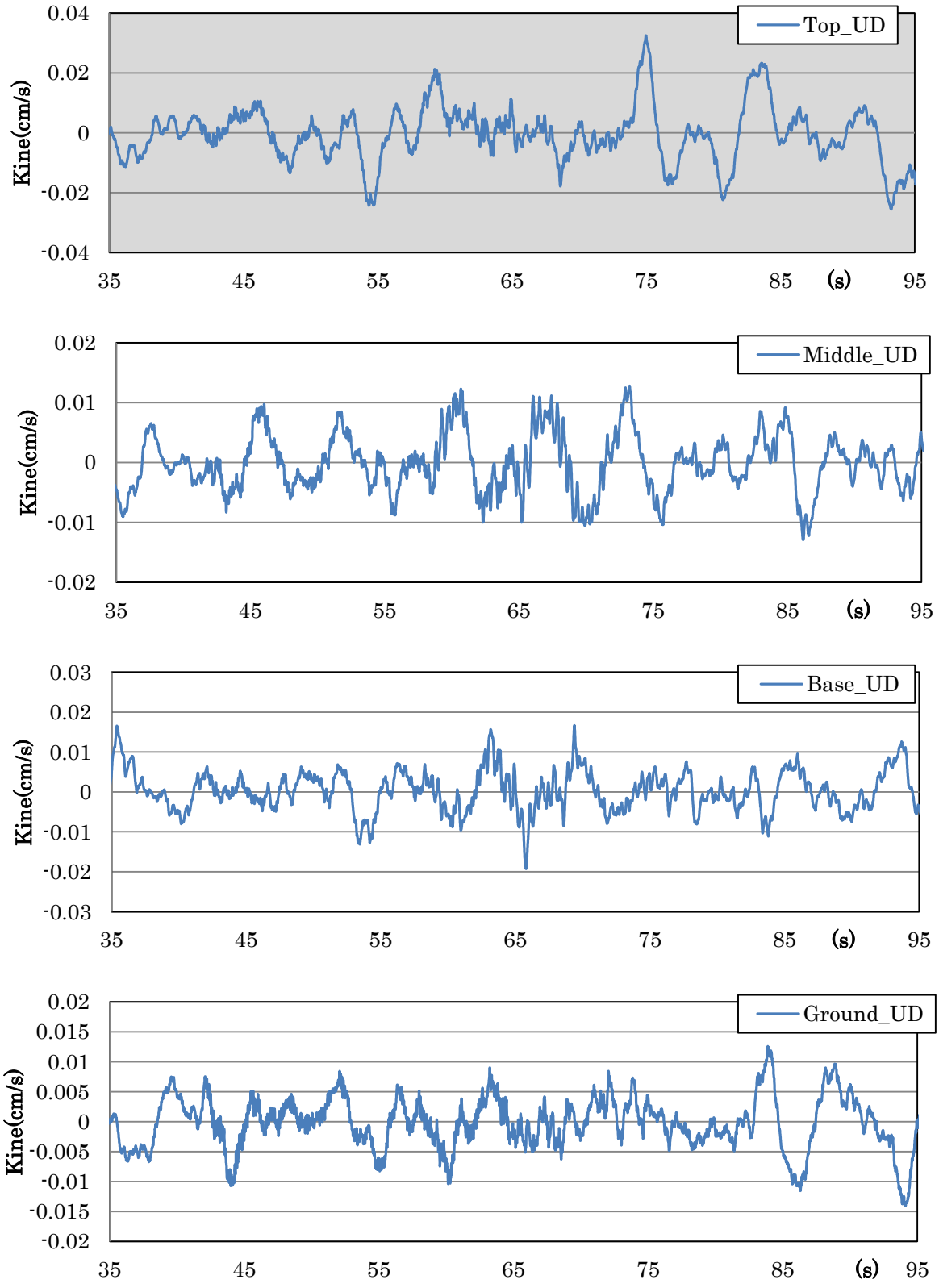

Fig. 3-86　Velocity time history of the record in EW direction

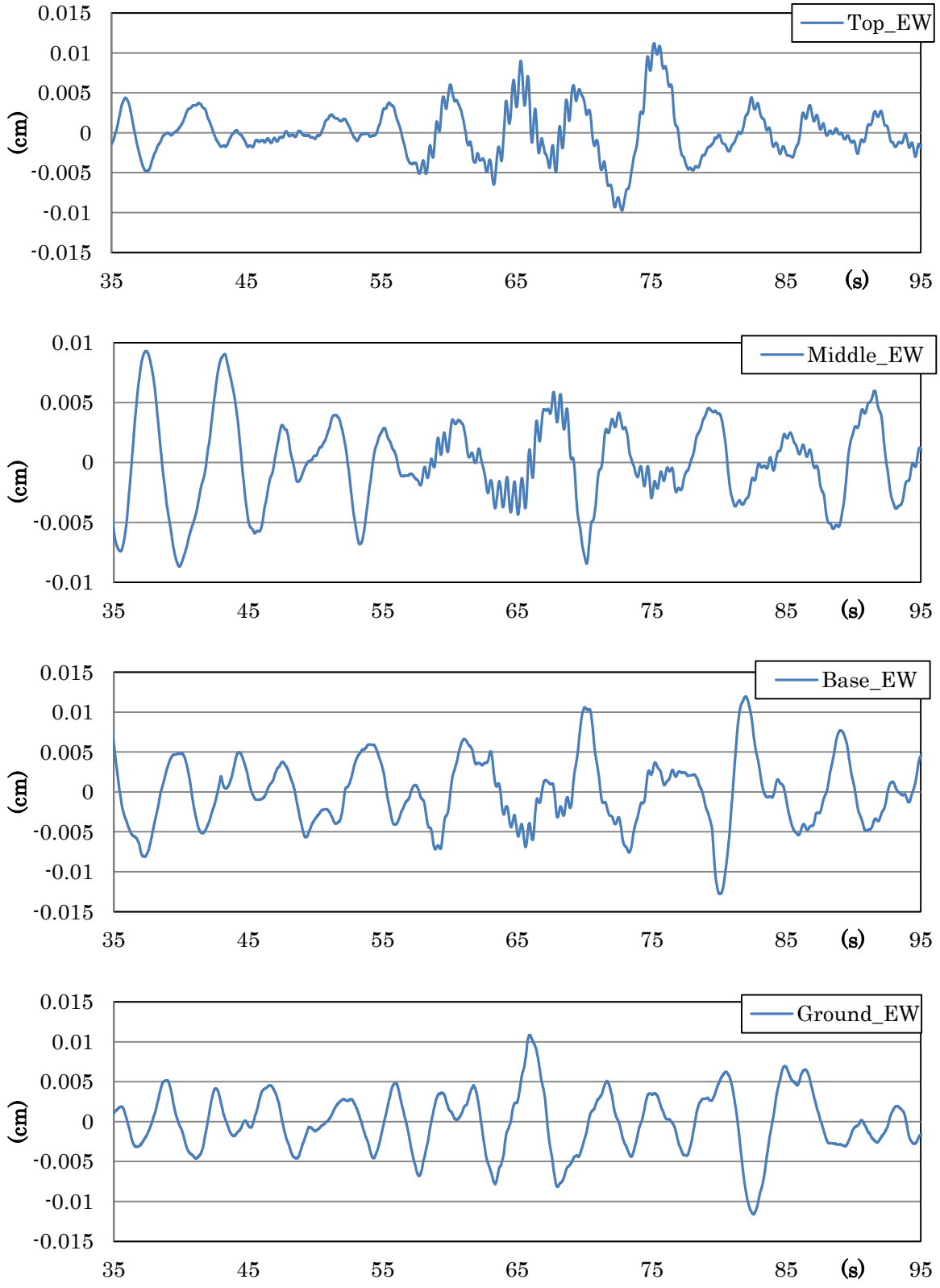

Fig. 3-87　Displacement time history of the record in EW direction

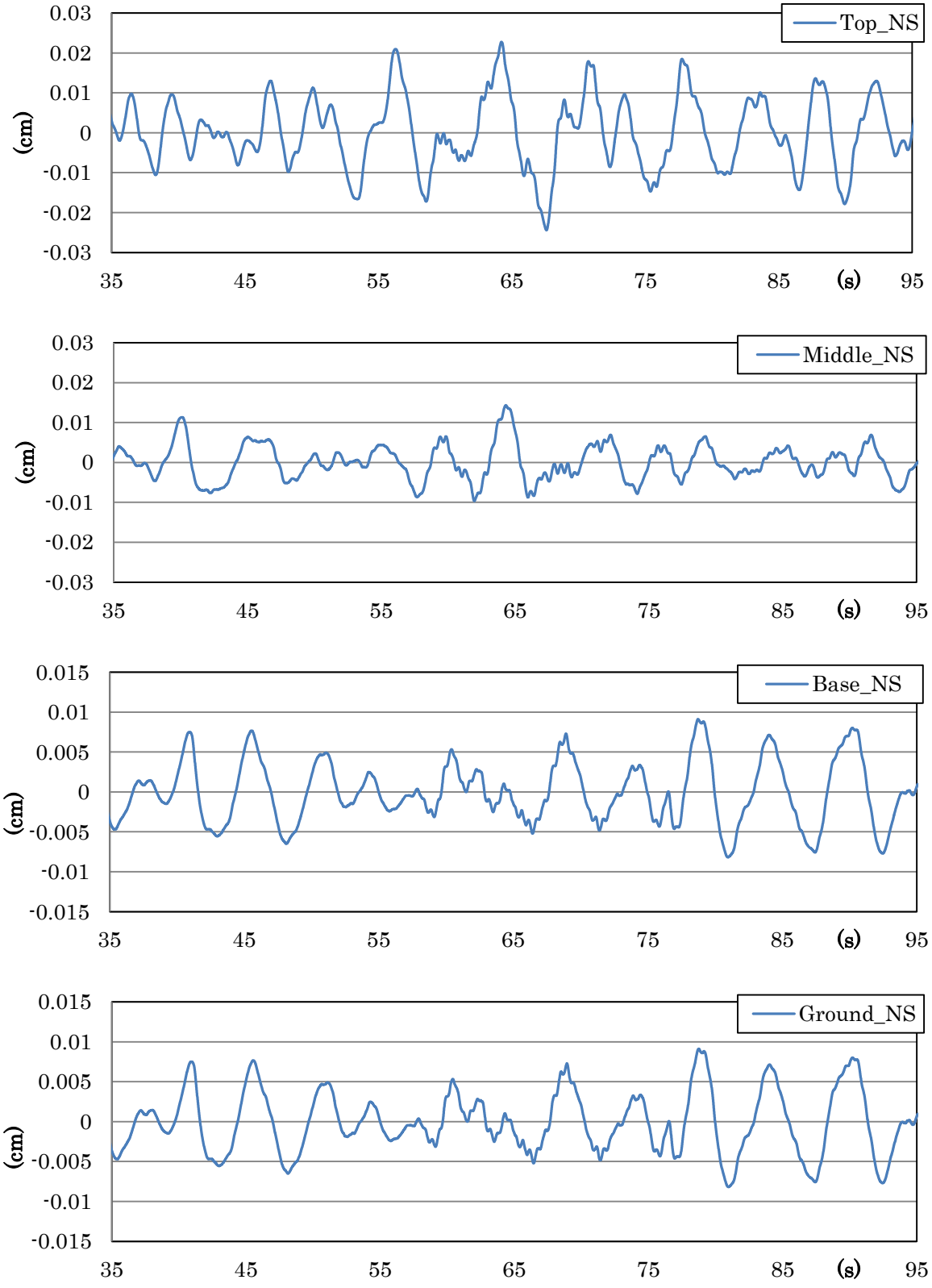

Fig. 3-88　Displacement time history of the record in EW direction

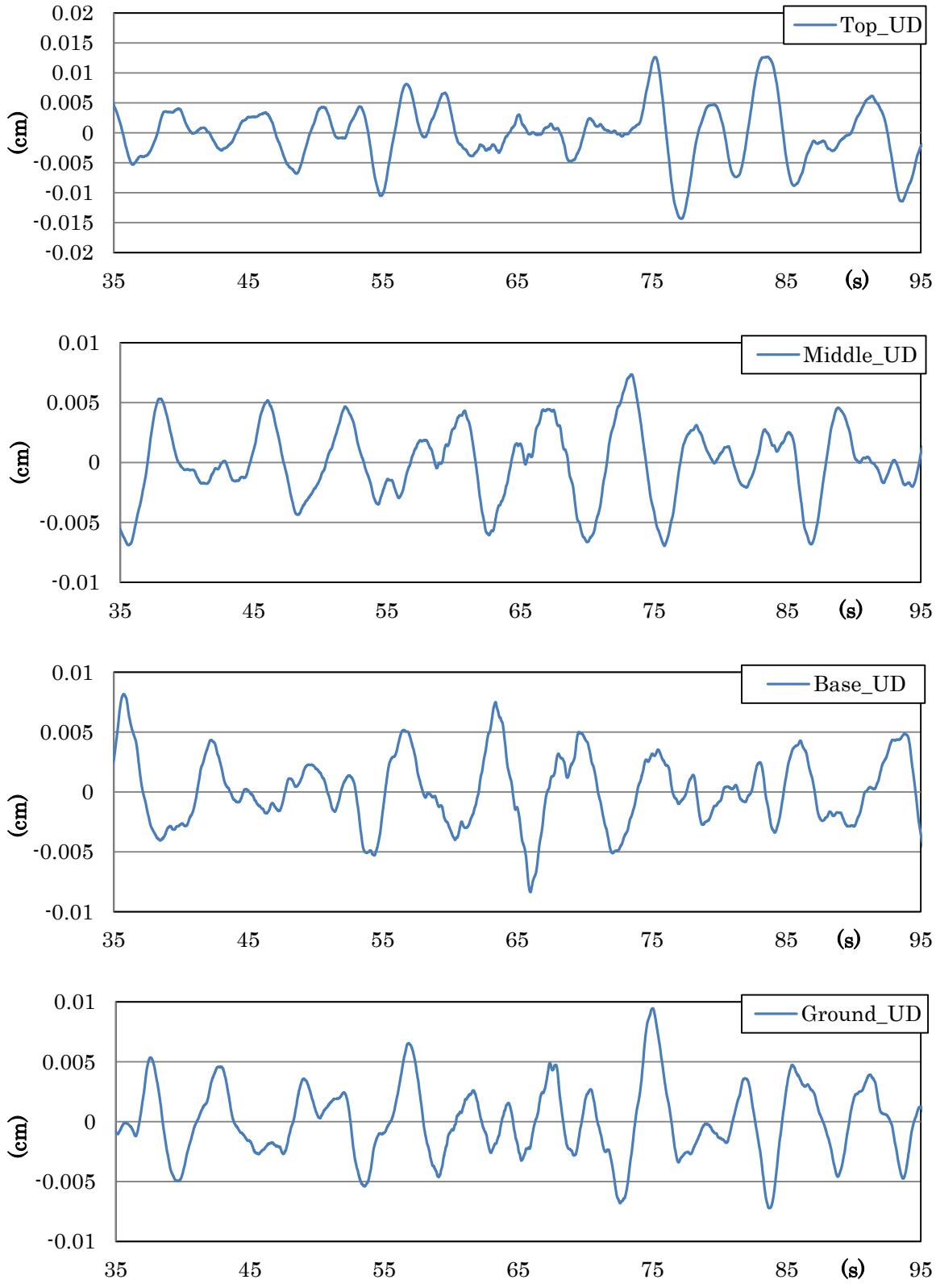

Fig. 3-89　Displacement time history of the record in EW direction

Fig. 3-90 shows the orbit at the Top, Middle, Base and Ground respectively.

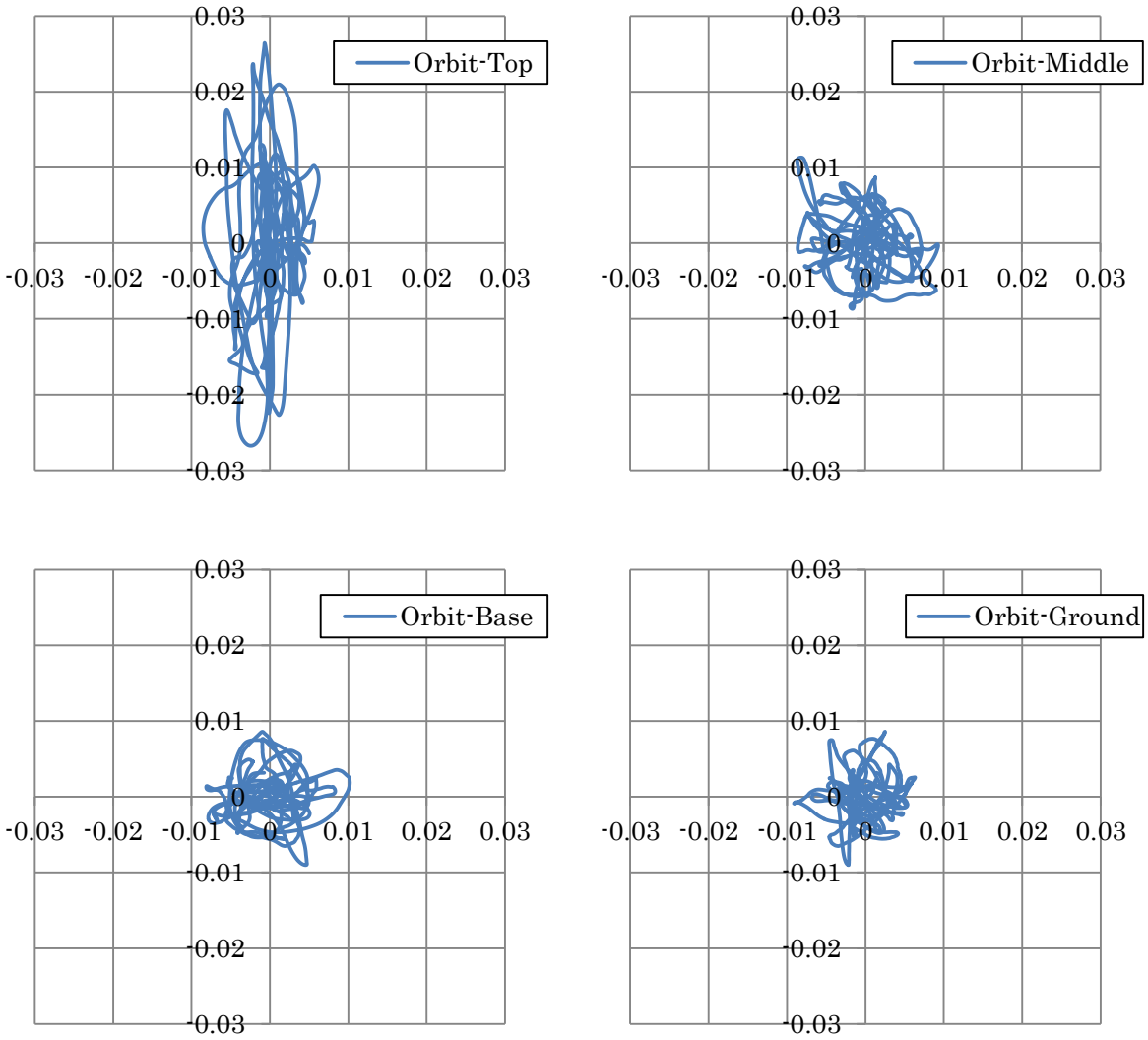

Fig. 3-90　Particle orbit at the point of the seismograms

Acceleration Fourier spectra, Acceleration response spectra and transfer functions are shown in Figs. 3-91 to 3-98. Acceleration Fourier spectra and transfer functions were smoothed with the Parzen Spectrum Window of 0.5 Hz.

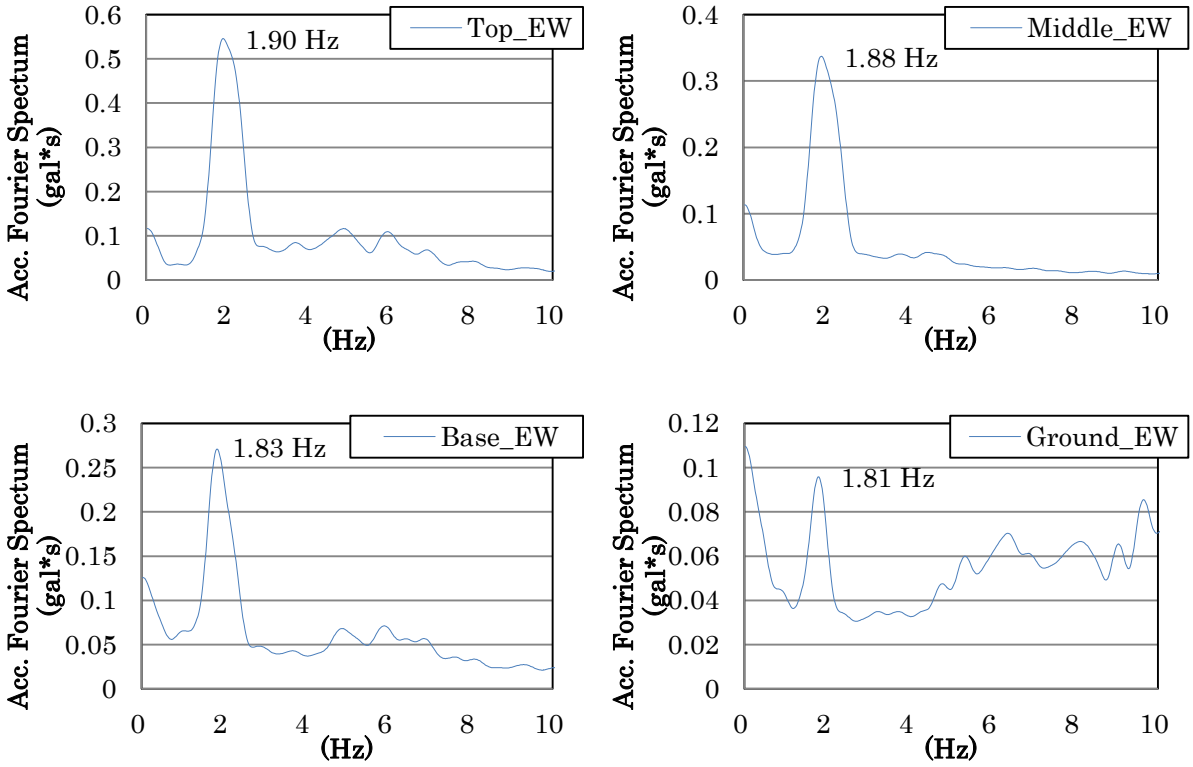

Fig. 3-91　Acc. Fourier Spectra; EW direction

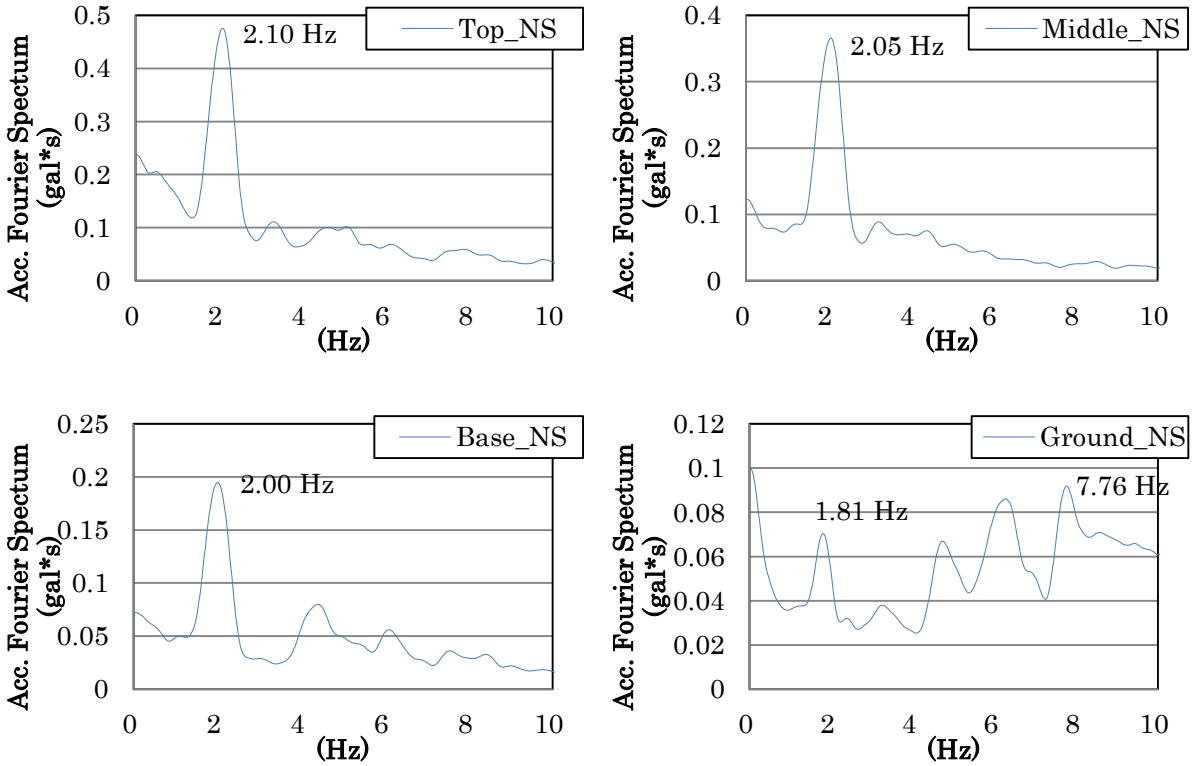

Fig. 3-92　Acc. Fourier Spectra; EW direction

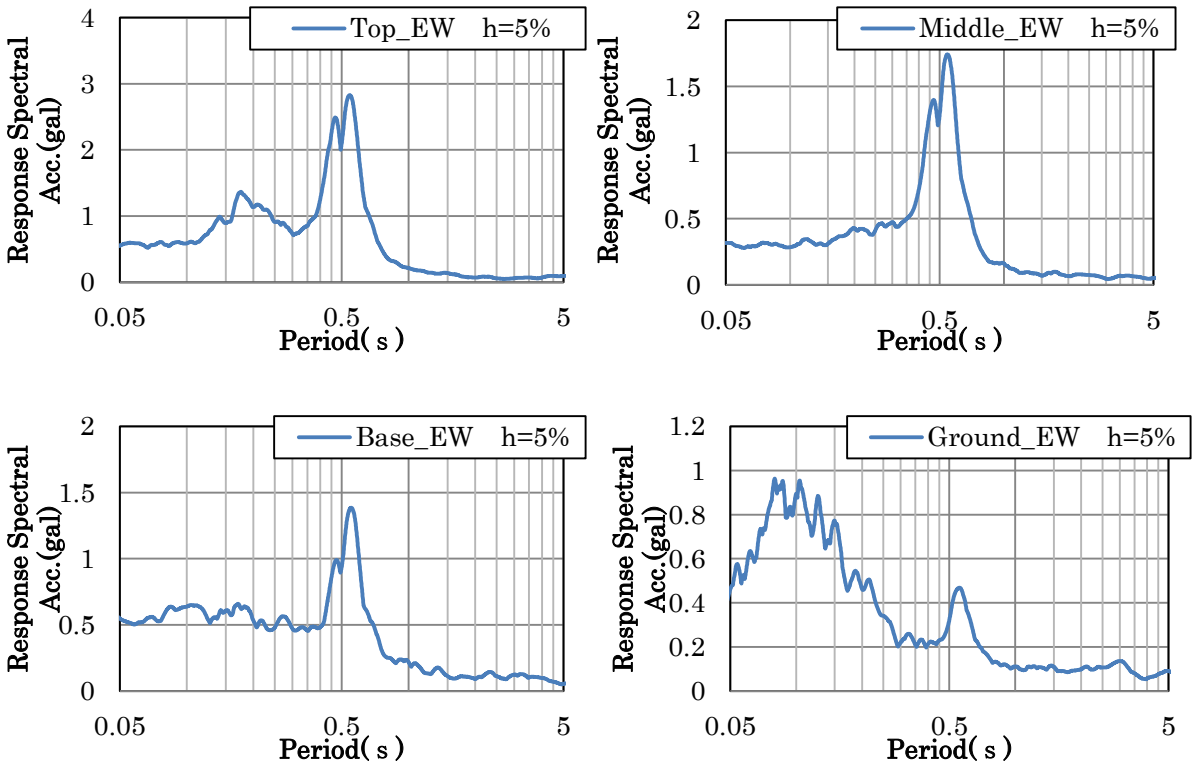

Fig. 3-93 Acc. Response Spectra; EW direction

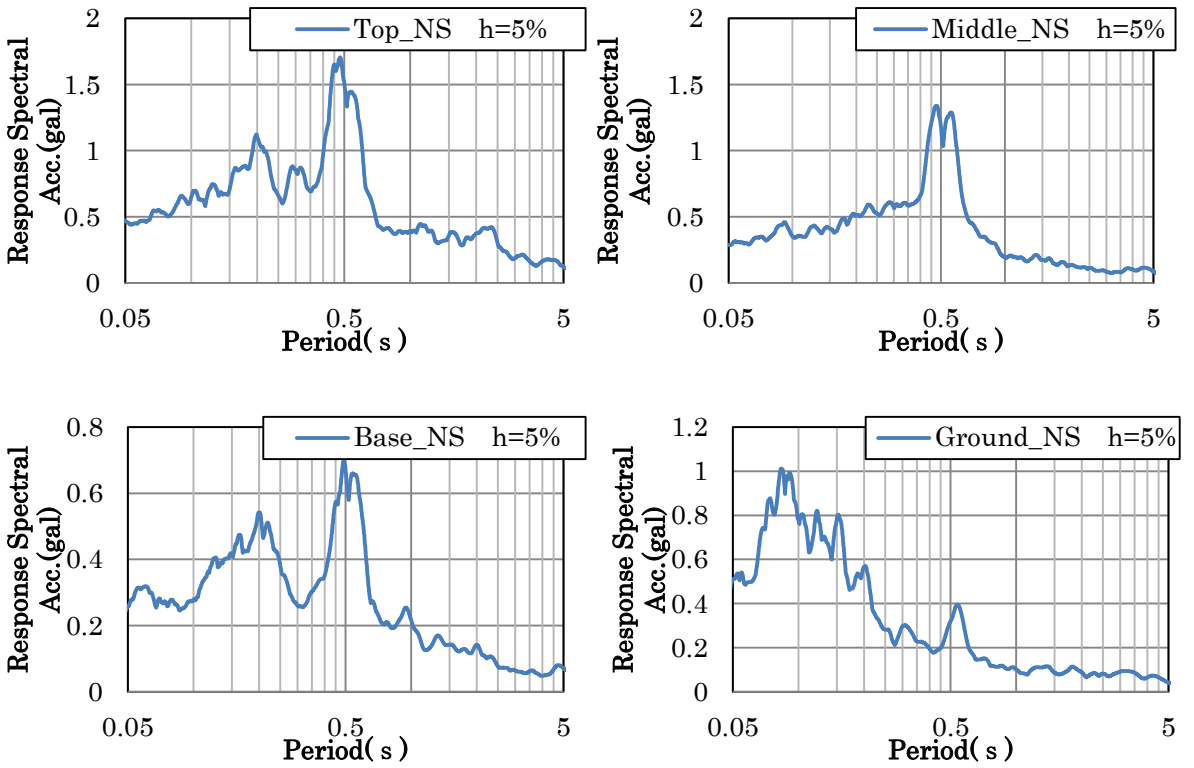

Fig. 3-94 Acc. Response Spectra; EW direction

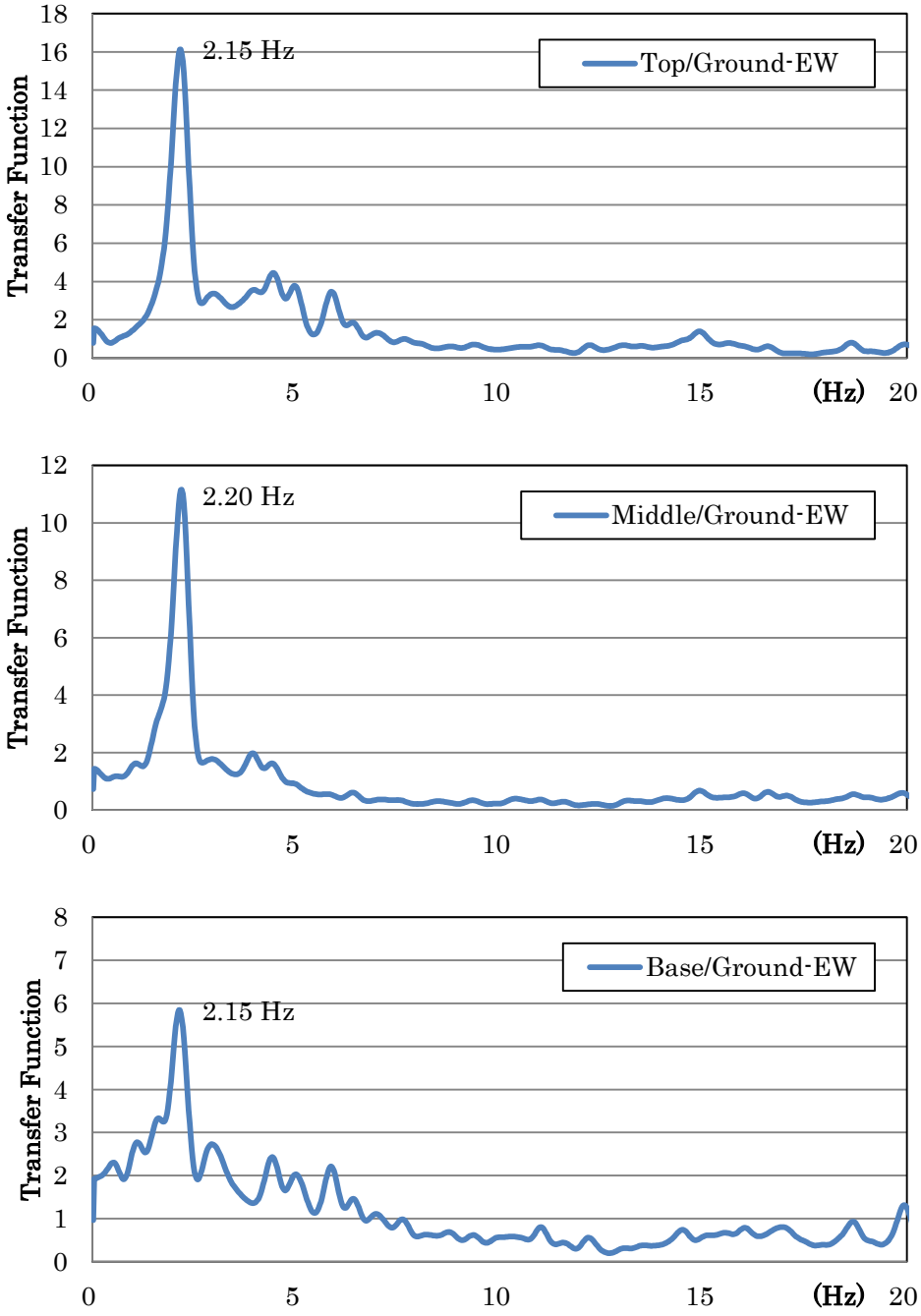

Fig. 3-95　Transfer Function of the record at the Ground; EW direction

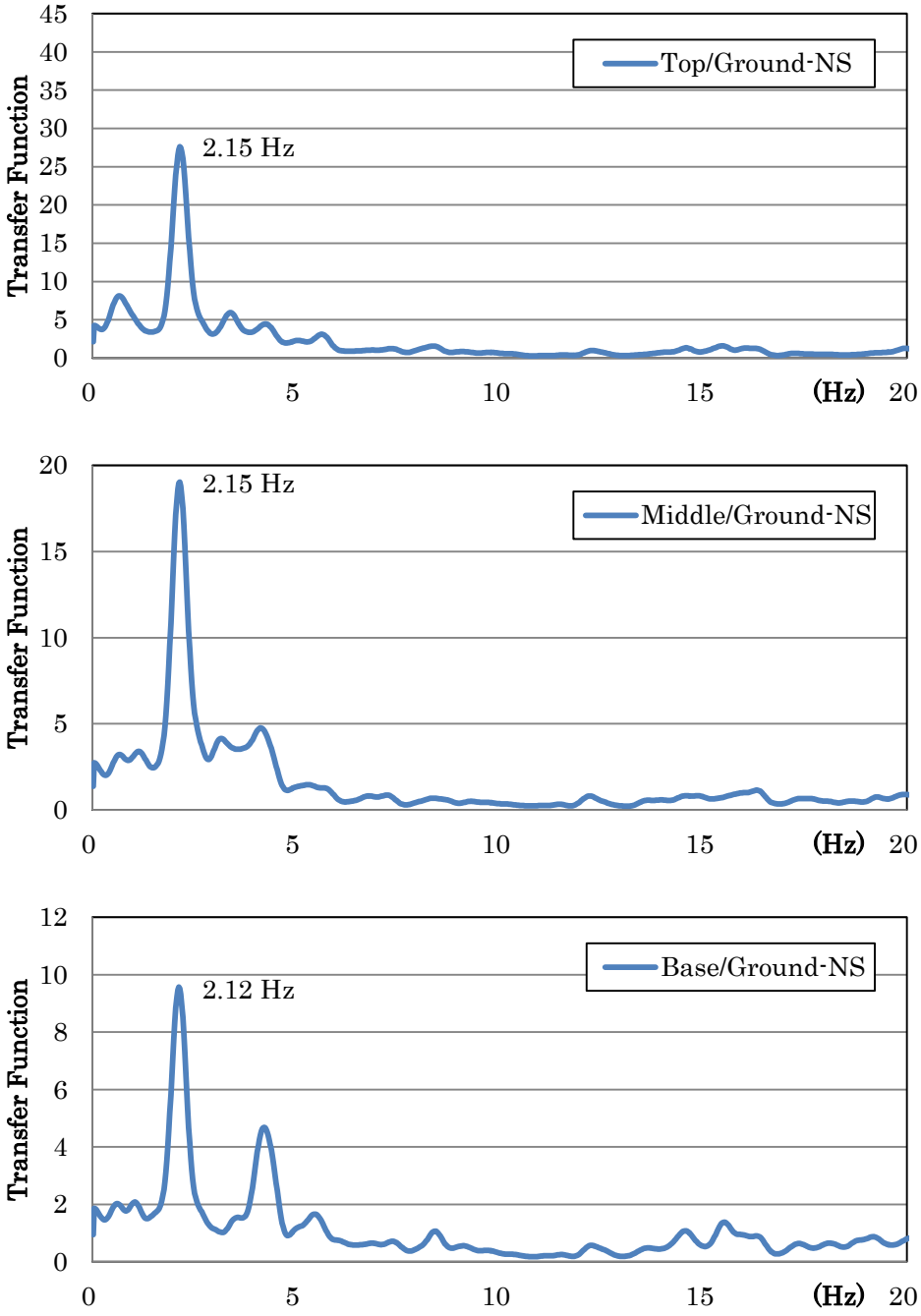

Fig. 3-96　Transfer Function of the record at the Base; NS direction

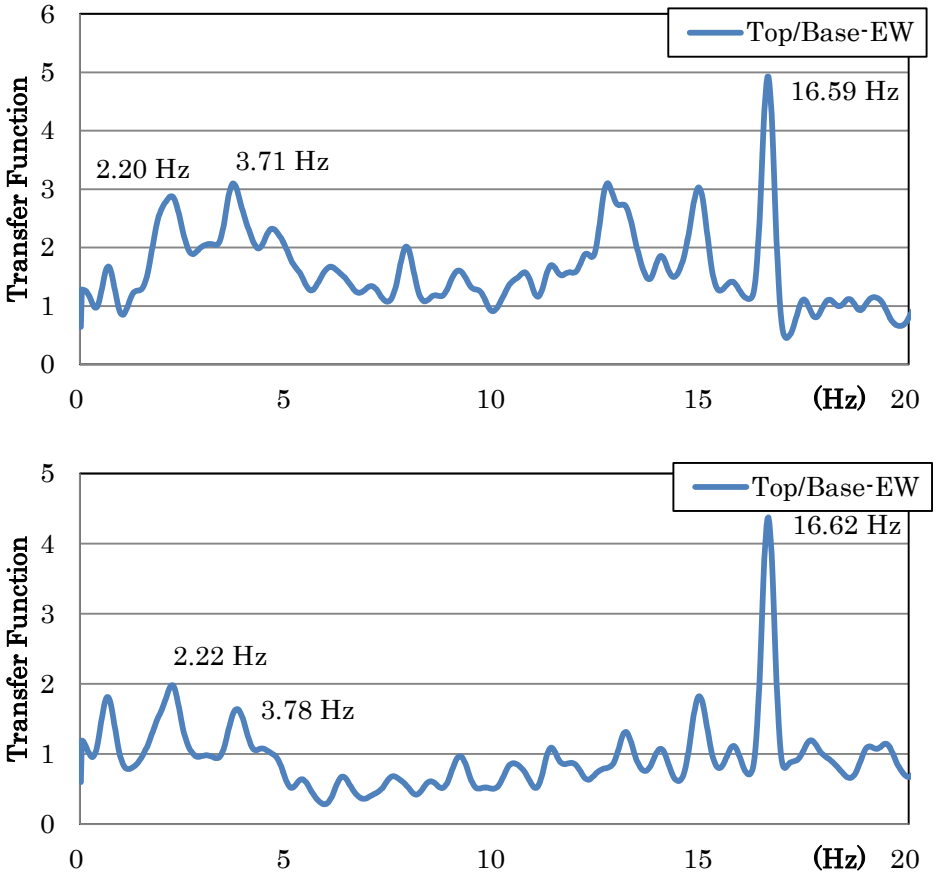

Fig. 3-97　Transfer Function of the record at the Base; NS direction

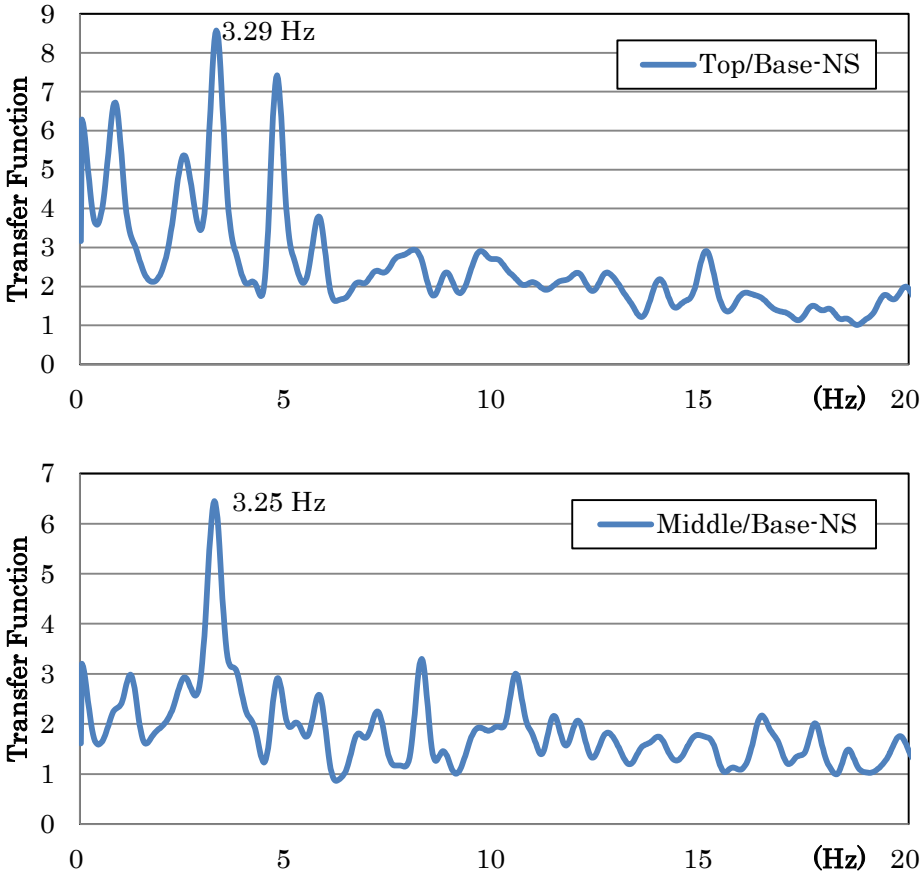

Fig. 3-98　Transfer Function of the record at the Base; NS direction

3.2.3 EARTHQUAKE MONITORING RESULTS

Amplitude of acceleration time histories of EW and NS component in September 12th, 2010 became larger as higher the monitoring point; Ground, Base, Middle, Top, shown in Figs. 3-99 and 3-100. On the other hand, in the case of two earthquakes on November 24th, 2011 and March 19th, 2012, such characteristic of amplification are not shown clearly (See Figs. 3-101 to 3-102). Although the peak ground acceleration of the event of 2012 was approximately 9 that was the same level as the earthquake of 2010, amplitude at the Top did not become clearly larger than at the Ground. This might be caused by the different characteristics in the earthquakes. Since level of the event on May of 2012 was so small, it was not in discussion in the present study.

Acceleration Fourier spectra indicated predominant frequency. Furthermore, transfer functions showed natural frequency from the three earthquakes (See Tables. 3-11, 3-12 and 3-13). On the other hand, the natural frequency of the structure of Chandi Shiva was measured 2.24 – 2.34 Hz in microtremor measurement conducted in 2006 and 2007. The natural frequency considering dynamic soil-structure interaction was 2.00 – 2.09 Hz, in the microtremor measurements. It should be noticed that the natural period became longer when earthquakes stroke.

The acceleration Response spectra shown in Fig. 3-107 indicated that the frequency characteristics of the ground motions when the earthquake occurred in 2010 were different from both those of 2011 and 2012. Those records showed that the natural frequency of soil-structure system was slightly affected by the ground motion characteristics. Furthermore, they showed that the natural frequency became longer as the response displacement was larger.

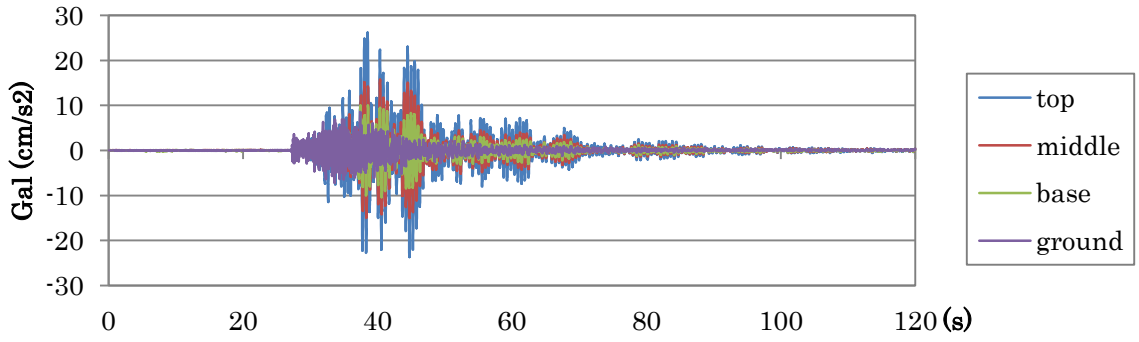

Fig. 3-99 Acceleration time history; EW direction (September 12th, 2010)

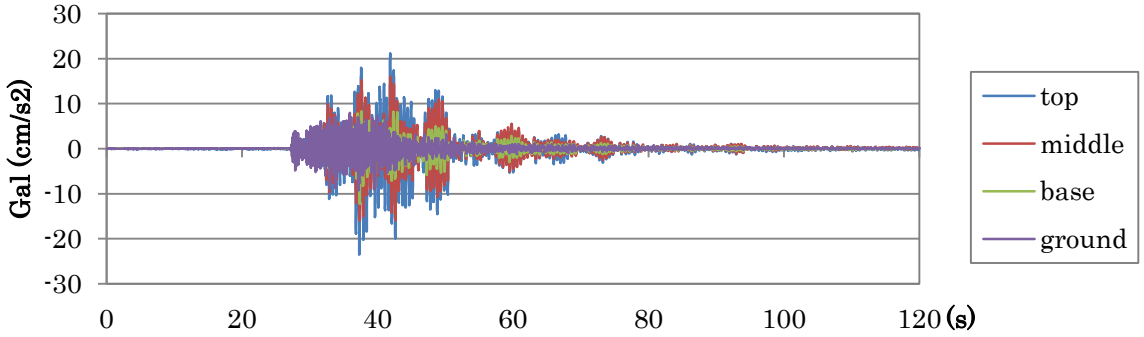

Fig. 3-100 Acceleration time history; NS direction (September 12th, 2010)

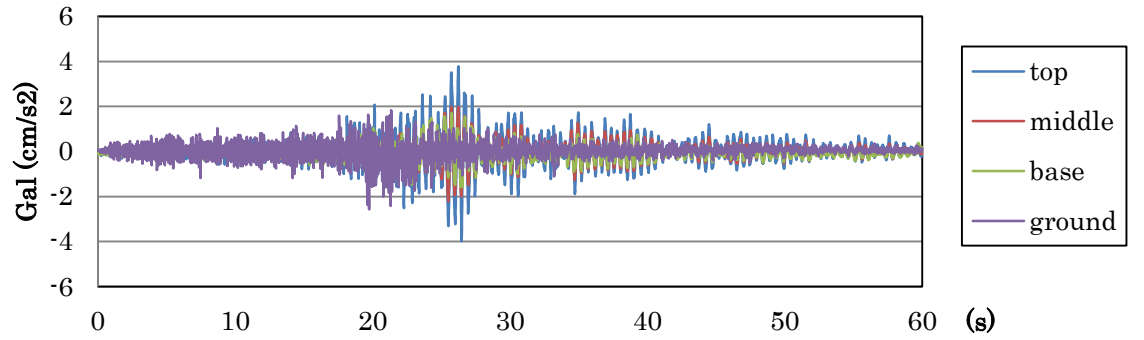

Fig. 3-101 Acceleration time history; EW direction (November 24th, 2011)

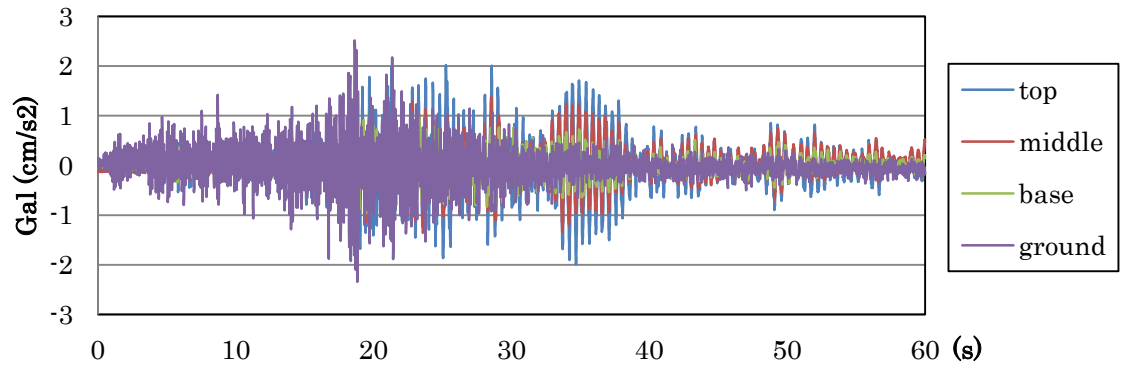

Fig. 3-102 Acceleration time history; NS direction (November 24th, 2011)

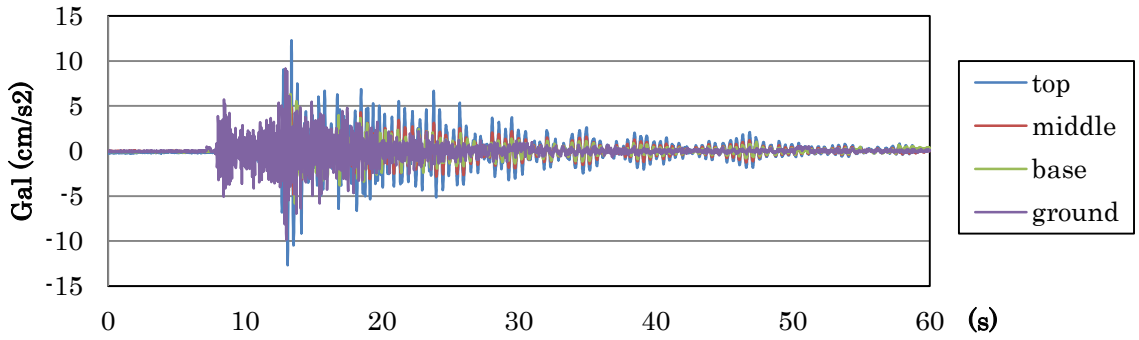

Fig. 3-103 Acceleration time history; EW direction (March 19th, 2012)

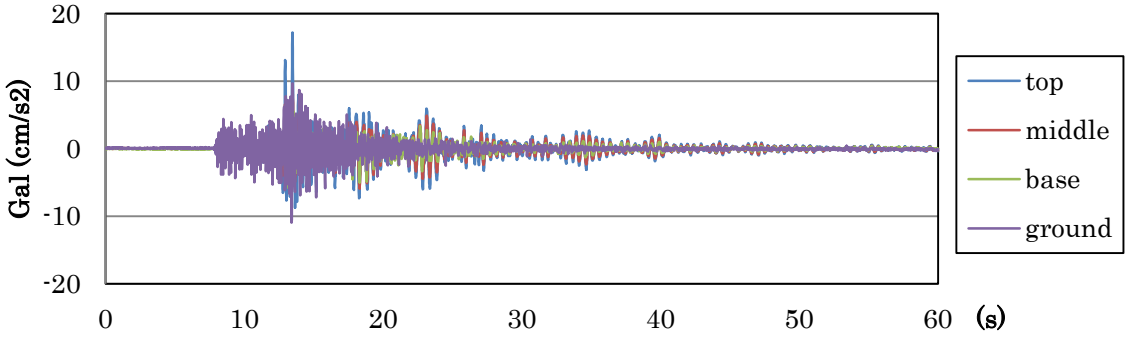

Fig. 3-104 Acceleration time history; NS direction (March 19th, 2012)

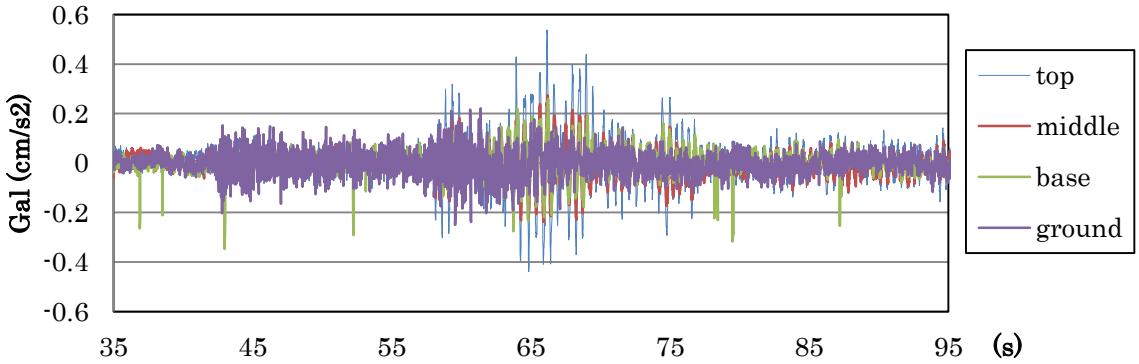

Fig. 3-105 Acceleration time history; EW direction (May 22th, 2012)

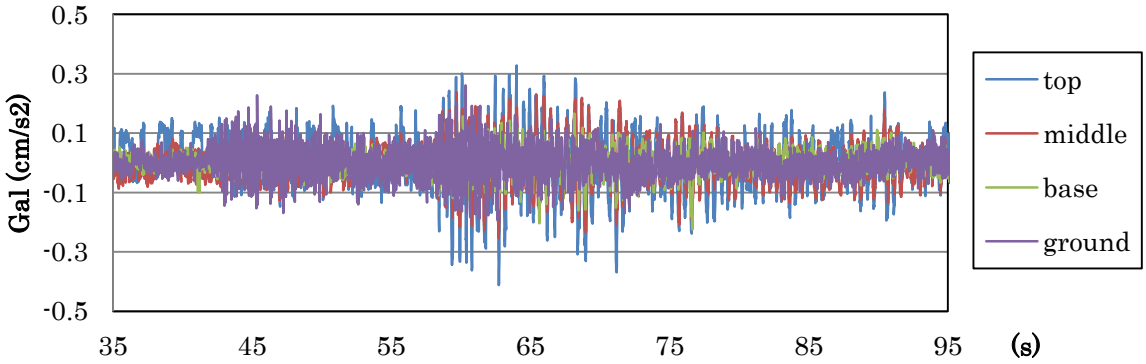

Fig. 3-106 Acceleration time history; NS direction (May 22th, 2012)

Table. 3-11 Predominant frequency from Acc. Fourier Spectra

		Predominant frequency (Hz)			
		2010/9/12	2011/11/24	2012/3/19	2012/5/22
EW	Top	1.91	1.95	2.04	1.90
	Middle	1.91	1.96	2.04	1.88
	Base	1.85	1.95	2.04	1.83
	Ground	1.72	8.38	7.94	1.81
NS	Top	1.93	2.05	1.96	2.10
	Middle	1.92	2.04	1.96	2.05
	Base	1.90	2.01	1.96	2.00
	Ground	7.98	8.52	7.91	7.76

Table. 3-12 Peak values from Transfer function to Ground

		Natural Frequency (Hz)			
		2010/9/12	2011/11/24	2012/3/19	2012/5/22
EW	top	1.97	2.07	2.01	2.15
	middle	1.96	2.06	2.01	2.20
	base	1.93	2.05	2.01	2.15
NS	top	1.99	2.05	2.00	2.15
	middle	2.00	2.01	1.99	2.15
	base	1.97	2.00	1.98	2.12

Table. 3-13 Peak values from Transfer function to Base

		Natural Frequency (Hz)			
		2010/9/12	2011/11/24	2012/3/19	2012/5/22
EW	top	3.07	3.36	3.49	3.71
	middle	2.78	3.33	3.54	3.78
NS	top	26.09	3.17	3.31	3.29
	middle	2.67	3.18	3.31	3.25

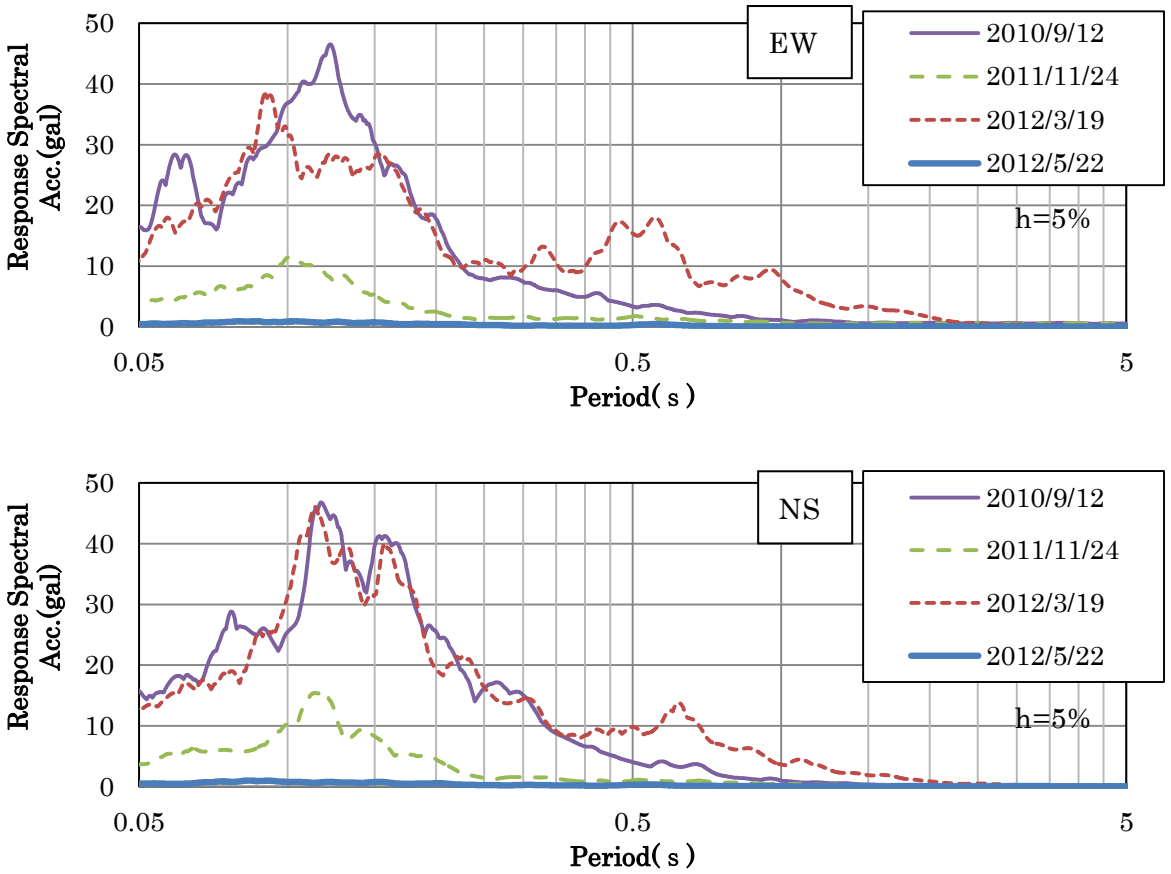

Fig. 3-107　Comparison of Acceleration response spectra of ground motions

Table. 3-14　Peak of Response Displacement (Top, Ground) and Amplification Factor

		Displacement (cm)							
		2010/9/12		2011/11/24		2012/3/19		2012/5/22	
		MAX.	min.	MAX.	min.	MAX.	min.	MAX.	min.
EW	Top	0.18	-0.22	0.02	-0.02	0.06	-0.04	0.01	-0.01
	Ground	0.06	-0.06	0.09	-0.07	0.08	-0.09	0.01	-0.01
NS	Top	0.02	-0.03	0.02	-0.02	0.02	-0.02	0.03	-0.03
	Ground	0.02	-0.02	0.02	-0.04	0.03	-0.05	0.01	-0.01
Amplification Factor	EW	2.33		0.24		0.80		1.03	
	NS	1.14		0.74		0.62		2.90	

3.3 MONITORING OF CRACK DISPLACEMENT, TEMPERATURE AND HUMIDITY

The inner structure of Chandi Shiva, the largest monument of the Prambanan Temples, has not been known clearly because there are neither documents nor records of drawings and specifications when it was reconstructed by Dutch engineers in the middle of 20th century. There found the serious cracks at the walls and the entrances of Chandi Shiva. In particular, the crack at the corner around the base was easily found. At some area, the surface of stones fell. Furthermore, some cracks reached to the wall of the rooms. The stones were displaced horizontally by maximum 50 mm at the west side wall. The west gate leaned westward by pushing the lintel of the gate and the entrance stairs as the displacement of the west wall. As structural monitoring has become of importance in the research area of structural engineering for conservation, the records would be expected to provide significant data to conduct the structural conservation.

Since October of 2011, the north, south room and the corridor of Chandi Shiva have been open to the public with limited entry. Covers were installed for displacement transducers in order to present disturbing, shown in Fig. 3-108.

Fig. 3-108 View of a displacement transducer with cover

3.3.1 MONITORING SYSTEM

Clack displacements have been monitoring by displacement transducers (PI-2, Tokyo Sokki Kenkyujo Co., Ltd.) connected with a Data logger (TDS-102-20, Tokyo Sokki Kenkyujo Co., Ltd.) four times in a day at intervals of 6 hours (0:00, 6:00, 12:00 and 18:00 by Indonesian time). Displacement data were stored by using Flash memory card. It was needed to extend the power cable from Chandi Hangsa to get electrical power for the Data logger. When the electricity is cut off the Data logger can work by four size D batteries.

As the structural stability should be investigated, the displacement of cracks has been monitored together with temperature and humidity since October 29th, 2008. However the

transducers at Ch 10 and Ch 16 had error to record since July 24th, 2009 at 12:00 and February 7th, 2009 at 12:00, respectively. To solve these problems the transducer at Ch 16 was replaced with new one. The transducer at Ch 10 was reconnected to get well connection between two cords from the gauge and the extension cord on May 8th to May 18th, 2010. While one thermocouple, Ch 0, did not work well since May 31st, 2009 at 18:00, the other thermocouple, Ch 1, also did not work since May 19th, 2009 at 0:00. To solve this problem they were replaced with new thermocouples. Structural monitoring was restarted after checking all equipment working correctly.

There was no record since November 1st, 2010 until February 2nd, 2011 for the reason that the volcano, Mount Merapi became active and erupted. During this period, the monitoring equipment was affected by lighting. There was a problem of the AC adaptor of the monitoring system since February 20th, 2011, therefore, the collected data were missing or unstable. DC batteries were used for electric power supply to the data logger since September 28th, 2011, as the AC adaptor did not work well. On December 15th, 2011, some transducers were exchanged their connection channel to the data logger in order to collect correct data of the transducers that have had no trouble. One thermocouple, Ch 0, was also replaced with new one at the same time.

Fig. 3-109 shows a block diagram of the present observation system.

Temperature and humidity were recorded every 1 hour in the devices (loggers) that were separately installed (see Figs. 3-110 and 3-111). To transfer data to a computer, Communication base was used. In the end of October 2012, four devices were replaced with new ones. Fig. 3-112 shows one of new temperature and humidity loggers.

Another type of temperature and humidity logger was set by one of members of Japanese experts, shown in Fig. 3-113. A diamond shape in Fig. 3-117 shows the location of this logger.

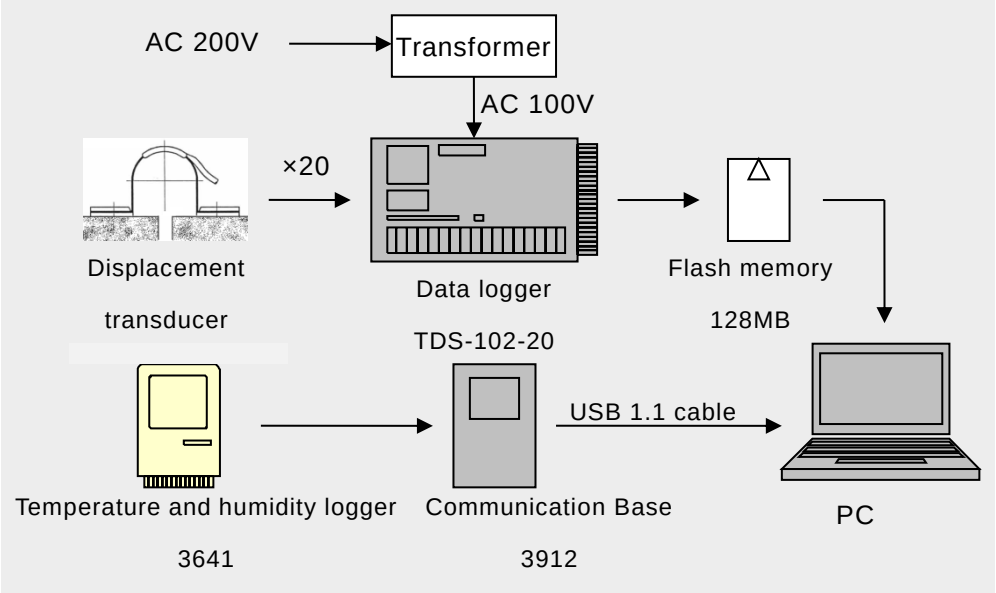

Fig. 3-109　Block diagram of observation system for crack, temperature and humidity

Fig. 3-110　Temperature and humidity logger

Fig. 3-111　View of a temperature and humidity logger

Fig. 3-112　Replaced temperature and humidity logger

Fig. 3-113　View of the temperature and humidity logger at the outside

Crack displacements have been monitored with displacement transducer (PI-2) at 14 points both of inside and outside the monuments. Fig. 3-117 shows the location of the data logger, displacement transducers, thermocouples and temperature/humidity loggers. Additional dummy equipment was installed at the outside 4 point, where the differences between daytime and nighttime temperatures are extreme, to revise the influence by swelling and shrinking of stone itself. A total 18 components of crack displacement have been recorded. Temperature and humidity also has been monitored with temperature and humidity logger at 4 points inside of each room. Furthermore, temperature has been recorded by two thermocouples outdoors and indoors. The data logger was set in the central room which has electricity, and connected with cables from crack transducers and thermocouples. The settlement method of displacement transducers (PI-2) was mentioned as the following.

i. Wash the stone where equipment would be installed with teeth brush and dry.

ii. Give an undercoat smooth on the stone with consideration to a space for screws and left for 24 hours.

iii. Glue both of the stone and baseplate and keep them for 1 minute after that stick together and keep under pressure for approximately 3 or 5 minutes until the glue dries. Leave them for 24 hours after filling the gap with glue.

iv. Attach the displacement transducer (PI-2) with screws on the baseplate (see Figs. 3-114 and 3-115).

v. Connect the displacement transducer and the data logger by using cable. Check the monitor of data logger for correct connection. (see Fig. 3-116)

vi. Cover connecter from dust and water along the wall not to interrupt passing. Be careful especially outside connecter with waterproof tape and vinyl tape.

Fig. 3-114 View of displacement transducer (PI-2-100)

Fig. 3-115 View of displacement transducer, dummy and thermo couple

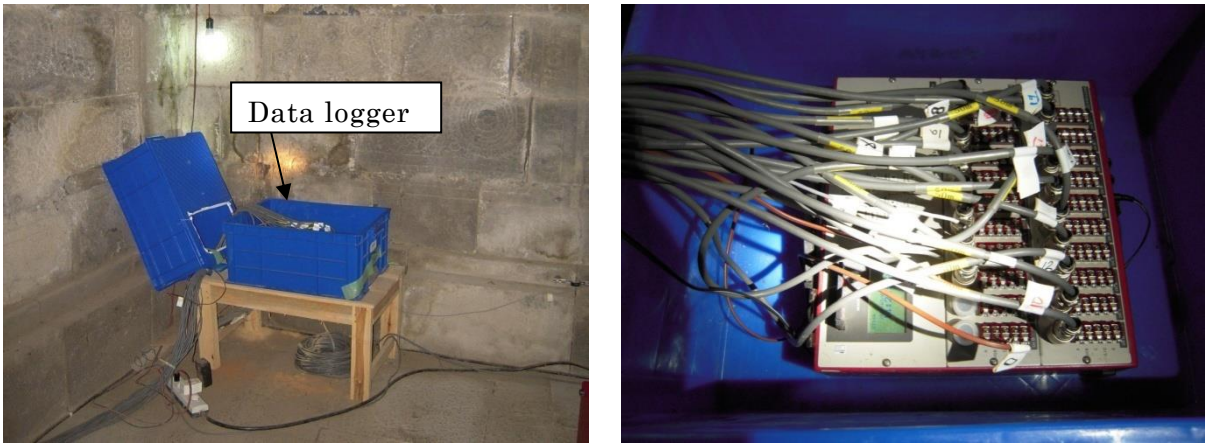

Fig.3-116　View of Data logger

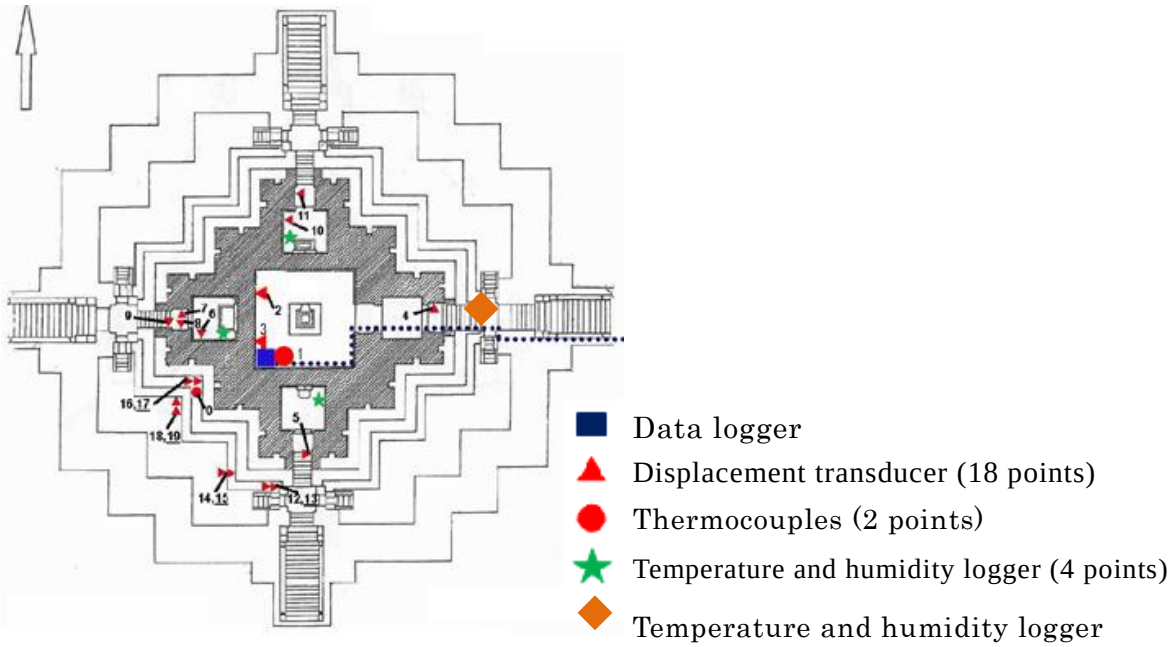

Fig. 3-117　Location and channel number of equipment

3.3.2　MONITORING RECORDS

Fig. 3-118 shows a record of thermocouples inside and outside of the room (Ch 0 and 1.) Figs. 3-119 to 3-122 show the data recorded by displacement transducers and dummy collected on October 29th, 2008 to January 10th, 2013. Fig. 3-123 shows the collected crack displacement values after revising with the data of the dummy (Ch 13, 15, 17 and 19.)

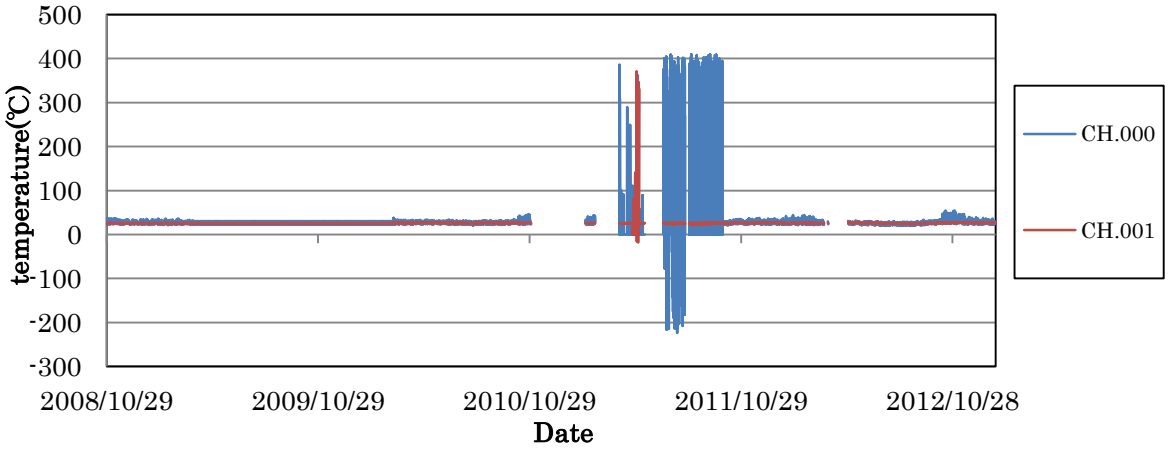

Fig. 3-118　Record of temperature from thermocouples (raw data)

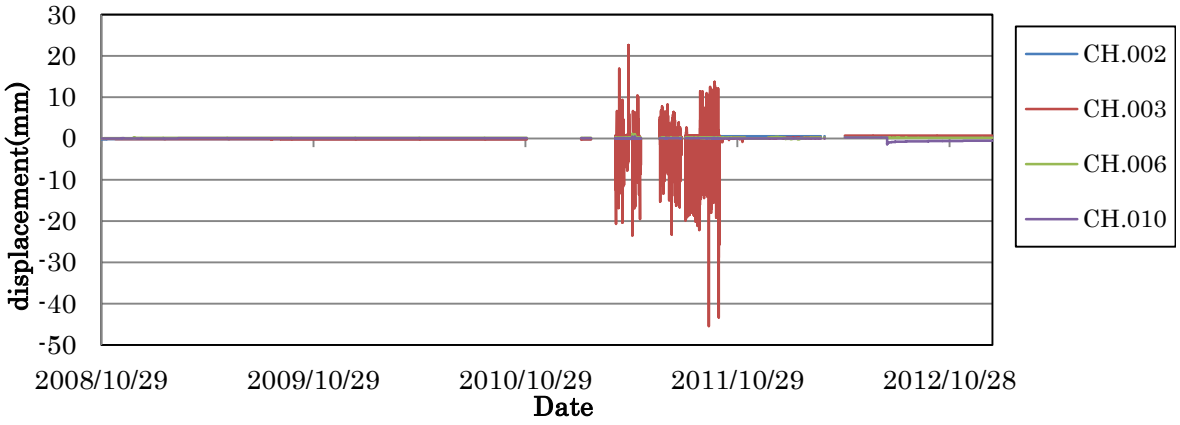

Fig. 3-119　Record of crack displacement inside the room (raw data)

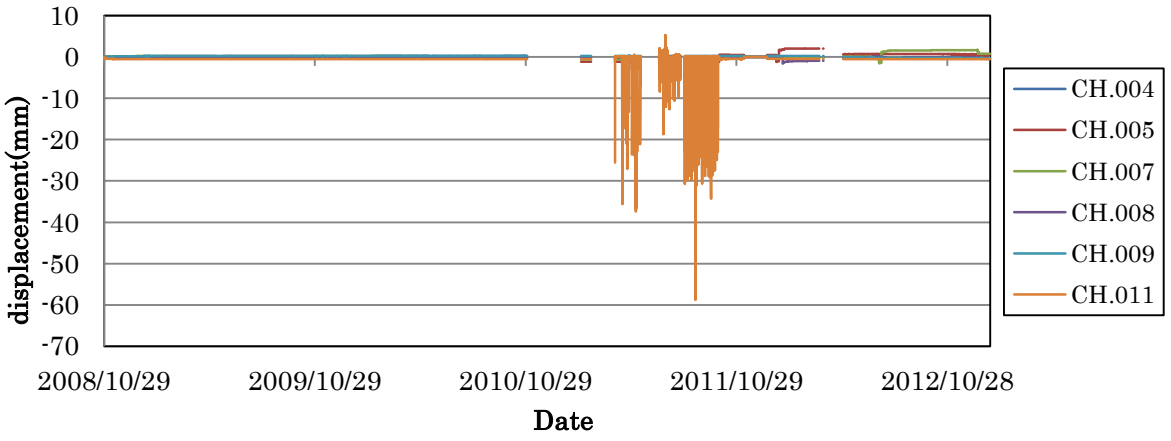

Fig. 3-120　Record of crack displacement around entrance of the room (raw data)

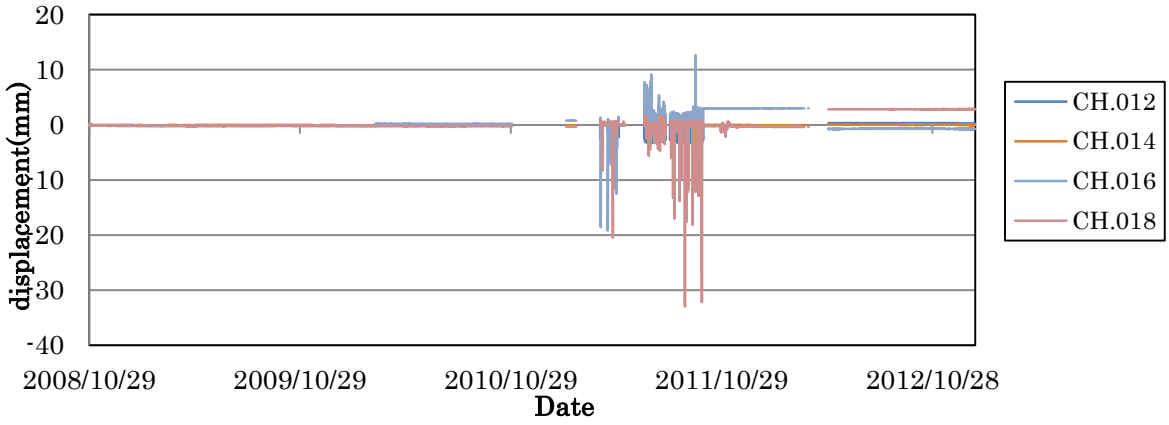

Fig. 3-121　Record of crack displacement outside the room (raw data)

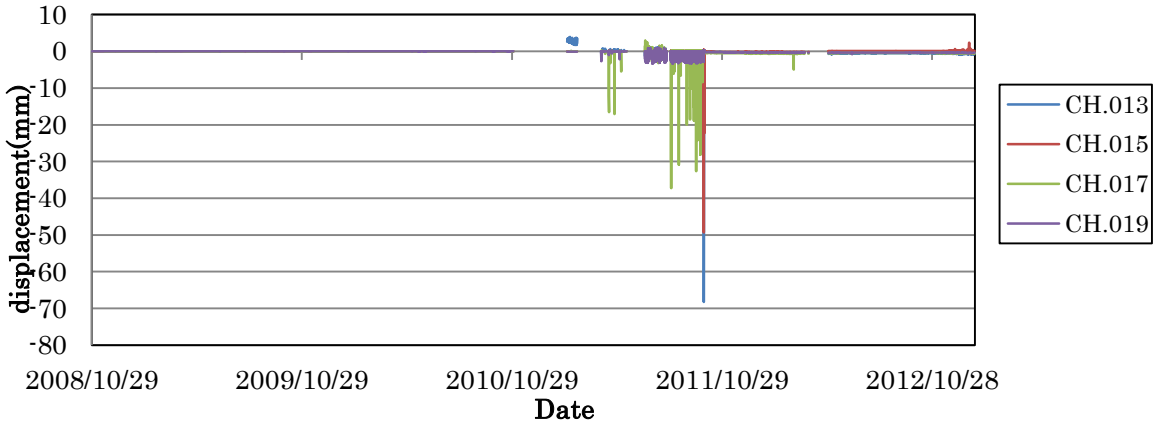

Fig. 3-122　Record of dummy outside the room (raw data)

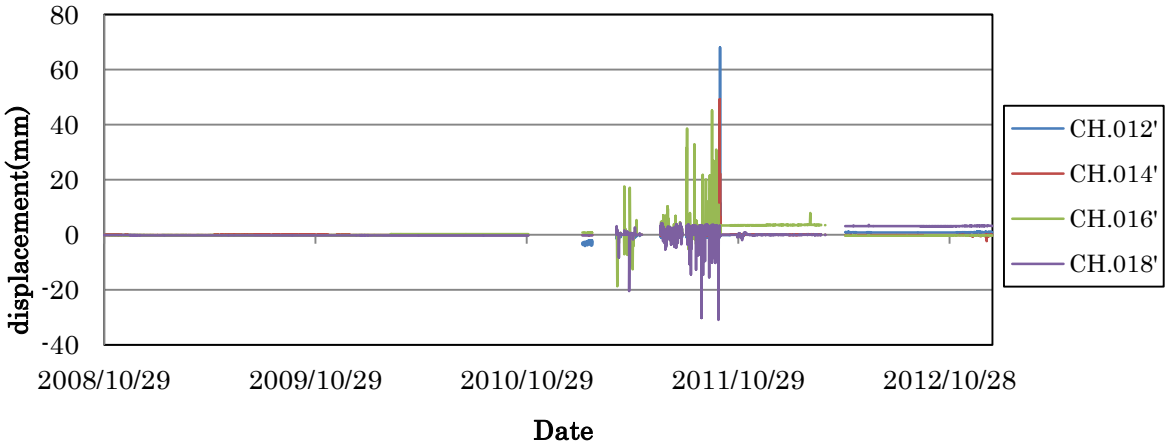

Fig. 3-123　Record of crack displacement outside the room (raw data revised with dummy)

All data show extraordinary values several times. It is considered that extraordinary values came from temperature revision of thermocouples when calculating the displacement data. The equation to calculate the displacement from temperature revision is below.

$$\mu\,\varepsilon(t) = a\,t^3 + b\,t^2 + c\,t + d$$

μ: conversion factor (με / mm)

ε(t): displacement (after revision) (mm)

a, b, c, d: correction coefficient

t: temperature (˚C)

The data are eliminated in the period between March of 2009 and March of 2010 in the figures. The thermocouples were replaced in March 8th to 10th, 2010. After the replacements, correct data of temperature could be recorded until July 31st, 2010. However, it is eliminated the unusual data of Ch 0 until September of 2011. After April 2011 to September 2011, the battery was started to use for power supply.

Figs. 3-125, 3-126 and 3-127 show the records of crack displacement. Some points which were no data due to personal or electrical factor were revised in consider with records of earthquake monitoring and the local seismic motions. These records were also eliminated the strange values as well as the records of temperature. The transducers of Ch5 and ch8 happen to be peeled off in July 5th, 2012 and in July 13th, 2012, respectively. These were glued again as the same process as described in the former section.

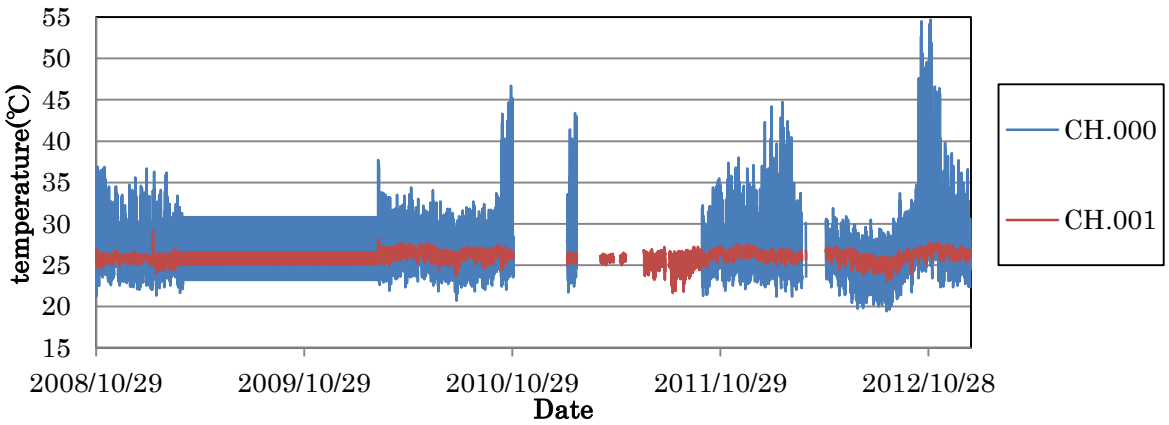

Fig. 3-124　Record of temperature from thermocouples (after revision)

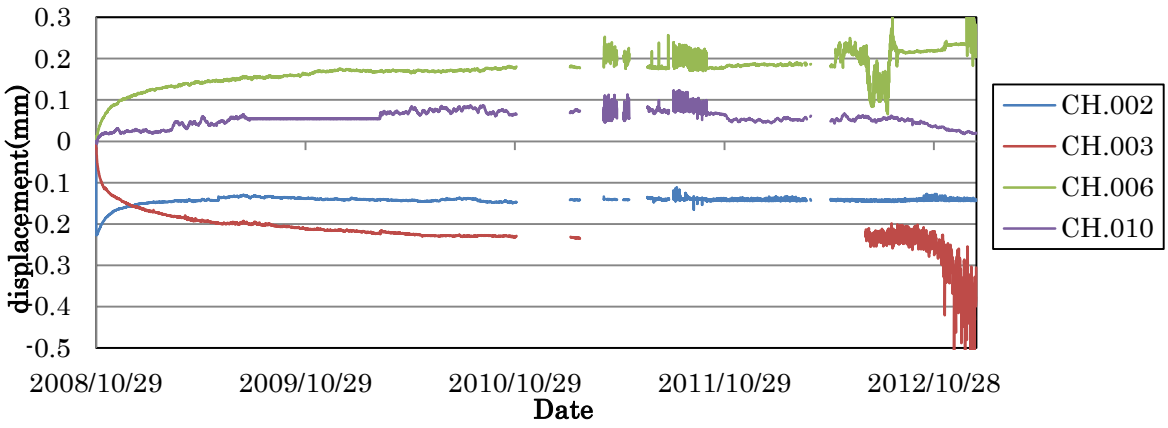

Fig. 3-125　Record of crack displacement inside the room (after revision)

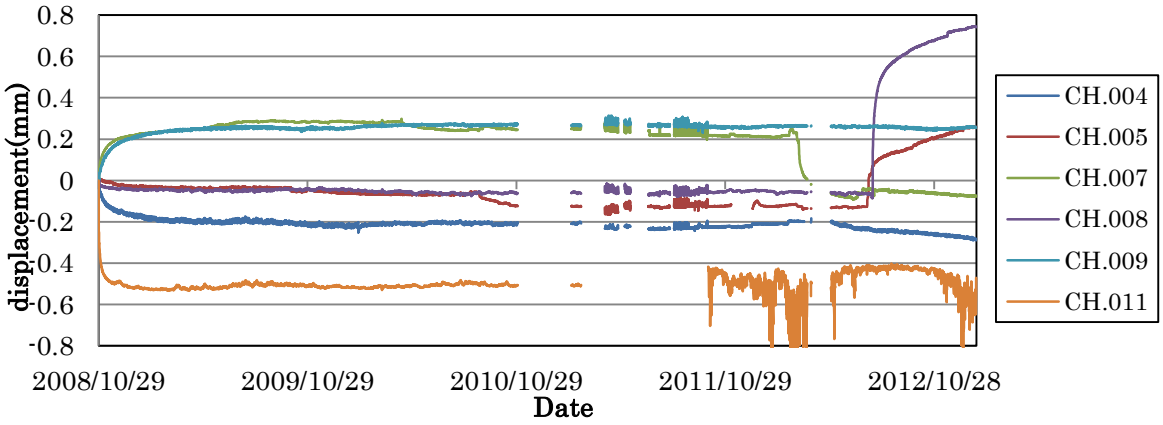

Fig. 3-126　Record of crack displacement around entrance of the room (after revision)

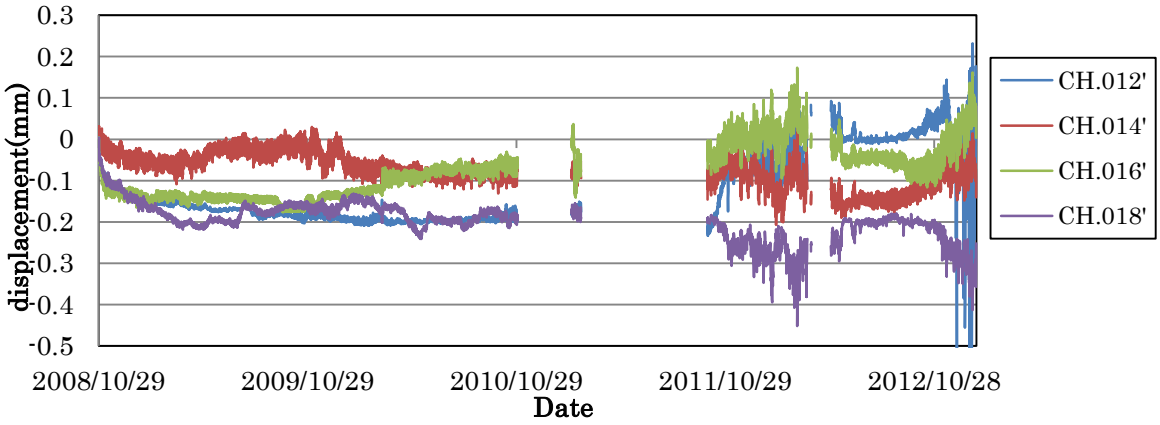

Fig. 3-127　Record of crack displacement outside the room (after revision)

Figs. 3-128 to 3-131 show the records of temperature and humidity logger from the October 29th, 2008 to January 10th, 2013. The records stopped on September 27th, 2009 by full memory of the data logger. The record of temperature and humidity logger at the central room had already collected on November 4th, 2009. Therefore, the graphs are separated, shown in Fig. 3-131. The record of thermocouple (Ch 1) is also drawn in this figure to show the condition in the central room. All of the equipment were restarted to record since November 4th, 2009. Though there were no data from March 10th, 2010 to June 16th, 2011, temperature and humidity monitoring was restarted since June 17th, 2011. On October 30th, 2012, all loggers were replaced with new ones as mentioned before.

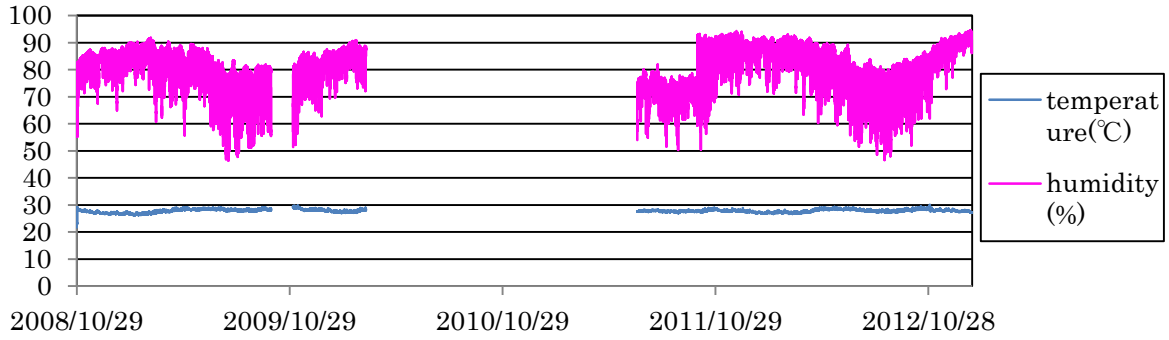

Fig. 3-128 Variation in temperature and humidity at the North

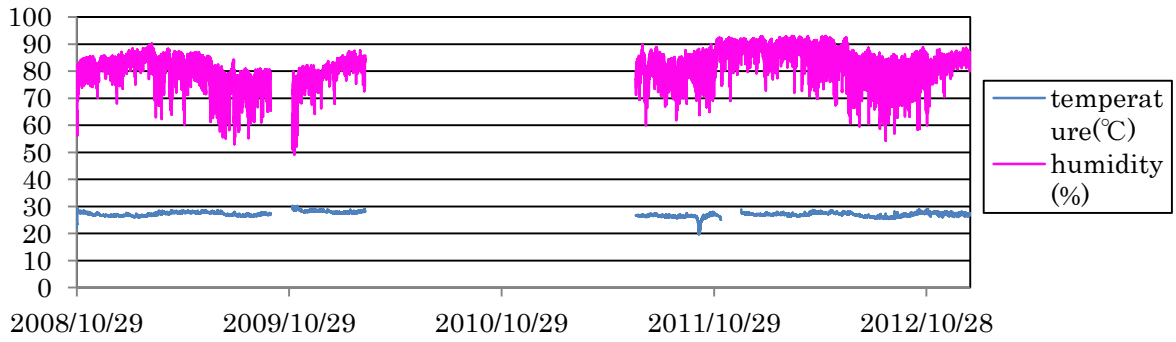

Fig. 3-129 Variation in temperature and humidity at the West

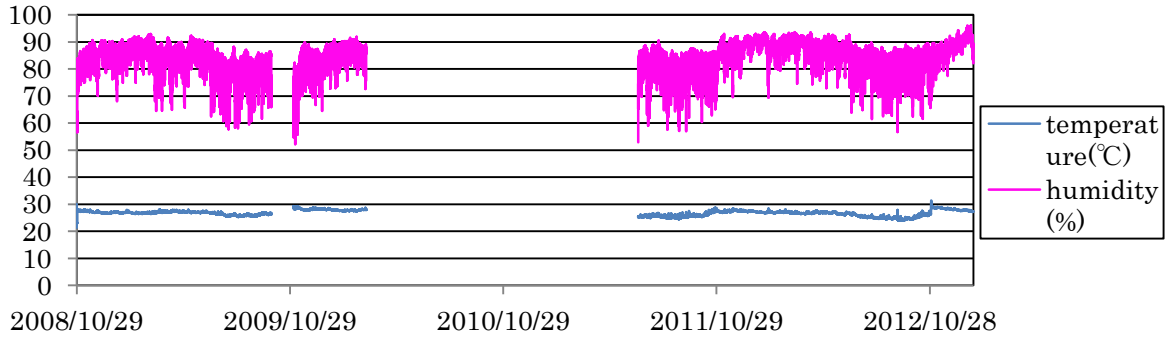

Fig. 3-130 Variation in temperature and humidity at the South

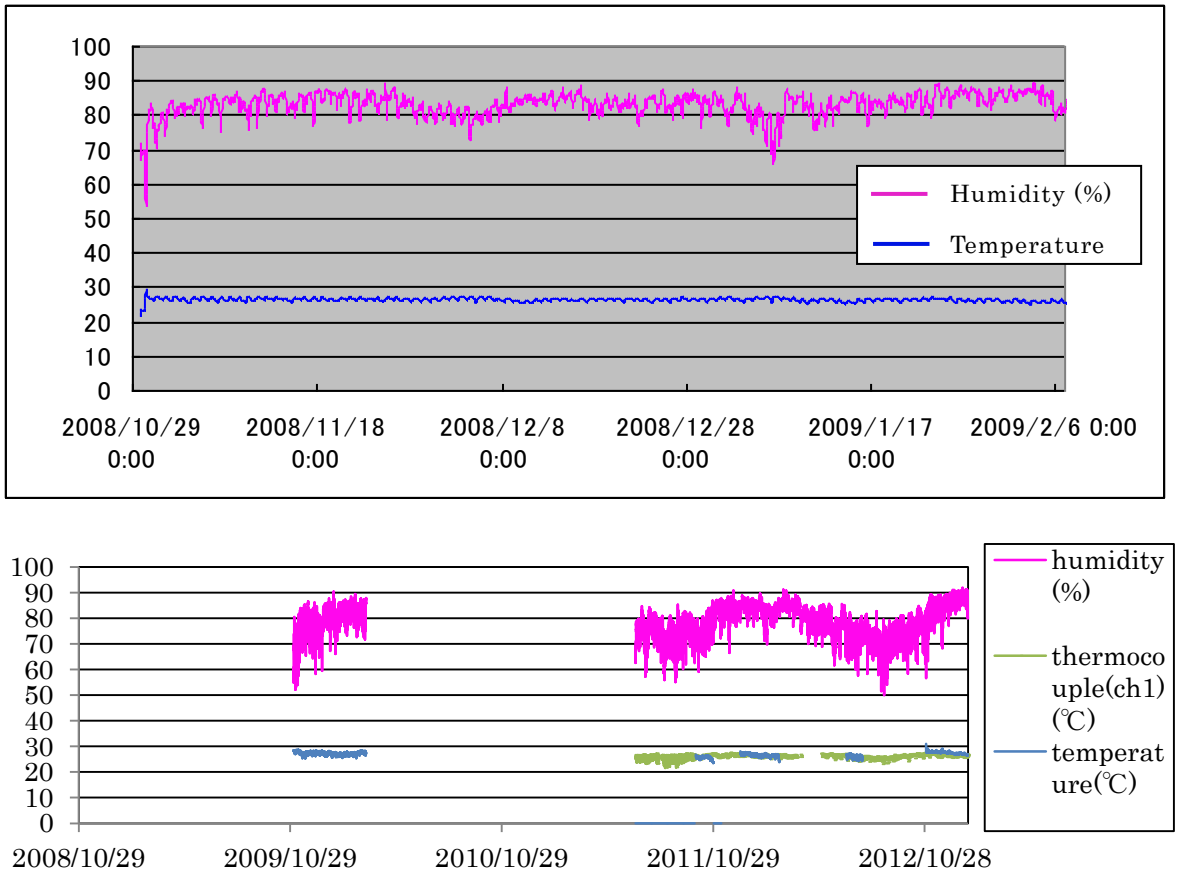

Fig. 3-131　Variation in temperature and humidity inside the central room

Fig. 3-132 shows the record of the temperature and humidity logger setting at the outside during March 9th, 2010 to August 30th, 2012.

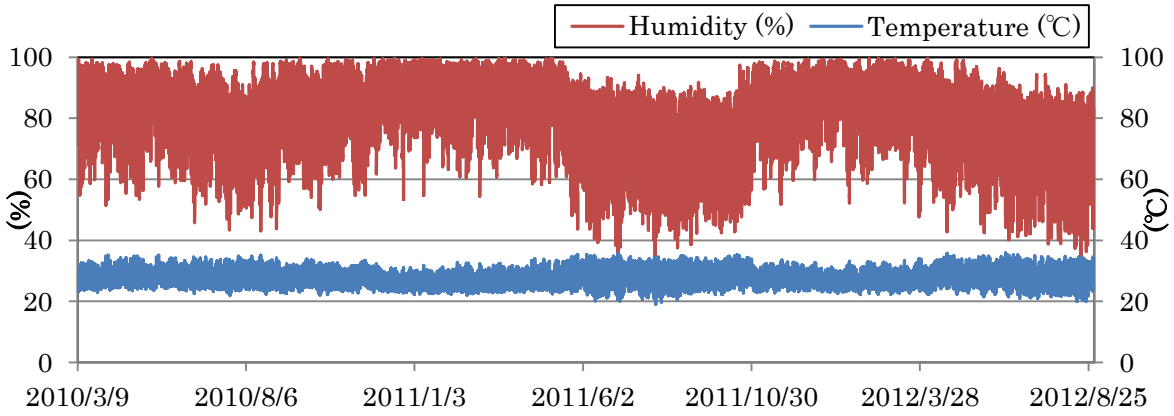

Fig. 3-132　Record of temperature and humidity at the outside

3.3.3 MONITORING RESULTS

Figs. 3-133 to 3-136 show the displacement movement before and after every earthquakes, mentioned in the former section. Judging from these figures, crack displacements at inside, entrance and outside of the central room were not affected by the earthquakes. This record indicated that the structure of Chandi Shiva was structurally stable. At the same time, this record suggested that emergency structural intervention would not be needed.

Three factors, humidity, crack displacement and temperature are composed in figures to find the relationship. Figs. 3-137 to 3-141 show those figures at central room, northern room, western room, southern room and outside of Chandi Shiva, respectively, from June 10th to 15th, 2012. There found no relation between crack displacement and humidity.

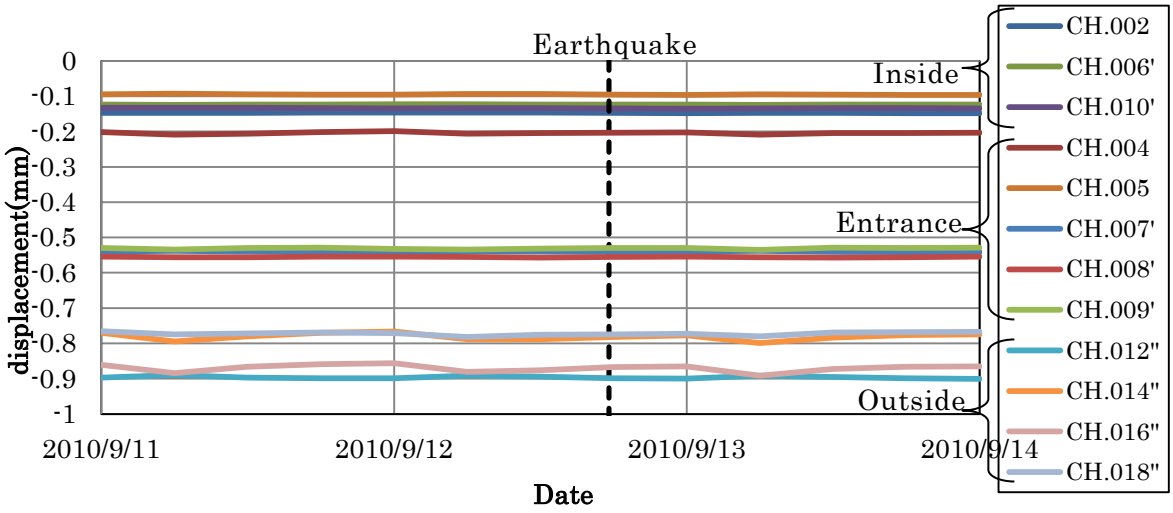

Fig. 3-133 Crack displacement before and after earthquake (September 12th, 2010)

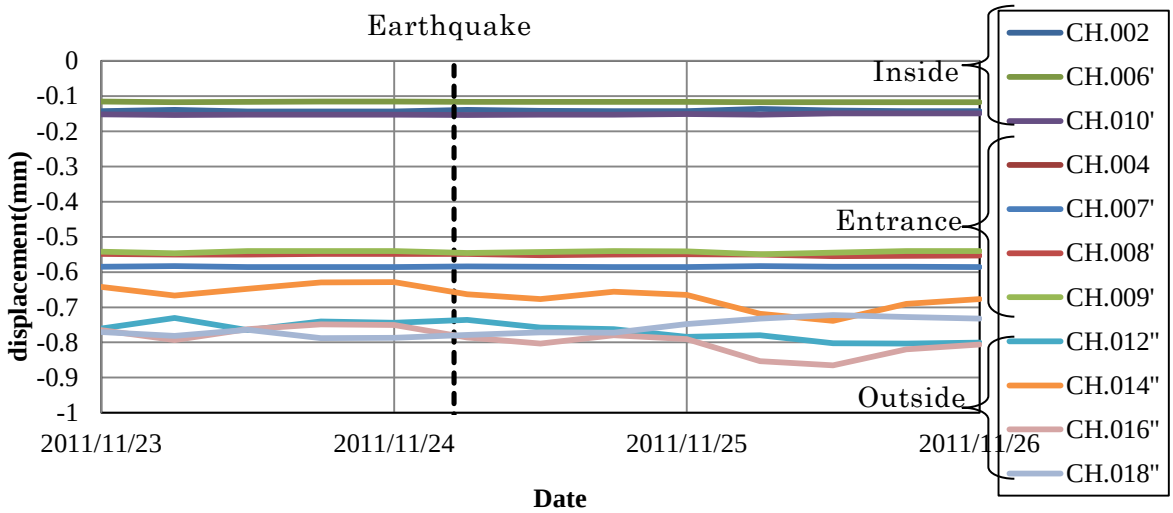

Fig.3-134 Crack displacement before and after earthquake (November 24th, 2011)

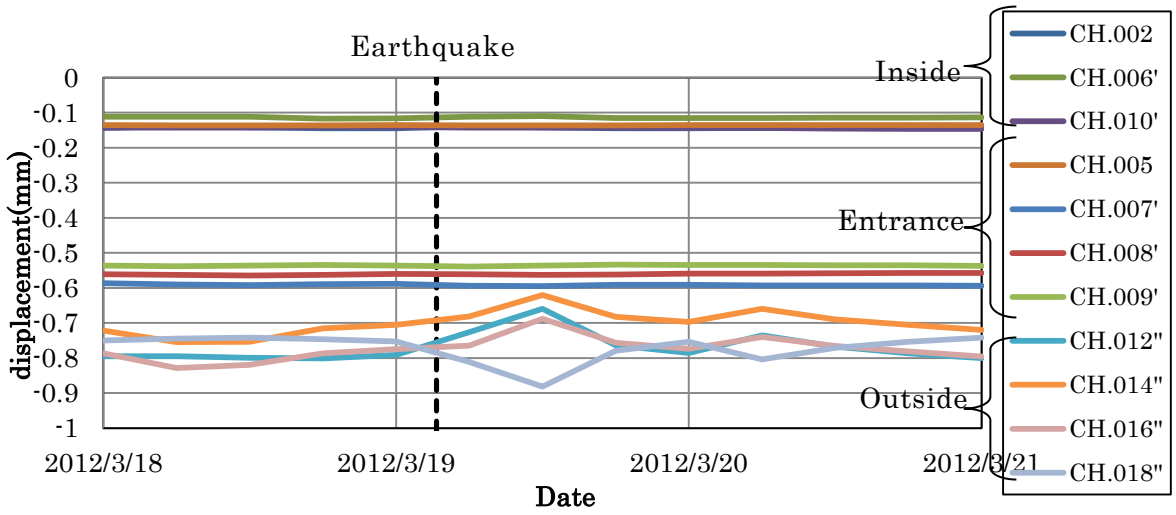

Fig.3-135 Crack displacement before and after earthquake (March 19th, 2012)

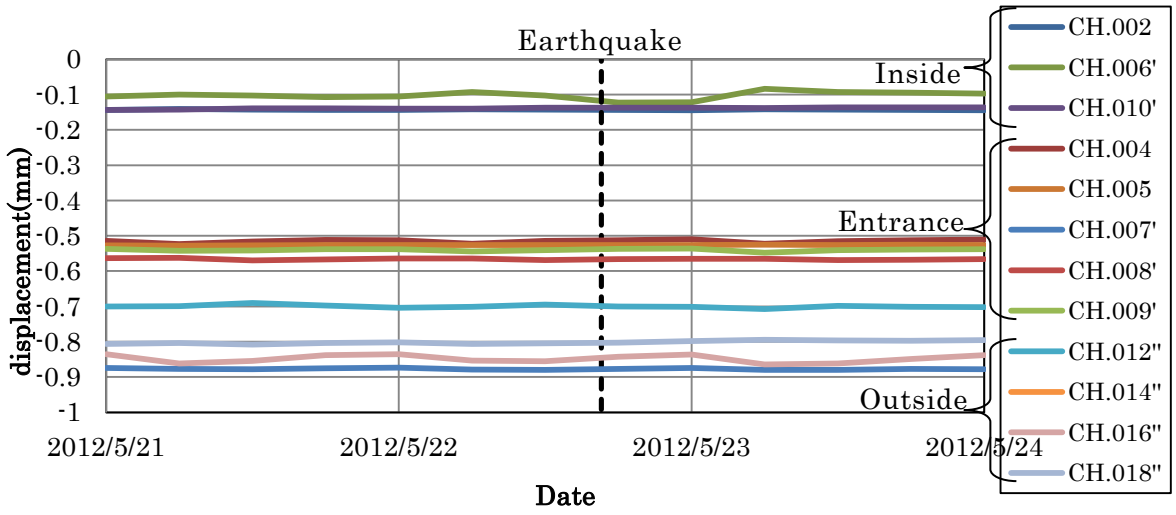

Fig. 3-136 Crack displacement before and after earthquake (May 22th, 2012)

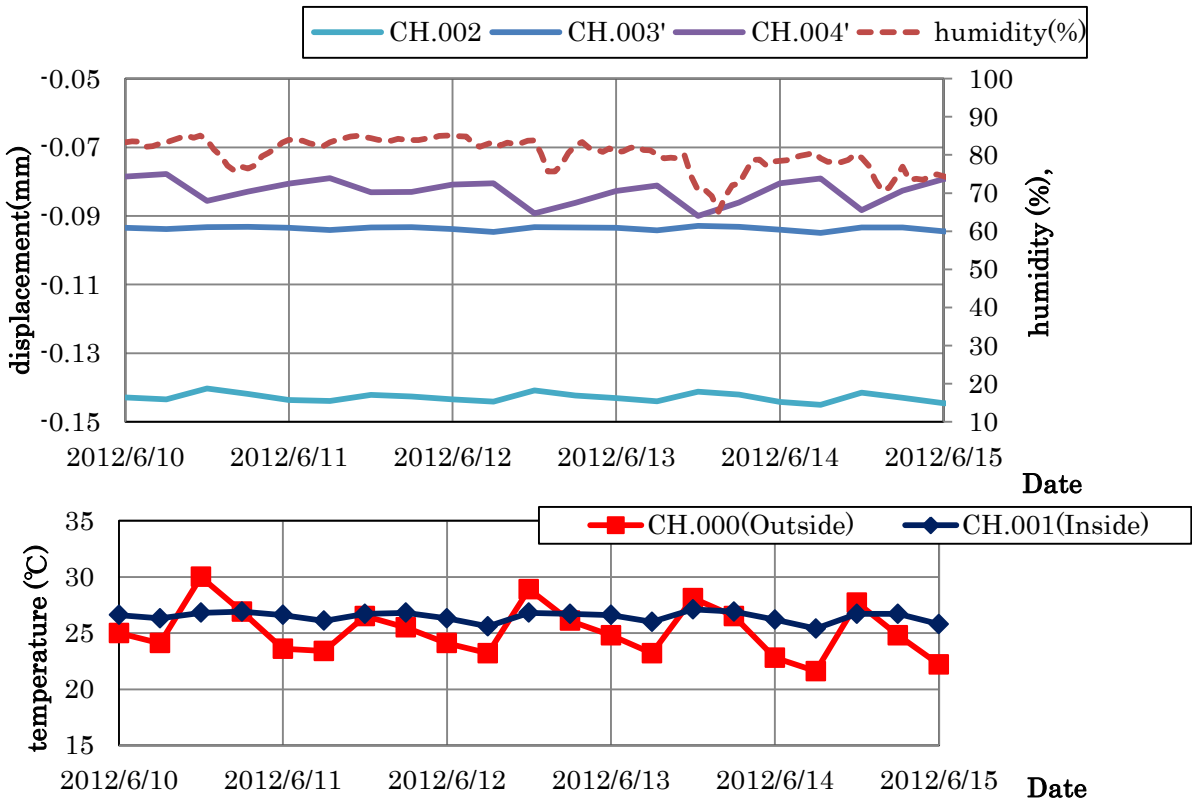

Fig. 3-137　Crack displacement, humidity and temperature; Central room

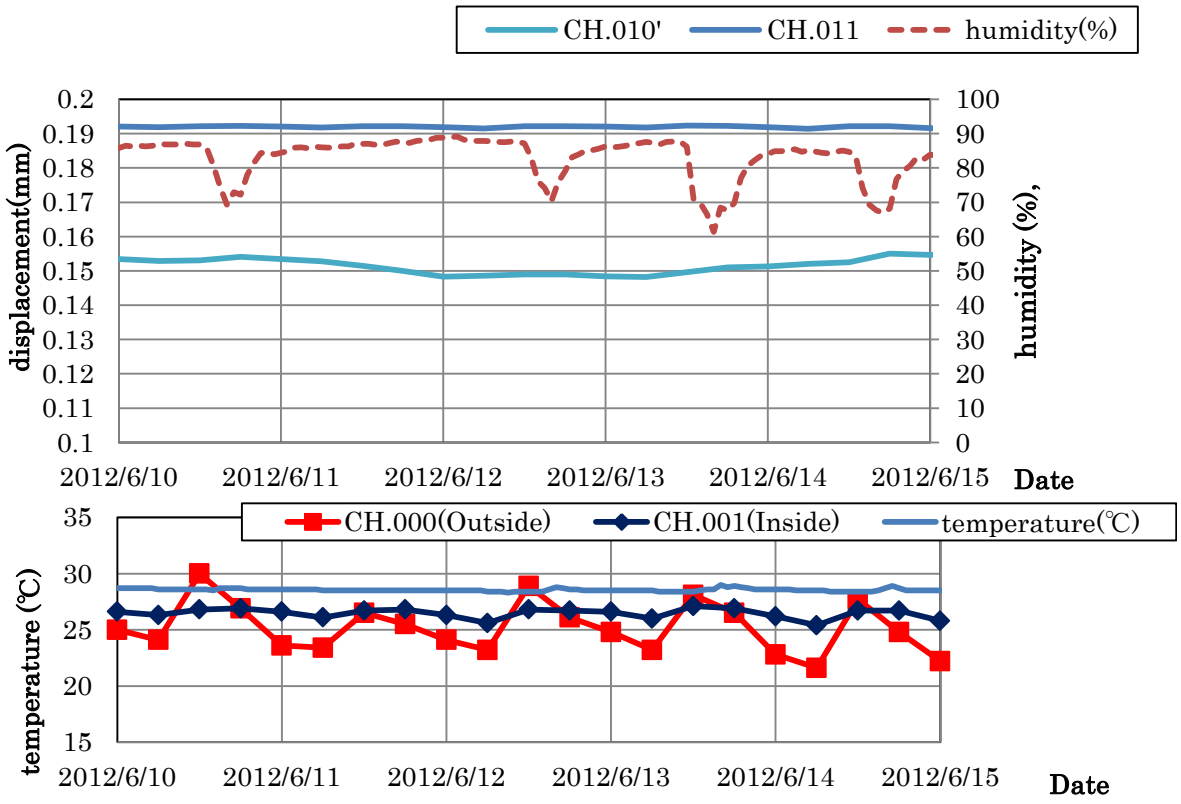

Fig. 3-138　Crack displacement , humidity and temperature; Northern room

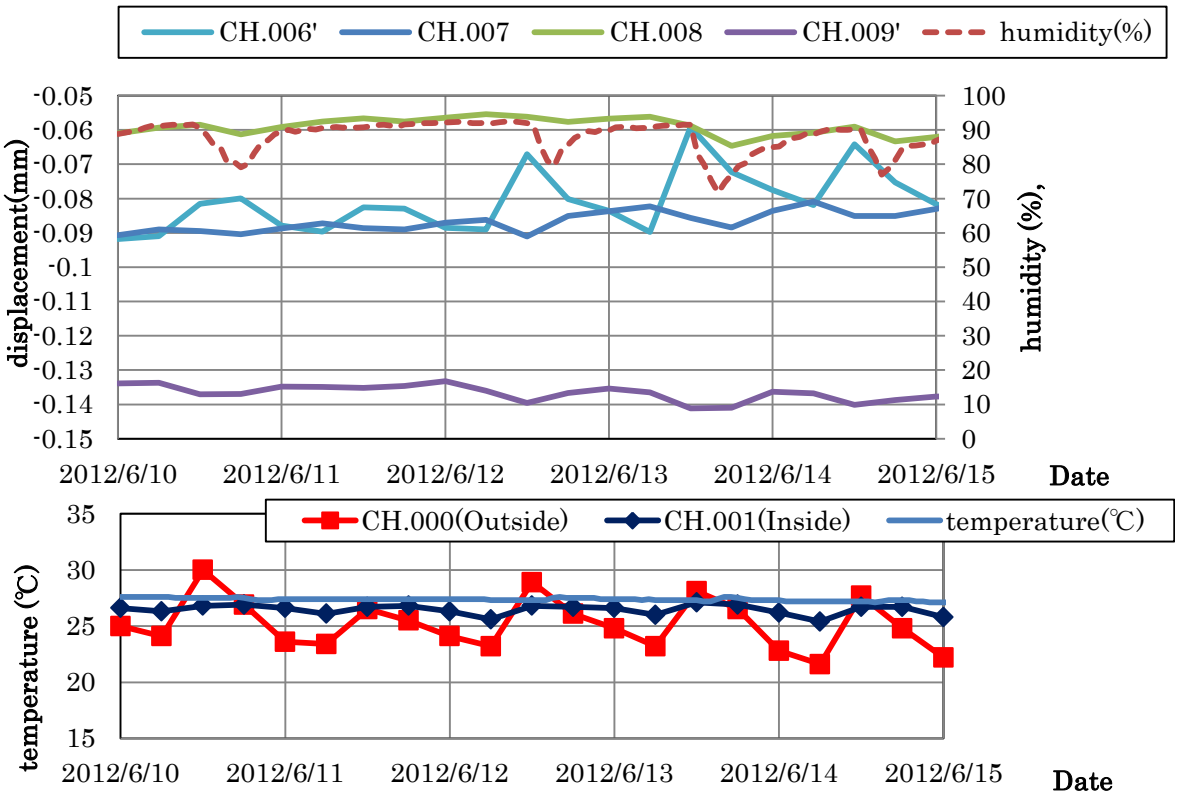

Fig. 3-139　Crack displacement, humidity and temperature; Western room

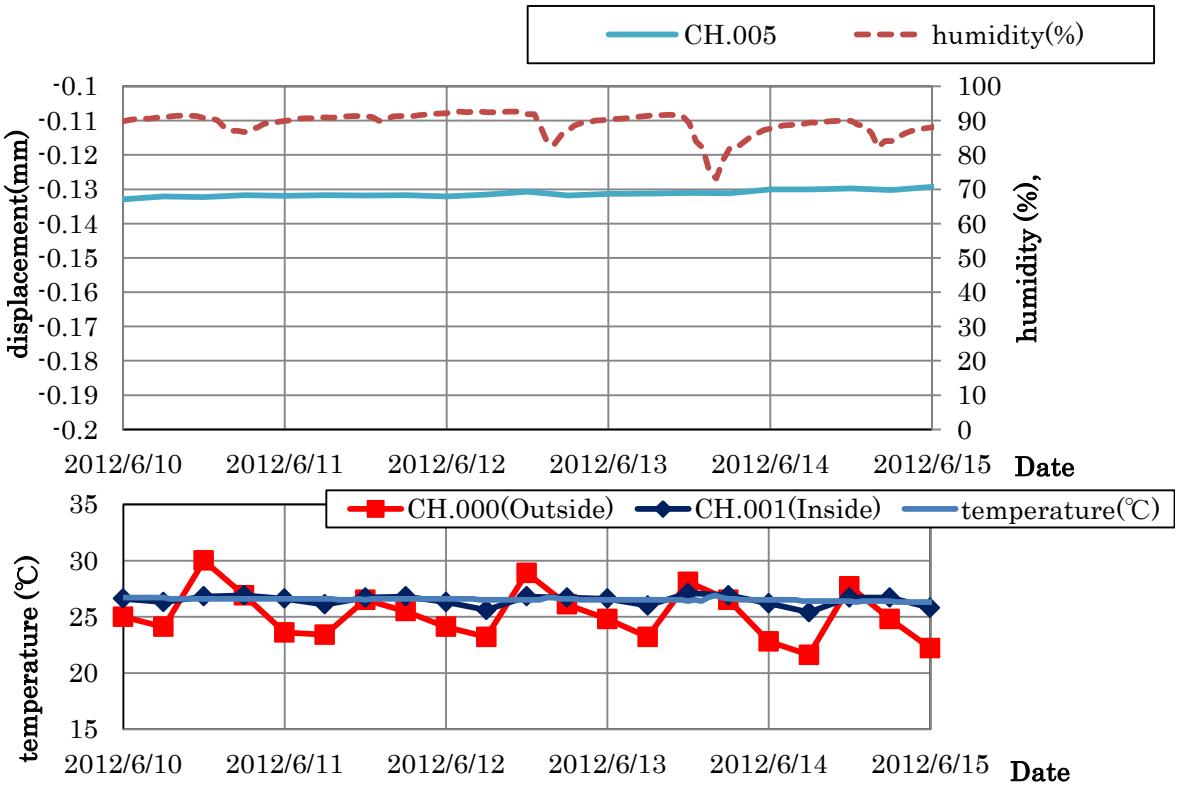

Fig. 3-140　Crack displacement, humidity and temperature; Southern room

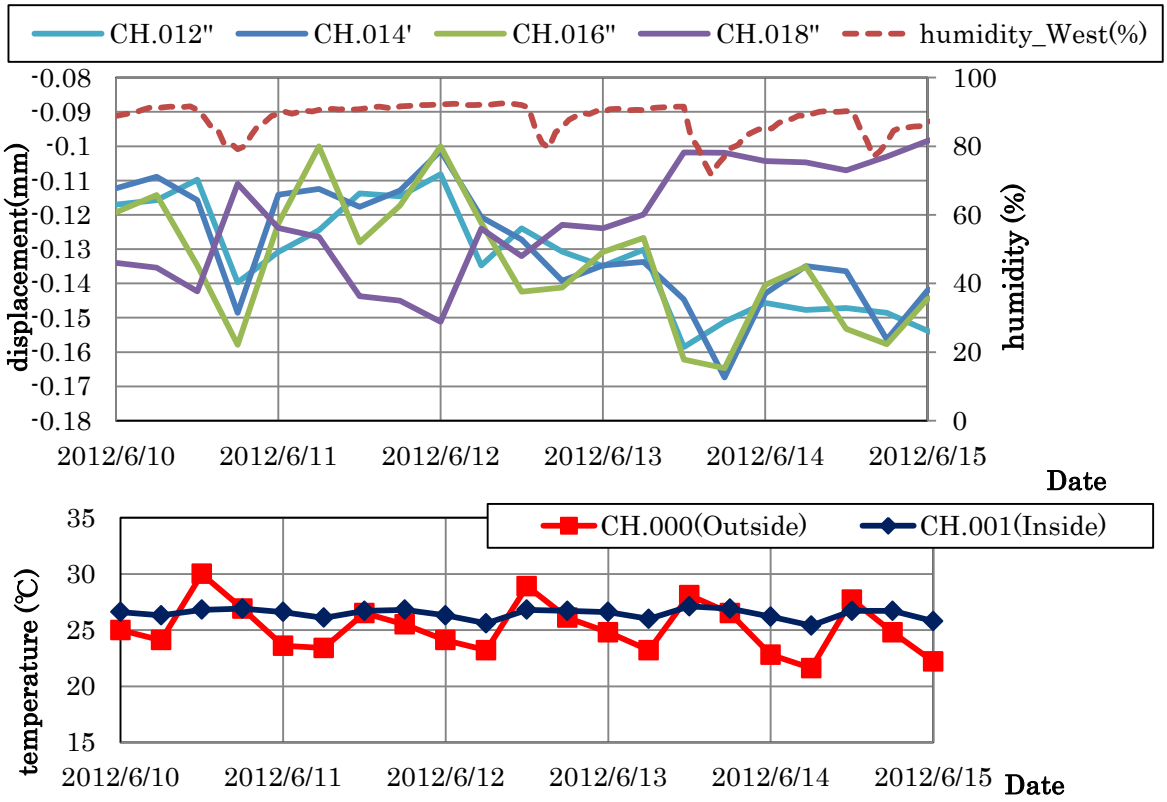

Fig. 3-141　Crack displacement, humidity in West room and temperature; Outside

Fig. 3-142 to 3-144 show monthly variations of each crack displacements. In the starting period, there found an effect of hardening of glue. In the figures of ch5 and ch8, the large displacement in July of 2012 was caused by hardening of glue as well (indicated by red arrow). Many figures show the large vibration since July of 2011. This phenomenon was caused by huge noise. Nevertheless, there were no vibration of displacement exceeding 1 mm.

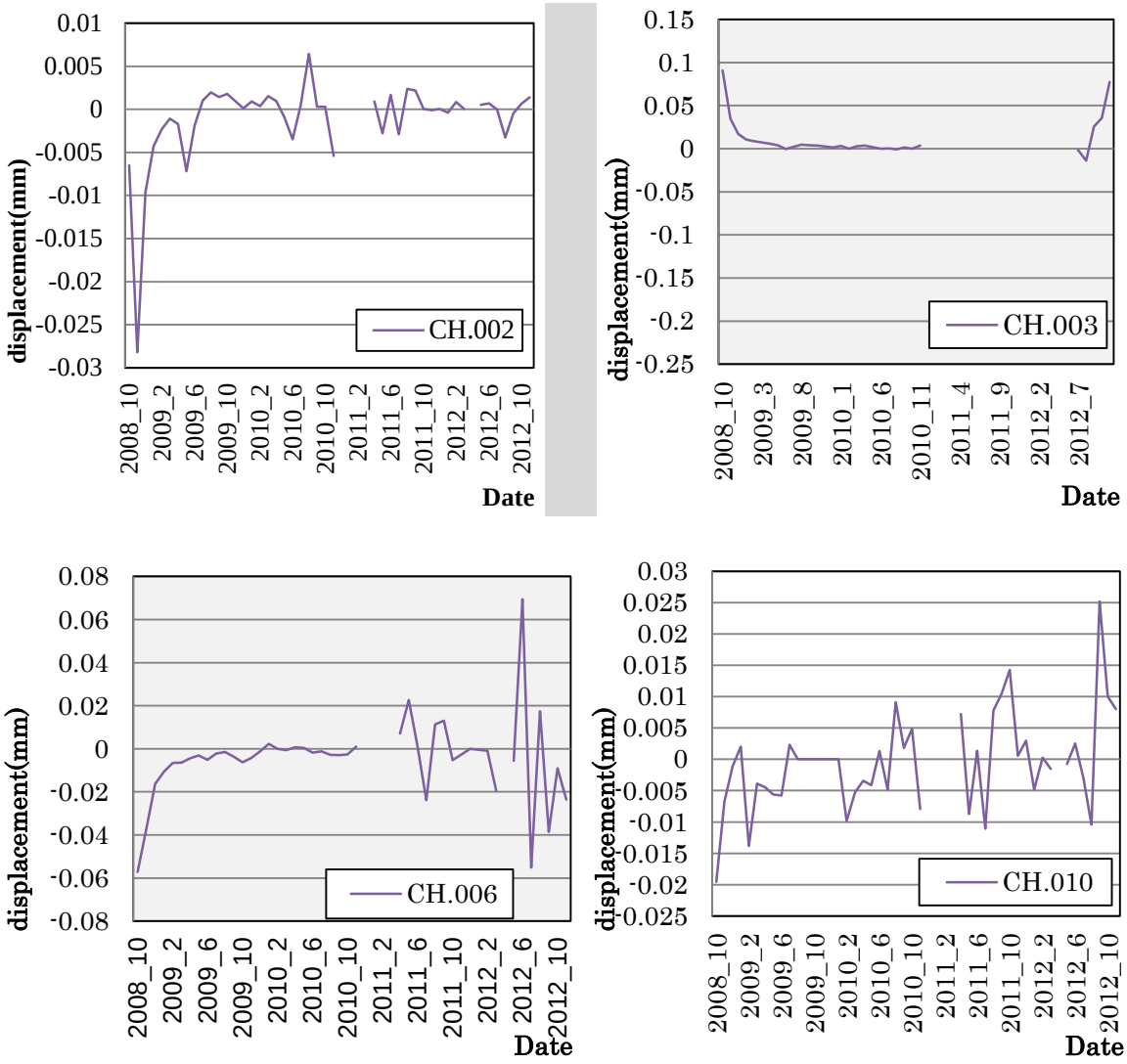

Fig. 3-142　Monthly vibration; Inside

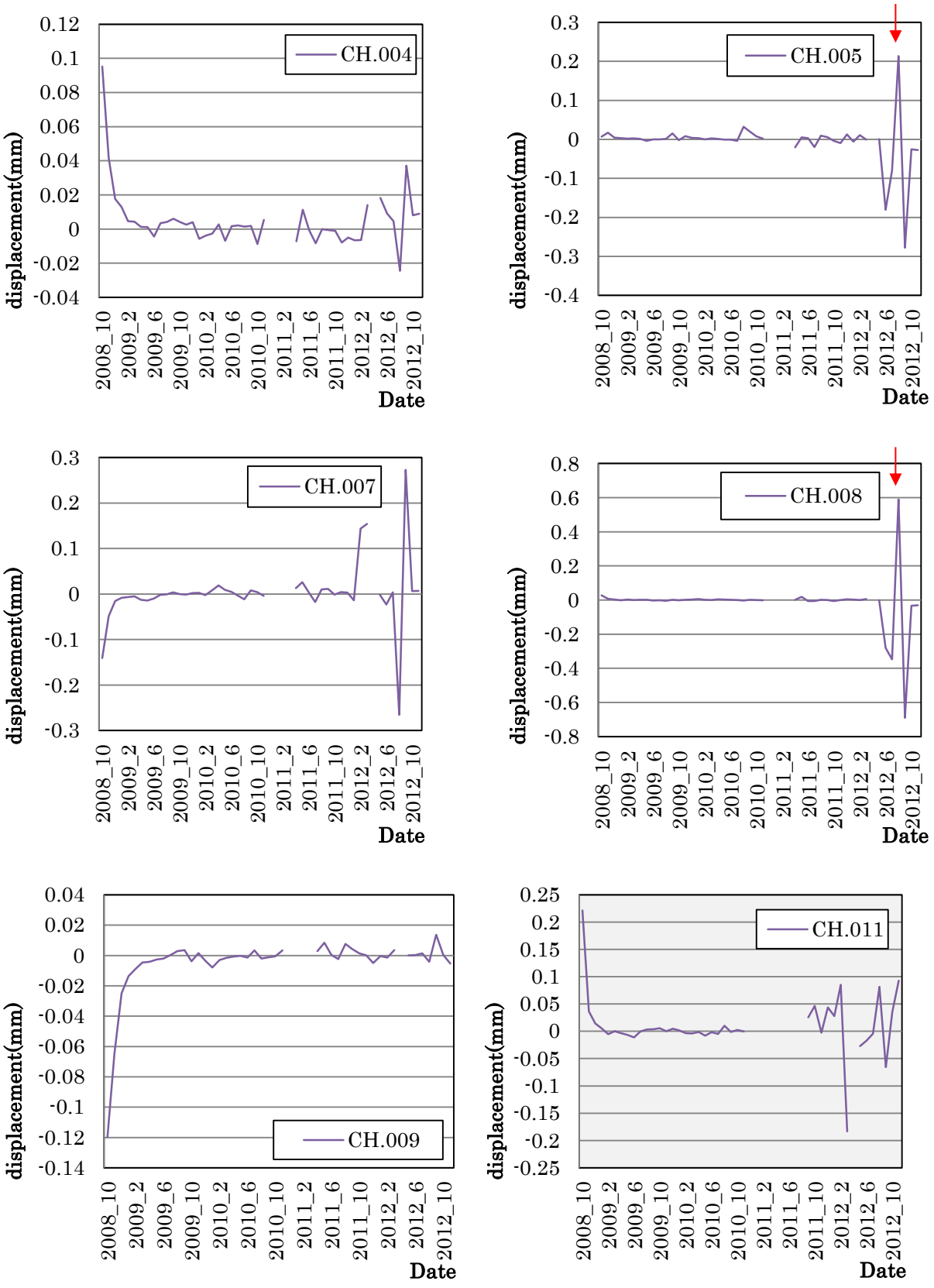

Fig. 3-143　Monthly vibration; Entrance

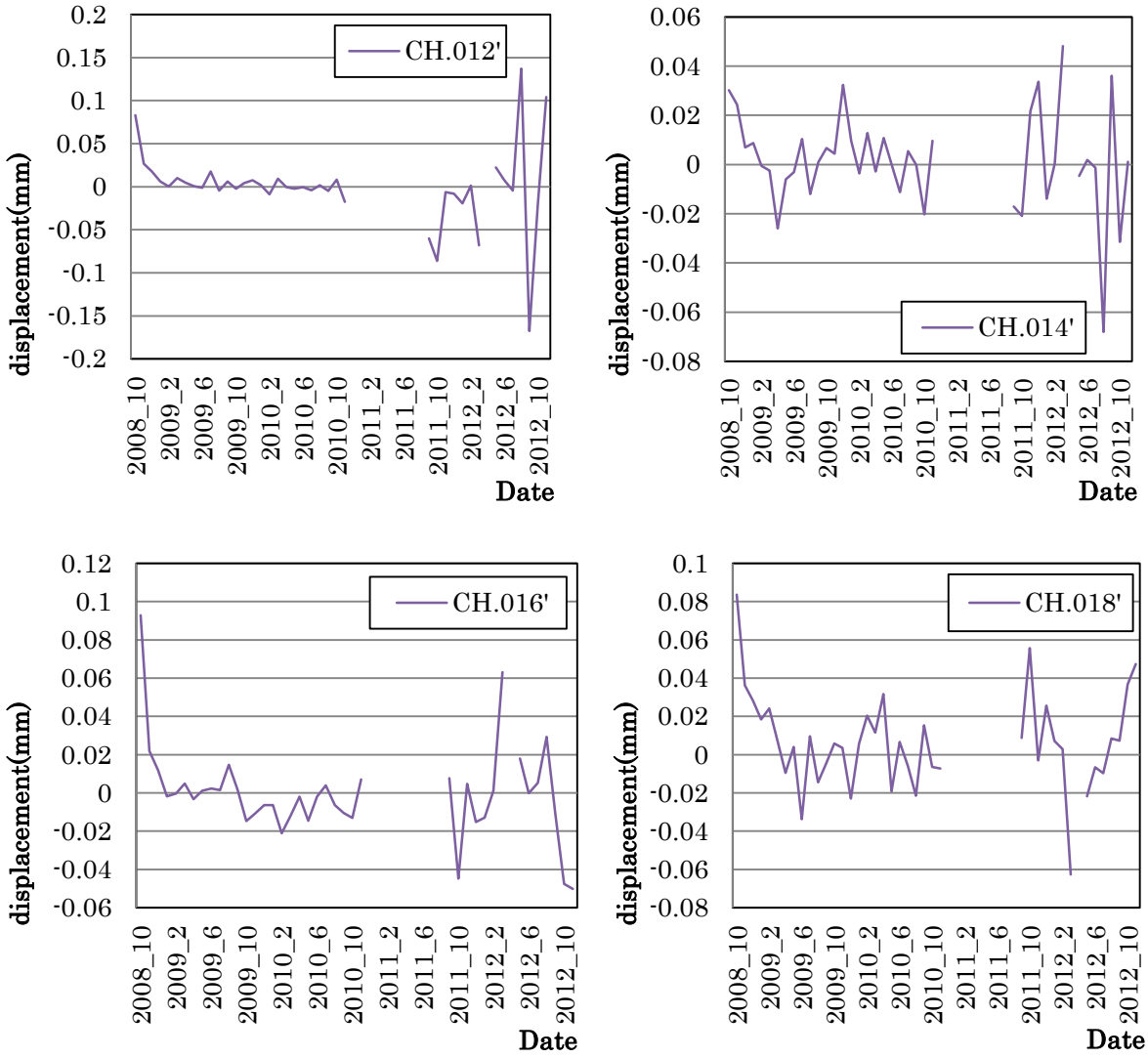

Fig. 3-144 Monthly vibration; Outside

The record of the temperature and humidity logger at the outside was compared with the thermocouples and another logger installed in the north room during August 20th to 30th in 2012 as shown in Figs. 3-145 and 3-146. One of the thermocouples and one temperature and humidity logger have been recorded the temperature at the outside. However, the former is at the Southwest, therefore, the monument shades this thermocouple from the sun. On the other hand, the latter is at the East. This difference in their condition caused approximately 5 degree difference in the highest temperature between at the Southwest and East. The lowest temperature did not show clearly difference as there was no factor effecting on the temperature.

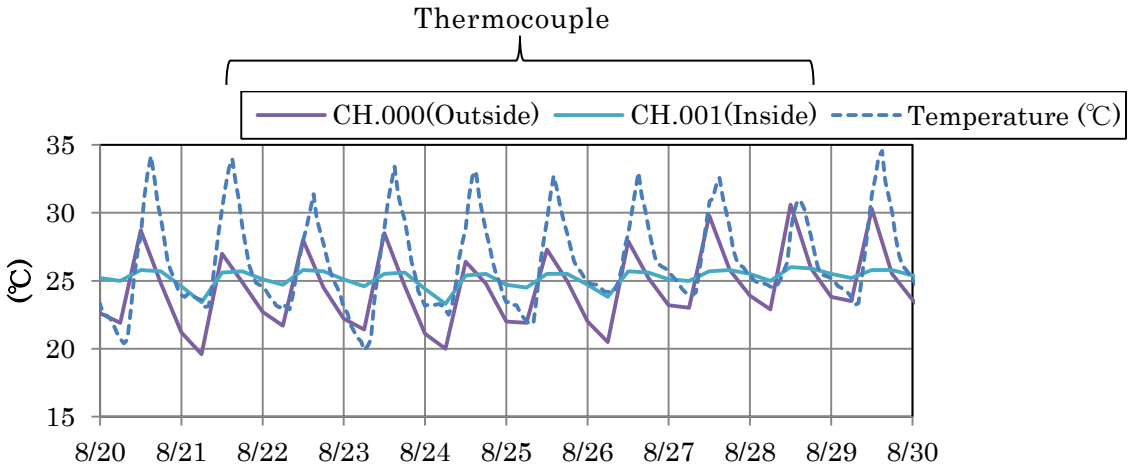

Fig. 3-145　Comparison of the thermocouples and the temperature of the logger

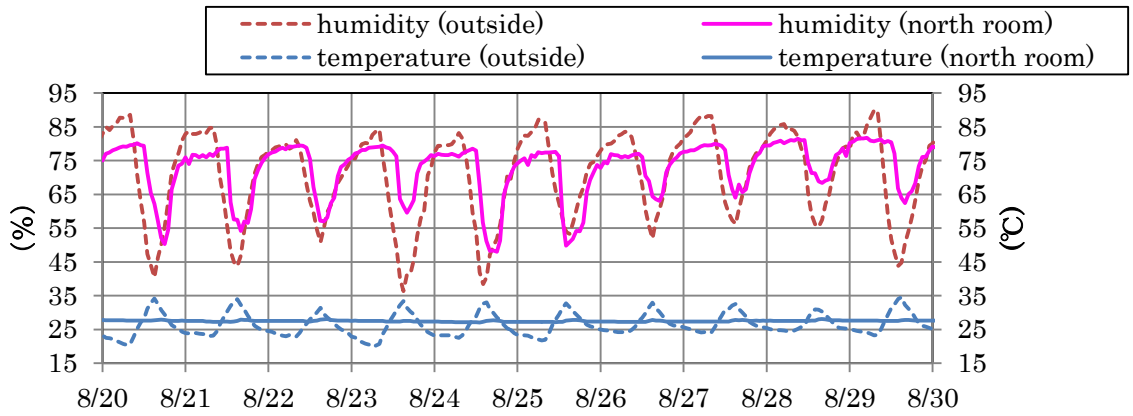

Fig. 3-146　Comparison of the records of data loggers at the outside and in the north room

3.4 SEISMIC RESPONSE ANALYSIS

3.4.1 LAMPED MASSES MODEL

A simplified analysis model, a lumped masses model, was introduced in the past study [15]. Three types of analysis models were assumed in the past study; A) rigid base model without dynamic soil-structure interaction, B) sway-rocking model without base embedding effect and C) embedding sway-rocking model with base embedding effect. As a result of the analysis with using these three models, model C was in good agreement with the monitoring record of 2010. Therefore in this thesis, the embedding sway-rocking model was employed to simulate the earthquake response of Chandi Shiva with consideration of dynamic soil-structure interaction presented in Fig. 3-147. Sway-rocking is called SR in the following sections in this thesis. Depth of embedding base was assumed to be 8 m, at the same time, the damping ratio of the soil spring was assumed to be 7 %. This damping ratio was evaluated to fit the analysis with the record. The natural frequency of the analysis model was 2.0 Hz being the same as that of the record. Table. 3-15 shows the parameters for the analysis. Table. 3-16 shows the material properties of concrete and soils of this analysis model.

The seismic behaviors of the event on September 12th, 2010, November 24th, 2011, March 19th and May 22th, 2012 were simulated as mentioned in the previous sections. The locations of the seismographs correspond with the level of lumped mass of the analysis shown in Fig. 3-148; Top and Mass No. 6, and Middle and Mass No. 4.

Parametric analysis of damping ratio and stiffness of the soil was conducted to the analysis of the earthquakes of 2011 and 2012.

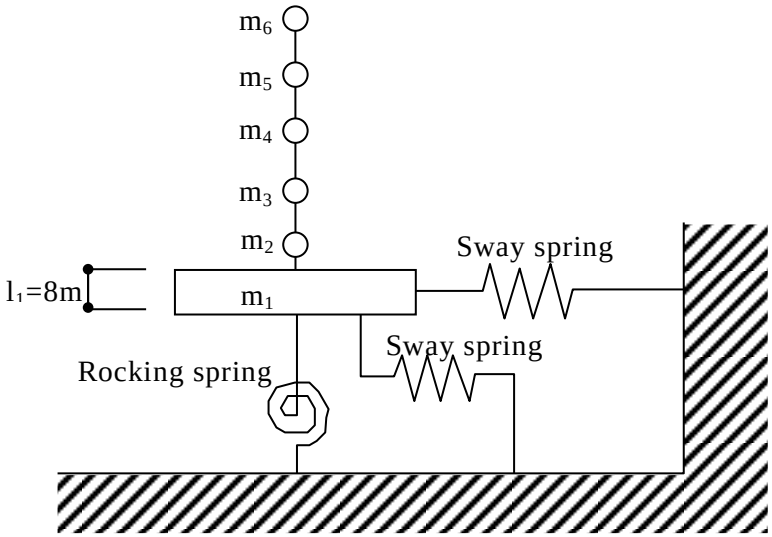

Fig. 3-147 Embedding SR model

Table. 3-15　Parameters for analysis

	Area (m^2)	Volume (m^3)	Equivalent Radius (m)	Second Moment of Area (m^4)
m2	921	7000	17.1	6.75×10^4
m3	408	3835	11.4	1.33×10^4
m4	279	2790	9.4	6.20×10^3
m5	144	1152	6.8	1.65×10^3
m6	17	175	2.3	23

Table. 3-16　Material properties for analysis

Concrete	ρ (kg/m^3)	2300
	ν	0.16
	E (N/m^2)	5.83E+09
Soil	ρ (kg/m^3)	240
	ν	280
	Vs (m/s)〈-8m～0m〉	1800
	Vs (m/s)〈under -8m〉	0.4

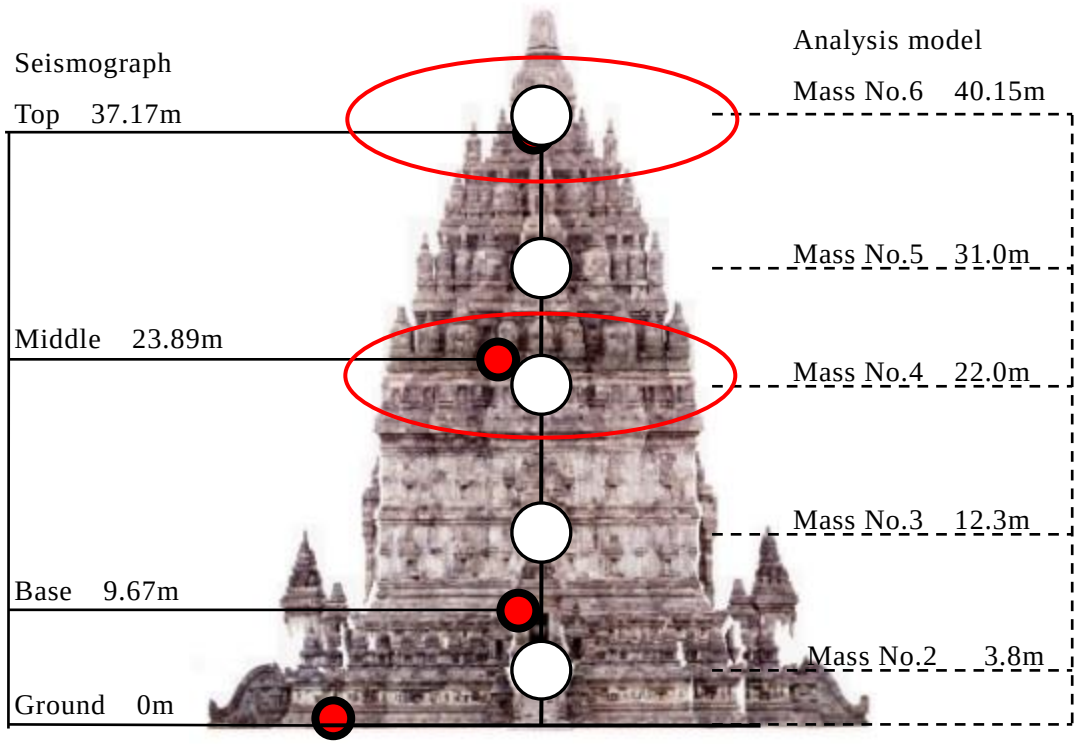

Fig. 3-148　Location of seismographs and lamped masses of the analysis model

3.4.2 RESULTS

Figs. 3-149 through 3-152 compare the peak response acceleration of the analysis with the monitoring the earthquakes in September of 2010, Nobember of 2011, March and May of 2012, respectively. In the analysis of 2010, Rayleigh damping model of the whole system was assumed to be 4 % (both for the primary and secondary modes). Parametric analysis of damping ratio and the soil stiffness were conducted for the analysis of the earthquakes of 2011 and 2012. Tables. 3-17 through 3-19 show the parameters for the model of December of 2011, March and May of 2012, respectively. For the analysis model of March of 2012 soil stiffness reduction due to strain dependency was taken into account. The condition of Model A shown in Table. 3-18 is the same as the model for the analysis of the earthquakes in 2010, 2011 and May in 2012. The soil stiffness of Model B was reduced by 30 %. As well as, the soil stiffness of Model C was reduced by 50 %.

Judging from Fig. 3-150, the model of which damping ratio was 4 % for both the primary and secondary modes was in best agreement with the monitoring of the earthquake of 2011. Furthermore, judging from Fig. 3-151, the model A of which damping ratio was 4 % was in best agreement with the monitoring of the earthquake of March in 2012. Judging from Fig. 3-151, the model of which damping ratio was 10 % for both the primary and secondary modes was in best agreement with the monitoring of the earthquake of May in 2012. To assess those results in more detail, Figs. 3-153 through 3-160 show the comparison of the acceleration wave forms of the analysis models with those of the monitoring.

Table. 3-17 Parameter for the analysis model of Nobember in 2011

	Damping ratio	
	h1	h2
Model	4%	4%
	4%	2%
	3%	2%
	2%	2%
	2%	1%

Table. 3-18 Parameter for the analysis model of March in 2012

	Damping ratio	
	h1	h2
Model A	4%	4%
	4%	2%
Model B	4%	4%
	4%	2%
Model C	4%	4%
	4%	2%

Table. 3-19　Parameter for the analysis model of May in 2011

	Damping ratio	
	h1	h2
Model	1%	1%
	2%	2%
	4%	4%
	5%	5%
	7%	7%
	10%	10%

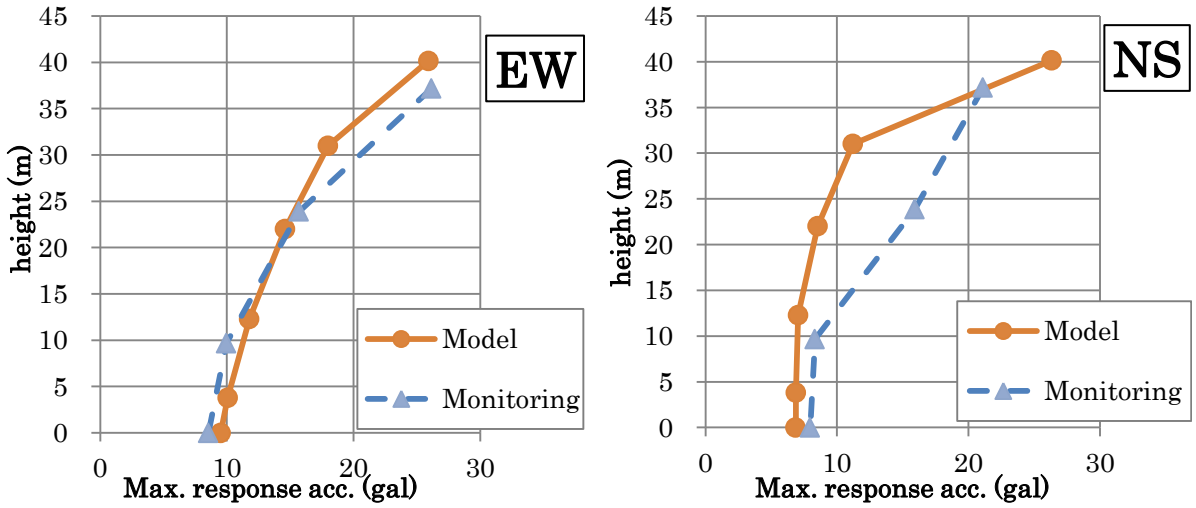

Fig. 3-149　Comparison of peak response acceleration (September 12th, 2010)

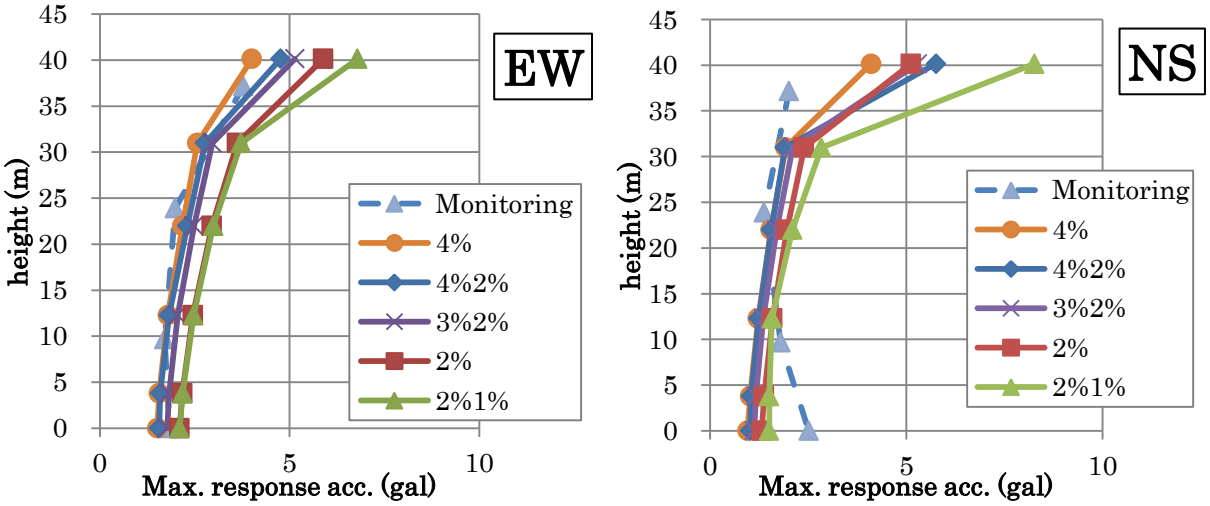

Fig. 3-150　Comparison of peak response acceleration (November 24th, 2011)

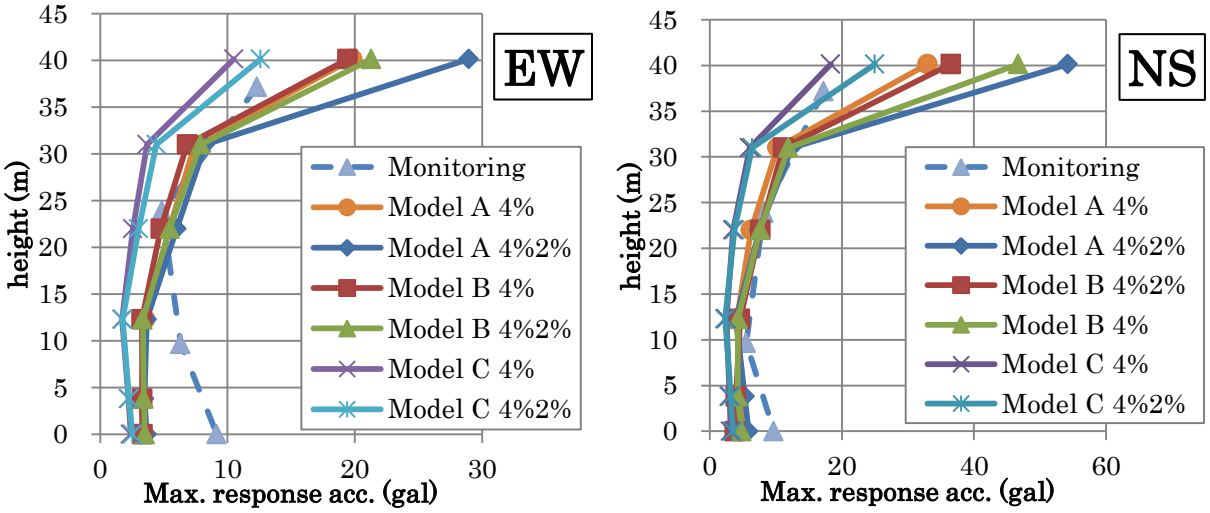

Fig. 3-151　Comparison of peak response acceleration (March 19th, 2012)

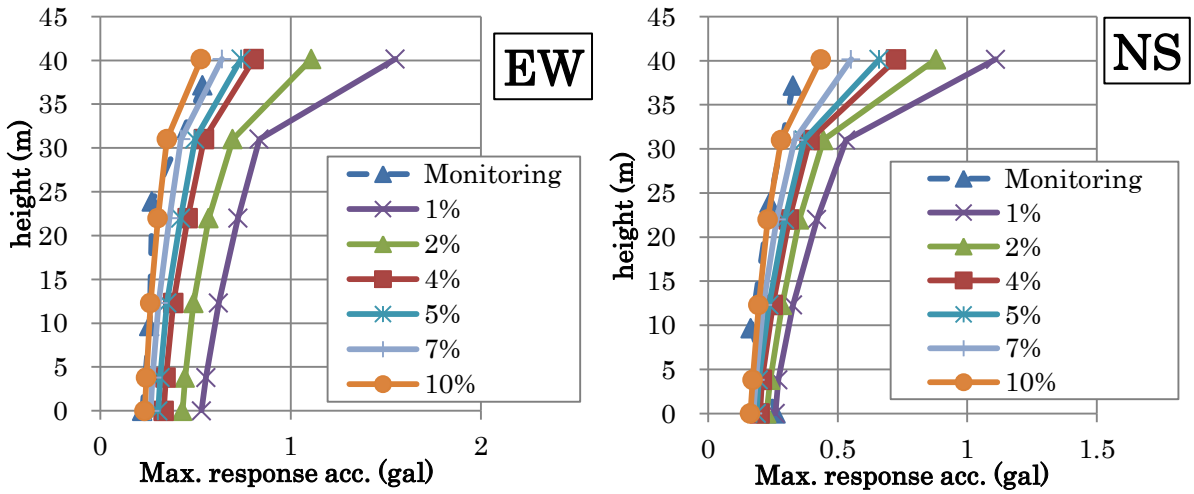

Fig. 3-152　Comparison of peak response acceleration (May 22th, 2012)

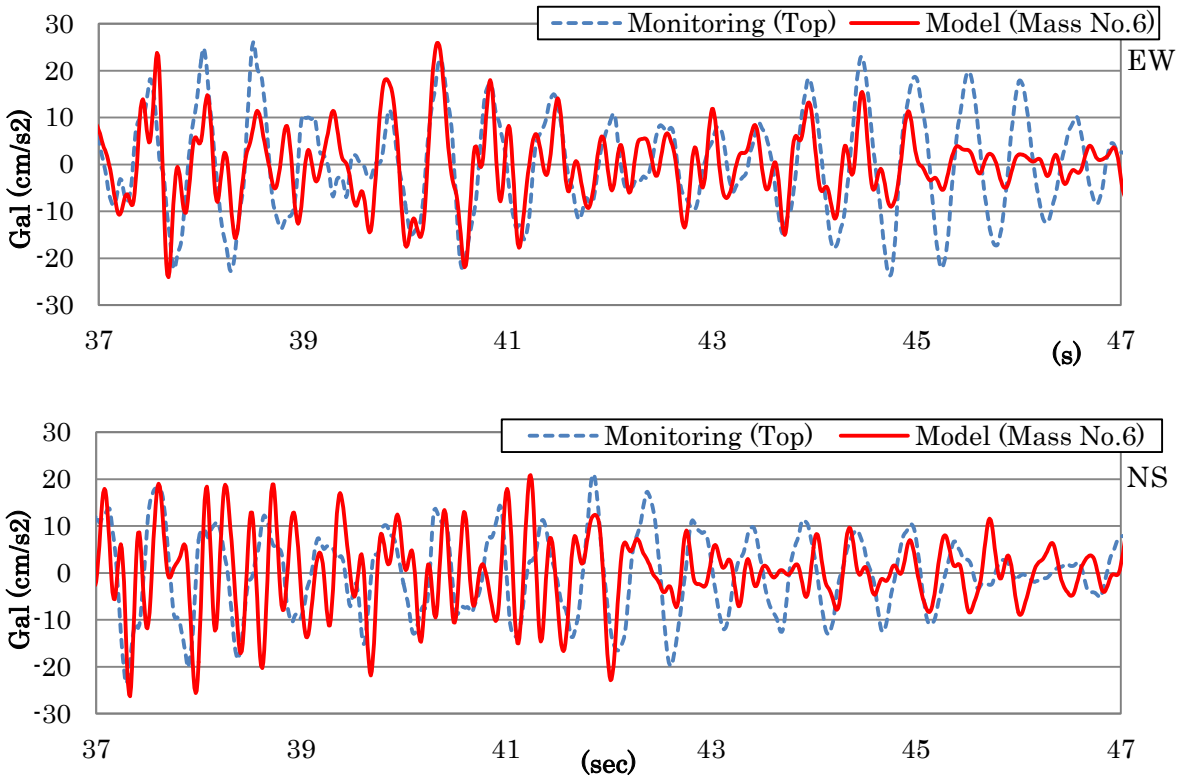

Fig. 3-153　Comparison of acc. wave form of Top and Mass No.6 (September 12th, 2010)

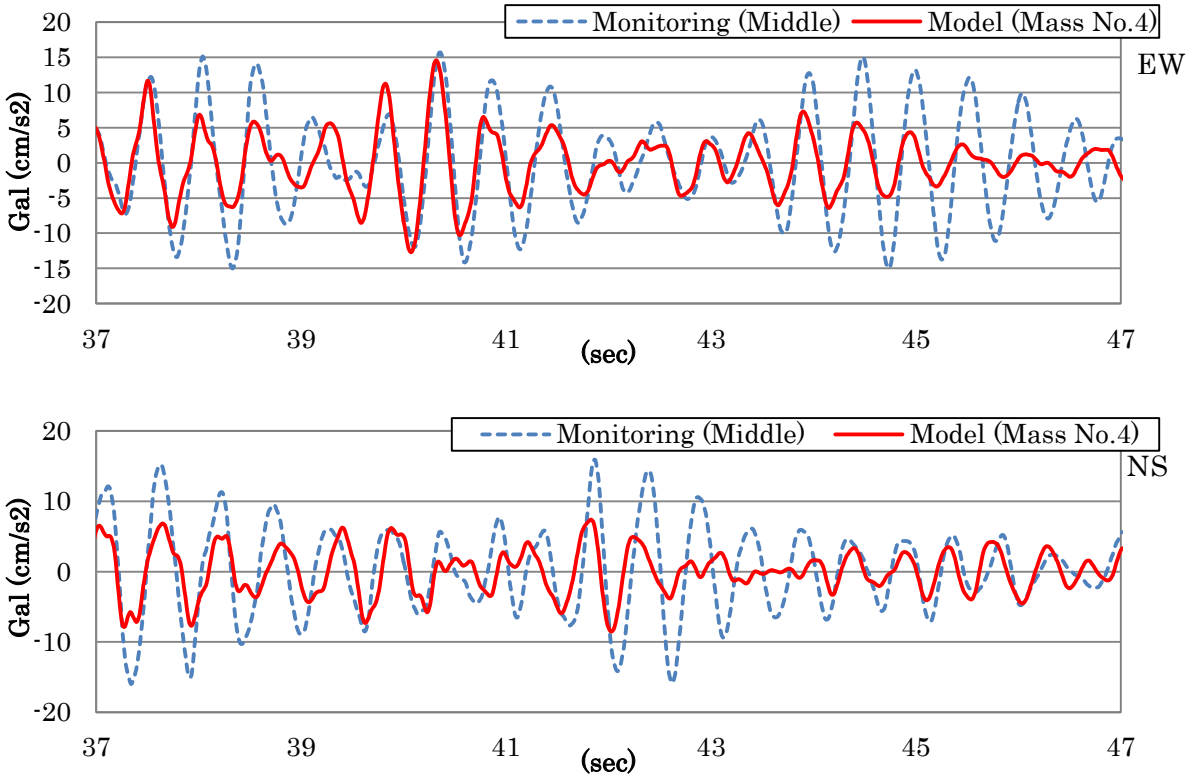

Fig. 3-154　Comparison of acc. wave form of Middle and Mass No. 4 (September 12th, 2010)

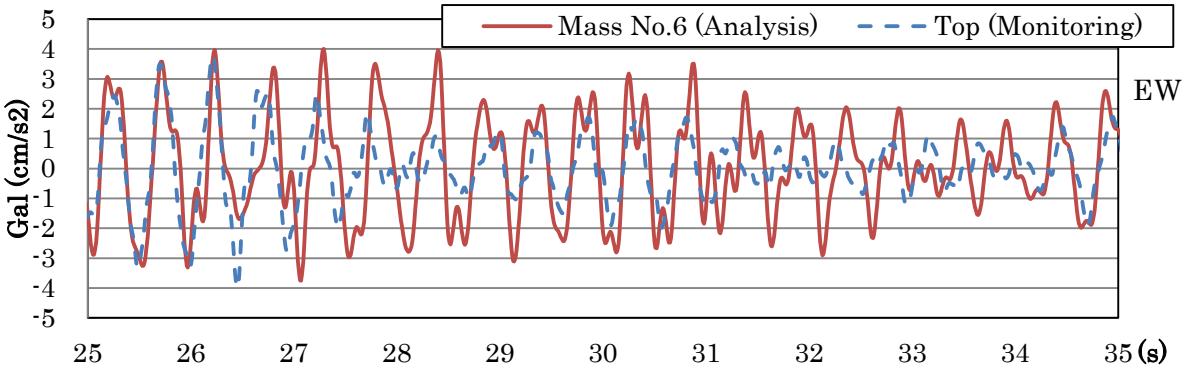

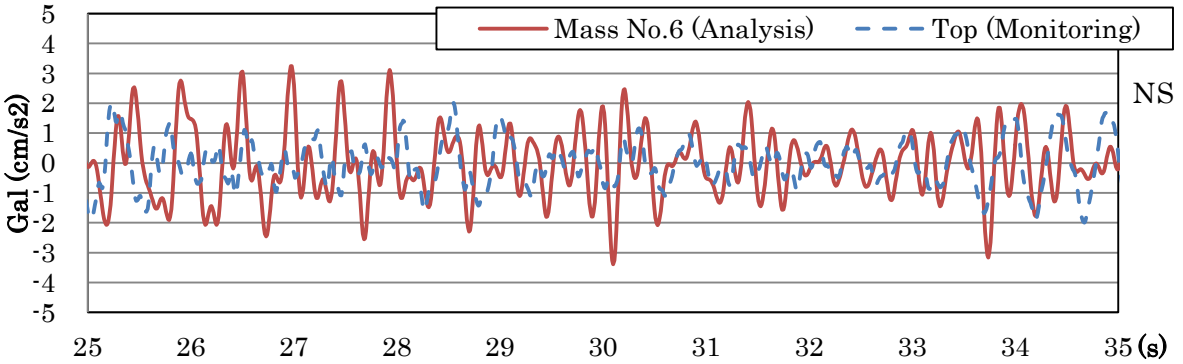

Fig. 3-155　Comparison of acc. wave form of Top and Mass No.6 (November 24th, 2011)

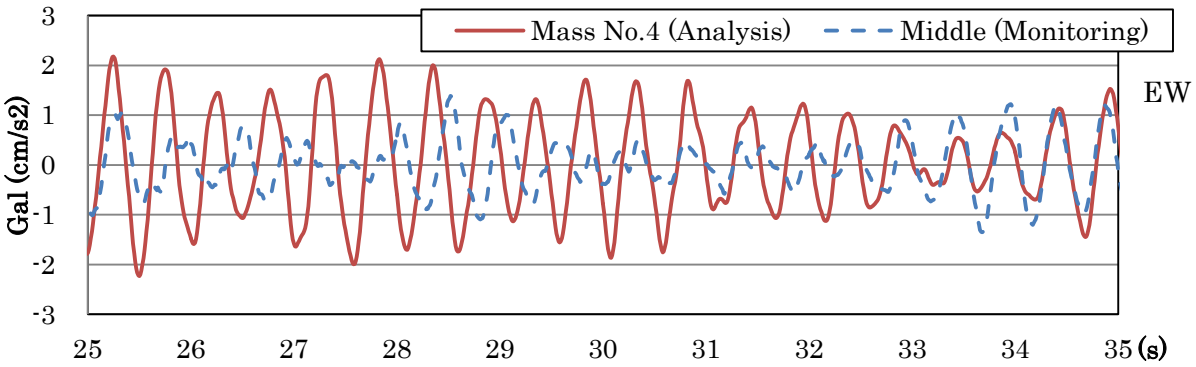

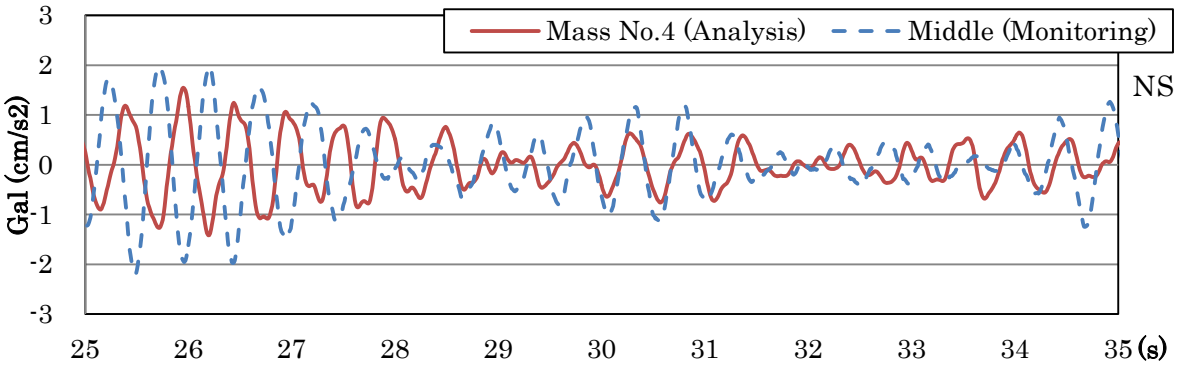

Fig. 3-156　Comparison of acc. wave form of Middle and Mass No. 4 (November 24th, 2011)

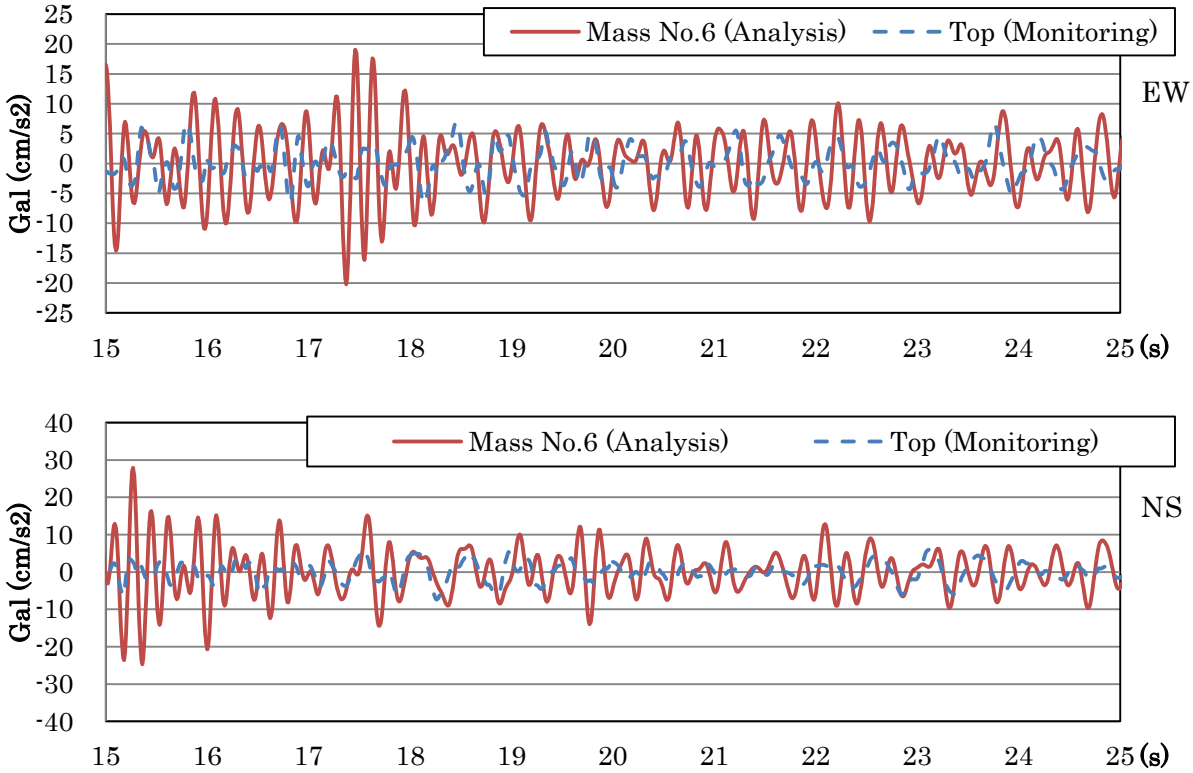

Fig. 3-157　Comparison of acc. wave form of Top and Mass No.6 (March 19th, 2012)

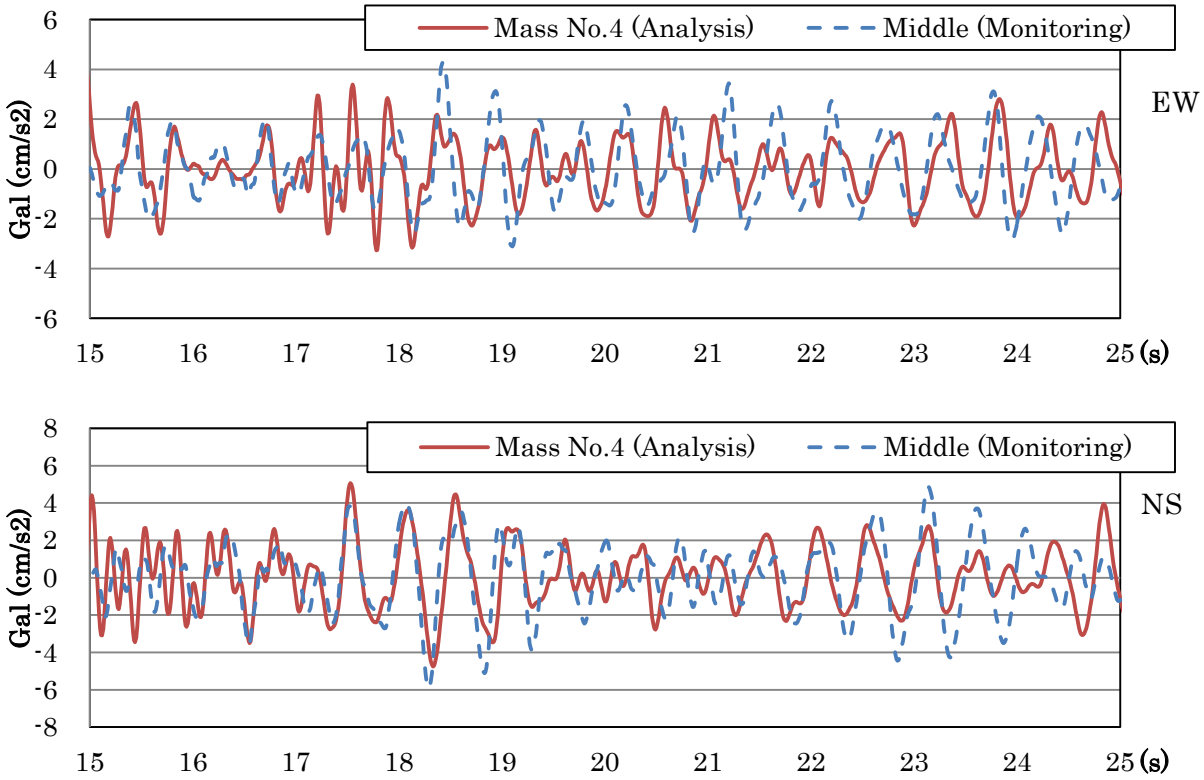

Fig. 3-158　Comparison of acc. wave form of Middle and Mass No. 4 (March 19th, 2012)

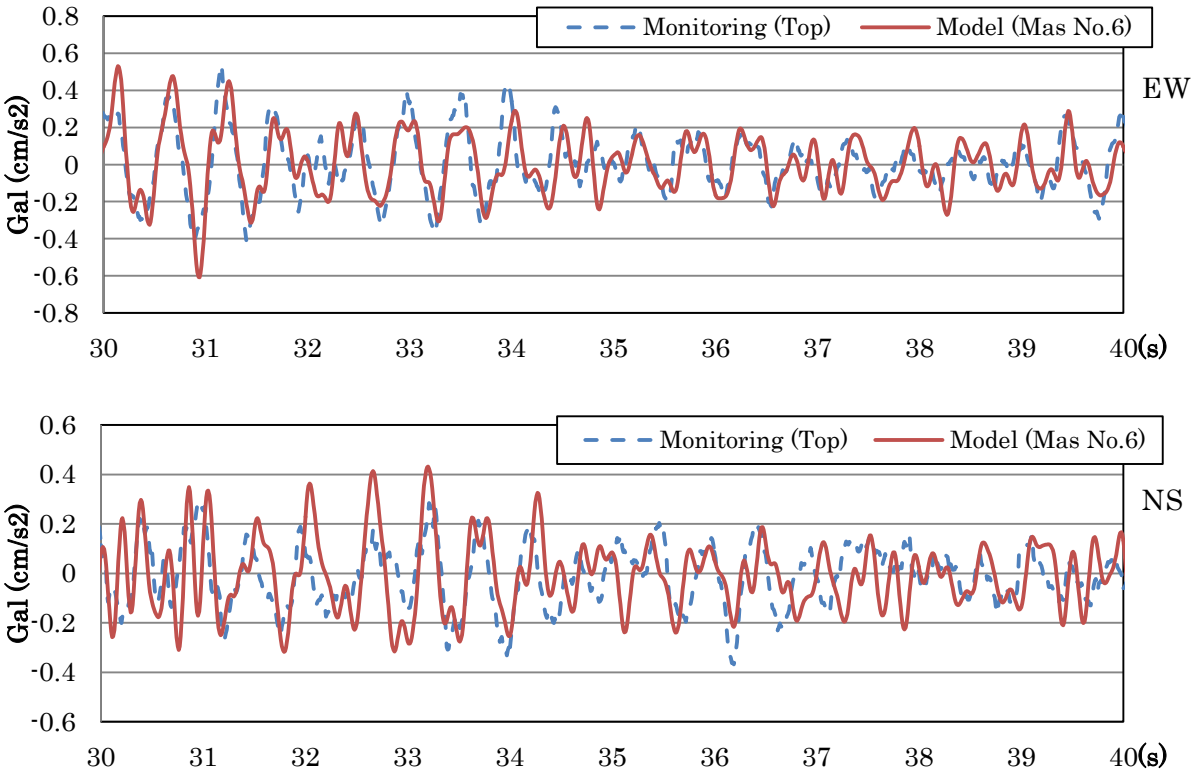

Fig. 3-159　Comparison of acc. wave form of Top and Mass No.6 (May 22th, 2012)

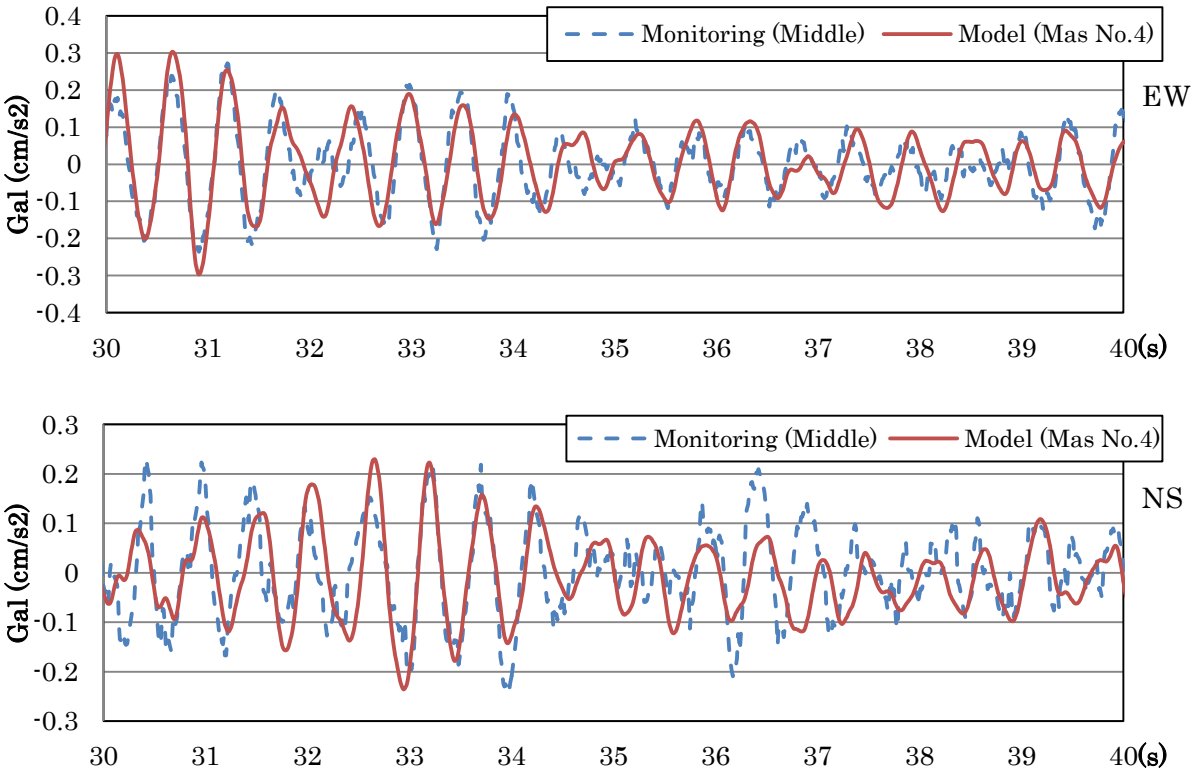

Fig. 3-160　Comparison of acc. wave form of Middle and Mass No. 4 (May 22th, 2012)

3.4.3 FINETE ELEMENT MODEL

The analysis model utilizing the 3-dimensional finite element was also employed for the analysis of Chandi Shiva. The model was assumed from the analysis model of Chandi Hangsa/Garuda, employed at the past study [14], taking into account the height of the structure; Chandi Shiva is 47m in height, while Chandi Hangsa/Garuda is 22m in height. On the assumption that the inner structural condition was the same as that of Chandi Hangsa/Garuda, the analysis model of Chandi Shiva was provided, because the inner structural condition of Chandi Shiva has not been known. Therefore, four types of models were analyzed. Fig. 3-161 shows specifications of these four models. Model 1 has the same cross section area of RC frame. On the other hand, the cross section area of RC frame of Model 2 was twice as large as that of Model 1. We examined the effect of the dynamic soil-structure interaction for each model. The parameters evaluated in the past study were used to determine the material properties of the model. This model was verified by comparison of the present analysis and the earthquake record of 2010. In this chapter, the results from the analysis by using Model 1 considering dynamic soil-structure interaction were presented. Fig. 3-162 shows the model. This finite element model consisted of a total of 52l,590 elements (of which 3 elements were as the three horizontal slabs, 651 elements were as the RC frame). Material properties were evaluated from the third survey in the international cooperative survey in 2006 to 2007, when the partial dismantlement of spire of Chandi Garuda was conducted [14]. The material properties were shown in Table. 3-20.

Fig. 3-163 shows the dimension of the representative column section at the lower part of the top of the roof of Model 1. Table. 3-21 shows the details of the RC frame. It contained 8 reinforced bars with the diameter 16 mm. We assumed that SD295 which is popular in Japan was used as reinforced bar (short-term tensile allowable stress 295 N/mm^2). If we assumed that the concrete was sufficiently strong and the yielding moment was decided by the tensile reinforced bar, the allowable bending moment M could be estimated by the following equation. As a result of this calculation, the allowable flexural moment of RC members at the top of the structure was evaluated to be 38.9 kNm.

$M = at \cdot ft \cdot 7/8 \cdot d$

- at: Cross section area of tensile bar
- ft: Short-term tensile allowable stress
- d: Distance from tensile edge to barycenter of reinforced bar

ft = 295 N/mm2

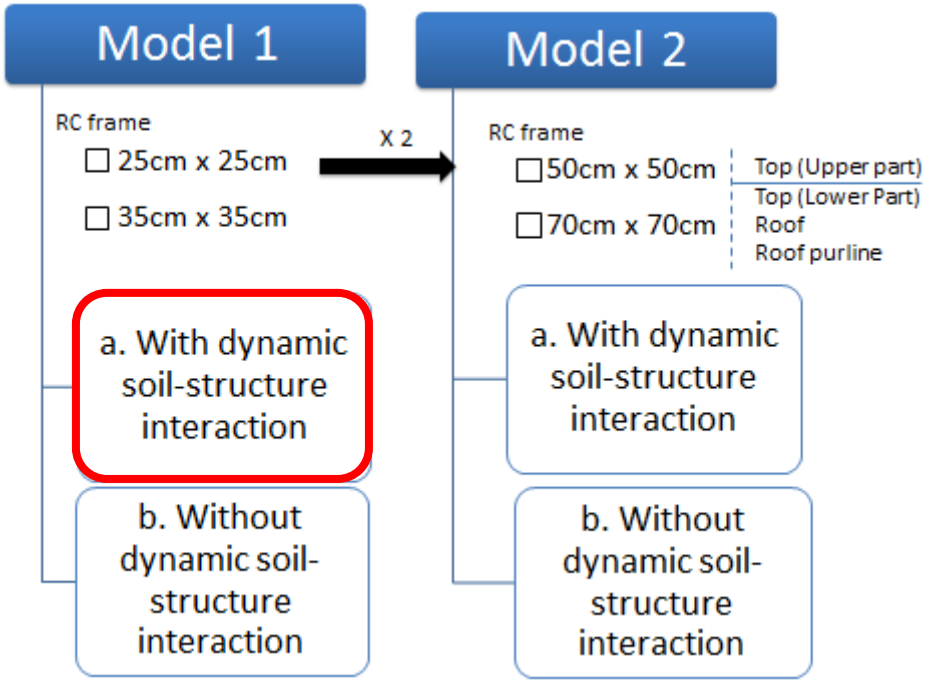

Fig. 3-161 Type of analysis models

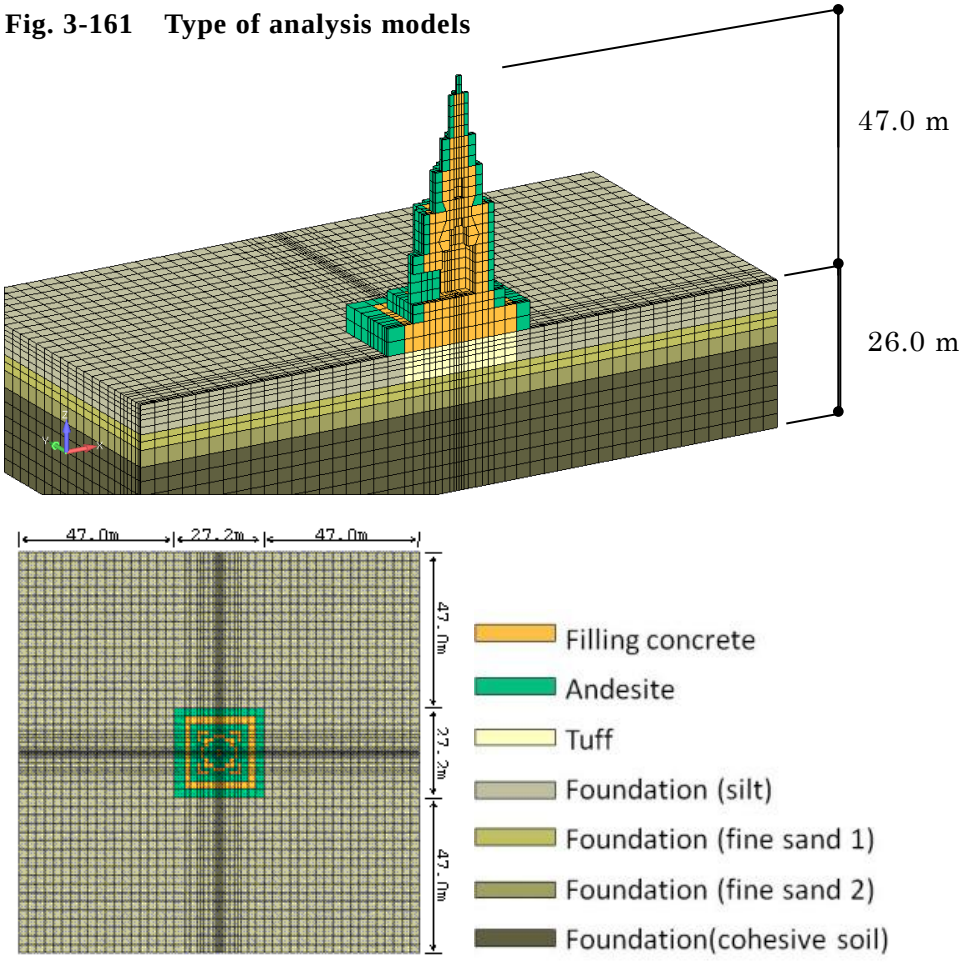

Fig. 3-162 Analysis model (Model 1, considering dynamic soil-structure interaction)

Table. 3-20 Material properties of the model

Material		Young's modulus (N/s^2)	Elastic shear modulus (N/s^2)	Poisson's ratio	Mass density (kg/m^3)	Shear wave velocity (m/s)
Filling concrete		1.60E+09	-	0.15	2330	-
Andesite Tuff		3.40E+09	-	0.30	2500	-
RC frame Horizontal slab		1.90E+10	-	0.20	2450	-
Foundation	Silt	-	1.9469E+07	0.45	1800	104
	Fine sand 1	-	8.2433E+07	0.33	1800	214
	Fine sand 2	-	1.8317E+08	0.33	1800	319
	Cohesive soil	-	1.1404E+08	0.45	1700	259

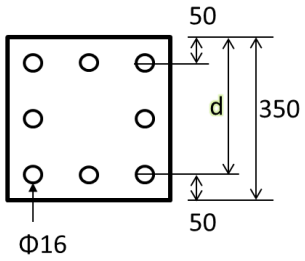

Fig. 3-163 Estimated column section of RC frame (Lower part of top of roof)

Table. 3-21 Cross sectional geometry (RC frame)

Part		Shape	Cross section (cm^2)	Torsional moment (m^3)	Area moment of inertia (m^4)
Top	Upper part	□- 25 cm x 25 cm	0.0625	5.501E-04	3.255E-04
Roof Roof purline	Lower part	□- 35 cm x 35 cm	0.1225	2.113E-03	1.251E-03

Input seismic motion that was used when the analysis of Chandi Hangsa/Garuda was conducted was also conducted. As there were no records of the event on May 25th, 2006, the Central Java Earthquake, both near the Prambanan Temples and in the epicentral area, the input ground motions were derived by using records of an earthquake. This earthquake occurred on September 7th, 1999 near Athens, Greece, which was the near-field earthquake with magnitude of 5.7 being similar to the Central Java Earthquake, as well as it brought significant damage to historical masonry buildings. It is called Athens Earthquake below. The record of the Athens Earthquake at the site SPLA 1 was used. The transverse component of the peak velocity was 12.4

kine (cm/s), and the peak acceleration was 217 gal (cm/s^2). This ground motion level could be accepted, according to estimation of the peak velocity of around 10 kine (cm/s) at the location of the Prambanan Temples on the basis of empirical equation of attenuation with distance. Figs. 3-164 and 3-165 show the acceleration waveform and the acceleration response spectrum of the input motion.

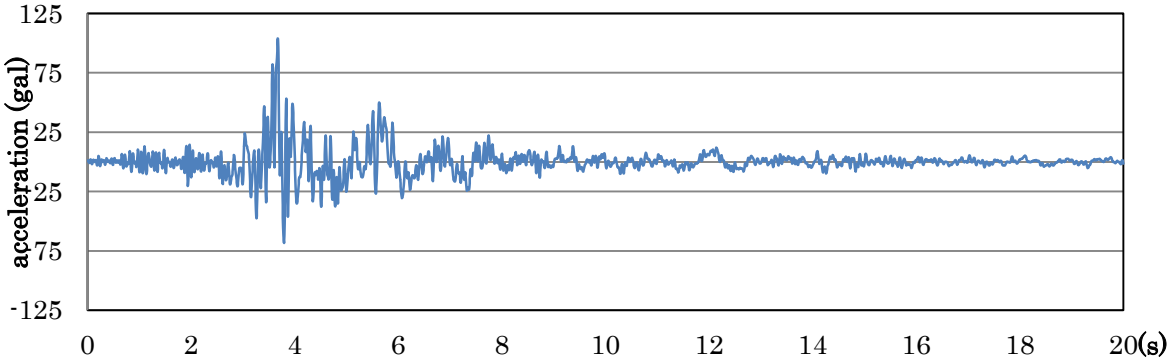

Fig. 3-164 Input seismic motion

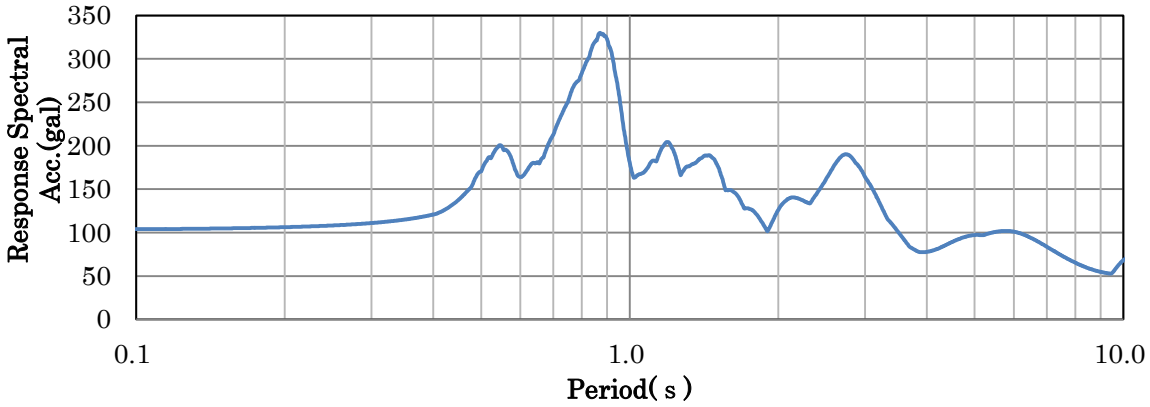

Fig. 3-165 Acceleration response spectrum of input seismic motion

3.4.4 RESULTS

Fig. 3-166 shows the contact pressure distribution at the base of foundation when only self-weight was induced. The maximum compressive stress was evaluated to be 115.7 kN/m^2. Fig. 3-167 shows the contact pressure distribution considering the dynamic effect induced by the earthquake. It could get the value 455.2 kN/m^2 as the maximum compressive stress. Fig. 3-168 and 3-169 show the distributions of tensile and compressive stress, respectively. As shown in Fig. 3-168, maximum tensile stress was 1,272.7 kN/m^2, on the other hand maximum compressive stress was 2,072.0 kN/m^2. Fig. 3-170 shows the distribution of shear stress. The maximum flexural bending moment induced on RC frame at earthquake was 11.4 kN/m^2, as shown in Fig. 3-171. Fig.

3-172 shows the vertical stress around the entrance affected by the self-weight under the same condition of Fig. 3-166. The maximum compressive stress was 845.0 kN/m^2. Fig. 3-173 shows the vertical stress around the entrance when earthquake was affected. It shows that the maximum compressive stress was 2,218.7 kN/m^2.

Table. 3-22 Compressive/tensile/shear stress and bending moment

		Compressive stress (kN/m^2)	Tensile stress (kN/m^2)	Shear stress (kN/m^2)	Bending moment (kNm)
Base of foundation	self-weight	115.7	-	-	-
		455.2	-	-	-
Short-term allowable bearing capacity		780.0	-	-	-
Around Entrance	self-weight	845.0	-	-	-
		2,218.7	-	-	-
Whole structure		2,072.0	1,272.7	432.3	-
Strength of the andesite		13,600.0	1,360.0	-	-
Strength of the inner concrete		22,000.0	2,200.0	-	-
RC frame		-	-	-	11.4
Flexural bending moment at short-term allowable stress		-	-	-	38.9

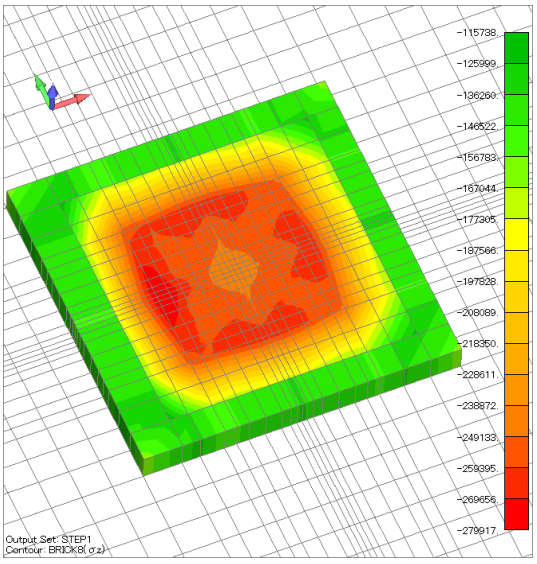

Fig. 3-166 Contact pressure distribution at the base of foundation (Self-weight)

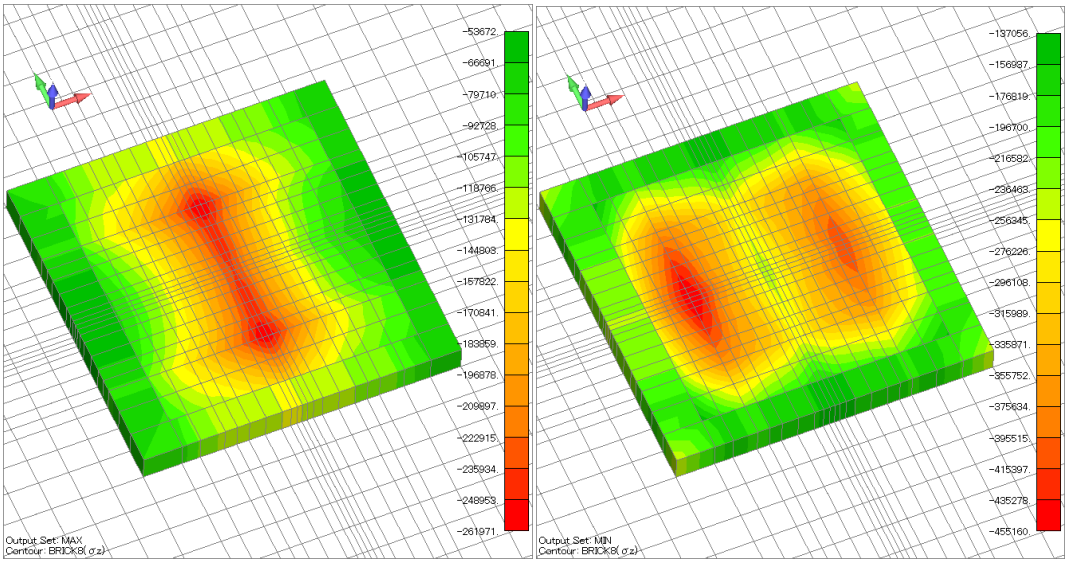

Fig. 3-167　Contact pressure distribution at the base of foundation (left: Max., right: min.)

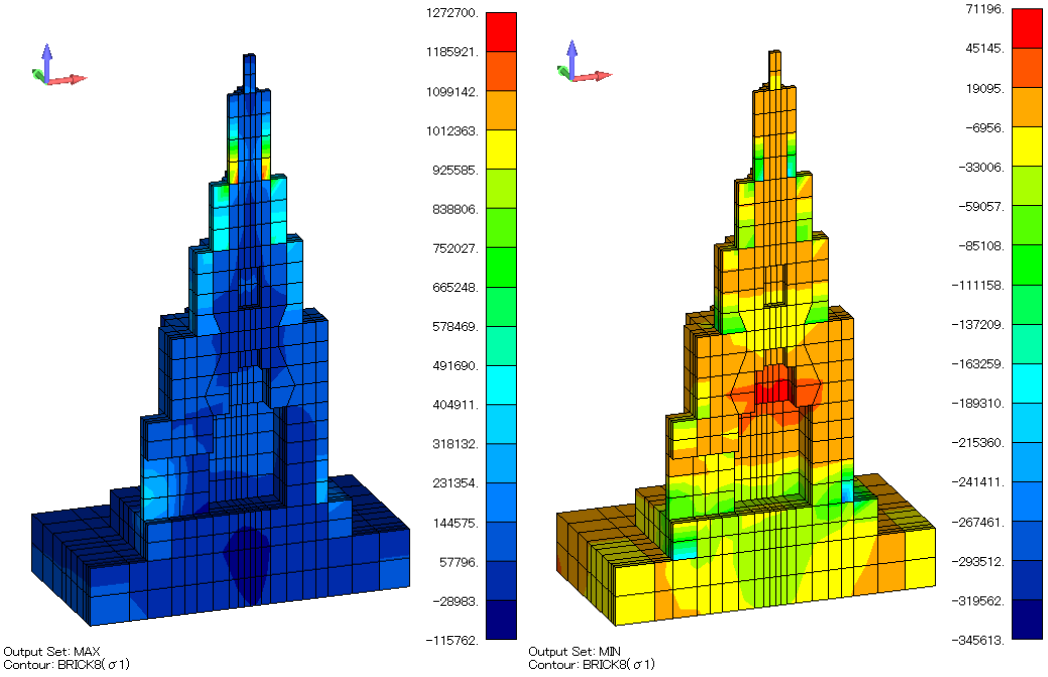

Fig. 3-168　Tensile stress distribution when the maximum and minimum stress induced

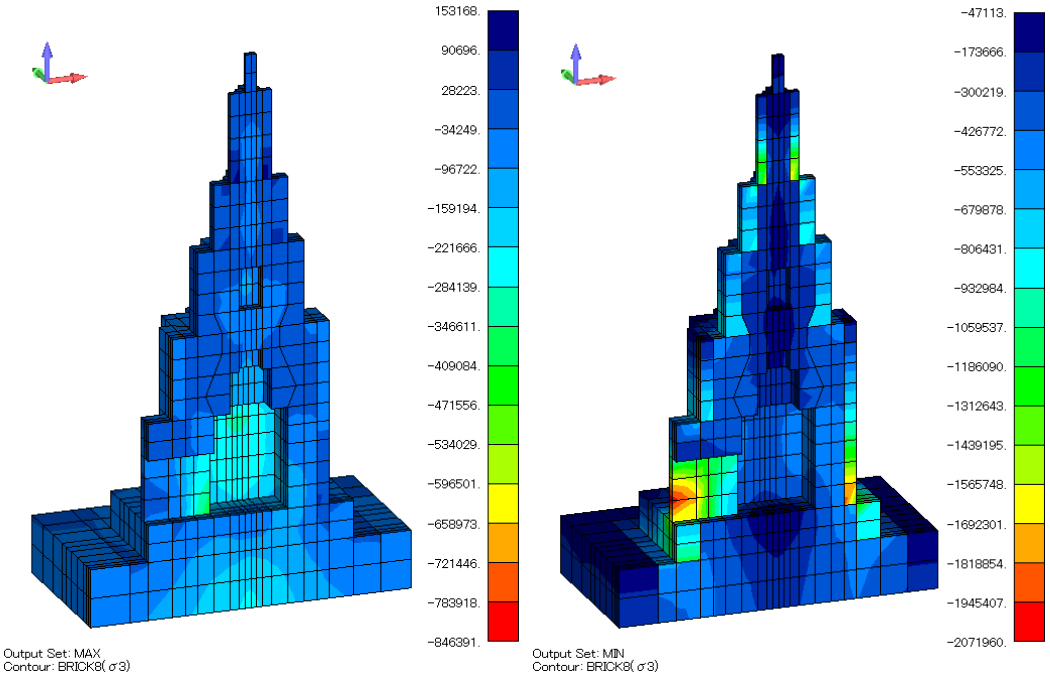

Fig. 3-169　Compressive stress distribution when the maximum and minimum stress induced

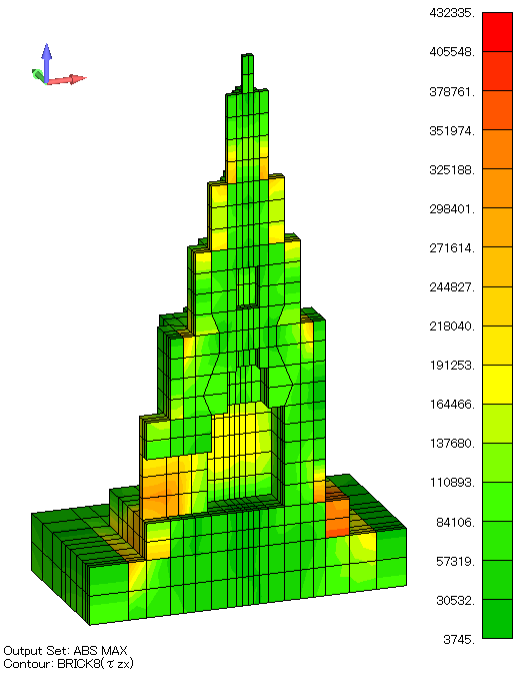

Fig. 3-170　Shear stress (τ_{zx})

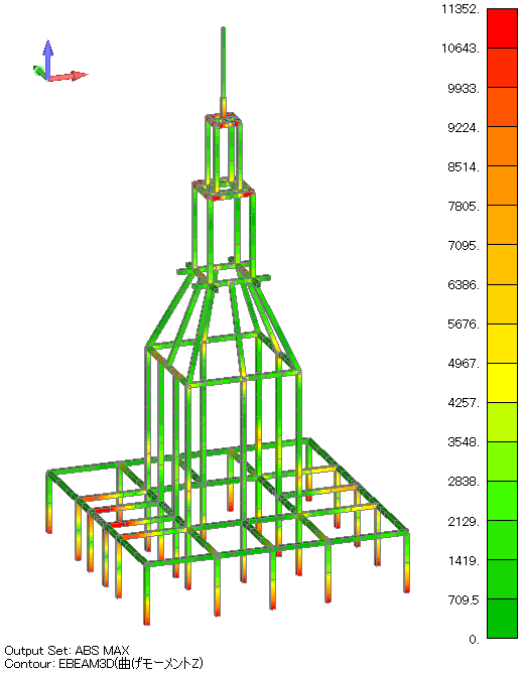

Fig. 3-171　Bending moment induced on RC frame

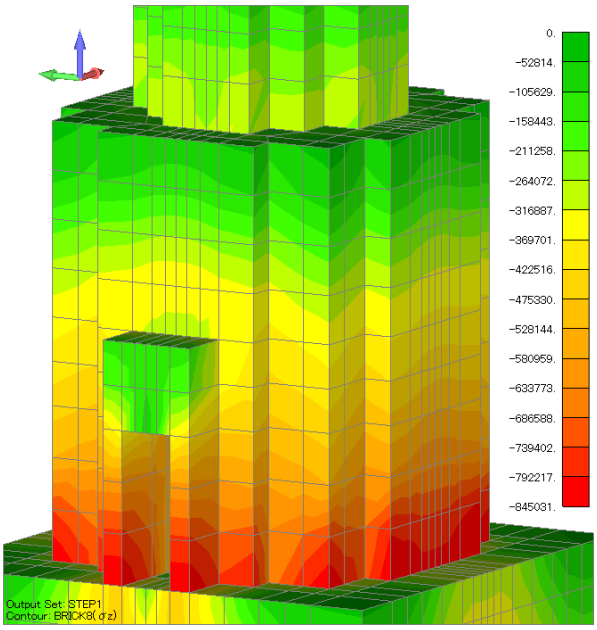

Fig. 3-172 Vertical stress around the entrance

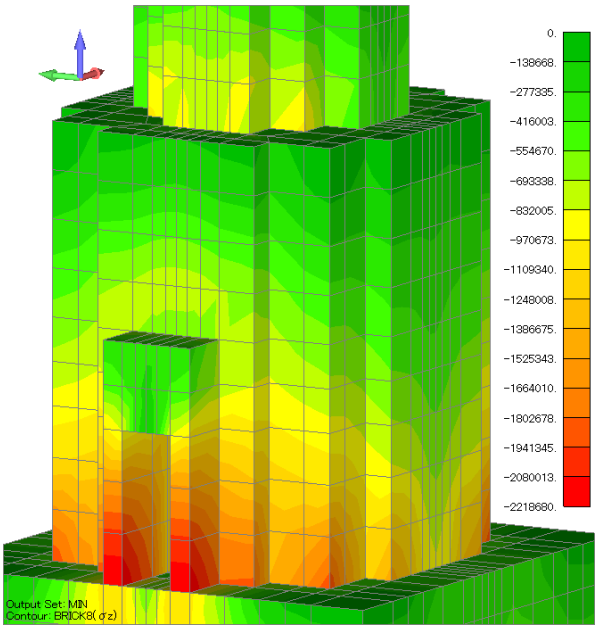

Fig. 3-173 Maximum vertical compressive stress

3.5 CONCLUDING REMARKS

The earthquake monitoring at Chandi Shiva performed for two and half years gave us a total of four records of minor earthquakes. The magnitude of the recorded earthquakes ranged from 4.2 to 5.1. The peak ground accelerations were smaller than 10 cm/s^2. Those monitoring records showed the fundamental dynamic characteristics of this large and massive masonry monument. Both the characteristics of the ground motions and those of the structural response were evaluated. The natural frequencies of Chandi Shiva, evaluated from the transfer functions from the ground to the structure, ranged from 1.9 to 2.2 Hz.

The crack displacement and temperature/humidity monitoring showed that the crack displacement was affected by the variation of the temperature. On the other hand, effect of humidity on crack displacement was not clearly found. These four earthquakes did not affect the variation of crack displacement at every monitoring point. The present monitoring indicated that the structure was stable during those earthquake motions.

The earthquake response analysis was conducted with employment of lamped masses models. The dynamic soil-structure interaction was taken into account. Four of the recorded earthquakes were utilized for the input motion.

The analysis utilizing the 3-dimentional finite element model was also carried out. The soil-structure interaction was taken into account as well. This model was verified by the monitoring record of 2010.

Chapter 4 Conclusions

4.1 CONCLUSIONS

In this study, the dynamic characteristics of the two World Heritage masonry monuments were studied by the structural monitoring. Those two objects were the Parthenon Athens in Greece and the Prambanan Temples in Indonesia. Earthquake response analyses of those monuments were conducted to simulate the earthquake records with the lamped masses models. Furthermore, the analysis model utilizing the 3-dimensioinal finite element was also employed for the analysis of Chandi Shiva of which inner structural condition has not been clearly known.

Firstly, the study of the Parthenon Athens was described. One earthquake monitoring record of December 8th, 2011 revealed the actual behavior during a small level earthquake of which peak ground acceleration was as small as 0.9 cm/s^2. The observed natural frequencies were 4.1 Hz and 3.8 Hz in EW and NS direction, respectively during this event. These natural frequencies were in good agreement with the ones of microtremor recorded just before this small earthquake. This earthquake record was compared with another small earthquake record of September 2nd, 2010. The acceleration response spectra of these two earthquakes did not show the predominant frequency depends on the topographic effect of the Acropolis hill.

The natural frequencies observed by the microtremor measurements in the past studies were compared with these of the earthquake event of 2011. The natural frequencies of the microtremor measurements in NS direction were in roughly good agreement with that of the earthquake. On the other hand, the natural frequencies in EW direction did not show good agreement.

Vibration due to restoration works was recorded at a number of times during the monitoring, as the peak acceleration exceeded trigger level at 0.5 cm/s^2. Those data also gave us the microtremor records. The natural frequency in NS direction has been approximately 3.8 Hz since July of 2011 until now. However, the natural frequency in EW direction has slightly varied.

The seismic response analysis utilizing the earthquake record of 2011 was conducted. The acceleration time histories at the rooftop were compared with those of the analysis model. As results, these acceleration waves were in roughly good agreement. The transfer functions in EW direction showed almost the same peak frequency at 4 Hz. However, in NS direction, the natural frequency of the analysis model showed the almost same peak frequency of the microtremor measurements in 2008. The reason of the disagreement of the natural frequencies in NS direction of monitoring and analysis was considered that this analysis model was verified by the natural frequencies of the microtremor measurements.

Secondary, the study of Chandi Shiva, the largest structure in the Prambanan Temples, was

described. A total of four minor earthquakes were successfully recorded by the seismographs at Chandi Shiva. The magnitude ranged from 4.2 to 5.1. The peak ground accelerations were evaluated from the earthquake response smaller than 10 cm/s^2. The natural frequencies of Chandi Shiva, observed by the transfer functions from the ground to the structure, ranged from 1.9 to 2.2 Hz. The larger the response displacement was, the higher the natural frequencies became. Moreover, it was found that the natural frequency was lower than that of the microtremor when earthquakes stroke it.

The crack displacement and temperature/humidity monitoring showed that the crack displacement was affected by the variation of the temperature. On the other hand, effect of humidity on crack displacement was not clearly shown. Four recorded earthquakes did not affect the variation of crack displacement at every monitoring point. The present monitoring indicated that the structure was stable during those earthquake motions.

The earthquake response analysis was conducted with employment of a lamped masses model. The dynamic soil-structure interaction was considered in the analysis model. Four earthquake records of September in 2010, November in 2011, March and May in 2012 were used for the simulation analysis.

The analysis utilizing the 3-dimentional finite element model was also carried out. The soil-structure interaction was taken into account. This model was verified by the monitoring record of 2010. In this analysis, the input earthquake record was assumed as the Central Java Earthquake of 2006. As a result of the calculation, the flexural bending moment induced in the RC frame did not exceed the flexural bending moment corresponding to the short-term allowable stress. As well as the tensile stress working in both the inner concrete and the andesite did not exceed the tensile strength. The present 3-dimentional finite element analysis showed that the structure did not suffer severe damage in its inner structure of RC on the assumption that the structure was subjected to the seismic event as large as 217 cm/s^2 of the peak acceleration. Furthermore, when we considered the dynamic earth pressure due to the seismic response, the contact pressure of the foundation base was smaller than the baring capacity estimated. It indicated that the irregular settlement was not caused by that earthquake.

4.2 FURTHER STUDY

To revise the analysis model, it would be needed to add monitoring points at the Parthenon Athens, at the same time, at the Acropolis hill in order to reveal the topographical effect.

The finite element model of Chandi Shiva would be needed to be revised to make a more accurate model, as the present model was based on Chandi Hangsa/Garuda.

ACKNOWLEDGEMENTS

The author is deeply grateful to Ass. Prof. H. P. Mouzakis from the National Technical University of Athens. The author also wants to thank Dr. M. Ioannidou as the former Director of Acropolis Restoration Service YSMA, and Dr. A. Miltiadou from Hellenic Ministry of Culture and Tourism for their kind cooperation in the international investigation of the Parthenon Athens.

In the international cooperative research of the Prambanan Temples, the author would like to express the gratitude to Prof. S. Pranumijoyo from the Gadjah Mada University. The project have been successfully performed in corporation with Department of history and archeology, Ministry of culture and tourism, Indonesia. Dr. C. Minowa and Mr. T. Suzuki's support were invaluable.

The author owes a very important debt to Prof. T. Hanazato for his schooling. And the author specially thanks all the member of Hanazato laboratory, since they always supported and encouraged me.

REFERENCE

[1] International Scientific Committee on the Analysis and Restoration of Structures of Architectural Heritage, Principles, "ICOMOS CHARTER –PRINCIPLES FOR THE ANALYSIS, CONSERVATION AND STRUCTURAL RESTORATION OF ARCHITECTURAL HERITAGE (2003)," (http://iscarsah.icomos.org/content/principles/ISCARSAH_Principles_English.pdf), browsing on February 2nd, 2013

[2] New Integrated Knowledge based approaches to the protection of cultural heritage from Earthquake-induced Risk, Workpackages, (http://www.niker.eu/workpackages/), browsing on February 2nd, 2013

[3] G. Creazza, "Structural Behaviour of San Marco Basilica, Venice," Journal of the International Association for Bridge and Structural Engineering (IABSE), SEI Volume 3, Number 1, pp.30-31, 1993

[4] T. Hanazato, "Earthquake Resistant Capacity of Historical Masonry Buildings : Structural Characteristics of World Heritage in Seismic Area," Architectural Institute of Japan, pp1087-1088, 2003 (in Japanese)

[5] H. Takayama, et. al., "Environmental Monitoring : Preliminary Report of Hagia Sophia Surveying Project No.8," Architectural Institute of Japan, pp23-24, 2001 (in Japanese)

[6] T. Hanazato, et. al., "Environmental Monitoring : Preliminary Report of Hagia Sophia Surveying Project No.9," Architectural Institute of Japan, pp25-26, 2001 (in Japanese)

[7] K. Hidaka, et. al., "Architectural-Structural Survey of HAGIA SOPHIA," chuokouronbijyutsu, pp195-216, 2003 (in Japanese)

[8] T. Hanazato, et.al., "Earthquake Resistant Capacity of Parthenon Athens and Five-story Pagoda," kenchikui, volume.4, No.2, pp30-34, 1996 (in Japanese)

[9] T. Ueshima, M. Shibuya, K.Kanazawa, H. Shiojiri and M. Nakamura, "System Identification, Detection of Proper Frequency Variation of an Aged Arch Dam and Its Dynamic Behavior during the 2011 Great East Japan Earthquake," Journal of 15WCEE LISBOA 2012, no. 0688, 2012

[10] N. Oyaizu, "Earthquake Ground Motions and Structural Damage at the Parthenon Athens," Bachelor thesis, Department of Architecture, Faculty of Engineering, Mie University, 2011

[11] M. Ohmura, "Fundamental Study on Dynamic Behaviors of the Parthenon Athens," Master's thesis, Graduate School of Engineering, Mie University, 2012

[12] D. Karnawati, S. Pranumijoyo, R. Anderson and S. Husein, "The Yogyakarta Earthquake of May 27, 2006," Star Publishing Company, Inc., 2008

[13] R. R. Putra, J. Kiyono, Y. Ono and H. R. Parajuli, “SEISMIC HAZARD ANALYSIS FOR INDONESIA,” Journal of Natural Disaster Science, Volume 33, pp.59-70, 2012

[14] Japan Center for International Cooperation in Conservation National Research Institute for Cultural Properties, Tokyo, “Survey Report and Restoration Plan on Prambanan World Heritage Temples,” National Research Institute For Cultural Properties, Tokyo, 2008

[15] A. Nakatani, “世界遺産プランバナン寺院シヴァ祠堂の耐震性に関わるモニタリング調査,” Bachelor thesis, Department of Architecture, Faculty of Engineering, Mie University, 2011